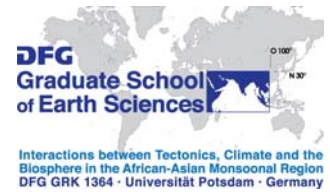Institut für Erd- und Umweltwissenschaften
Mathematisch-Naturwissenschaftliche Fakultät
Universität Potsdam

Climate variability and glacial dynamics in the Himalaya

Dirk Scherler

Für Kalle

"[...] if we speak of the general uniformity of Nature we must do so in a wide sense, remembering the wide epochs, it may be, of thousands of years, which represent but as it were one or two footsteps in the progress of Nature, which is the self-revelation of Him with whom a thousand years is as one day."

[Arthur Neve, Journeys in the Himalayas and Some Factors of Himalayan Erosion, 1911]

Abstract

In the high mountains of Asia, glaciers cover an area of approximately 115,000 km² and constitute one of the largest continental ice accumulations outside Greenland and Antarctica. Their sensitivity to climate change makes them valuable palaeoclimate archives, but also vulnerable to current and predicted Global Warming. This is a pressing problem as snow and glacial melt waters are important sources for agriculture and power supply of densely populated regions in south, east, and central Asia. Successful prediction of the glacial response to climate change in Asia and mitigation of the socioeconomic impacts requires profound knowledge of the climatic controls and the dynamics of Asian glaciers. However, due to their remoteness and difficult accessibility, ground-based studies are rare, as well as temporally and spatially limited. We therefore lack basic information on the vast majority of these glaciers.

In this thesis, I employ different methods to assess the dynamics of Asian glaciers on multiple time scales. First, I tested a method for precise satellite-based measurement of glacier-surface velocities and conducted a comprehensive and regional survey of glacial flow and terminus dynamics of Asian glaciers between 2000 and 2008. This novel and unprecedented dataset provides unique insights into the contrasting topographic and climatic controls of glacial flow velocities across the Asian highlands. The data document disparate recent glacial behavior between the Karakoram and the Himalaya, which I attribute to the competing influence of the mid-latitude westerlies during winter and the Indian monsoon during summer.

Second, I tested whether such climate-related longitudinal differences in glacial behavior also prevail on longer time scales, and potentially account for observed regionally asynchronous glacial advances. I used cosmogenic nuclide surface exposure dating of erratic boulders on moraines to obtain a glacial chronology for the upper Tons Valley, situated in the headwaters of the Ganges River. This area is located in the transition zone from monsoonal to westerly moisture supply and therefore ideal to examine the influence of these two atmospheric circulation regimes on glacial advances. The new glacial chronology documents multiple glacial oscillations during the last glacial termination and during the Holocene, suggesting largely synchronous glacial changes in the western Himalayan region that are related to gradual glacial-interglacial temperature oscillations with superimposed monsoonal precipitation changes of higher frequency.

In a third step, I combine results from short-term satellite-based climate records and surface velocity-derived ice-flux estimates, with topographic analyses to deduce the erosional impact of glaciations on long-term landscape evolution in the Himalayan-Tibetan realm. The results provide evidence for the long-term effects of pronounced east-west differences in glaciation and glacial erosion, depending on climatic and topographic factors. Contrary to common belief the data suggest that monsoonal climate in the central Himalaya weakens glacial erosion at high elevations, helping to maintain a steep southern orographic barrier that protects the Tibetan Plateau from lateral destruction.

The results of this thesis highlight how climatic and topographic gradients across the high mountains of Asia affect glacier dynamics on time scales ranging from 10^0 to 10^6 years. Glacial

response times to climate changes are tightly linked to properties such as debris cover and surface slope, which are controlled by the topographic setting, and which need to be taken into account when reconstructing mountainous palaeoclimate from glacial histories or assessing the future evolution of Asian glaciers. Conversely, the regional topographic differences of glacial landscapes in Asia are partly controlled by climatic gradients and the long-term influence of glaciers on the topographic evolution of the orogenic system.

Zusammenfassung

In den Hochgebirgen Asiens bedecken Gletscher eine Fläche von ungefähr 115,000 km² und ergeben damit, neben Grönland und der Antarktis, eine der größten Eisakkumulationen der Erde. Die Sensibilität der Gletscher gegenüber Klimaschwankungen macht sie zu wertvollen paläoklimatischen Archiven in Hochgebirgen, aber gleichzeitig auch anfällig gegenüber rezenter und zukünftiger globaler Erwärmung. Dies kann vor allem in dicht besiedelten Gebieten Süd-, Ost- und Zentralasiens zu großen Problem führen, in denen Gletscher- und Schnee-Schmelzwässer eine wichtige Ressource für Landwirtschaft und Stromerzeugung darstellen. Eine erfolgreiche Prognose des Gletscherverhaltens in Reaktion auf den Klimawandel und die Minderung der sozioökonomischen Auswirkungen erfordert fundierte Kenntnisse der klimatischen Steuerungsfaktoren und der Dynamik asiatischer Gletscher. Aufgrund ihrer Abgeschiedenheit und dem erschwerten Zugang gibt es nur wenige glaziologische Geländestudien, die zudem räumlich und zeitlich sehr begrenzt sind. Daher fehlen bisher grundlegende Informationen über die Mehrzahl asiatischer Gletscher.

In dieser Arbeit benutze ich verschiedene Methoden, um die Dynamik asiatischer Gletscher auf mehreren Zeitskalen zu untersuchen. Erstens teste ich eine Methode zur präzisen satelliten-gestützten Messung von Gletscheroberflächen-Geschwindigkeiten. Darauf aufbauend habe ich eine umfassende regionale Erhebung der Fliessgeschwindigkeiten und Frontdynamik asiatischer Gletscher für die Jahre 2000 bis 2008 durchgeführt. Der gewonnene Datensatz erlaubt einmalige Einblicke in die topographischen und klimatischen Steuerungsfaktoren der Gletscherfließ-geschwindigkeiten in den Gebirgsregionen Hochasiens. Insbesondere dokumentieren die Daten rezent ungleiches Verhalten der Gletscher im Karakorum und im Himalaja, welches ich auf die konkurrierenden klimatischen Einflüsse der Westwinddrift im Winter und des Indischen Monsuns im Sommer zurückführe.

Zweitens untersuche ich, ob klimatisch bedingte Ost-West Unterschiede im Gletscher-verhalten auch auf längeren Zeitskalen eine Rolle spielen und gegebenenfalls für dokumentierte regional asynchrone Gletschervorstöße relevant sind. Dazu habe ich mittels kosmogener Nuklide Oberflächenalter von erratischen Blöcken auf Moränen ermittelt und eine glaziale Chronologie für das obere Tons Tal, in den Quellgebieten des Ganges, erstellt. Dieses Gebiet befindet sich in der Übergangszone von monsunaler zu Westwind beeinflusster Feuchtig-keitszufuhr und ist damit ideal gelegen, um die Auswirkungen dieser beiden atmosphärischen Zirkulationssysteme auf Gletschervorstöße zu untersuchen. Die ermittelte glaziale Chronologie dokumentiert mehrere Gletscherschwankungen während des Endstadiums der letzten Pleistozänen Vereisung und während des Holzäns. Diese weisen darauf hin, dass Gletscher-schwankungen im westlichen Himalaja weitestgehend synchron waren und auf graduelle glaziale-interglaziale Temperaturveränderungen, überlagert von monsunalen Niederschlags-schwankungen höherer Frequenz, zurück zu führen sind.

In einem dritten Schritt kombiniere ich Satelliten-Klimadaten mit Eisfluss-Abschätzungen und topographischen Analysen, um den Einfluss der Gletscher Hochasiens auf die Reliefentwicklung im Hochgebirge zu untersuchen. Die Ergebnisse dokumentieren ausgeprägte

meridionale Unterschiede im Grad und im Stil der Vergletscherung und glazialen Erosion in Abhängigkeit von topographischen und klimatischen Faktoren. Gegensätzlich zu bisherigen Annahmen deuten die Daten darauf hin, dass das monsunale Klima im zentralen Himalaja die glaziale Erosion schwächt und durch den Erhalt einer steilen orographischen Barriere das Tibet Plateau vor lateraler Zerschneidung bewahrt.

Die Ergebnisse dieser Arbeit dokumentieren, wie klimatische und topographische Gradienten die Gletscherdynamik in den Hochgebirgen Asiens auf Zeitskalen von 10^0 bis 10^6 Jahren beeinflussen. Die Reaktionszeit der Gletscher auf Klimaveränderungen sind eng an Eigenschaften wie Schuttbedeckung und Neigung gekoppelt, welche ihrerseits von den topographischen Verhältnissen bedingt sind. Derartige Einflussfaktoren müssen bei paläoklimatischen Rekonstruktion und Vorhersagen über die Entwicklung asiatischer Gletscher berücksichtigt werden. Desweiteren gehen die regionalen topographischen Unterschiede der vergletscherten Gebiete Asiens teilweise auf klimatische Gradienten und den langfristigen Einfluss der Gletscher auf die topographische Entwicklung des Gebirgssystems zurück.

Contents

List of Figures

x

List of Tables

Acknowledgements

I am particularly indebted to my advisor, Manfred Strecker, for making this project possible and for the confidence he has shown to me from the very beginning onwards. He guided and supported me in every possible way, and allowed me to pursue research topics of my choice. I thank Bodo Bookhagen and Rasmus Thiede, for their friendship and support and for paving the way to work in the Himalaya. Bodo served as a mentor and project collaborator, and I am thankful for his helpful feedback and constructive criticism.

Much of this work would not have been possible without the generous support of Tashi Tsering Lonpo. He proved invaluable during my field work and became a dear friend with whom I share many joyful and adventurous memories.

I thank Friedhelm von Blanckenburg, now at GFZ, for allowing me to work in his lab at University Hanover, and for sharing his exhilarant scientific curiosity. I appreciate the kind support by Kevin Norton, Hella Wittmann, and Jane Willenbring who taught me the chemical procedures of processing cosmogenic nuclide samples. I am especially indebted to Sébastien Leprince, from Caltech, who developed the program COSI-Corr that I used in my studies and who patiently helped me whenever problems arose. I acknowledge the invitation to Pasadena by Jean-Phillipe Avouac, from Caltech, and to Boulder by Robert S. Anderson, from the University of Colorado. The supporting help of Arvid K. Jain and Sandeep Singh from IIT Roorkee, India, and of Sampat K. Tandon, from University Delhi, contributed to the accomplishment of this thesis project.

I am grateful to many colleagues in Potsdam for their continuous support and help. Martin Trauth is thanked for his support in various MATLAB-issues, Gerold Zeilinger for his expertise in GIS-related problems, and Mathias Ohrnberger for his assistance with mathematical problems. Ed Sobel, Taylor Schildgen, Oliver Korup, Barbara Carrapa, Estelle Mortimer, and Gregory Hoke contributed to making Golm a scientifically rich place. Antje Musiol, Birgit Fabian, Ines Münch, René Muschkogel, and Daniel Vollmer are thanked for their support in various technical issues. During my PhD, I benefited a lot from interactions with my fellow PhD colleagues with whom sharing labs, rooms, and discussions has always been great fun. I thank Hendrik Wulf for the time we spent together in the field and for interesting discussions and joint projects. I appreciated spending time with Mauricio Parra, Andres Mora, Henry Wichura, Esther Hintersberger, Paolo Ballato, Angela Landgraf, Katrin Rehak, Gudrun Richter, and many others at University Potsdam, and Burch Fisher and Ryan Perroy at UC Santa Barbara. I also want to thank Andreas Bergner for managing the Graduate School and all students who helped in different ways, in particular Johanna Meyer for her assitance in the lab. The list of individuals

1   Introduction

Climatic change influences the dynamics of earth-surface processes, most directly through changes in temperature and precipitation [e.g., *Bull*, 1991]. Against the backdrop of global change this has and increasingly will have important socioeconomic consequences in many regions on Earth [*IPCC*, 2007a; b]. Long-term increases of land surface temperatures in monsoonal Asia, for example, are expected to intensify the hydrological cycle and increase monsoon precipitation [*Meehl and Washington*, 1993]. In fact, meteorological data from central India already indicate an intensification of severe monsoonal rainstorm events, at the expense of more moderate events [*Goswami et al.*, 2006]. Such hydrological changes have potentially far-reaching consequences for the frequency and magnitude of catastrophic floods and slope failures, and thus erosion rates [e.g., *Kale and Hire*, 2004; *Bookhagen et al.*, 2005a, b].

At present, one of the most conspicuous effects of climate change in mountainous Asia is the widespread melting and retreat of glaciers [*Mayewski and Jeschke*, 1979; *Dyurgerov and Meier*, 2005; *Kulkarni et al.*, 2005; *Kehrwald et al.*, 2008; *Bolch et al.*, 2008; *Raina*, 2009]. Shrinking glaciers and shorter periods of snow cover continuously modify river discharge, which is important for the livelihood of densely populated areas in central, south, and East Asia [*Barnett et al.*, 2005; *Cruz et al.*, 2007; *Ren and Karoly*, 2008]. The glacial demise is frequently accompanied by formation of moraine-dammed lakes that are prone to catastrophic outburst floods and which pose serious hazards to mountain communities and infrastructure [e.g., *Richardson and Reynolds*, 2000; *Cenderelli and Wohl*, 2001]. Clearly, mitigating the glacial responses to climate change requires profound knowledge of the past and present dynamics of these glaciers. However, due to their remoteness and difficult acessibility, Asian glaciers are amongst the least studied glaciers on Earth [*Dyurgerov and Meier*, 2005; *WGMS*, 2008], and current knowledge of their behavior from short to long time scales is limited [e.g., *Benn and Lehmkuhl*, 2000; *Berthier et al.*, 2007; *Owen*, 2009].

The goal of this thesis is to contribute to a better understanding of the dynamics of Asian glaciers. To achieve this, I employ different techniques, including remote-sensing analysis and cosmogenic nuclide surface exposure dating. These methods cover different length and time scales and provide the opportunity to study various aspects of glacial dynamics. Key for linking the different time scales is the response of glaciers to present-day climate change on decadal time scales as well as longer-term climate oscillations during the Quaternary.

Pronounced climatic changes during the Quaternary [e.g., *Zachos et al.*, 2001], resulted in periodic waxing and waning of mountain glaciers all over the world [e.g., *Penck and Brückner*, 1909; *Hays et al.*, 1976]. In monsoonal Asia, Quaternary climate changes are associated with periodic oscillations in monsoon strength due to glacial-interglacial cycles and orbitally controlled insolation changes [*Kutzbach*, 1981; *Prell and Kutzbach*, 1992; *Wang et al.*, 2001; *Cheng et al.*, 2009]. Strengthening of the monsoon circulation at the Pleistocene/Holocene transition, for example, increased landward moisture flux and precipitation [e.g., *Sinha et al.*, 2005; *Wang et al.*, 2005; *Dykoski et al.*, 2005; *Herzschuh*, 2006] and resulted in widespread glacial advances in the Himalaya during the early Holocene [*Phillips et al.*, 2000; *Finkel et al.*,

2003; *Barnard et al.*, 2004]. Towards the western end of the Asian highlands, however, an increasing proportion of precipitation is related to the northern-hemisphere westerlies, and it is not yet clear whether glacier advances in these areas are more directly related to oceanic and atmospheric changes in the North Atlantic region [*Seong et al.*, 2009; *Chen et al.*, 2008; 2010; *Rupper et al.*, 2009; *Yadav et al.*, 2009].

Viewed on geologic time scales, the superposition of low to high-frequent climate oscillations and associated disturbances of geomorphic systems [e.g., *Schumm and Lichty*, 1965; *Church and Slaymaker*, 1989; *Tucker*, 2004] has regionally distinctive impacts on landscape development and may ultimately affect the tectonic evolution of mountain belts [e.g., *Willett*, 1999; *Montgomery et al.*, 2001; *Beaumont et al.*, 2001; *Zeitler et al.*, 2001; *Thiede et al.*, 2005; *Willett et al.*, 2006; *Whipple*, 2009]. Some of the most pertinent questions in Earth Sciences are related to the causes and effects of Quaternary glacial cycles and their links with the climatic, biologic, and geologic evolution of the Earth [e.g., *Penck and Brückner*, 1909; *Imbrie and Imbrie*, 1979; *Molnar and England*, 1990; *Raymo and Ruddiman*, 1992]. High mountainous landscapes in particular, with their U-shaped valleys, cirques, and overdeepenings, provide rich evidence of Quaternary glaciation and erosion. Current hypothesis posits that formerly more extensive and repeatedly oscillating glaciers limit the topographic height of the Himalaya and other glaciated mountain ranges by efficient glacial erosion near the long-term snowline, irrespective of tectonic rates [*Brozovic et al.*, 1997; *Brocklehurst and Whipple*, 2002; *Mitchell and Montgomery*, 2006; *Berger et al.*, 2008; *Egholm et al.*, 2009]. Yet, the details of this mechanism, known as the 'glacial buzz saw', such as how glacial erosion rates adjust to gradients in uplift rates, are not clear [e.g., *Brocklehurst and Whipple*, 2007].

In summary, current research identifies several key questions related to mountain glaciers in general, and to glaciers in the Asian highlands in particular that can be cast in the following questions:

1) How have glaciers responded to Quaternary climatic changes, and how will they respond to present day and future climate change?

2) How do climatic and topographic gradients influence the dynamic behavior of glaciers?

3) What are the long-term effects of glacial erosion on the topographic evolution of glaciated mountains?

To provide answers to these and related questions, I focus on mountain glaciers along the southern and western margin of the Tibetan Plateau that are influenced by monsoonal and westerly moisture sources. I provide a more detailed introduction to the study area and its climatic characteristics, in the following, second chapter.

In chapter 3, I investigate the potential of a new technique for image orthorecification, co-registration, and correlation, to measure glacier-surface velocities in alpine terrain with high accuracy. For this purpose I used the program COSI-Corr [*Leprince et al.*, 2007] in conjunction with ASTER (Advanced Spaceborne Thermal Emission and Reflection Radiometer) satellite images. Through application of filtering procedures and several quality tests, I validated the consistency of the results, providing confidence in the remotely sensed velocity measurements despite lack of ground control. This approach allows fast, easy, and economically viable acquisition of detailed glaciological data in areas of difficult access and provides a means for large-scale, spatially extensive monitoring of glaciers in high mountainous terrain.

In chapter 4, I employ the methodology developed in chapter 3 to conduct the first comprehensive regional synthesis of the topography and flow characteristics of Asian glaciers

using digital elevation analysis and remotely sensed glacier-surface velocities. The study revealed how along- and across-strike variations in snowline elevation, climate, and topography account for regional differences in the size and steepness of snow accumulation areas, which control the relative amounts of direct snowfall and avalanching. These factors are tightly linked with the extent of supraglacial debris cover and its effect on glacial flow velocities, which have not been identified previously.

Debris cover is long known to influence glacial-mass balances and to modulate the response of glaciers to climate change [*Ogilvie*, 1904; *Østrem*, 1959; *Mattson et al.*, 1993], suggesting that regional differences in debris cover may also lead to contrasting glacial behavior. In chapter 5, I present a closer inspection of flow velocities along the lower reaches of the previously studied glaciers, augmented with mapped frontal changes between 2000 and 2008, to investigate the relationship between debris cover, quasi-stagnant ice and frontal dynamics. The data show that many debris-covered glaciers with shallow terminus regions are stagnant and in-situ downwasting for kilometers upstream from their stable fronts. Such glaciers are most frequent in the steep central Himalaya but nearly absent in the Karakoram, where more than half of the studied glaciers were stable or advancing during the study period. This suggests presently different glacial conditions between the Karakoram and the Himalaya that are unrelated to differences in debris cover, and most likely due to the different atmospheric circulation regimes that influence these regions.

The competing influence of westerly and monsoonal moisture sources along the southern and western edge of High Asia is an outstanding problem in regional palaeoclimatic and glacial research [e.g., *Gillespie and Molnar*, 1995; *Benn and Owen*, 1998; *Owen et al.*, 2008; *Rupper et al.*, 2009; *Chen et al.*, 2008; 2010]. In chapter 6, I investigate the climatic controls on glaciations in the western Himalaya, by using cosmogenic nuclide surface exposure dating on moraines in western Garhwal, an area situated within the transition zone between dominant monsoonal and northern hemisphere westerlies influence. The new glacial chronology documents multiple glacial oscillations during the termination of the last glacial period and the Holocene with steadily decreasing glacial extents. Comparison with other glacial chronologies and palaeoclimatic records from the western Himalaya suggests largely synchronous glacial changes during this time period that are related to gradual glacial-interglacial temperature changes, superimposed with monsoonal precipitation changes of higher frequency.

The long-term effects of Quaternary climatic change on mountain glaciation and associated landscape development in High Asia is the subject of chapter 7. I used the glacier velocity data presented in chapter 4, to estimate mean annual ice-flux near the equilibrium line altiude (ELA) of the studied glaciers and use it as a proxy for glacial erosion potential [e.g., *Hallet et al.*, 1996]. The ice flux-based estimates of glacial erosion potential suggest an approximately linear increase with the size of glaciers and thus their accumulation areas. Digital elevation analysis reveals that regional differences in present-day and Quaternary snowline elevations result in significant differences in accumulation areas, hence glacier sizes, and erosion potential. These observations are supported by marked gradients in topographic relief which indicate an east-west gradient in glacial dissection of the southern and western Tibetan Plateau edges.

The contents of chapter 3 to 7 form individual studies that have been submitted to peer-reviewed journals. Chapter 3 ("Glacier-surface velocities in alpine terrain from optical satellite imagery – Accuracy improvement and quality assessment" by Dirk Scherler, Sébastien Leprince and Manfred R. Strecker) has been published in *Remote Sensing of Envrionment* [*Scherler et al.*, 2008]; chapter 4 ("High Asian gaciers: impact of topography and climatic gradients on debris

cover and flow velocities" by Dirk Scherler, Bodo Bookhagen and Manfred R. Strecker) has been submitted; chapter 5 ("Influence of debris cover on the frontal dynamics of High Asian glaciers" by Dirk Scherler, Bodo Bookhagen and Manfred R. Strecker) is in submission; chapter 6 ("Timing and extent of Late Quaternary glaciation in the Western Himalaya constrained by 10Be-moraine dating in Garhwal, India" by Dirk Scherler, Bodo Bookhagen, Manfred R. Strecker, Friedhelm von Blanckenburg and Dylan Rood) has been published in *Quaternary Science Reviews* [*Scherler et al.*, 2010]; chapter 7 ("Atmospheric moisture sources, snowline elevations, and glacial erosion potential across High Asia" by Dirk Scherler, Bodo Bookhagen, Manfred R. Strecker and Rasmus C. Thiede) has been submitted.

Apart from the AMS-measurements of the samples presented in chapter 6, which were analyzed by Dylan Rood at the Center for Accelerator Mass Spectrometry at the Lawrence Livermore National Laboratories, USA, I did all analyses for this thesis personally.

2   Geologic and climatic setting

"Im Gletschergebiete des Himalaya ist die Gebirgsgestaltung ganz so wie in den Alpen, aber alle Verhältnisse sind weit großartiger."

[H. von Schlagintweit, Reisen in Indien und Hochasien, 1871]

The Himalayan orogen stretches for almost 2,500 km from the Nanga Parbat massif in the western syntaxis at ~74°E, to the Namche Barwa massif in the eastern syntaxis at ~95°E (Figure 2.1). Physiographically, the orogen forms the transition between the Indo-Gangetic Plain to the south, which lies at elevations of less than 0.5 km, and the Tibetan Plateau to the north, with mean elevations of ~5 km over most of its area [*Fielding et al.*, 1994]. At the north-western end the Himalaya is adjoined by the Karakoram, Pamir, and Hindu Kush mountains and at the south-eastern end by the Nyainqentanglha Shan.

Formation of the Himalaya and the Tibetan Plateau is related to closure of the Tethyan Ocean and collision of the Indian subcontinent with the Eurasian landmass since at least the Eocene [e.g., *Molnar and Tapponnier*, 1975; *Allégre*, 1984; *Harrison et al.*, 1992]. At large scale, the Himalaya can be divided into four physiographic zones that run parallel along strike the mountain belt and often mark distinct lithotectonic units [e.g., *Gansser*, 1964; *Fuchs*, 1975; *Hodges*, 2000; *Yin*, 2006]. The mostly less than 1500-m-high hills of the Sub-Himalayan molasse are bound by the Main Frontal Thrust to the Indo-Gangetic Plain in the South, and by the Main Boundary Thrust to the sedimentary and low-grade metamorphic rocks of the Lesser Himalaya in the North, which reaches elevations of less than about 3000 m. The Main Central Thrust marks the boundary to the high-grade metamorphic rocks of the steep Higher Himalaya with peaks of more than 6000 m. Sedimentary rocks of the Tethyan Himalaya follow beyond a series of normal faults related to the South Tibetan Detachment System, and commonly form the physiographic transition to the Tibetan Plateau at a distance of around 200 km from the Main Frontal Thrust. Farther north, the Indus-Tsangpo Suture zone defines the northern limit of rocks derived from the Indian subcontinent.

The extensive highlands of the Tibetan Plateau and surrounding orogens, collectively referred to as High Asia [*von Wissmann*, 1959], exert strong influence on atmospheric processes. On a global scale, the elevated land mass of High Asia forms an orographic obstacle that influences atmospheric circulation patterns and plays a vital role in the establishment of the Asian monsoons [e.g., *Hahn and Manabe*, 1975; *Boos and Kuang*, 2010] and north African and central Asian dry regions [e.g., *Broccoli and Manabe*, 1992; *Rodwell and Hoskins*, 1996]. At regional scale, these orographic barriers form borders of distinctive climatic zones that control surface processes and the occurrence and style of glaciation.
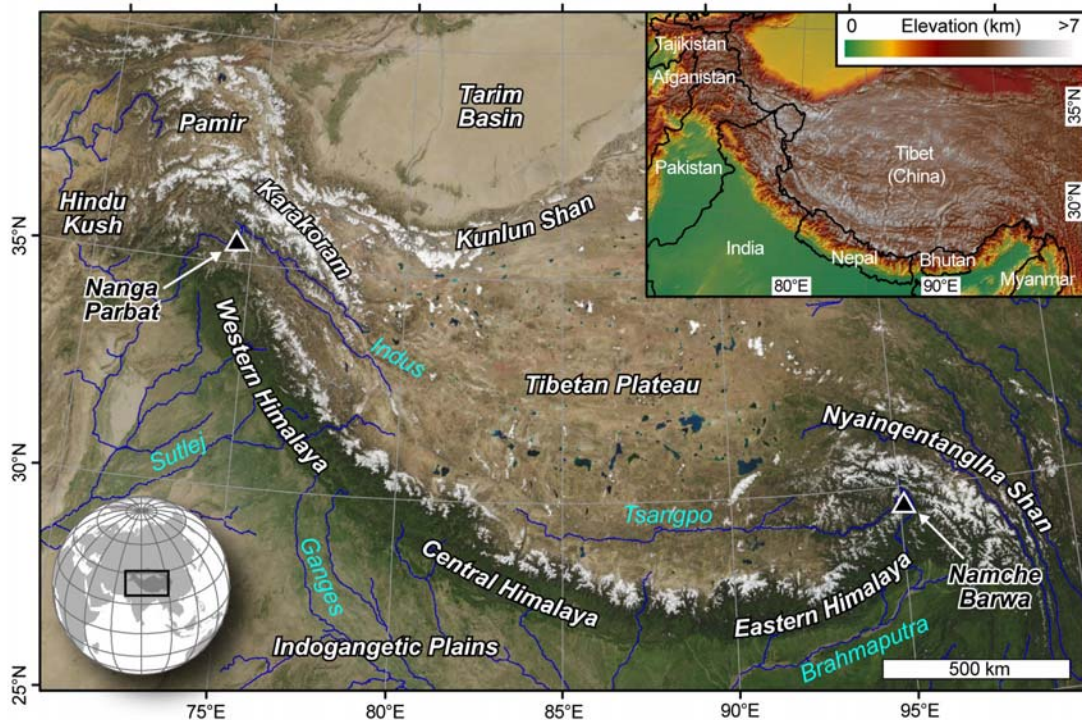
Figure 2.1: Geographic overview of the Himalaya, Tibetan Plateau, and adjoining mountain ranges. Background is a mosaic of MODIS (MODerate resolution Imaging Spectroradiometer) images that were acquired in August between 2000 and 2008 (image provided by NASA's Earth Observatory). Glacially covered areas make up ~33,050 km² in the Himalaya, ~16,600 km² in the Karakoram, ~12,260 km² each in the Kunlun Shan and Pamir, and ~7,500 km² in the Nyainqentanglha Shan [*Dyurgerov and Meier*, 2005]. Inset figure shows surface elevation and political borders.

Present-day climate in High Asia is dominated by two atmospheric circulation systems: the northern-hemisphere westerlies and the Asian monsoons (Figure 2.2) [*Flohn*, 1957; *Barry and Chorley*, 2003]. Both circulation systems follow a pronounced seasonal cycle that leads to a distinct annual peak in precipitation. During summer, when the land surface and the Tibetan Plateau heat up, a strong pressure gradient develops between the relatively warmer Asian land mass and the relatively cooler Indian Ocean [*Flohn*, 1957; *Hahn and Manabe*, 1975]. In effect, the Inter-Tropical Convergence Zone (ITCZ) is shifted far to the north and a persistent northward directed air flow advects moisture from the Indian Ocean towards the continent [*Gadgil*, 2003]. As the trades cross the equator, the Coriolis Effect induces a southwesterly wind that encounters the western coast of India and gives rise to high amounts of precipitation associated with the Indian summer or Southwest monsoon. Moisture that reaches the Himalaya during summer originates in the Bay of Bengal from where it is transported northwestward along the monsoon trough by mesoscale depressions [*Gadgil*, 2003; *Barros et al.*, 2004]. Orographically forced monsoonal precipitation in the Himalaya is highest at elevations <3-4 km [*Seko*, 1987; *Putkonen*, 2004; *Bookhagen and Burbank*, 2006], and only small amounts cross the Himalaya, which effectively insulates warm and moist air masses to the south from drier and colder air to the north [*Boos and Kuang*, 2010]. At small spatial and temporal scales, significant precipitation differences between valleys and ridges, and day and night have been observed [*Yasunari*, 1976; *Yasunari and Inuoe*, 1978; *Bollasina et al.*, 2002; *Barros et al.*, 2000, 2004]. During the summer months, the upper-tropospheric westerlies flow north of the Tibetan Plateau and rarely interact with the Tibetan Plateau. However, this may occur when an upper-level trough that displaces the westerly jet stream far to the south is located over the Pamir and leads to a southerly air flow along its front [*Weiers*, 1994]. Such upper-level air flow enables

monsoonal moisture from deep convection to cross the orographic barrier of the Higher Himalaya and reach areas as far north as the Karakoram [*Flohn*, 1956; *Weiers*, 1994].

Figure 2.2: Climatic conditions in central Asia in July and January. Black lines indicate coasts and topography >3 km elevation. Vectors mark direction and magnitude of mean-monthly surface winds and east-west oriented thick lines with arrowheads mark the position of the upper level westerly jet stream, derived from the mean-monthly 500-hPa geopotential heights and wind fields. Grey shading indicates monthly precipitation. Letters denote the position of persistent surface pressure systems. Dashed thick line shows position of the Inter-tropical convergence zone (ITZC). Wind and pressure based on NCEP Reanalysis data [*Kalnay et al.*, 1996] provided by the NOAA/OAR/ESRL PSD, Boulder, Colorado, USA; downloaded from their Web site at http://www.cdc.noaa.gov/. Precipitation based on CRU 2.0 data [*New et al.*, 2002] provided by the Climatic Research Unit at the University of East Anglia, Norwich, UK; downloaded from their Web site at http://www.cru.uea.ac.uk/.

During winter, the atmospheric pressure gradient between the continent and the Indian Ocean reverses and at the longitude of the HMA, the ITCZ is located near the equator. Descending air masses over the continent cause a pronounced dry season and monsoonal precipitation is restricted to the east coasts of the continent (Figure 2.2). At the same time, however, the westerlies are displaced southward and split up in two branches, located north and south of the Tibetan Plateau. They blow strongest in winter and transport moisture from the Mediterranean, Black, and Caspian Seas to the western edge of the HMA [*Hoskins and Hodges*, 2002]. Precipitation during winter and spring is associated with westward traveling cyclones known as Western Disturbances [e.g., *Lang and Barros*, 2004; *Yadav et al.*, 2009] and therefore decreases in amount from west to east. Despite orographic interception of moisture in the HK and WH, snowfall occurs even in areas that are located in the orogen interior, which is much drier during summer [*Singh and Kumar*, 1997; *Wulf et al.*, in press].

Over geologic timescales, the topographic evolution of Asia, particularly the rise of the Tibetan Plateau during the Cenozoic, are believed to have exerted a fundamental influence on the climatic history of this region and even to have contributed to long-term Cenozoic global cooling [*Raymo et al.*, 1988; *Raymo and Ruddiman*, 1992]. Furthermore, atmospheric-moisture influx and resulting precipitation patterns control the efficacy of fluvial and glacial surface processes and provide feedback mechanisms to tectonic processes by crustal mass removal and redistribution [*Beaumont et al.*, 1992; *Avouac and Burov*, 1996; *Willett*, 1999; *Sobel et al.*, 2003]. Such feedbacks have been postulated for the monsoon-dominated Himalaya, based on numerical modeling [e.g., *Beaumont et al.*, 2001], and thermochronologic studies [e.g., *Thiede et al.*, 2004; *Wobus et al.*, 2003; 2005]. However, these studies have focussed on the effects of fluvial erosion, whereas inferences on the long-term effects of glacial erosion in the Himalaya are controversial and largely speculative [*Brozovic et al.*, 1997; *Burbank et al.*, 2003; *Harper and Humphrey*, 2003]. This is mainly due to difficulties in measuring or estimating glacial

erosion rates [Hallet et al., 1996]. More data is needed to evaluate current glacial erosion laws and develop models of the glacial impact on landscape development and orogenesis in diverse topographic and climatic settings.

3   Glacier-surface velocities in alpine terrain from optical satellite imagery – accuracy improvement and quality assessment

Abstract

The worldwide retreat of mountain glaciers has important consequences for the water, food, and power supply of large and densely populated areas in South and Central Asia. Successful mitigation of the hydrological impacts on societies as well as assessing glacier-related hazards require large-scale monitoring of glacier dynamics. However, detailed glaciological data from the Asian highlands are lacking, due to its size and difficult accessibility. We have applied a novel technique for precise ortho-rectification, co-registration, and sub-pixel correlation of Advanced Spaceborne Thermal Emission and Reflection Radiometer (ASTER) satellite imagery to derive surface velocities of Himalayan glaciers. Our approach allows for the correction of offsets due to attitude effects and sensor distortions, as well as elevation errors if a digital elevation model (DEM) from the Shuttle Radar Topography Mission (SRTM) was used for orthorectification. After post-processing, the error on the displacements is on the order of 2-4 m per correlation. Translated into annual velocities, this error is reduced (increased) when the correlated images are more (less) than a year apart. Through application of a filtering procedure and several quality tests, the consistency of the results is validated to provide confidence in the remotely sensed velocity measurements, despite the lack of ground control. This novel approach allows fast, easy, and economically viable acquisition of detailed glaciological data in areas of difficult access and provides a means for large-scale monitoring of glaciers in high mountainous terrain.

3.1   Introduction

The global warming of climate has continued to cause the retreat of glaciers in many mountainous regions, and even the most optimistic scenarios for future temperature change involve pronounced glacier retreat over many decades to come [e.g., *Oerlemans*, 1994; *IPCC*, 2007a]. This has important consequences for the global hydrological cycle, particularly in climatic threshold areas characterized by water stress. For example, the water, food, and power supply of densely populated regions in South and Central Asia are to a large degree dependent on snow and glacier melt water [*Karim and Veizer*, 2002; *Winiger et al.*, 2005; *IPCC*, 2007b]. Successful mitigation of the climate-related hydrological changes and their impacts on society therefore poses a pressing challenge, which calls for large-scale monitoring of glaciers and a better understanding of their dynamics [e.g., *Haeberli et al.*, 2000, 2007; *Kargel et al.*, 2005]. Due to the large extent and difficult accessibility of high mountainous terrain, especially in Asian orogens, remote sensing techniques provide an efficient way to collect data in disparate regions. For example, satellite images have been used to track changes in glacier geometry [e.g., *Paul et al.*, 2002; *Khalsa et al.*, 2004; *Aizen et al.*, 2007]; analyze and monitor supraglacial lakes [*Wessels et al.*, 2002]; determine the equilibrium line altitude [*Rabatel et al.*, 2005], and estimate annual mass balances of glaciers [*Berthier et al.*, 2007]. Remote sensing tools can also be efficiently used to determine the ice velocity of a glacier, which is a particularly crucial

variable because it determines ice discharge [e.g., *Scambos et al.*, 1992; *Goldstein et al.*, 1993; *Joughin et al.*, 2004, *Rignot and Kanagaratnam*, 2006].

Although glacier-surface velocities can be measured directly on the glacier with high accuracy at arbitrary spatial and temporal resolutions [e.g., *Hubbard and Glasser*, 2005], observations over long periods involve frequent revisits of the survey points, which can only be located on the accessible parts of a glacier. Therefore, field measurements commonly result in very sparse spatial coverage. In contrast, remote sensing-based measurements provide the opportunity to achieve large and possibly complete spatial coverage, even in very remote areas. Currently, three methods are commonly employed to derive glacier-surface velocities: interferometry of synthetic aperture radar (SAR) imagery, SAR tracking techniques, and cross correlation of optical satellite images.

Velocity measurements by interferometry of SAR imagery (InSAR) may achieve high accuracies, but require that coherence between the images is not lost due to modification of the glacier surface by, e.g., melting or snowfall [*Strozzi et al.*, 2002; *Trouvé et al.*, 2007]. This requirement, together with limitations regarding the resolvable displacement gradients, result in InSAR-derived velocity measurements that are typically constrained to time spans of 1, 3 or 6 days [e.g., *Massonet and Feigl*, 1998; *Joughin et al.*, 1996]. Thus, the obtained velocity data may be representative only for the observation period and an extrapolation to annual velocities is difficult.

Offset tracking in SAR imagery [*Michel and Rignot*, 1999; *Joughin*, 2002, *Strozzi et al.*, 2002] is similar to cross correlation of optical satellite imagery [*Lucchita and Ferguson*, 1986; *Bindschadler and Scambos*, 1991]. The basic approach is to track features from one scene to another and to calculate their velocity given the temporal separation and the measured displacement. In the case of SAR images, this can be done using either the intensity or coherence of the complex radar images [*Strozzi et al.*, 2002]. Compared to InSAR, tracking techniques using SAR images are more useful for measuring flow velocities over longer periods. However, a general drawback of SAR imagery in steep mountainous terrain is the high incidence angle of the sensor, which may inhibit visibility of the target glacier, and require very accurate DEMs to correctly orthorectify the measurements [*Trouvé et al.*, 2007].

Using optical satellite imagery, the detail and accuracy of the measurements is largely limited by the ground resolution of the sensor, and by the ability to precisely co-register images acquired at different dates. The latter task is usually the most difficult and has led to inaccuracies on the order of one pixel, i.e., 15m if ASTER imagery were used [*Kääb*, 2005; *Stearns and Hamilton*, 2005]. Further errors may arise from changes in the satellite attitude during scanning of the images [*Van Puymbroeck et al.*, 2000], and from an inaccurate DEM during orthorectification using a rigorous model [e.g., *Toutin*, 2004]. A principle drawback of optical imagery is the dependency on cloud-free conditions.

In summary, velocity measurements by InSAR are most appropriate for analyzing very short time scales, i.e., days, or where extrapolation to longer time scales is justified, e.g., in ice sheet studies [*Joughin et al.*, 2002]. Feature tracking, using SAR or optical imagery is more appropriate for analyses over longer periods. Although limited by cloud cover during image acquisition, cross correlation of optical imagery provides a quick and efficient way of measuring glacier surface velocities. Importantly, a huge and global archive of optical images from glaciers already exists and new images are continuously acquired. In order to achieve the measurement accuracy required to infer, e.g., annual velocity variations, the co-registration

requires high accuracy and errors due to attitude effects or inaccurate DEMs need to be minimized.

Here, we evaluate the potential and the limits of a new application for orthorectification, co-registration and correlation of optical imagery, COSI-Corr [Co-registration of Optically Sensed Images and Correlation; *Leprince et al.*, 2007], to measure glacier-surface velocities in mountainous terrain. We provide guidelines to improve the accuracy of the measurements and to assess their quality without available ground-truth data. This includes correction of offsets in the displacement maps due to attitude effects and due to elevation-errors in the DEM. The methodological principles are applicable to a wide variety of optical satellite imagery and are demonstrated here using ASTER images.

We have studied the glaciers in two Himalayan regions: Khumbu in Nepal and Garhwal in India, where glacier shrinking is observed. First, we demonstrate the methodological principles, including quality assessment, on the relatively slow Khumbu glacier at Mount Everest. Second, we investigate and model displacement errors induced by systematic elevation errors in the SRTM-based DEM, at the Gangotri glacier group in Garhwal. In a further step, the recent velocity history of Gangotri glacier, situated in the headwaters of the Ganges, is analyzed to demonstrate the capabilities and the limits of the method to monitor glacier dynamics.

Table 3.1: List of ASTER scenes.

Region	Granule ID	Date [yyyy-mm-dd]	Sun azimuth [°]	Sun angle [°]	Incedence angle [°]	Orientation [°]	Cloud cover [a] [%]
Khumbu	ASTL1A 0009280513510312080	2000-09-28	155.78	57.51	-2.870	9.26	63
(Case study 1)	ASTL1A 0010140513270106251	2000-10-14	161.76	52.29	0.022	9.26	70
	ASTL1A 0112200502290201111	2001-12-20	160.96	36.18	0.025	9.26	43
	ASTL1A 0210040500380210261	2002-10-04	152.76	54.87	-2.829	9.26	49
	ASTL1A 0211210500340212070	2002-11-21	162.48	40.26	-0.041	9.26	36
	ASTL1A 0301080500160303170	2003-01-08	157.48	36.44	-0.030	9.26	48
	ASTL1A 0310230459290311050	2003-10-23	158.65	48.60	0.019	9.26	25
	ASTL1A 0410090458390410220	2004-10-09	154.41	52.87	0.022	9.26	72
	ASTL1A 0410250458240411040	2004-10-25	158.11	47.51	-2.873	9.26	77
	ASTL1A 0411100458190411210	2004-11-10	160.38	42.70	-1.480	9.26	55
	ASTL1A 0511130458410511190	2005-11-13	161.12	41.93	0.022	9.26	47
	ASTL1A 0511290458400512020*	2005-11-29	161.18	38.58	-0.019	9.26	45
	ASTL1A 0512060504390512090	2005-12-06	162.41	37.35	8.588	9.31	76
	ASTL1A 0512150458320512180	2005-12-15	160.27	36.29	0.016	9.26	43
	ASTL1A 0602010458090602040	2006-02-01	151.87	39.99	-2.876	9.26	40
	ASTL1A 0701190459340701220	2007-01-19	154.56	37.74	-2.867	9.26	67
Garhwal	ASTL1A 0109090542130109210	2001-09-09	149.10	60.91	5.699	9.56	52
(Case study 2)	ASTL1A 0310100529250310220	2003-10-10	156.13	49.64	-5.727	9.56	44
	ASTL1A 0310100529340310220	2003-10-10	155.70	50.21	-5.727	9.51	13
	ASTL1A 0407240529140408100	2004-07-24	116.65	68.37	-8.586	9.56	40
	ASTL1A 0508190534580508220	2005-08-19	133.17	65.31	5.729	9.56	87
	ASTL1A 0510150528360510180	2005-10-15	157.07	47.74	-8.583	9.56	69
	ASTL1A 0609230535100609260	2006-09-23	151.63	55.82	2.878	9.56	52
	ASTL1A 0610090534580610120*	2006-10-09	158.14	50.61	5.729	9.56	62
	ASTL1A 0611100535050611130	2006-11-10	163.20	40.39	2.873	9.56	57

All given data were extracted from the metadata of the images. The orientation measures the angle between the along-track direction and North in a clockwise direction. The images that were used as the master images in the coregistration procedure are marked with a star (*). [a] The listed cloud cover is taken from the images metadata and usually overestimates the true cloud cover.

3.2   Methods & data

Table 3.1 presents the imagery analyzed in this study, along with details on the acquisition parameters. Although we generally avoided scenes with heavy cloud and snow cover, we included a number of less than optimal scenes to test their suitability for velocity measurements.

The different steps of our approach are organized in two work flows and presented in Figure 3.1. The first group of tasks comprises orthorectification, co-registration, and correlation of the satellite imagery, followed by post-processing of the correlation results using COSI-Corr. COSI-Corr is a new software package that has originally been developed for the detection of coseismic displacement [*Leprince et al.*, 2007; 2008; available for download from the Caltech Tectonics Observatory website, http://www.tectonics.caltech.edu]. The software package is an IDL-based module for the remote sensing platform ENVI© by RSI. The application allows processing of aerial as well as satellite imagery from the SPOT, ASTER, and Quickbird sensors. A detailed description of the methodological background and COSI-Corr can be found in *Leprince et al.* [2007], and applications in *Leprince et al.* [2008] and *Avouac et al.* [2006]. The second group of tasks is related to data filtering and assessing the quality of the results. In case of more than one correlation, i.e., more than two ortho-images, further steps may involve the comparison and the combination of the acquired data.
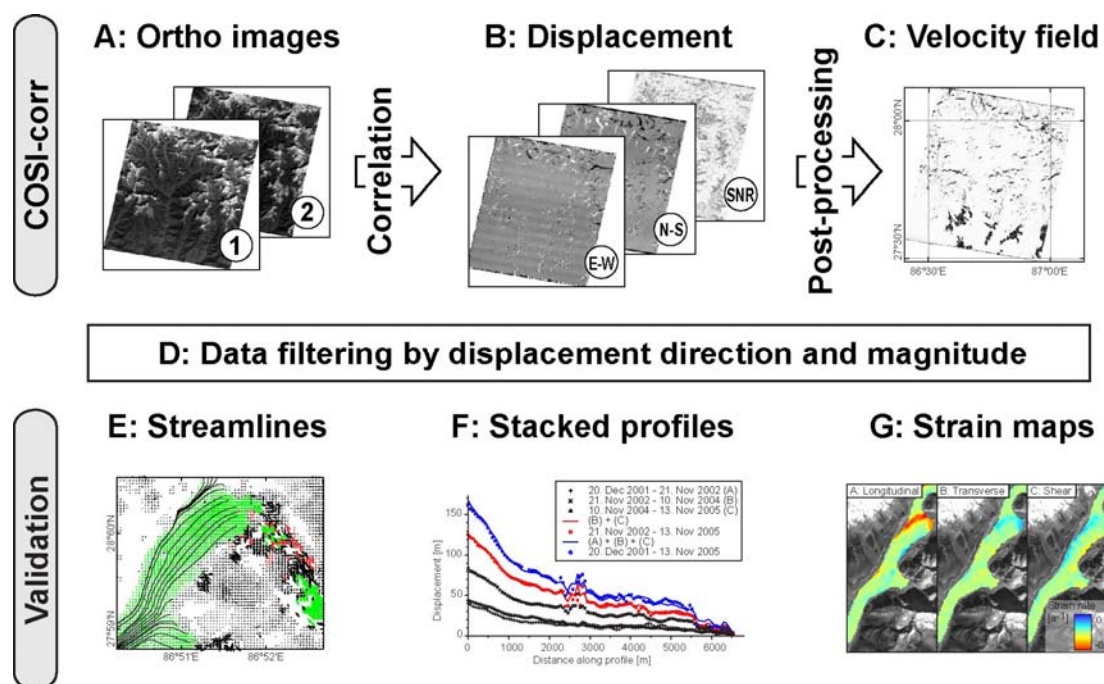
Figure 3.1: Processing chain to derive accurate glacier surface velocities. The first work flow comprises the orthorectification and co-registration of multitemporal satellite images (A), their correlation (B), and post-processing (C) to improve the accuracy of the displacement measurements. These steps were done using ENVI© with COSI-Corr. The correlation results are filtered (D) and then checked for their consistency using streamlines (E), stacked profiles (F), and strain maps (G) in the second work flow.

3.2.1   Orthorectification, co-registration and sub-pixel correlation of satellite images using COSI-Corr

The orthorectification procedure relies on the automatic generation of ground control points (GCPs). A precise set of GCPs is generated from a raw image (slave), with respect to an already orthorectified image (master), by iteratively refining an initial rough selection of manually defined tiepoints. Image patches from the raw slave image are orthorectified and their misregistrations with the master image are estimated from correlation. A precise set of GCPs is produced when the misregistration measured at each patch converges to a minimum. Importantly, generating GCPs is independent of any ground data by using a shaded image of the DEM as the first orthorectified master. The first orthorectified image produced will then become the new master for subsequent slave images. This approach is globally applicable,

wherever DEMs are available. However, the DEM needs to be free of voids, which is a common problem in mountainous terrain. Smaller gaps can be safely interpolated using standard methods while larger patches should be replaced with other data sources, as described in numerous studies [e.g., *Luedeling et al.*, 2007; *Crippen et al.*, 2007]. Alternatively, SRTM tiles from many mountainous regions in the world, where most of the largest voids have been patched with data from topographic maps, are publicly available from Jonathan de Ferranti (http://www.viewfinderpanoramas.org). Such DEMs have been used in this study.

Once a set of precise GCPs has been produced, the mapping matrices that associate ground coordinates with raw pixel coordinates are computed. They define the resampling grid from the raw image to the orthorectified image (Figure 3.1A). Special care is brought to the resampling operation in order to avoid the introduction of aliasing in the orthorectified image.

Horizontal ground displacements are retrieved from the sub-pixel correlation of multitemporal orthorectified images (Figure 3.1B). Image correlation is achieved with an iterative, unbiased processor that estimates the phase plane in the Fourier domain. This process leads to two correlation images, each representing one of the horizontal ground displacement component (East-West and North-South), and to a Signal-to-Noise-Ratio (SNR) for each measurement, assessing the confidence of the results. In a typical process, images are wrapped onto the topography within the DEM resolution, and co-registered in pairs with 1/50-1/20 pixel accuracy, allowing for the measurement of horizontal offsets with an accuracy on the order of 1/20-1/10 of the pixel size.

All data produced for this study have been obtained using ASTER band 3N 15 m resolution images. To allow the measurement of large displacements without losing resolution on the displacement fields, the COSI-Corr multiscale correlation analysis was performed using a window size of 128 down to 32 pixels. Steps of 4 pixels between adjacent correlations yielded ice flow velocity maps sampled at every 60 m.

3.2.2   Post-processing procedures

3.2.2.1   Removal of residual attitude effects

Data on the roll, pitch, and yaw of the satellite during image acquisition come with the imagery's metadata, and are accounted for during orthorectification. However, the ASTER sensor samples the attitude information not frequently enough to allow for full compensation of the resulting image distortions [*Teshima and Iwasaki*, 2008]. As a result, the correlation maps of two ortho-images will show wave artifacts in the across-track direction of the image (cf. Figure 3.4). A gentle long wavelength distortion in the along-track direction is attributed to focal plane distortions, e.g., spherical aberration from the optical system or distortion of the CCD sensor [*Leprince et al.*, 2008]. Such systematic distortions can be removed using post-processing tools within COSI-Corr. The possibility to remove these artifacts depends on the fraction of visible, stable ground, i.e., ground that does not involve any glacier flow, in the two ortho-images. Generally, the higher the amount of stable and visible ground, the better the possibilities of removing attitude effects. However, distortions resulting from attitude effects may be obscured when other distortions are present, e.g., due to inaccurate DEMs.
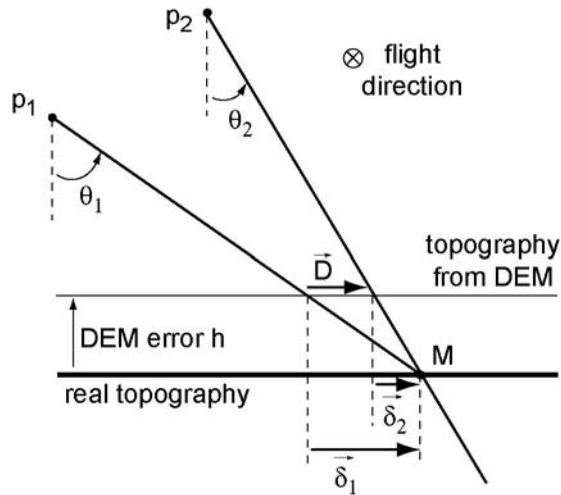
Figure 3.2: Effect of DEM error on displacement measurements. Assume a pixel p_1 from an image I_1 acquired at a date t_1 sees the ground point M, and a pixel p_2 from an image I_2 acquired at a date t_2 sees the same point M on the ground, and that both images are orthorectified and co-registered according to a DEM with an elevation error h. For simplicity, it is assumed that locally, around the ground point M, the topography and the elevation error are well approximated by constants. θ_1 and θ_2 are the angles between the line of sight of the pixels p_1 and p_2, and the vertical. When the orthorectified images I_1 and I_2 are correlated, a disparity $D = \delta_1 - \delta_2$, induced by the elevation error h, is measured.

3.2.2.2   Removal of DEM-related errors

Although COSI-Corr was explicitly designed for correlating satellite images irrespective of their incidence angles, different incidence angles may lead to distortions in the orthorectification in case of an inaccurate DEM. As these distortions cannot yet be corrected a priori, i.e., during orthorectification, they will be transferred to the displacement maps. In our case studies, errors were most prominent in the E-W displacement maps, as the ASTER sensor can only be inclined in the across-track direction and the orbital path of the carrying satellite TERRA is only a few degrees off north over sub-tropical latitudes. If we assume that all pixels in an image have a comparable sight angle that is well approximated by the instrument incidence angle, the measured ground disparity D relates to the incidence angles of the correlated scenes, θ1 and θ2, and to the elevation error of the DEM, h, by

$$D = h * (\tan(\theta 1) - \tan(\theta 2)). \tag{1}$$

The disparity increases with the difference in incidence angles and the elevation error of the DEM (see Figure 3.2). As the SRTM data is the principal source of DEMs in many studies, it is useful to assess any systematic errors that can be modeled to improve the accuracy of the displacement measurements. It has been shown in earlier studies that elevation errors of SRTM-based DEMs contain a component which linearly increases with terrain slope, and another which depends on terrain aspect [*Bourgine and Baghdadi*, 2005; *Gorokhovich and Voustianiouk*, 2006; cf. *Toutin*, 2002a]. The dependency on terrain aspect is presumably related to the orbital path of the Space Shuttle and to the look direction of the antenna [*Bourgine and Baghdadi*, 2005]. Accordingly, elevations of foreslopes, i.e., with a northwesterly aspect, are generally underestimated and elevations of backslopes, i.e., with a southeasterly aspect, are generally overestimated. Because the ortho-images and correlation maps are well co-registered with the DEM used for orthorectification, the ground disparities can be compared with the topography to produce a model for correcting the displacement errors. We found that the residual displacement error, ε, can be estimated with the model

$$\varepsilon = K * s * \cos(a + \varphi) + z \tag{2}$$

where s is the slope of the topography surface, a is the topography aspect, and K, φ, and z are constants to be determined from, e.g., a least squares procedure. In all cases we investigated, φ was around 1.3 rad, i.e., 75 degrees, which implies that the largest offsets occur at aspects of approximately 105 and 285 degrees (see Table 3.2). K can be interpreted as the maximum offset among all aspects, per slope radian. In this study, the absolute value of K, for the E-W displacement, was always around 13 m/rad, i.e., about 23 cm per degree slope angle. The last term, z, is not related to the DEM-error but may be regarded as the mean error due to attitude effects. This term could be set to zero if the correlation results, after correcting for DEM-error effects, allow removal of the attitude effects with the destriping tool (chapter 3.2.2.1). In some cases (see below), this is not possible due to residual noise in the correlation map, which stems from (1) inaccurate slope and aspect values and (2) erroneous sampling of miscorrelations or moving ground for estimating the parameters K and φ. Before fitting equation (2) to the displacement, aspect and slope data, we used a signal-to-noise ratio threshold of 0.99 and a data range between –20 m and +20 m for the E-W and –10 m and +10 m for the N-S displacement to minimize noise and erroneous sampling.

Table 3.2: Details on the error evolution during post-processing of the correlations that were used in the study of the recent velocity history of Gangotri Glacier.

Correlation details					Residual offset [m]						Parameters for the correction model		
Ortho 1	Ortho 2	Time span [a]	Inc. angle diff. [°]		Raw		DEM-error corr.		Attitude-effect corr.		K [m/°]	Phi [°]	z [m]
					Mean	Std	Mean	Std	mean	std			
Aug 05	Sep 06	1.08	2.85	E-W	-1.140	3.756	\	\	-0.255	3.394	\	\	\
				N-S	1.723	4.239	\	\	-0.752	3.720	\	\	\
Aug 05	Okt 06	1.17	0.00	E-W	-0.741	3.921	\	\	-0.070	3.499	\	\	\
				N-S	-0.197	4.336	\	\	-0.038	3.732	\	\	\
Aug 05	Nov 06	1.25	2.86	E-W	-1.021	4.110	\	\	-0.104	3.682	\	\	\
				N-S	-1.065	4.428	\	\	-0.221	3.989	\	\	\
Jul 04	Okt 05	1.25	0.00	E-W	0.200	3.705	\	\	0.039	3.489	\	\	\
				N-S	-0.062	3.978	\	\	-0.016	3.600	\	\	\
Jul 04	Aug 05	1.08	14.32	E-W	0.132	5.251	0.114	4.446	-0.074	4.070	-0.2393	63.5869	-1.068
				N-S	1.465	4.157	0.109	3.487	0.191	3.179	0.048	68.4856	0.079
Okt 03	Jul 04	0.75	2.86	E-W	-1.406	4.189	\	\	0.116	3.366	\	\	\
				N-S	1.337	3.558	\	\	0.308	3.276	\	\	\
Okt 03	Aug 05	1.84	11.46	E-W	1.593	5.182	0.174	5.033	0.230	4.842	-0.2142	78.2087	-4.585
				N-S	0.175	4.573	0.145	4.536	0.385	4.251	0.04339	86.7859	-0.040
Okt 05	Okt 06	1.00	14.31	E-W	0.086	5.252	-0.007	4.546	-0.036	4.371	-0.2438	71.3332	-1.020
				N-S	0.123	3.576	0.049	3.484	\	\	0.04672	86.4857	0.002
Okt 05	Sep 06	0.92	11.46	E-W	-0.173	5.315	0.066	4.972	0.045	4.614	-0.2381	70.7483	0.240
				N-S	-0.742	3.796	-0.091	3.768	-0.021	3.591	0.04901	78.6315	0.955
Okt 05	Nov 06	1.08	11.46	E-W	0.090	5.367	0.009	4.844	-0.008	4.428	-0.2322	73.2567	-0.321
				N-S	0.208	3.733	0.113	3.485	0.226	3.423	0.05598	59.6355	-0.164
Okt 03	Okt 06	3.00	11.46	E-W	1.410	5.092	0.135	4.449	\	\	-0.2237	72.838	-3.540
				N-S	0.070	3.668	0.107	3.275	\	\	0.03684	76.6675	-0.040
Sep 01	Okt 03	2.08	11.43	E-W	-1.560	5.066	-0.060	3.612	0.003	3.487	0.2532	69.1628	3.971
				N-S	-0.030	4.115	-0.033	2.851	-0.007	2.811	-0.0446	76.6162	-0.100
Sep 01	Aug 05	3.95	0.03	E-W	1.052	4.023	\	\	0.299	3.268	\	\	\
				N-S	0.111	4.232	\	\	-0.218	3.269	\	\	\

When the differences in incidence angles were low, corrections of DEM-induced errors were not necessary. Residual offsets were determined from all displacement data in a range between -10 m and +10 m. Thus, slow moving glacier ice has also unwillingly been sampled, and the residual offset estimates should be regarded as upper bounds.

As an alternative to using SRTM-based DEMs, one could use the ASTER images from the 3N and 3B bands to construct the DEM used for orthorectification. However, it should be noted that the above mentioned attitude effects, as well as steep slopes, shadows, clouds, and snow fields will cause problems in the DEM generation. Consequently, ASTER-derived DEMs from steep,

mountainous terrain are usually associated with many gaps and large errors [e.g., *Toutin*, 2002b; *Kääb*, 2002; *Eckert et al.*, 2005; *Fujisada et al.*, 2005], and thus we preferred to use the SRTM-based DEM.

3.2.3   Data Filtering

Once all systematic errors have been removed, the measurements were filtered to exclude miscorrelations and to identify reasonable correlations obscured between miscorrelated patches (Figure 3.1D). Excluding measurements with a low signal-to-noise ratio is a starting point to quickly filter the displacement maps. However, this does not exclude all miscorrelated points, and we have found that in addition, a simple directional filter is very efficient in getting rid of most remaining miscorrelations [e.g., *Kääb*, 2005]. This was done by defining the flow direction from flow features on the glacier surface in the ortho-images and allowing for some deviation, e.g., of up to 20°. An additional filter is applied to the magnitude of the displacement to acknowledge that velocities do not change abruptly, but rather gradually. Both filter procedures need to be applied with variable parameters (e.g., directions, sizes, and thresholds) on different patches of the glacier and thus require some manual tuning. Overlaying the displacement field in form of vector arrows on one of the ortho-images helped to identify whether the results were consistent with the flow features on the glacier surfaces. We designed an interface in MATLAB© that allows for a quick definition of thresholds and patch sizes to apply the filters.

3.2.4   Quality assessment and validation techniques

The lack of ground-truth velocity measurements hampers simple evaluation of remotely sensed measurements in most cases. Yet, in order to assess the quality of the measurements, we designed a number of tests to check the consistency of the results with regard to the displacement direction, magnitude, and gradient. These include (1) a test of the displacement direction by using the displacement field to construct streamlines, i.e., displacement paths, which can be checked against flow features on the glacier surface in the ortho-images (Figure 3.1E); (2) a test of the displacement magnitude by comparing the sum of incremental measurements (e.g., the sum of displacements measured from images between 2001-2002, 2002-2003 and 2003-2004) with a displacement measurement over the complete observation period (i.e., 2001-2004) (Figure 3.1F); (3) a check of the displacement gradients by overlying the ortho-images with strain-rate maps calculated from the displacement data (Error! Reference source not found.G), using the method by *Nye* [1959] as shown in studies by *Bindschadler et al.* [1996]. For the calculation of strain rates, only filtered displacement values have been used and small gaps in the displacement maps have been linearly interpolated. Furthermore, in order to suppress small-scale dynamics and noise in the strain rates, the displacement maps have been smoothed with a 5x5 pixel convolution filter [*Bindschadler et al.*, 1996]. An error estimation of the strain-rate calculations was performed by bootstrapping (n = 1000) the calculations using the E-W and N-S displacements with added uncertainties. The uncertainties have been randomly drawn from a normal distribution described by the residual error over stable ground. The resulting strain-rate maps describe the longitudinal, transverse, and shear strain rates over the glacier surface. The reference frame is the local flow direction. With this suite of tests, we determined whether the correlation procedure was stable and we produced consistent results that are supported by flow features on the glacier surface.

3.3   Study area

Currently, approximately 116,000 km² of mountainous terrain are glacierized in South and Central Asia [*Dyurgerov and Meier*, 2005], making this region the largest glacierized continental area outside the polar regions. Despite the great number of glaciers in the Himalaya and Karakoram and their important role for water supply to the region, glaciological data are surprisingly limited [e.g., *Wagnon et al.*, 2007]. The available measurements of glacier areas and mass-balance calculations have shown that glaciers in the Asian highlands are generally retreating [*Mayewski and Jeschke*, 1979; *Dyurgerov and Meier*, 2005], in some cases at high rates, like the Parbati glacier in India, retreating at almost 52 m/yr [*Kulkarni et al.*, 2005]. Conversely, some glacier advances have been observed in the eastern Himalaya and the Karakoram, which have been linked to increased precipitation [*Liu et al.*, 2006] and/or decreased summer temperatures [*Hewitt*, 2005; *Fowler and Archer*, 2006].
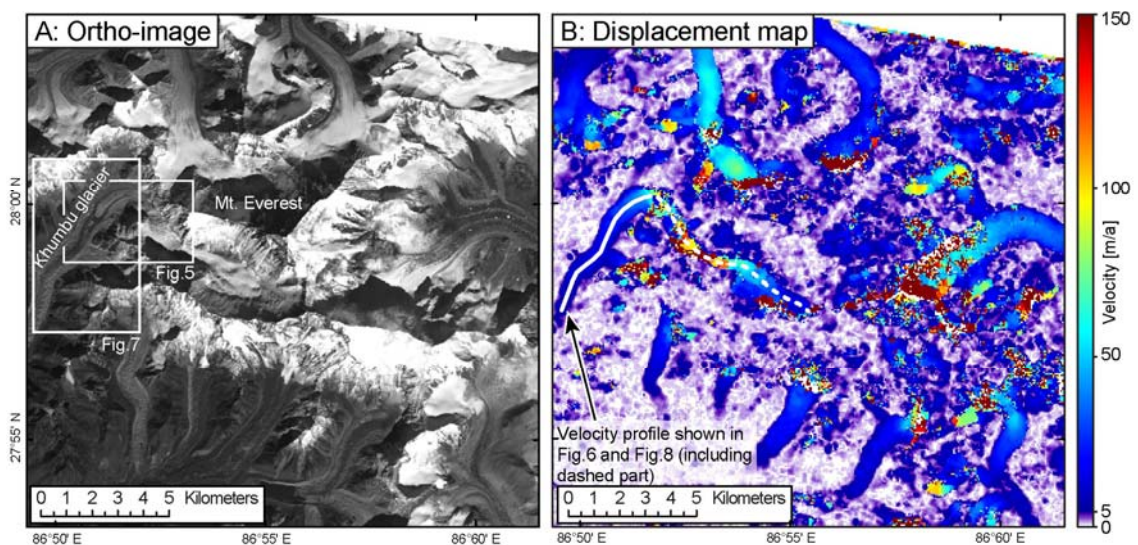
Figure 3.3: Example of orthorectified image and displacement map derived from image correlation from the Mount Everest region, Nepal. (A) Ortho-image acquired on Nov. 10th 2004. (B) Displacement map produced by correlating the ortho-image in A with another ortho-image acquired on Nov. 29th 2005. The displacement values were normalized to annual velocities. The subsets in A are shown in Figure 3.5 and Figure 3.7 and glacier-surface velocity along the profile in B is displayed in Figure 3.6 (short profile) and Figure 3.8 (long profile).

Because of the low latitudinal position between 27 and 37° N, Himalayan glaciers usually occur at elevations of more than 4 km, although some descend to elevations of less than 3 km. Such advances to relatively low altitudes are commonly thought to be driven by a high amount of supraglacial debris cover that shields the ice from ablation, lowering the accumulation-area ratios compared to that of debris-free glaciers [*Benn et al.*, 2003]. The debris cover is an important feature for deriving surface velocities from optical satellite imagery as it creates and preserves pronounced surface morphology over relatively long timescales [*Luckman et al.*, 2007]. However, the correlation procedure tends to fail when illumination conditions are grossly different between scenes. During summer, frequent cloud cover due to the Indian Southwest Monsoon limits the choice of suitable satellite scenes.

In our study we have chosen the Mount Everest region, Khumbu, in the Nepalese Himalaya, and the Gangotri glacier group, Garhwal, in the Indian Himalaya. We selected these sites because they hold abundant glaciers of different sizes that are important water resources [e.g., *Singh et al.*, 2006] and some of them, due to recent down-wasting, are prone to catastrophic outburst flooding [e.g., *Cenderelli and Wohl*, 2001; *Kattelmann*, 2003], making them prime

targets for monitoring strategies. The high elevation sectors in both regions are characterized by a moderately wet monsoonal climate, with more influence of the Winter Westerlies in Garhwal.

3.4   Results

3.4.1   Case study 1: Khumbu Himal, Nepal

Figure 3.3 shows an ASTER ortho-image from the Mount Everest region, acquired in November 2004, and a displacement map produced by correlation with another ortho-image from November 2005. The acquisition setting of both ASTER scenes with identical near-vertical incidence angles, similar shading, absence of clouds, and only limited snow cover, provide ideal conditions for orthorectification and correlation (Table 3.1).
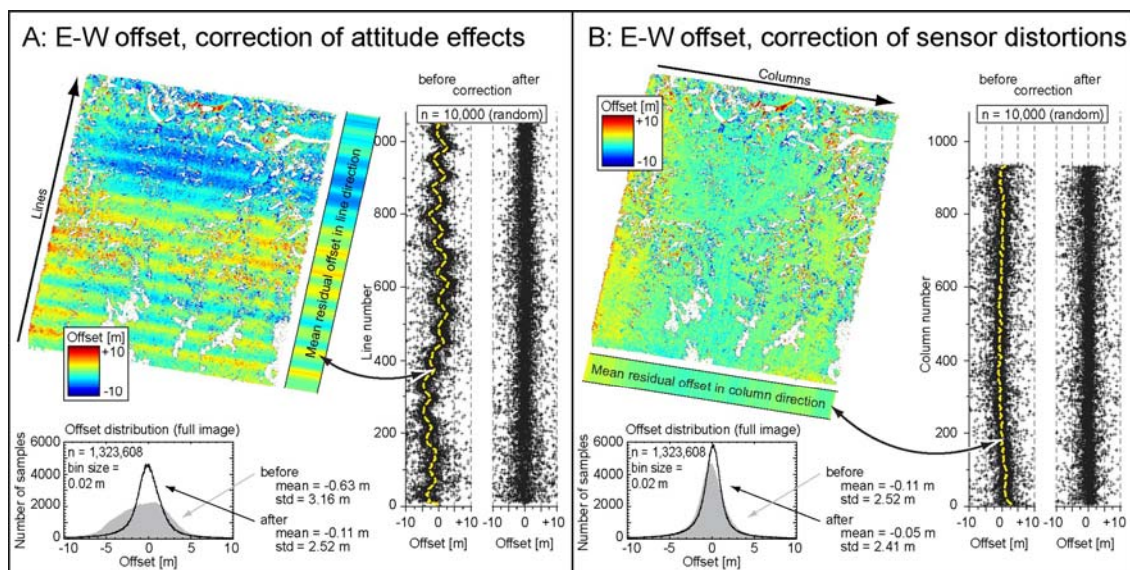
Figure 3.4: Correction of attitude effects and sensor distortions. The corrections are calculated from the mean residual E-W offset in the column- (A) and in the line-direction (B) of the correlation shown in Figure 3.3B. The scatter plots depict the individual offsets of a randomly sampled set of 10,000 pixels, and the histograms show the entire population arranged in 0.02 m offset bins.

3.4.1.1   Accuracy improvement

Well-identifiable stripes in the E-W displacement map are due to attitude variations and are a first sign of low noise and successful orthorectification (Figure 3.4). The stripes have been removed with the COSI-Corr destriping-tool. This has improved the accuracy of the measurements as is shown in Figure 3.4. Before the correction, the residual displacement in the E-W direction, as measured from all data points lying within –10 m to +10 m, had a mean value of –0.63 m and a standard deviation (1σ) of 3.16 m. After removing the distortions in the line direction of the image, the residual displacement decreased to a mean value of -0.11 +/- 2.52 m. Further removal of the more gentle distortion in the column direction improved the accuracy only somewhat to a mean of –0.05 +/- 2.41 m. Most likely, optimal results from the destriping procedure would be achieved if the destriping model was defined using stable ground only. However, this would have been a laborious task, and we found that simply thresholding the displacement map to a range that encompasses the undulations due to attitude effects, e.g., -10 m to +10 m, works well enough to remove any systematic undulations. Indeed, most of the glaciers have moved by more than 10m during our study period, and thus most of the ice-flow related measurements are discarded from simple thresholding.
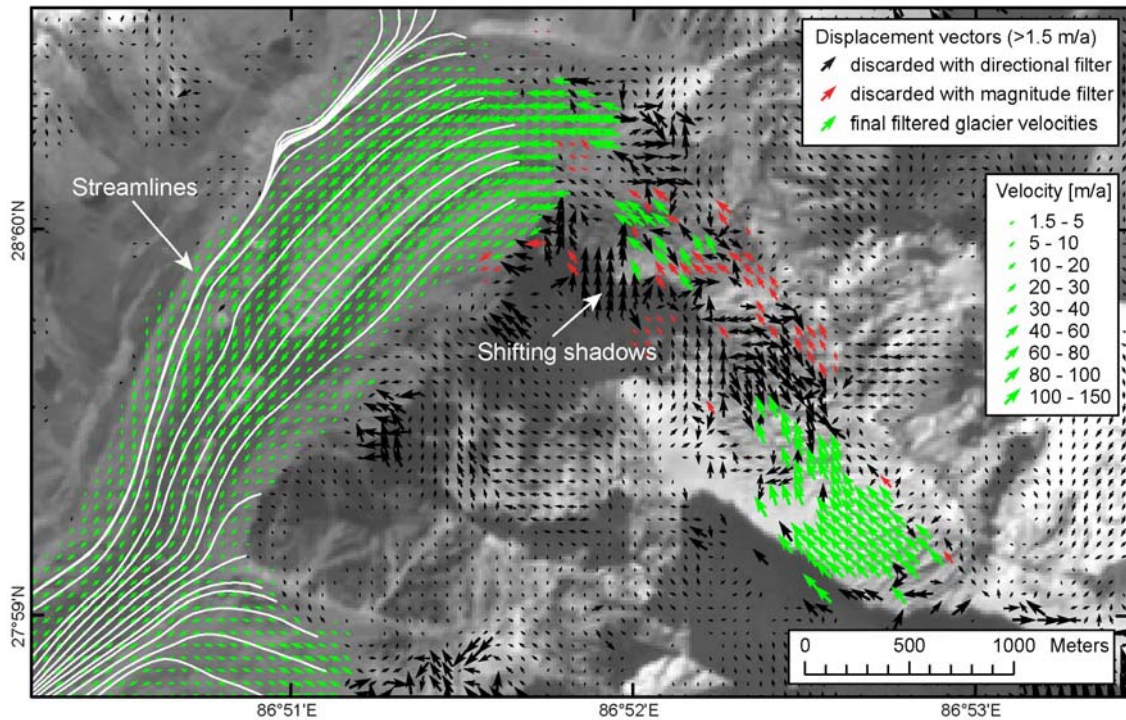
Figure 3.5: Velocity field of the central part of Khumbu glacier. Annual velocities derived from the correlation shown in Figure 3.3B. The ortho-image in the background is from Nov. 10th 2005. The arrows depict displacements of more than 1.5 m/a. Through filtering the data by direction, most miscorrelations are discarded. Further filtering by magnitude removed measurements pointing in the right direction, but that showed anomalously high or low velocities (green arrows). Red arrows mark the filtered velocity vectors that are consistent with flow features on the glacier surface. Streamlines are shown in white and were constructed using the retrieved velocity vectors.

3.4.1.2   Filtering

After removal of obvious systematic distortions in the displacement images, the displacement measurements over the glacier area have been filtered to eliminate miscorrelations. This approach is used on Khumbu glacier (N27.9806, E86.8766), which is an intermediate-size glacier (16.5 km length) located southwest of Mount Everest. Based on an analysis by *Luckman et al.* [2007], the glacier appears to be stagnant over its lowermost 2 km.

As was already apparent in the displacement map in Figure 3.3B, the correlation procedure failed in certain parts and returned erroneous displacements (see Figure 3.5). This is particularly the case in the steep portions of the glacier where the velocity gradient, and thus deformation of the glacier surface, is large. Another problem that may not be apparent at first sight is artificial displacement due to moving shadows [e.g., *Berthier et al.*, 2005]. If the sun angles are different in the scenes to be correlated, the correlation procedure will possibly detect the shifting shadows and record an artificial displacement. In order to exclude such miscorrelations, we have filtered the data over the area of the glacier as described in chapter 3.2.3. The result of the filter procedure in the central part of Khumbu glacier is shown in Figure 3.5. Most of the obvious erroneous vectors have been discarded using the directional filter (black arrows). The magnitude filter discarded another group of displacement vectors that were pointing in the correct direction, but showed anomalously high or low displacement values (green arrows). In this case, we applied the filters on patches of up to 1 km², depending on changes in flow direction and magnitude, and allowed for +/- 20° deviation from the defined flow direction. The magnitude filter was applied more variably according to nearby, well identifiable velocities, usually within a range of +/- 30 m/a. Clearly, unless filtering is performed very carefully with tight thresholds and on small patches, erroneous results may survive and correct results may be discarded, e.g.,

some displacement vectors at the edges of Khumbu glacier in Figure 3.5. However, the proportion of these cases among the entire population of retrieved data is usually very small, even if the filtered patches are relatively large.
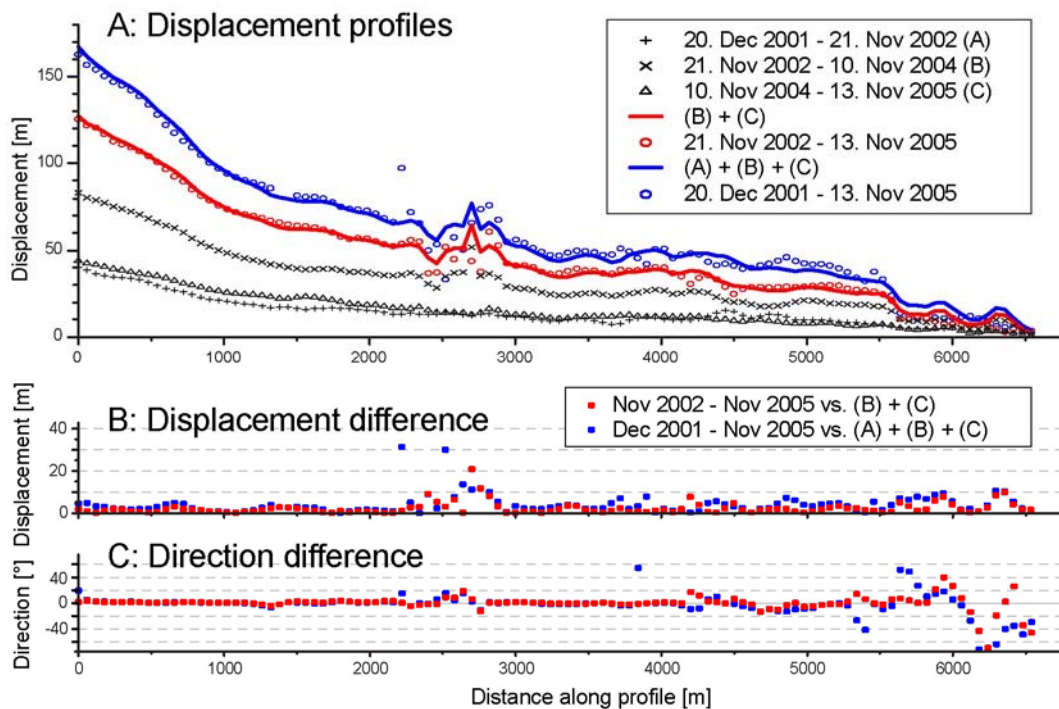
Figure 3.6: Stacked displacement profiles from the lower part of Khumbu Glacier. See Figure 3.3B for footprint. The data points depict the displacement over the time span given in the figure's legend. The red line (blue line) is the sum of the 2 (3) displacements denoted by '+' and 'x' (and 'Δ'). The red (blue) circles depict the displacement measured over the same periods as covered by the red (blue) lines. The overall good correspondences provide us with confidence in the reliability of the individual measurements.

3.4.1.3   Quality assessment

The first consistency test using streamlines is applied on the lower part of Khumbu glacier, which has good and continuous data coverage (Figure 3.5). The streamlines agree quite well with the flow features on the glacier surface. In the lower part of Khumbu glacier the streamlines are narrow, due to the confluence with a tributary glacier. A minor mismatch of the streamlines coming from the tributary glacier and the banding on the glacier surface (hardly visible in the figure) does not appear to be an artifact, as it is observable in all other correlations we performed. Instead, the mismatch appears to reflect a relative increase in ice discharge from this tributary compared to the upper Khumbu glacier.

For the second consistency test we used four ortho-images from the years 2001, 2002, 2004, and 2005 (see Table 3.1). An example from the lower part of Khumbu glacier is given in Figure 3.6. For this profile the raw, unfiltered data have been used to show the good agreement over most parts of the profile. The displacements derived between 2002 and 2004, and all time spans encompassing this period, show some suspicious velocity variations in the center of the profile. From visual inspection it was found that these variations are due to the enlargement of a supraglacial pond, where the retreat of the bounding margins caused an apparent reduction in velocity at the up-glacier side and an apparent increase in velocity at the down-glacier side of the pond. The stacked profiles show that the magnitudes of the displacement measurements agree very well in the upper part of the profile but contain larger scatter in the lower part, where surface degradation due to melting is higher. Furthermore, at lower displacement values, the

distorting influence of the noise increases, especially regarding the displacement direction. These poor quality data points have been excluded using the filter procedure. It should be noted that the measured displacements are always straight and may thus lead to an underestimation of the true displacements if their paths were curved. However, as the magnitudes of the displacement vectors are generally small compared to the local curvatures of the flow, the displacement paths are well approximated linearly. Problems may occur when measuring flow in strong bends over longer time spans.
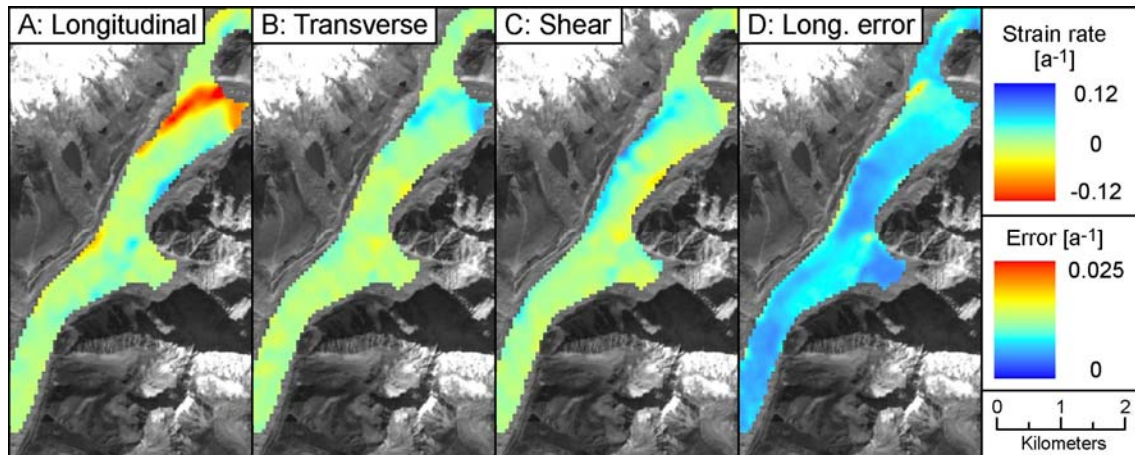
Figure 3.7: Longitudinal, transverse, and shear strain rate maps and error on the longitudinal strain rates over Khumbu Glacier. Maps derived from the filtered velocity vectors shown in Figure 3.5. The distribution and magnitude of transverse and shear strain rate errors look similar to the longitudinal strain rate errors and are not shown. See text for details on the calculation of the strain rates and strain rate errors.

For the third consistency test, we calculated strain rates from the displacement field and examined its compatibility with regard to the glacier surface, e.g., the occurrence of crevasses. However, the correlation failed in the central part of Khumbu glacier where crevasses are formed. Nevertheless, an examination of the pattern of strain rates still allows identification of unexpected displacement gradients. Figure 3.7 shows the components of the calculated surface strain rates over Khumbu glacier and the error in longitudinal strain rates. While most of the glacier is characterized by moderately low strain rates, some areas stand out with much higher strain rates. First, in the highest parts on Khumbu glacier where the velocity data were retrieved, the glacier slows down considerably, which causes high values of negative strain rates, i.e., shortening rates. This happens just below a steep part along the glacier profile, where numerous crevasses have formed, and presumably closed again. Second, approximately 500 m west, along-flow shortening reaches a peak at the confluence with a tributary glacier coming from the north. When looking at the velocity vectors and streamlines in Figure 3.5 and at the transverse strain rates in Figure 3.7, it is apparent that ice near the edge of Khumbu glacier has divergent flow towards the tributary glacier. Consequently, the tributary ice, which flows with velocities of less than 3 m/a near the confluence, is being pushed aside and not incorporated into the main ice stream of Khumbu glacier. Therefore, the contribution of ice from the tributary glacier appears to be reduced, which causes Khumbu glacier to expand laterally. Newly formed crevasses with a NW-SE orientation can be seen in high-resolution satellite images (e.g., in Google Earth©), supporting this conclusion.

In the upper part of the covered area of Khumbu glacier, shear-strain rates at the glacier margins are high and of opposite sign, as would be expected. In the lower part, where surface velocities as well as velocity gradients across the width of the glacier are low, shear-strain rates are lower too. The error on the longitudinal strain rates (Figure 3.7D) is highest in the regions of

low velocities, as the flow direction is strongly affected by the noise, which consequently results in considerable scatter of the velocity gradients. The errors on the transverse and shear-strain rates are similar to that of the longitudinal-strain rates, and are therefore not shown.
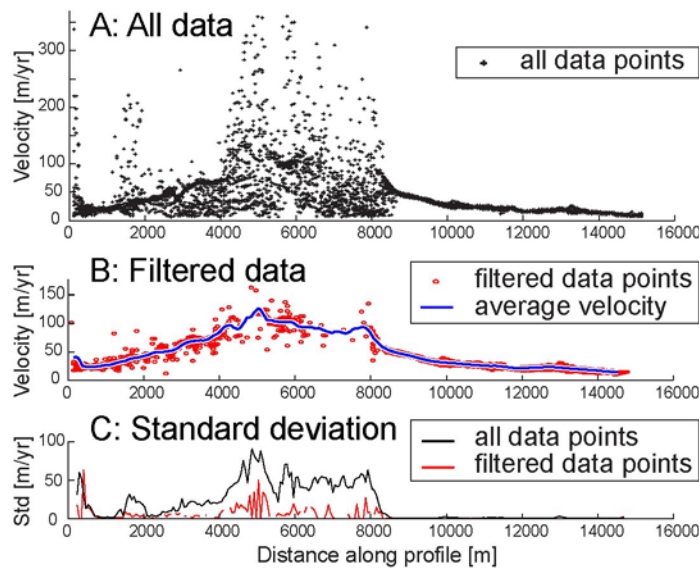
Figure 3.8: Continuous velocity profile of Khumbu Glacier derived from 22 correlations. The unfiltered data points (A) show considerable scatter in the central and upper part. The filtered data points (B) display less scatter as is shown in the plot of the standard deviation (C) of the data points from all the correlations. Note that not all correlations provide measurements over the entire glacier.

3.4.1.4   Data combination: continuous velocity profile from Khumbu Glacier

Because most correlation maps contain some areas where the procedure failed or returned erroneous data, it may be useful to combine the results from several correlations to enhance the spatial coverage across a glacier. A comparison of the filtered velocity measurements (not shown) has yielded very similar results throughout the observation period, from 2001 to 2007. In order to arrive at a continuous velocity profile of Khumbu glacier, we extracted the displacement data of all correlations we performed along a profile that extends from the highest point in the accumulation zone, down to the toe of the glacier (Figure 3.3B). We applied our filtering procedure, with the same parameters, simultaneously to all displacement maps to only extract the meaningful data from our profile (Figure 3.8). A large data set of 22 displacement maps enabled us in this case to produce a relatively well-constrained velocity profile, even though the results of the correlations are not equally good over the whole glacier. The lower part is especially consistent and the standard deviation among data points from different displacement maps is well below 5 m/a. In the central part, where the glacier flows over steep topography and attains high velocities and strain rates, strong surface modifications between the images complicated the correlation procedure and resulted in miscorrelations.

It should be emphasized that the combination of velocity measurements from different time periods is only possible when the glacier shows no signs of velocity change over the period of observation. This condition has to be examined, e.g., using velocity profiles, before compiling the data.

3.4.2   Case study 2: Garhwal Himalaya, India

The Gangotri glacier group is situated in western Garhwal, India, and forms part of the headwaters of the Ganges. The Gangotri glacier is, with more than 30 km length, one of the largest glaciers in the Indian Himalaya. We obtained 9 ASTER scenes, covering a period from

September 2001 to November 2006, that are characterized by differences in incidence angle of up to 14 degrees (see Table 3.1), which caused additional errors (chapter 3.2.2.2).
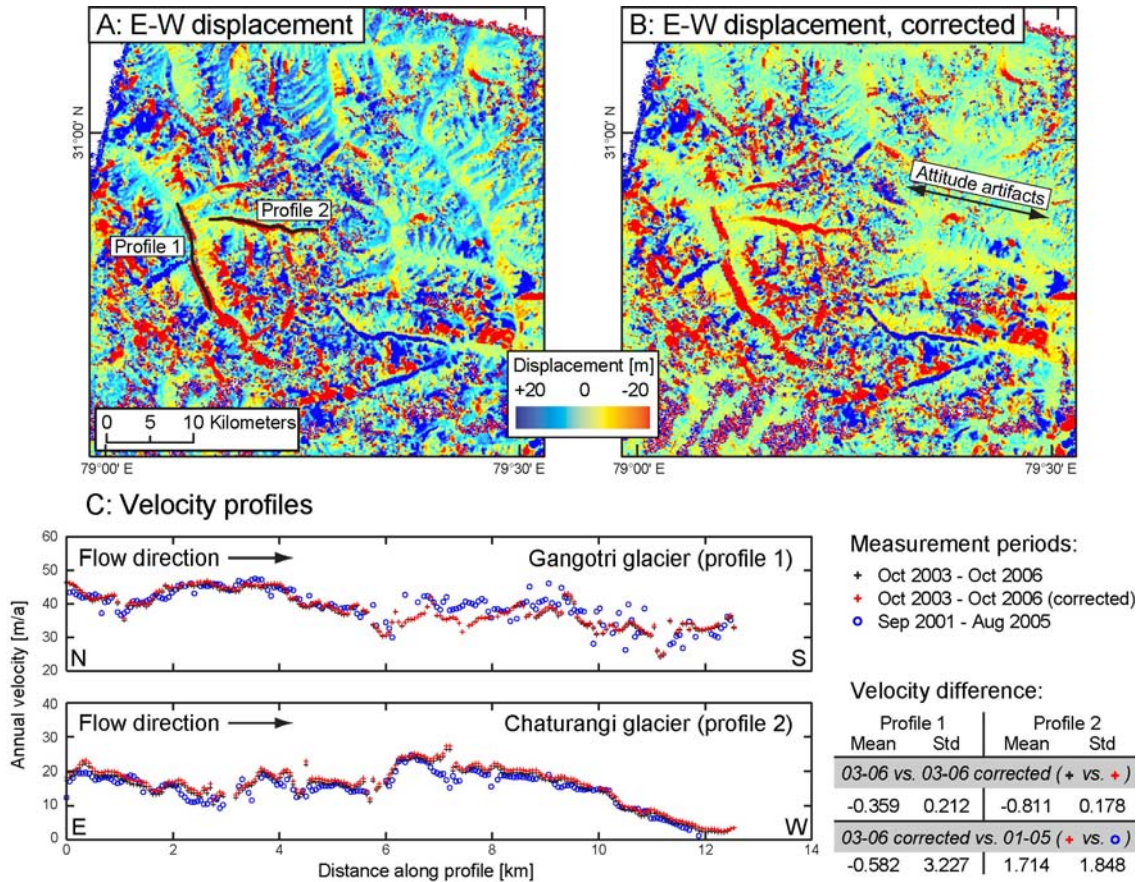
Figure 3.9: Correction of DEM-induced distortions. Images show E-W displacement in the Gangotri glacier group derived from correlation of ortho-images acquired on Oct 10th, 2003, and Oct 9th, 2006. Color-coding applies to pixels with displacement values in between +20 m and –20 m. Pixels with values outside this range are assigned the last color of the respective side of the color bar. The aspect dependence of the SRTM-based DEM-error produces an artificial hill shade effect in (A). After correction of DEM-induced offsets, distortions due to attitude artifacts become visible (B). Velocity profiles of the Gangotri and Chaturangi glaciers are shown in (C). For comparison, the uncorrected and corrected velocity measurements from the period 2003-2006 are plotted together with velocity measurements from the period 2001-2005, where topography-related artifacts are absent as the incidence angles during acquisition of the images were similar (see Table 3.2).

3.4.2.1   Correcting for DEM-related distortions

Figure 3.9 depicts the E-W displacement over Gangotri glacier and adjacent areas, derived from a correlation of ortho-images from October 2003 and October 2006 (see Table 3.1). The difference in incidence angles between the ortho-images is 11.5 degrees. In Figure 3.9A it is seen how displacement errors over stable ground produce an artificial shading effect, which highlights the dependence of the elevation error on terrain aspect. The variation of the mean E-W and N-S offsets with terrain aspect and slope angle is given in Figure 3.10. We modeled the offsets using equation (2), with $K = -12.817$ m/rad, $\varphi = 1.271$ rad, and $z = -3.54$ m for the E-W component, and $K = -2.111$ m/rad, $\varphi = 1.338$ rad, and $z = -0.04$ m for the N-S component, determined from least squares adjustment. The applied correction improved the measurement accuracy to the degree that distortions due to the attitude effect became visible (Figure 3.9). However, in this case we were not able to further correct the attitude effects more precisely as described in chapter 3.2.2.1, due to a high level of noise and a small fraction of stable, correlated ground that could be used for defining the destriping model. Thus, the negative z

value in the E-W component represents the mean attitude effect which is biased towards higher values in the upper part of the image, where more stable, correlated ground exists. The correction improved the mean residual errors determined from all displacement values between -10 m and +10 m, from 1.41 +/- 5.1 (errors are 1σ) m to 0.13 +/- 4.4 m for the E-W component, and from 0.07 +/- 3.6 m to 0.11 +/- 3.2 m for the N-S component. Better results were obtained in cases where additional destriping was possible (Table 3.2). Nevertheless, given that distortions from DEM-errors increase linearly with slope angle, the impact on the derived glacier velocities is only small as glaciers mostly occur on low-gradient terrain. This is shown in Figure 3.9C, which depicts the surface velocities of the Gangotri and the adjacent Chaturangi glaciers along profiles from different correlations. A measurement from September 2001 to August 2005, with no difference in incidence angle, is used as a reference. Although natural velocity variations may occur, these should be rather small due to the length of the observation period. The velocity difference between the uncorrected and corrected correlation (October 2003 – October 2006) is small and almost not visible. Furthermore, the velocity measurements from the corrected correlation and the correlation from September 2001 to August 2005, yield very similar values.
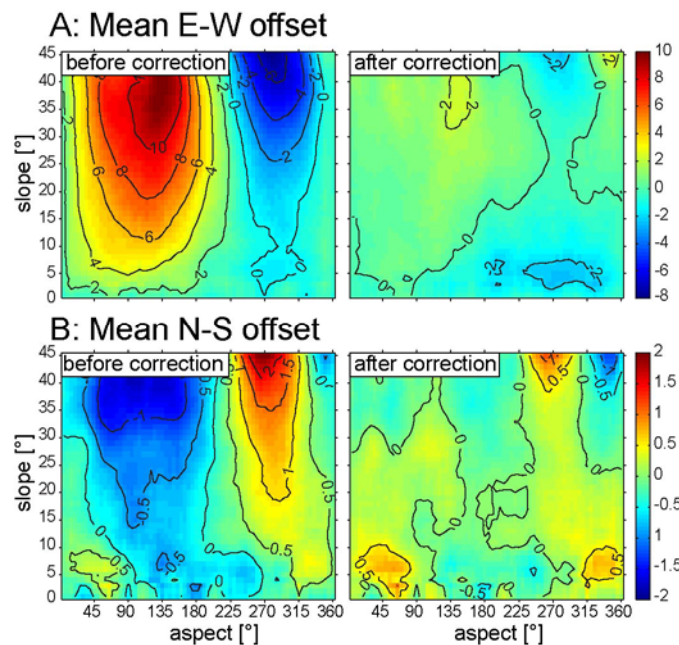
Figure 3.10: Slope and aspect dependency of DEM-induced distortions. Mean E-W (A) and N-S offset (B) from the correlation of the Oct 2003 and Oct 2006 ortho-images from the Gangotri glacier group (see Table 3.1). The mean offsets were determined from the E-W and N-S displacement values ranging between –20 m and +20 m, and –10 m and +10 m, respectively. Slope angles were sampled in 1-degree intervals and aspect in 5-degree intervals. The resulting distribution was smoothed with a 5x5-convolution filter. At slope angles of more than 45 degrees (not shown), fewer data points lead to more scatter.

The results from the error-modeling and removal of other correlations used in this study are given in Table 3.2. At incidence angle differences of more than 10 degrees, DEM-induced errors were visible, modeled and removed. In most cases it was possible to correct the displacement maps for attitude effects after removal of the DEM-induced errors. The residual errors of the corrected displacement are similar to the residual errors of correlations with low incidence angle differences. Thus, the error removal was successful.

3.4.2.2   Data comparison: recent velocity history of the lower part of Gangotri Glacier

Velocity measurements from the correlations presented in Table 3.2 were used to investigate the recent velocity history of Gangotri glacier. For this purpose, we picked a profile along the central flow line of the glacier and plotted the annual velocity, with the associated errors given as shaded areas around some of the measurements, in Figure 3.11.

Over most of the profile, the annual velocity from October 2003 to July 2004 was faster than during the period from July 2004 to October 2005 (Figure 3.11A). The difference is greater than the combined error on the measurements, and is therefore significant. The annual velocity from October 2003 to August 2005 rests in between the analyzed periods as would be expected. Whether or not this velocity difference is a true decrease in ice discharge over time or an effect of the sampled period, e.g., a seasonal effect, is not clear from this analysis.

In order to elucidate the role of the seasonal coverage of the observation periods, we investigated annual velocities over different periods within one hydrological year, although only available from 2005 to 2006. Figure 3.11B depicts a less obvious, but still visible difference in annual velocity when comparing a time period starting in August 2005 with one starting in October 2005. Velocities from October 2005 to October 2006 appear faster than velocities from August 2005 to October 2006. Very similar velocity profiles from two more correlations ending in late September 2006 lend additional credibility to the results. Importantly, the occurrence of the velocity difference spatially coincides with the larger velocity difference observed in the earlier time periods in Figure 3.11A.

The main difference of the seasonal coverage between the observation periods with slower and faster surface velocities is the extension of the slow velocity observations into the third quarter of the year, i.e., over late July to early October in the first case (Figure 3.11A) and over late August to early October in the second case (Figure 3.11B). Hence, the flow velocity during this time appears to have been relatively slower compared to the average velocity during the rest of the year. The larger velocity difference in the first case (Figure 3.11A) can be explained if periods of slower velocities extended from July to October in both years, 2004, and 2005. Therefore, we conclude that the measured difference in annual velocities from 2003 to 2005 may be due to the same reason as for the observed difference in velocity during the period from 2005 to 2006.

Several studies on alpine glaciers as well as outlet glaciers of ice sheets have shown that glacier flow velocities can vary significantly over daily to annual time scales [*Bindschadler et al.*, 1977; *Gudmundsson et al.*, 2000; *Anderson et al.*, 2004; *Bartholomaus et al.*, 2008]. Such variations have commonly been attributed to melt water induced changes in subglacial hydrology that lead to variations in the speed of basal sliding. Importantly, many mountain glaciers show the highest flow velocities during spring to early summer, and before maximum ablation and proglacial stream discharge occurs [*Willis*, 1995; *Fountain and Walder*, 1998; *Harper et al.*, 2007].

Such phenomena may explain the observed variations in flow velocity of the Gangotri glacier as well. During early summer, velocities may be higher as temperatures are high and melting occurs. However, as melting decreases from August to October, flow velocities may be slower than the annual average. Such inferences are supported by meteorological and hydrological studies near the terminus of Gangotri glacier [*Singh et al.*, 2006, 2007]. Therefore, we speculate that subsequent to peak melting and discharge in July/August, flow velocities decrease to slower

than average levels. Hence, the observed decrease in average annual velocity from 2003 to 2005 may be the result of the observation period and may not reflect an overall decrease in flow velocity and ice discharge.
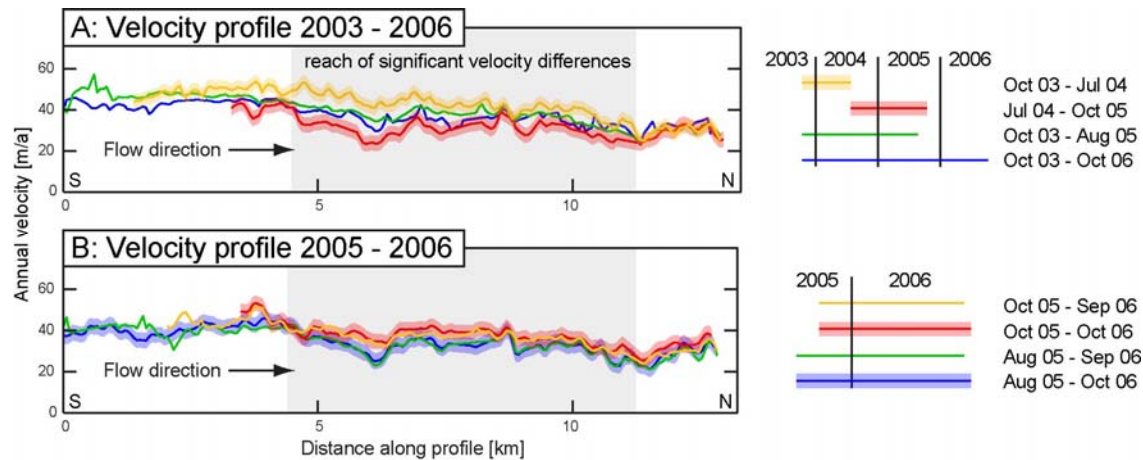
Figure 3.11: Recent velocity history of the lower part of Gangotri Glacier. Data derived from the correlation of ortho-images from the years 2003 to 2006. The shaded rims around selected profiles give the one-sigma error range, calculated from the residual offsets (see Table 3.2). (A) shows the annual velocity during the period 2003 to 2006. Significant differences exist between the period 2003-2004 and 2004-2005 over the reach marked by a gray background. (B) shows the annual velocity from different observation periods from 2005 to 2006. Although of lower magnitude, a similar velocity difference is visible over the same reach as in A. The footprint of the profile is shown as Profile 1 in Figure 3.9A.

3.5   Discussion

3.5.1   Measurement errors

All data in this study are reported as horizontal glacier-surface velocities or displacements. The data have not been converted to surface-parallel velocities. This can be easily achieved with the DEM used for orthorectification, as the topographic and kinematic data are well co-registered. However, such conversion does not account for the emergence velocity, which is the vertical velocity due to accumulation and ablation [e.g., *Reeh et al.*, 2003].

We estimated the residual errors on the measurements by analyzing the distribution of offsets with absolute values of less than 10 m. This means that "slow" moving ice is erroneously sampled, hence skewing the distribution to higher offsets. Applying an additional threshold of 0.99 to the signal to noise-ratio map usually limits the data to low-relief areas. This results in much lower residual offset values on the order of zero mean and a standard deviation of 1 m. However, as we cannot assume that the residual errors on measurements of moving glaciers can be characterized by stable ground with high SNR values, we applied the rather conservative error estimation without using a high SNR threshold. Hence, the errors presented in this study should be regarded as upper bounds.

As in many regions worldwide, the most accurate DEM available to date for high mountainous terrain is based on SRTM data, and thus problems associated with systematic topographic errors may occur frequently. Our method presents a means to model and correct for the resulting displacement errors. Yet, at slope angles greater than ~45 degrees, the model does not fit the offset data as good as at lower slope angles, due to large scatter and insufficient data points. Fortunately, glaciers occupy mostly low-gradient terrain, where such topography-related errors are small, providing good possibilities for correction. Furthermore, an advantage of ASTER imagery over most other sensors is that the incidence angle of the 3N band (VNIR), which should be used for velocity measurements, is always close to nadir, hence assuring small

distortions due to topographic errors. Note that the presented error description and modeling is related to our use of an SRTM-based DEM specifically, as we observe the bias of the DEM, scaled by a function of the incidence-angle difference (eq. 1). The error modeling may be applied to all correlation results of ortho-images produced with SRTM-based DEMs, but the fitting parameters are specific to each correlation.

3.5.2   Comparison with SAR-derived velocity measurements

When comparing our velocity measurements of Khumbu glacier with those obtained by *Luckman et al.* [2007] using InSAR and feature tracking, important differences emerge. First, the SAR-derived data show significant scatter over most of the profile, which is not seen in our data. Second, the measurements obtained from feature tracking and interferometry over two time periods each, differ considerably between the techniques and also between two periods using one technique. Problems with InSAR in the lower parts of the analyzed glaciers are acknowledged by these authors and more confidence is put on the data obtained from feature tracking. *Luckman et al.* [2007] also analyzed Kangshung glacier on the eastern slopes of Mt. Everest. In this area, they obtained results that are much more consistent with our data. However, the errors given by these authors are quite high, sometimes exceeding the velocity and on average reach 50% of it. These errors are thus too high to reliably detect velocity changes and assign them to natural causes and not to measurement problems. Despite these difficulties it should be noted that tracking techniques using SAR imagery may complement the use of optical imagery in areas where the glacier surface lacks visible features, e.g. in extensive accumulation troughs.

3.5.3   Other optical sensors

Apart from ASTER, imagery from other satellites, as well as aerial photos, can also be used with COSI-Corr to measure ground displacement [e.g., *Leprince et al.*, 2007]. Satellite Pour l'Observation de la Terre (SPOT) imagery in particular has proven useful in deriving glacier-surface velocities [*Berthier et al.*, 2005; *Leprince et al.*, 2008]. Compared to ASTER, SPOT images have a more accurate attitude description (attitude variations are sampled at a higher rate), and do not usually require the correction of attitude effects in the displacement maps. However, as the incidence angles in SPOT images can be high, DEM-errors in steep terrain may cause larger distortions. It is also useful to know that the broader spectral bandwidth of the panchromatic sensor of SPOT (500-730 nm) has often led to high gains of many earlier SPOT images, when high mountainous terrain was not among the main target areas of satellite-data acquisitions. This resulted in saturated images that are useless for velocity measurements over snow covered areas. More recent SPOT5 imagery is now adapted and provides images with lower gains over snow-covered mountains.

  It is not possible to process satellite images from the Landsat Thematic Mapper (TM) or Enhanced Thematic Mapper+ (ETM+) with sub-pixel accuracy. This is due to the unknown attitude variations of the satellite and the imaging system. Whereas SPOT and ASTER are pushbroom sensors, i.e., they scan across-track lines of 60 km instantaneously, TM and ETM+ sensors sample the ground along 16 across-track lines of 185 km (this is a whiskbroom system). Hence, attitude variations do not only occur in the along-track direction, but also in the across-track direction, which makes their removal virtually impossible.

3.5.4   Implications for glacier monitoring

The suitability, global coverage, and low cost of ASTER scenes make this imagery a viable option among other alternatives to conduct large-scale and long-term monitoring campaigns of remote glacial systems [e.g., *Kargel et al.* 2005]. In comparison with other sensors, the use of ASTER imagery, along with COSI-Corr, provides reliable results, as inherent problems with attitude effects and inaccurate DEMs can be solved. To successfully derive accurate glacier surface velocities in mountainous terrain, a number of important points should be kept in mind.

First, cloud cover should be low. However, when the master image has been successfully orthorectified, all other slave images require only three tie points to be accurately co-registered. Thus, even cloudy images with 3 patches (approx. 3 km x 3 km in size) of stable ground can be accurately co-registered. Importantly, thin, partly transparent clouds do not pose a problem. Therefore, even though cloud cover restricts the use of optical imagery to derive glacier-surface velocities, in many cases, images with even 50% of cloud cover or more can be used as long as the glacier of interest is visible.

Second, images with grossly different snow-cover characteristics, such as winter and summer scenes, are difficult to correlate. The problem is not the snow cover itself, but the difference. That is why images from the same season usually work well, whether with or without snow cover. As the degree of snow cover is usually not identical between two images, parts on the glacier where the correlation procedure obtained poor results or failed are commonly encountered. Such data gaps may be filled with another correlation if images are present and the velocity did not change, as in the case of Khumbu glacier in the first case study.

Third, surface modifications, like snow cover change, complicate the correlation procedure. This applies directly to the resolvable time span and measurable velocities. When velocities are high, shorter time spans between the ortho-images lead to better results. For example, a surging glacier, which may flow at rates of several hundred meters per year, requires a narrow temporal separation of the images (in such a case, the use of InSAR may be more appropriate). When velocities are low, a longer temporal separation of the images is preferred, if surface degradation by melting or down-wasting does not interfere. Time spans exceeding one year also reduce the residual error when normalizing the results to annual velocities. For instance, we succeeded in measuring annual velocities of approx. 10 m/a on glaciers with little surface degradation in Garhwal.

Finally, we emphasize the need to properly understand the flow characteristics of the investigated glaciers before inferring any long-term trends. Our study of the velocity history of Gangotri glacier has shown that slight differences in the seasonal coverage of the observation periods may result in considerable velocity differences. Therefore, velocity analyses over different seasons should always be undertaken, if possible.

3.6   Conclusions

In this study we have used the new application COSI-Corr to orthorectify, co-register, and correlate ASTER satellite imagery and derive surface velocities from glaciers in the Himalayas. We have shown how to minimize residual offsets of the displacement measurements due to attitude effects, and we have presented a way to detect, model, and correct for additional offsets induced by elevation errors of the SRTM-based DEM. Additionally, we developed techniques to check the quality and consistency of the results despite lack of ground control. The achieved measurement accuracies allowed us to detect seasonal velocity variations of 10 – 20 m/a in the lower part of the Gangotri glacier, in India. The results of individual correlations may be

combined to enhance the spatial coverage across a glacier, which is particularly useful for synoptic studies aiming at continuous velocity profiles or maps from glaciers over large areas.

We find that COSI-Corr is a powerful remote-sensing tool to perform detailed, as well as synoptic comparisons of glacier dynamics in remote, high mountainous terrains. Furthermore, the accurate co-registration of the ortho-images, the displacement maps, and the DEM used for orthorectification, provide the possibility to investigate links between surface features on the glacier, glacier dynamics, and topography. This may prove useful for future modeling studies that require tuning to recent conditions.

Finally, our analysis of glacier dynamics using combined ASTER imagery and COSI-Corr has shown that this methodology is well suited to derive accurate, low-cost glacier-surface velocity measurements from remote regions where ground instrumentation is costly and difficult to implement. This is important in light of global warming and the need for water-management plans to take account of shrinking glaciers and the associated hazards.

4   High Asian glaciers: Impact of topography and climatic gradients on debris cover and flow velocities

Abstract

A large fraction of Earth's valley glaciers outside the Polar Regions is located in High Asia, fringing the southern and western margin of the Tibetan Plateau. The present-day climate in these regions is dominated by the westerlies during the winter and the Indian monsoon during the summer season, with distinct spatial precipitation patterns coupled to topographic gradients. Here, we provide the first comprehensive regional synthesis of the topography and flow characteristics of 287 glaciers across High Asia using digital elevation analysis and remotely-sensed glacier-surface velocities. High Asian glacial landscapes have large variations in topographic relief which controls the size and steepness of snow accumulation areas and thus the relative amounts of direct snow fall and avalanching. In regions of steep and rugged topography avalanche-fed glaciers have large areas of supraglacial debris cover and flow velocities are highest along short segments near their head but greatly reduced along their debris-mantled lower parts. In contrast, glaciers situated in low-relief areas are mainly nourished by direct snow fall, have little or no debris cover and a more symmetrical distribution of flow velocities. The along- and across-strike variations in snowline elevations, climate, and topography result in accumulation areas with strikingly different relief characteristics. In monsoonal areas, snowlines are generally high and accumulation areas are largely confined to steep, high-reaching massifs within the Himalaya. Regions influenced by the westerlies have lower snowlines and larger accumulation areas of lower relief within internal parts of the orogen. This cumulates to some of the largest valley glaciers in the Karakoram with exceptionally high flow velocities.

4.1   Introduction

Currently, approximately 115,000 km² in High Asia are covered with glaciers [*Dyurgerov and Meier*, 2005]. A large fraction of these areas are found along the edges of the Tibetan Plateau, and are characterized by steep gradients in topography and climate. Due to the remoteness, routinely ground-based monitoring is unfeasible and consequently, not much is known about the majority of glaciers [*Dyurgerov and Meier*, 2005; *WGMS*, 2008]. Important data on glacial properties and mass balances have been collected by a number of glaciological studies on individual glaciers in the Himalaya and on the Tibetan Plateau [e.g., *Ageta and Higuchi*, 1984; *Ageta et al.*, 1989; *Fujita et al.*, 1998]. However, most of these glaciers are relatively small and devoid of debris cover, with the notable exception of Khumbu Glacier in eastern Nepal [*Inoue*, 1977; *Nakawo et al.*, 1999; *Kajastha et al.*, 2000], although it is known that many Himalayan glaciers are extensively covered by debris [e.g., *Schlagintweit*, 1871; *Hedin*, 1900; *Odell*, 1925]. It is commonly assumed that valley glaciers in steep topography receive most of their supraglacial debris through mass movements from steep hillslopes [*Boulton and Eyles*, 1979; *Benn and Evans*, 1998]. The importance of debris cover for melting and glacial mass-balances has long been recognized [*Ogilvie*, 1904; *Flint*, 1942; *von Wissmann*, 1959; *Clayton*, 1964; *Mattmon et al.*, 1993; *Kayastha et al.*, 2000], but its consequences for glacial flow velocities are far less studied [e.g., *Russell*, 1895; *Kirkbride*, 1995].
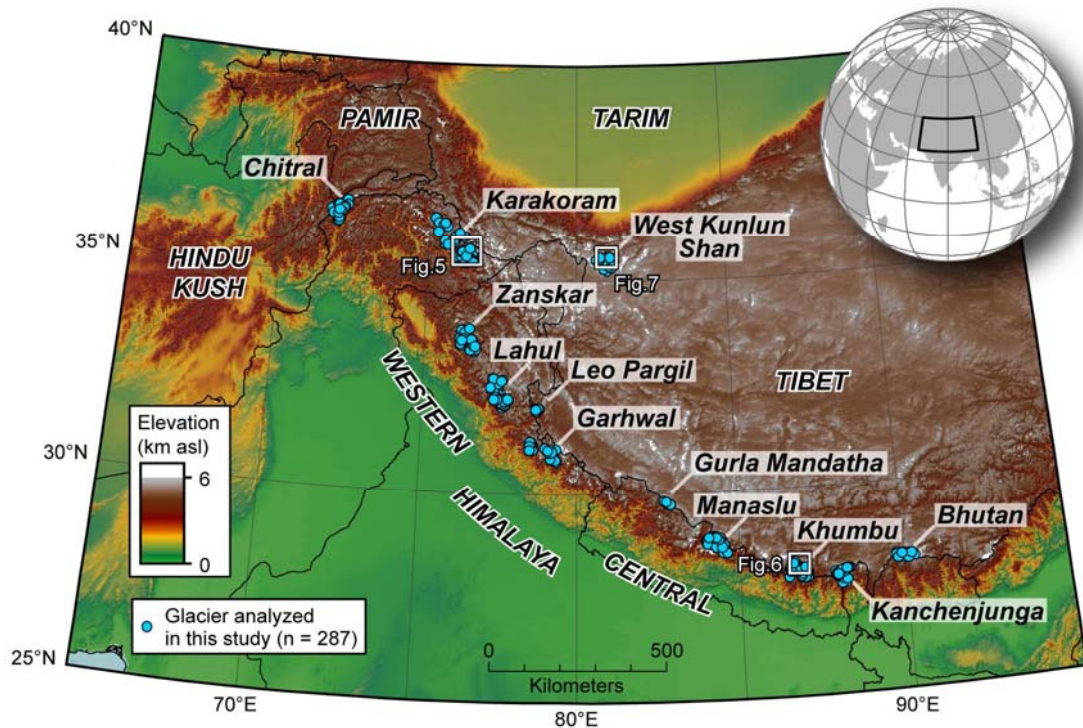
Figure 4.1: Geographic setting of the study areas in High Asia. Blue circles indicate the location of analyzed glaciers, black lines mark international borders. Elevation source is SRTM data.

Rapid advances in space-based Earth observation and sensors with increasingly better image resolution provide new opportunities in studying glaciers in remote areas [e.g., *Bindschadler*, 1998; *Kargel et al.*, 2005; *Kääb et al.*, 2005]. In particular, correlation of mulitemporal satellite imagery allows measuring glacier-surface velocities across large areas and at relatively low cost [e.g., *Scambos et al.*, 1992; *Kääb*, 2005; *Berthier et al.*, 2005]. *Scherler et al.* [2008] tested a new method of image orthorectification, co-registration and correlation [*Leprince et al.*, 2007, 2008] on High Asian glaciers and achieved measurement accuracies on the order of 2-3 m/yr using Advanced Spaceborne Thermal Emission and Reflection Radiometer (ASTER) imagery. Such accuracies allow constructing spatially meaningful and dense velocity fields on short timescales [*Leprince et al.*, 2008].

In this study, we use remotely-sensed glacier-surface velocities in combination with digital elevation analysis to investigate how climate and topography influence the flow behavior of 287 High Asian glaciers (Figure 4.1). In particular, we explore what conditions promote the formation of debris cover and how it affects glacier-surface velocities. Furthermore, we conduct a large-scale regional survey of glacial topographic characteristics, debris-covered areas, amount of snow-avalanching contribution, and flow velocities to decipher regional trends and their relation to climatic gradients. We have divided our approach into two steps: First, we analyze the topographic setting and debris-covered area of the studied glaciers and how these are related to the amount of snow accumulation by avalanches. We hypothesize that debris cover increases with topographic relief as more snow avalanches with entrained debris from steep hillslopes are accumulated on the glacier. Second, we analyze glacier-surface velocities, obtained from remote-sensing imagery between 2000 and 2008, to assess mean annual glacier flow characteristics. Our study shows that the downstream distribution of flow velocities reflects a complex interplay between topography, moisture supply, debris cover, and snow avalanching.
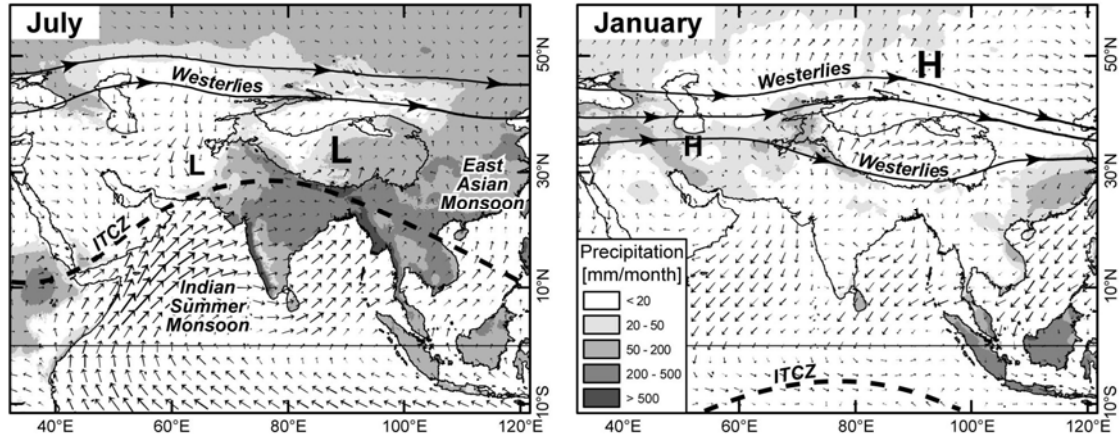
Figure 4.2: Climatic conditions in central Asia in July and January. Black lines indicate coasts and topography >3 km elevation. Vectors mark direction and magnitude of mean-monthly surface winds and east-west oriented thick lines with arrowheads mark the position of the upper level westerly jet stream, derived from the mean-monthly 500-hPa geopotential heights and wind fields. Grey shading indicates monthly precipitation. Letters denote the position of persistent surface pressure systems. Dashed thick line shows position of the Inter-tropical convergence zone (ITCZ). Wind and pressure based on NCEP Reanalysis data [*Kalnay et al.*, 1996] provided by the NOAA/OAR/ESRL PSD, Boulder, Colorado, USA (http://www.cdc.noaa.gov/). Precipitation based on CRU 2.0 data [*New et al.*, 2002] provided by the Climatic Research Unit at the University of East Anglia, Norwich, UK (http://www.cru.uea.ac.uk/).

4.2   Study area and regional climatic context

High Asia encompasses an extensive region of high elevations influenced by different atmospheric circulation systems (Figure 4.2). The center of this region is the Tibetan Plateau with mean elevations of ~5 km asl [*Fielding et al.*, 1994]. The Tibetan Plateau forms an important orographic obstacle for the mid-latitude westerlies and the South and East Asian monsoons [*Hahn and Manabe*, 1975; *Broccoli and Manabe*, 1992; *Boos and Kuang*, 2010]. In this study, we focus on regions along the southern, western and northwestern margins of the Tibetan Plateau (Figure 4.1). Glaciers in the central Himalaya are dominated by a monsoonal climate, with a distinct rainy season during summer (June to September) and a dry season in winter [*Gadgil*, 2003] (Figure 4.2). These glaciers have been termed summer-accumulation type glaciers, according to the main accumulation season [*Ageta and Higuchi*, 1984]. Although monsoon precipitation can reach very high amounts over the Himalaya [*Bookhagen and Burbank*, 2006; in press], most moisture is orographically forced out at elevations <4 km asl, and the high glacierized sectors of the orogen are more arid [*Harper and Humphrey*, 2003]. From east to west, monsoon influence decreases and moisture supply by the mid-latitude westerlies becomes more important (Figure 4.2). Notably, at 78° longitude near the Sutlej Valley lies the moisture boundary, where eastern regions receive most precipitation during summer and western regions receive most precipitation during winter [*Bookhagen and Burbank*, in press]. Westerlies precipitation sourced in the Mediterranean, Black and Caspian seas, is highest in winter and early spring when low-pressure systems known as Western Disturbances encounter the western margin of High Asia [*Barry and Chorley*, 2003]. Glaciers in the western Himalaya are influenced by monsoonal and westerlies moisture regimes. At the northern rim of the Tibetan Plateau, the West Kunlun Shan is the most continental setting that we studied. In this region, limited precipitation is mainly derived from the East Asian monsoon during summer resulting in glaciers confined to high elevations [*Ohata et al.*, 1989]. In all of these areas little is known on mass-balance profiles and potential temporal changes in accumulation rates [*Weiers*, 1994; *Bhutiyani*, 1999; *Winiger et al.*, 2005; *Hewitt*, 2005].

4.3   Topography and debris cover

4.3.1   Methods

4.3.1.1   Glacier and debris cover mapping and topographic analysis

We digitized glacier outlines by using Advanced Spaceborne Thermal Emission and Reflection Radiometer (ASTER) band 3N images with 15-m ground resolution in the visible and near infrared (VNIR) spectral range taken between the years 2000 and 2008 (Table A1). Additionally, we processed a number of Système Pour l'Observation de la Terre (SPOT) 4 and 5 panchromatic images with ground resolutions of 10 and 5 m, respectively. We orthorectified these images using the orthorectification and correlation tool COSI-Corr [*Leprince et al.*, 2007, 2008], and a 90-m resolution Shuttle Radar Topographic Mission (SRTM)-based digital elevation model (DEM) [*Farr et al.*, 2007].

Mapping of debris-free ice and snow was automatically done using orthorectified LANDSAT TM and ETM+ imagery. We selected late summer scenes with high snowlines and low snow cover (Table A1), and identified snow or ice covered areas from band TM4/TM5 ratios [e.g., *Paul et al.*, 2004]. With the aid of the digitized glacier outlines we can distinguish between debris cover and clean ice.

We investigated the topography of the analyzed glaciers and corresponding catchments with the SRTM-based DEM. Contributing areas above the glacier surfaces were calculated using the DEM and the D8 flow-routing algorithm [*O'Callaghan and Mark*, 1984] to identify upstream cells. We manually checked all results for consistency. Local topographic relief was taken as the elevation range measured in circular moving windows of a 5-km radius.

4.3.1.2   Snowlines, equilibrium-line altitudes (ELA) and accumulation-area ratios (AAR)

We obtained estimates of the position of the snowline as a proxy for the transient equilibrium line altitude (ELA) of the analyzed glaciers, using orthorectified satellite images (ASTER, SPOT, and Landsat) that were acquired near the end of the hydrological year, when snow cover is lowest. We manually determined the surface elevation at the boundary between relatively fresh, bright snow and darker ice. The temporal coverage of the observation period with suitable scenes varies from region to region and only allows an approximate estimate of the transient ELA. Consequently, we associated an estimated uncertainty to our ELA estimates, which is based on the observed temporal and spatial variability in snowlines for each glacier. This approach is to some degree subjective and the relative discrepancies can vary, but it is clearly the only available data. On average ~20 images are available per region and most of them are from near the end of the hydrological year. Thus, the reported ELAs provide reasonable first-order estimates for the investigated time period [cf. *Meier and Post*, 1962]. We used the ELA estimates and propagated associated uncertainties to calculate accumulation-area ratios (AAR). These ELAs are transient and are likely different from the zero-net mass balance steady-state ELAs and their corresponding AARs. Furthermore, earlier studies have suggested that glaciers dominantly nourished by avalanches commonly have ELAs that are significantly lower than the climatic snowline would suggest [*Benn and Lehmkuhl*, 2000].

4.3.1.3   Identifying avalanche accumulation

From visual interpretation of the satellite images, we identified glaciers inferred to be fed by avalanches and classified them into three categories: low, intermediate, and high amount of

accumulation by avalanches. This classification included criteria such as presence of snow-avalanche cones and steep accumulation areas on hillslopes above the glacier surfaces (Figure 4.3). We acknowledge that an objective, continuous measure for the degree of avalanche accumulation would increase the detection of variability, but as no suitable data is available, we content ourselves with this classification.
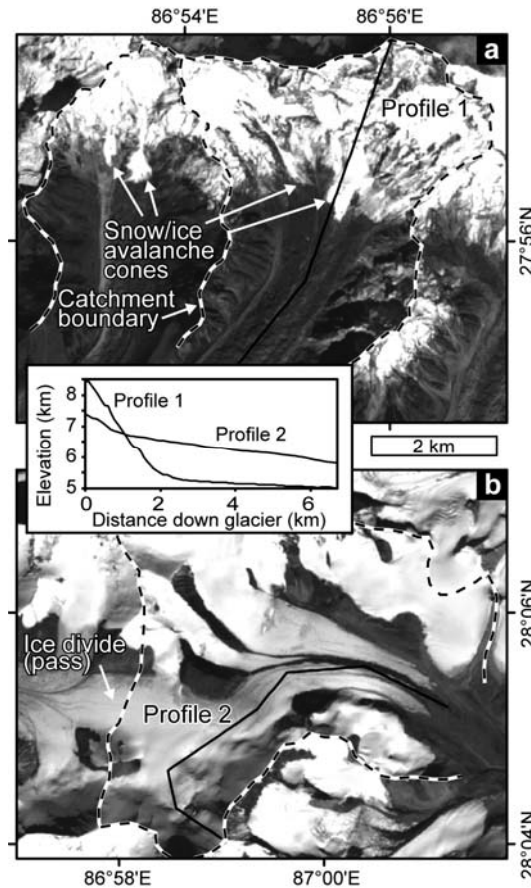
Figure 4.3: End-member examples of avalanche accumulation. Orthorectified ASTER images of glaciers with (a) high contribution of avalanches to accumulation, and (b) low contribution of avalanches to accumulation. Inset plot shows topographic profiles from each glacier. Examples in a and b are located ~7 km south and ~11 km north of Mt. Everest, respectively.

4.3.2   Results

4.3.2.1   Regional differences in topographic setting

We collected data in 12 different regions ranging from the high Hindu Kush to the eastern central Himalaya (Figure 4.1) and grouped these into six greater geographic regions, based on similarities in climate and topography. Following decreasing influences of the westerlies and increasing influences of the Asian monsoons, from west to east these are: (1) the high Hindu Kush (HK), (2) Karakoram (K), (3) western Himalaya (WH), (4) West Kunlun Shan (WKS), and (5+6) central Himalaya (CH). In the central Himalaya, we further distinguish between glaciers that are situated south (CHS) or north (CHN) of the main topographic divide between the Himalaya and the Tibetan Plateau. Glaciers in the Hindu Kush, Karakoram, and western Himalaya are located at similar mean elevations and are usually lower than glaciers in the central Himalaya and West Kunlun Shan (Figure 4.4a). The mean elevations of northern central Himalayan glaciers are on average at ~6.0 km, whereas the mean elevations of southern glaciers are on average at ~5.0-5.5 km with a larger elevation range. Differences in mean elevation are

partly accompanied by differences in mean local relief of the corresponding catchments (Figure 4.4b). Mean local relief is lowest for the analyzed catchments in the West Kunlun Shan and in the northern central Himalaya, but it is significantly higher for catchments in the Hindu Kush, Karakoram, and the southern central Himalaya. The western Himalaya takes an intermediate position. Regional variations in catchment relief are also reflected in the mean slope values of the associated glaciers (Table 4.1). The average fraction of glacierized areas of the analyzed catchments is ~40% and similar in most regions except for the Karakoram, where it is ~50%, and the West Kunlun Shan, where it is ~73%.
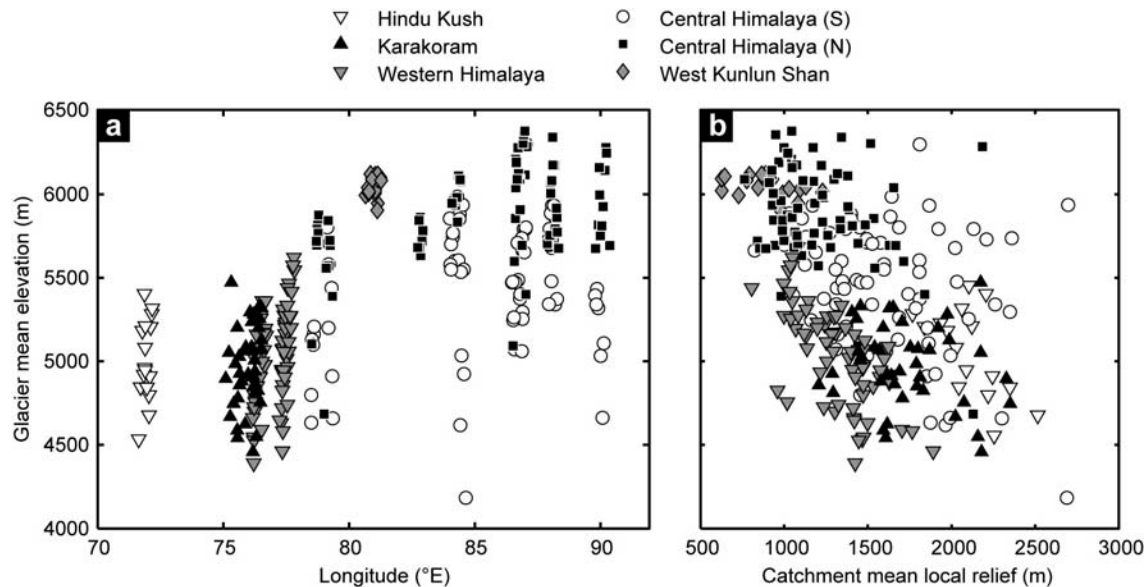
Figure 4.4: Topographic setting of the studied glaciers. Mean elevation of the studied glaciers versus (a) zonal position, and (b) mean local relief, calculated over a 5-km radius of their catchment.

4.3.2.2 Variations in debris-covered area, avalanche accumulation, and accumulation-area ratio (AAR)

Glaciers with significant debris cover exist in all regions except for the West Kunlun Shan, where the debris-covered area is generally <10% (Table 4.1). The highest mean value and variability in debris-covered area is found for glaciers from the southern central Himalaya, whereas in the northern part of the central Himalaya, debris-covered areas are lower. Importantly, the mean debris-covered area is generally lower when excluding glaciers with high and intermediate amounts of avalanche accumulation. For example they decrease from ~35% to ~19% in the southern central Himalaya (Table 4.1). Excluding these glaciers reduces the differences between glaciers from the southern and northern central Himalaya.

Our three-class system of accumulation by avalanches inevitably misses gradual changes, but nevertheless highlights several important aspects (Figure 4.5). First, glaciers with more avalanche accumulation tend to have a higher fraction of debris cover, largely unrelated to glacier size, although the variability in the fractions of debris cover is greater for smaller glaciers (<20 km length). Consequently, glaciers with high fractions of debris-covered areas have low AARs and vice versa, although a few cases of low debris-cover and low AARs exist. Second, mean catchment relief divided by the glacierized fraction of the catchment serves as a proxy for the amount of bedrock protruding above the glacier surfaces. It is positively correlated with the fraction of debris-covered areas, but variability is high (Figure 4.5c). Third, glaciers with high amounts of avalanche accumulation tend to have on average steeper catchment areas above the snowline than glaciers without. This is also reflected in lower hypsometric integrals

(HI) of the glacier and catchment areas of avalanche-fed glaciers (Figure 4.5d, e). The hypsometric integral measures the distribution of planimetric area with respect to elevation; a low value indicates that the bulk of area is found at lower elevations and vice versa. Finally, the median (and mean) elevation of glaciers subjected to high amounts of avalanche accumulation is often located far below the approximate position of the snowline or ELA obtained from the satellite images (Figure 4.5f).

Table 4.1: Regional statistics of selected catchment and glacier properties.

| | Geographic region | | | | | |
	HK	K	WH	CHS	CHN	WKS
Glacier area as a function of catchment area (y = ax)						
a	0.40	0.50	0.43	0.37	0.43	0.73
+/-	0.05	0.03	0.02	0.02	0.03	0.03
R²	0.9	0.97	0.94	0.94	0.78	0.98
Mean catchment relief (m)						
Mean	2016	1734	1314	1618	1202	912
Median	2062	1675	1311	1552	1112	888
SD	282	283	216	398	283	179
Mean glacier slope (°)						
Mean	21.2	18.8	15.4	17.5	15.8	12.8
Median	20.2	18.7	15.0	17.6	15.0	12.4
SD	3.2	3.4	2.9	3.5	4.1	4.3
Debris cover (%)						
Mean	22.9	20.5	21.3	34.6	17.9	2.8
Median	23.0	19.8	15.9	30.0	12.6	2.2
SD	10.3	12.8	16.3	22.8	16.0	2.2
Debris cover (%), excluding avalanche-accumulation glaciers						
Mean	19.8	18.3	15.9	19.3	12.2	2.8
Median	22.5	15.8	12.4	15.7	9.0	2.2
SD	9.4	9.8	11.9	12.2	9.2	2.2
Accumulation area ratio (AAR)						
Mean	0.46	0.58	0.48	0.42	0.60	0.80
Median	0.45	0.62	0.53	0.47	0.63	0.81
SD	0.09	0.16	0.21	0.26	0.18	0.07
AAR, excluding avalanche-accumulation glaciers						
Mean	0.48	0.62	0.54	0.58	0.65	0.80
Median	0.47	0.64	0.55	0.61	0.66	0.81
SD	0.07	0.14	0.16	0.16	0.12	0.07

Geographic regions are the high Hindu Kush (HK), Karakoram (K), western Himalaya (WH), southern central Himalaya (CHS), northern central Himalaya (CHN), and West Kunlun Shan (WKS). The uncertainties for factor a in the catchment area glacier area relationship correspond to the 90%-confidence intervals.

4.4   Glacier-surface velocities

4.4.1   Methods

We obtained glacier-surface velocities from sub-pixel correlation of orthorectified ASTER and SPOT images in the frequency domain using COSI-Corr [*Leprince et al.*, 2007, 2008] and following the methodology described by *Scherler et al.* [2008]. In short, two scenes taken at different times are orthorectified, co-registered and correlated, and the sub-pixel displacement of features on the glacier surface is recorded at every 4th pixel in the 15-m resolution orthorectified ASTER images, providing measurements of the horizontal surface velocity for every 60 m. Uncertainties in the velocity measurements are on the order of 2-4 m/y (Table A4) and mainly relate to inaccuracies in the DEM used for orthorectification and noise in the correlation results. For more details on the procedure, see the auxiliary material and *Kääb* [2005], *Berthier et al.* [2005], *Leprince et al.* [2007] and *Scherler et al.* [2008].
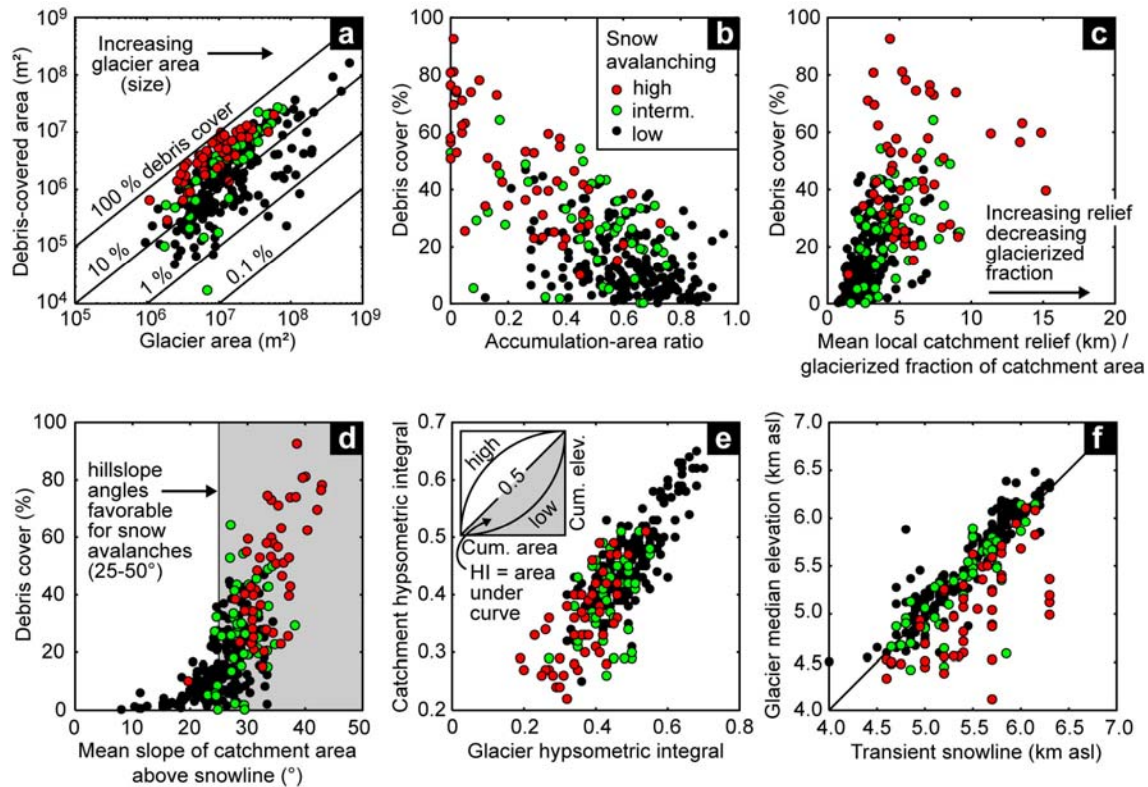
Figure 4.5: Debris cover and topographic characteristics of avalanche-accumulation glaciers. Marker colors depict degree of avalanche accumulation estimated from visual interpretation of satellite images. (a) Glacier area vs. debris-covered area, which is largely unrelated. (b) Accumulation-area ratio (AAR) vs. debris-covered area. High debris-cover usually implies lower AARs and vice versa. (c) Ratio of mean local-catchment relief and glacierized fraction of catchment area vs. debris-covered area. Glaciers with more ice-free and steep topography above them tend to have higher debris cover. (d) Mean slope of catchment area above snowline vs. debris-covered area. Hillslope angles favorable to snow avalanching after *Luckman* [1977]. (e) Glacier hypsometric integral vs. catchment hypsometric integral. Avalanche-fed glaciers and their catchments have areas skewed to lower elevations. (f) Equilibrium line altitude (ELA), estimated from satellite image vs. glacier median elevation. Avalanche-fed glaciers typically have most areas below the snowline.

For the purpose of data comparison, we measured the surface velocity along a manually identified central flow line of each glacier. This reduces the data complexity and also facilitates comparing a large number of glaciers of different lengths. In the case of complex branching glaciers, we selected the main valley glacier and did not consider multiple profiles along the tributary glaciers. The profile points are spaced at 60 m, and on average ~10 velocity measurements from different velocity maps and years were available per point. In order to minimize miscorrelations, we filtered the velocity data by direction and magnitude [cf. *Scherler et al.*, 2008]. A continuous velocity profile was generated for each glacier by computing the average velocity for each profile point and interpolation at profile points with no measurements. Final velocities are obtained by smoothing the velocity profile with a 5-point moving average filter.

A peculiar feature of glaciers from the Karakoram is the large number of surging glaciers [e.g., *Barrand and Murray*, 2006; *Hewitt*, 2007]. During phases of active surging, these glaciers usually have anomalously high velocities, rapidly advancing fronts, and the formation of crevasses in an extended area where there were none before. Such glaciers were omitted from our analysis. However, glaciers with at least some apparent surging behavior in the past, identified from distorted medial moraines at confluences with other glaciers, but no sign of any active surging were included in our analysis. None of the examined Himalayan glaciers showed

any signs of surging behavior. Even distorted medial moraines, indicating velocity variations, are extremely rare.

4.4.2   Results

To demonstrate the applicability of image-cross correlation techniques, we present glacier-surface velocity profiles of two glaciers from three key regions: the central Karakoram, the Khumbu Himal in the central Himalaya, and the West Kunlun Shan. We selected these regions due to their differences in topographic and climatic setting (Figure 4.6), which highlight characteristic features in the glacier-surface velocities that are widespread among many other glaciers.
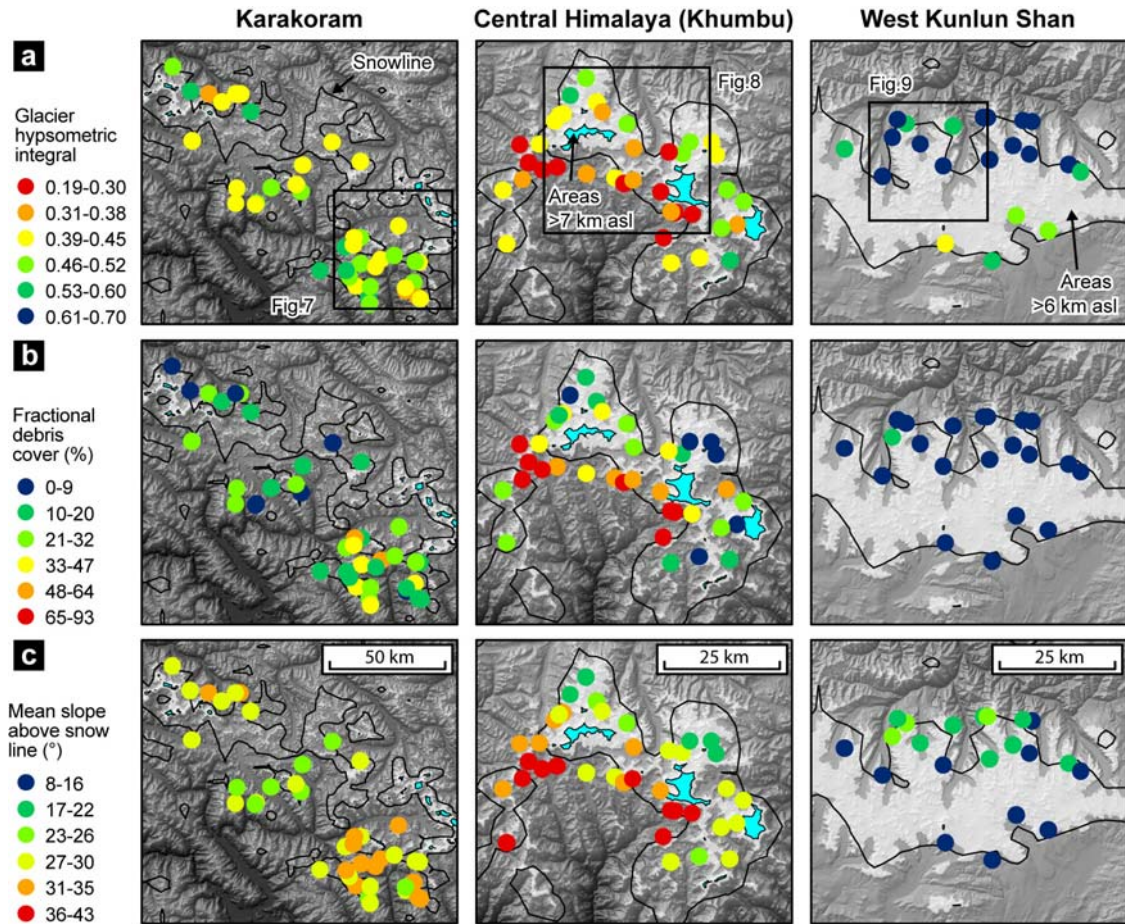
Figure 4.6: Topographic characteristics of the three case-study regions: Karakoram (K), Khumbu Himal in the central Himalaya (CHS), and west Kunlun Shan (WKS). Each point represents a glacier and is plotted at the center position of a glacier-bounding rectangle. (a) Glacier hypsometric integral (HI). High HIs indicate glaciers in plateau-like landscapes with wide and shallow accumulation basins, whereas low HIs indicate glaciers in dissected landscapes with steep headwalls and high relief. (b) Percentage of debris-covered areas. (c) Mean slope of glacier and catchment areas above snowline. Black line indicates present-day regional climatic snowline after *von Wissmann* [1959].

4.4.2.1   Case study 1: central Karakoram

With >16,600 km² of ice-covered area, the Karakoram is the most heavily glacierized region in High Asia [*Dyurgerov and Meier*, 2005]. It hosts some of the world's largest valley glaciers, such as the Siachen (70 km), Baltoro (62 km), and Biafo (63 km) glaciers. Shorter glaciers that are suitable for constructing velocity profiles were mostly found in the southeastern part of the Karakoram, south of Baltoro Glacier (Figure 4.6). In the central and northwestern part, however, the glaciers are generally larger and interconnected, limiting the number of individual,

non-overlapping velocity profiles. On average, the glaciers have AARs of ~0.58 ± 0.16 (1σ), and ~20 % of their surface area is covered with debris. Mean catchment relief is ~1700 m and the glaciers have mean slopes of ~19°. Most of the glaciers have relatively large firn basins of lower relief and at high elevations, but flow down into deeply incised valleys with steep hillslopes.
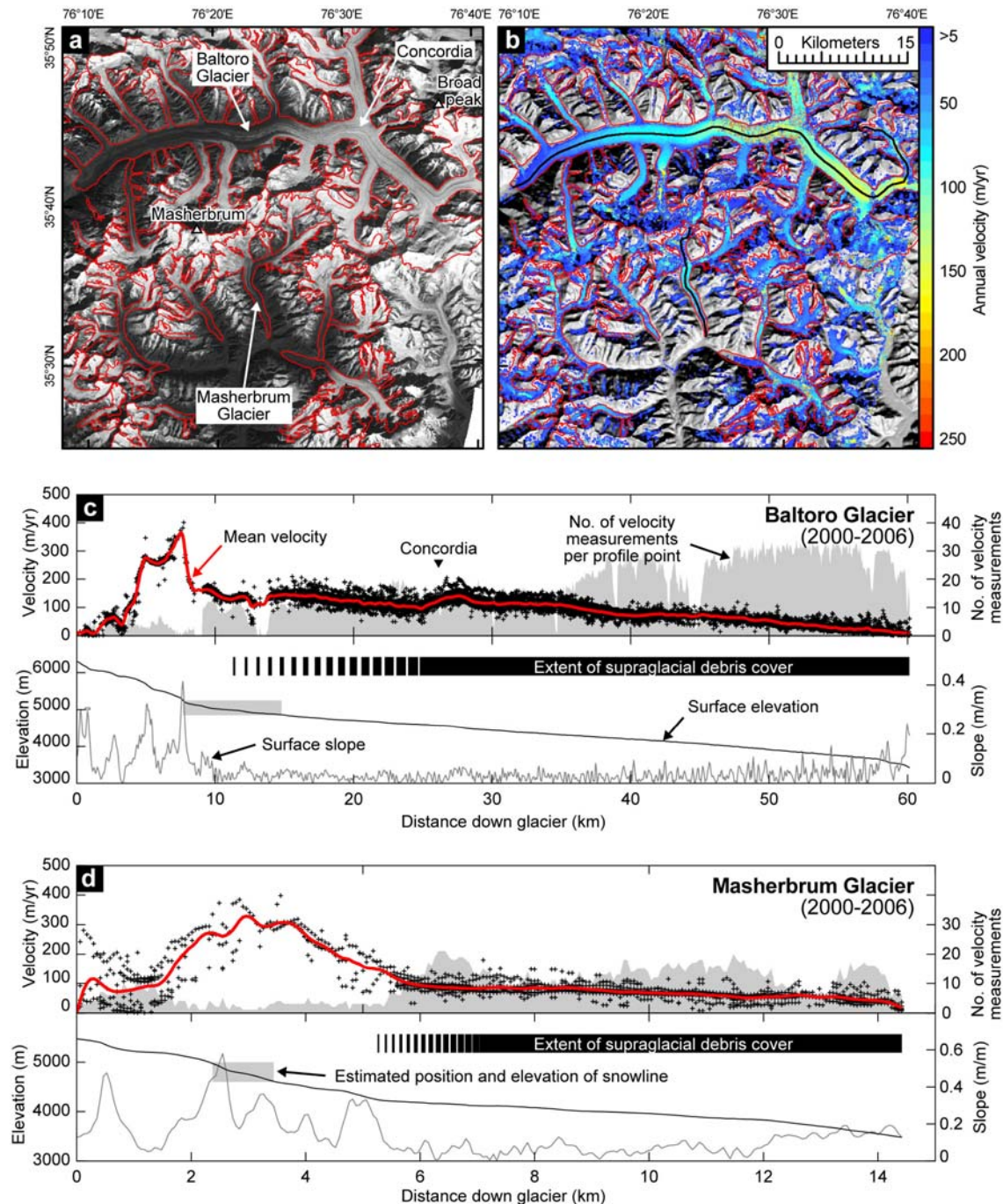
Figure 4.7: Case studies from the central Karakoram. (a) Orthorectified ASTER-satellite image from October 2003. Red polygons delineate the studied glaciers. (b) Velocity map derived from correlation of the image in A with another image from October 2002. Only velocities >5 m/yr are shown. The black lines show the trace of the profiles in C and D. (c) Velocity, surface elevation, and along-profile surface slope of Baltoro Glacier. Black crosses are the available velocity measurements after filtering. Red line depicts the mean annual velocity, derived from averaging the velocity measurements at each profile point, interpolating over no-data profile points and smoothing with a 5-point running-average filter. Concordia is the place where the northern and southern branches of Baltoro glacier meet (see B). (d) Same as C, but for Masherbrum Glacier.

In the Karakoram, we measured some of the highest velocities of the study area. The Baltoro Glacier, for example, locally attains peak velocities of almost 400 m/yr (Figure 4.7c). Even smaller glaciers, like Masherbrum Glacier, located southeast of Masherbrum peak (7821 m asl), reach equally high velocities in steep segments (Figure 4.7d). Flow velocities are usually low in the uppermost accumulation basins, but quickly increase to high velocities within steeper reaches along the flow path. The larger glaciers, with multiple tributaries, eventually reach a point of reduced steepness and flow velocities, after which velocities decrease steadily toward the glacier's terminus with less variability in surface slope and velocity. Where major tributaries join the ice stream, flow velocities usually increase somewhat, unless the joining glacier shows surging behavior or does not contribute any significant ice discharge. The two main branches of the upper part of Baltoro Glacier, for example, meet at Concordia and the surface velocities increase by ~30-40% over a distance of ~3 km (Figure 4.7). In contrast, the joining of small-tributary glaciers downstream of Concordia results in only subtle velocity variations.

Considerable scatter in the velocity data can be seen along different segments of the velocity profiles. Some of the scatter in the steep, upper parts of the accumulation basin is due to correlation difficulties (see below). In the slower flowing, lower parts of the glaciers, however, interannual velocity variations of ~50-100 m/yr or more are frequently observed.

4.4.2.2   Case study 2: Khumbu Himal (central Himalaya)

The Khumbu Himal is a region of horseshoe-shaped high topography in the central Himalaya of eastern Nepal, with Mount Everest (8848 m asl) located on the topographic divide between the Himalaya and the Tibetan Plateau (Figure 4.6). The glacierized areas stretch from the steep and high-relief areas in the southern Himalaya to the less steep and lower-relief areas on the edge of the Tibetan Plateau to the north, covering a horizontal distance of ~50 km at most (Figure 4.3). For the glaciers in the south, we inferred large amounts of avalanche accumulation and measured high areal fractions of debris cover (Figure 4.6), and low AARs (Table 4.1). Conversely, glaciers to the north of the topographic divide provide little evidence for avalanche accumulation, have lower debris cover, and higher AARs.

Measured glacier-flow velocities are on average lower than in the Karakoram. In the south, accumulation areas are often located on steep hillslopes and segmented in several small sub-basins that are connected by steep ice falls. Ngojumba Glacier, for example, originates at the southern slopes of Cho Oyu peak (8188 m asl) and descends ~1500 m over a horizontal distance of ~3 km, before it flows another ~17 km with an elevation drop of only ~800 m (Figure 4.8c). Ice flow over steep bedrock is associated with large changes of the glacier surface and commonly results in poor correlations between the multi-temporal satellite images. Such problems particularly pertain to glaciers with accumulation basins that are partly or fully disconnected from the main valley glacier below, such as Ngojumba Glacier. Here, it is difficult to accurately measure velocities in the highest part and the continuous, composite velocity profile that we constructed and velocities may not have been correctly depicted (Figure 4.8c).

High flow velocities in the steep upper part of the glaciers contrast with low flow velocities observed in their shallow sloping lower parts. Velocity decreases farther downstream, sometimes occur relatively abrupt and do not coincide spatially with slope changes, but with the joining of tributary glaciers. In the velocity profile of Ngojumba Glacier, for example, a marked velocity drop at ~9-10 km distance from the glacier head coincides with the confluence of the slow moving eastern branch of Ngojumba Glacier (Figure 4.8a, c). A similar phenomenon can be observed at ~8-10 km distance from the glacier head of Rongbuk Glacier (Figure 4.8d). In

the northern part of the central Himalaya, however, topographic relief is lower than to the south and the glaciers have generally more balanced gradients, receive less avalanche accumulation and carry less debris cover (Figure 4.8d).
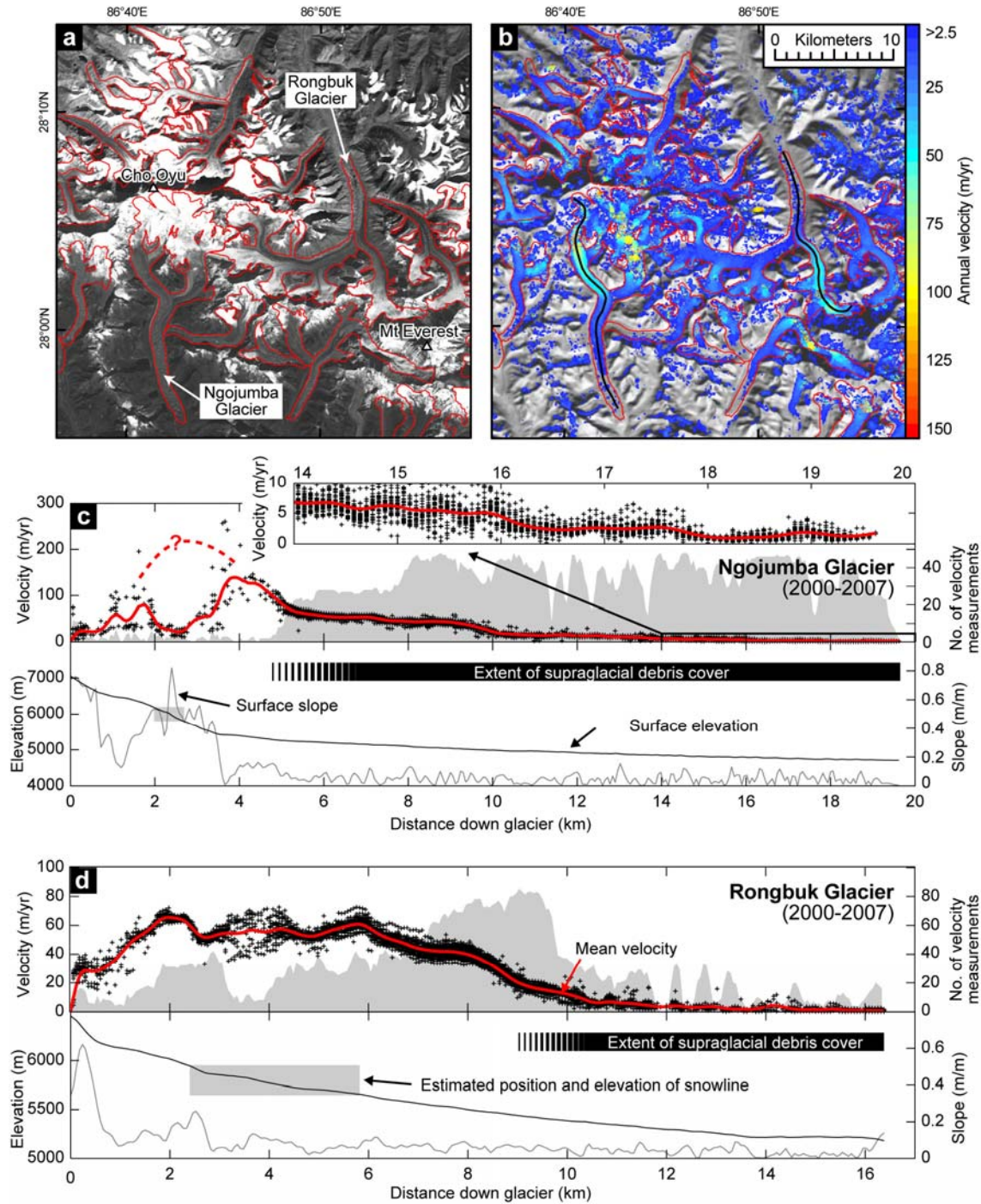
Figure 4.8: Case studies from Khumbu Himal in the central Himalaya. Symbols as in Figure 4.7. The orthorectified image in (a) is a mosaic from two images acquired in November 2004. The velocity map in (b) is also a mosaic and was produced by correlation of the image in (a) with another image from November 2005, and from correlation of images acquired in October 2003 and 2004. Inset in (c) has the Y axis on the right and depicts velocities over the lower ~5-6 km of Ngojumba Glacier. Note changes in the y-axis scaling from (c) to (d).

In several cases the flow velocities at the lowest part of the glacier reach values that are on the order of the uncertainties (<2-4 m/yr), and we cannot confidently tell whether the ice is flowing or stagnant and downwasting (in-situ decay) (see inset of Figure 4.8c). Interannual velocity

variations, if not related to correlation difficulties are generally much smaller than in the Karakoram and on the order of ~20 m/yr.
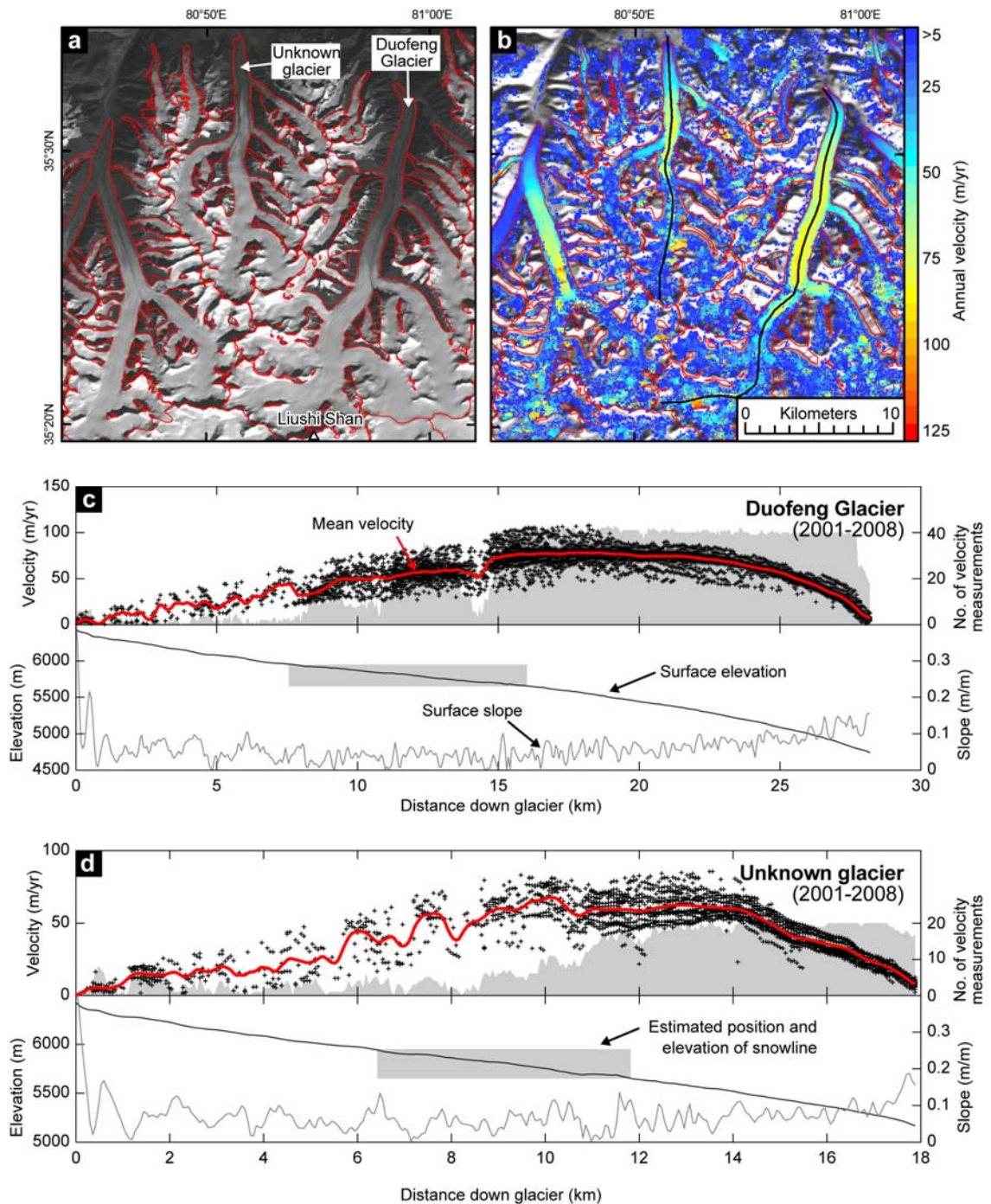
Figure 4.9: Case studies from the West Kunlun Shan. Symbols are the same as in Figure 4.7. The orthorectified image in (a) is a mosaic of images acquired in December 2004 and February 2005. The velocity map in (b) was produced by correlation of images taken in March 2005 and February 2006. The name of the glacier displayed in (d) is unknown.

4.4.2.3   Case study 3: West Kunlun Shan

Glacierized areas in the West Kunlun Shan are smaller than in the Karakoram [*von Wissmann*, 1959], but the areal fraction of ice cover within catchments is higher (Table 4.1). Most of the range is covered by a continuous glacier surface that connects north and south flowing glaciers with nunataks (exposed ridges or mountains) protruding not more than a few hundred meters above the ice surface. North-flowing valley glaciers reach minimum elevations of ~5,000 m asl,

whereas the south-flowing glaciers are of piedmont type and terminate at ~5,500 m asl. Compared to the other study regions, mean catchment relief is lower (912 ± 179 m), the glaciers rest on shallower mean slopes (12.8 ± 4.3 °), and have large AARs (0.8 ± 0.07) and virtually no debris cover, with average values of 2.8 ± 2.2 % (Figure 4.6). None of the investigated glaciers appeared to receive significant amounts of avalanche accumulation.

The pattern of glacier-flow velocities in the West Kunlun Shan is unique among all studied regions. The typical evolution of flow velocities from the glacier head towards the toe is shown by two velocity profiles in Figure 4.9. In the upper accumulation area of the glaciers, velocities are relatively low. In this part of the glacier, image correlation is complicated due to permanently snow-covered glacier surfaces with few crevasses or other markers, making feature tracking difficult. However, in such settings, along-flow variations in slope are low and thus interpolation between limited velocity measurements still provides reasonable results. Despite considerable scatter due to measurement difficulties, the available data suggest an approximately monotonic increase in velocities over approximately two-thirds of the profile length. Beyond the subdued velocity-peak, the velocity decreases in a parabolic to linear fashion (Figure 4.9).

A notable characteristic in the surface profiles of many glaciers in the West Kunlun Shan is the lack of a steep portion in the uppermost part. Farther downstream, surface slopes are similar to glaciers of the other regions, but eventually steepen towards the glacier terminus. Local, steep portions with associated velocity peaks are generally absent.

Significant interannual variations in flow velocities of up to ~40 m/yr can be observed in the lower parts of the glaciers. Such variability is usually largest (in absolute terms) where velocities are highest and decreases in magnitude up- and downstream. However, fewer data in the upper parts of the glaciers does not allow deciphering potential variability more accurately.

4.4.2.4   Regional distribution of glacier-surface velocities

Our case studies have shown that the magnitude and distribution of flow velocities varies between regions, glacier sizes, and topography. To better depict the regional differences and patterns in glacier-surface velocities across the landscape, we show all velocity profiles in map view and by region in Figure 4.10.

We measured the highest glacier-surface velocities in the Karakoram, where most flow velocities are >25 m/yr. Several of the largest glaciers (>20-30 km length), such as Baltoro, Biafo, Yazghil, and Virjerab, show flow velocities >100 m/yr over much of their length, and along steep segments peak velocities, locally up to 1000 m/yr. In all other study areas, most of the measured velocities are below 25 m/yr, and velocities >100 m/yr are only found where a long glacier (>15 km length) flows across a steep valley reach. Such glaciers are exclusively found near the highest topography, where the largest accumulation areas exist, but are absent in the West Kunlun Shan, where topographic relief is subdued (Figure 4.9). The Khumbu Glacier, for example, originates on the southern slopes of Mount Everest and attains >100 m/yr at the Khumbu ice fall, approximately half-way down its length. However, glaciers with steep accumulation areas (shown by closely spaced contours in Figure 4.10), such as Ngojumba Glacier (Figure 4.8), and other south-flowing glaciers in the central Himalaya, have relatively low gradients over much of their course and a steep portion along the flow path is either absent or confined to their headwalls and short horizontal distances (Figure 4.11). In such cases, flow velocities are highest near the glacier head but quickly diminish downstream.
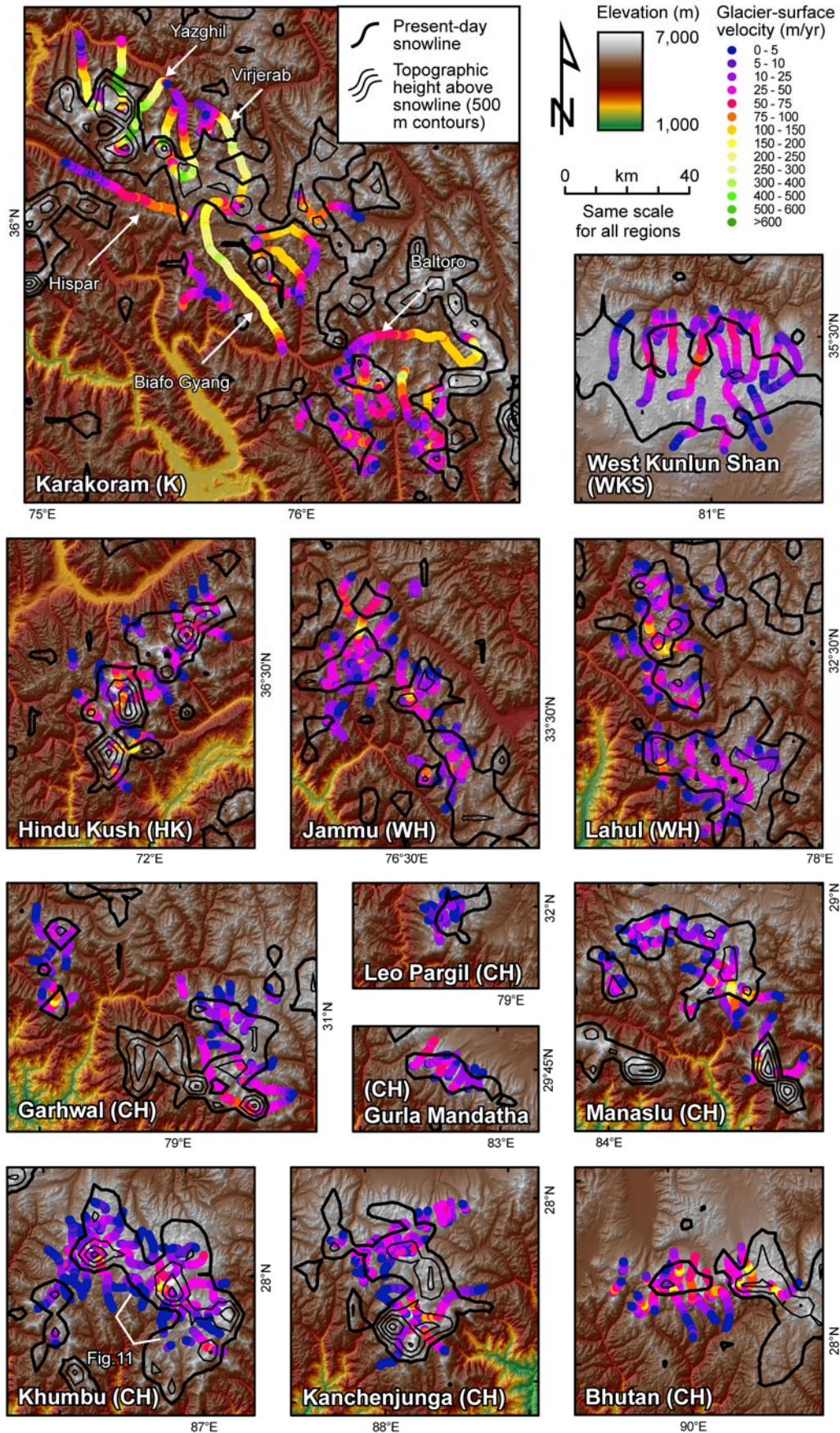
Figure 4.10: Regional patterns of glacier-surface velocities. See Figure 4.1 for regional setting of study areas. Only surface velocities following the central-flow line of the studied glaciers are shown and only those glaciers with sufficient data are used to construct velocity profiles covering the entire glacier. For each glacier we picked only one velocity profile to prevent overlap. Thus, the number of studied glaciers in the Karakoram is relatively low with respect to the

much greater glacierized areas. Present-day regional climatic snowlines after *von Wissmann* [1959]. This dataset comprises contour lines that we digitized and interpolated on a coarse (5-km resolution) grid. Note that present-day snowlines are likely somewhat too high in the Karakoram and too low in the southern central Himalaya.

In summary, the highest flow velocities in each region are associated with the highest topography, where the largest accumulation areas are located. Particularly steep accumulation areas exist in the southern central Himalaya, the Hindu Kush, and in the northwestern part of the Karakoram, whereas in the western Himalaya, the northern central Himalaya, and the central and southeastern part of the Karakoram, accumulation areas are less steep. In the West Kunlun Shan, where the topography and relief are more subdued, the largest interconnected accumulation areas exist but flow velocities are relatively low and local velocity peaks are absent.
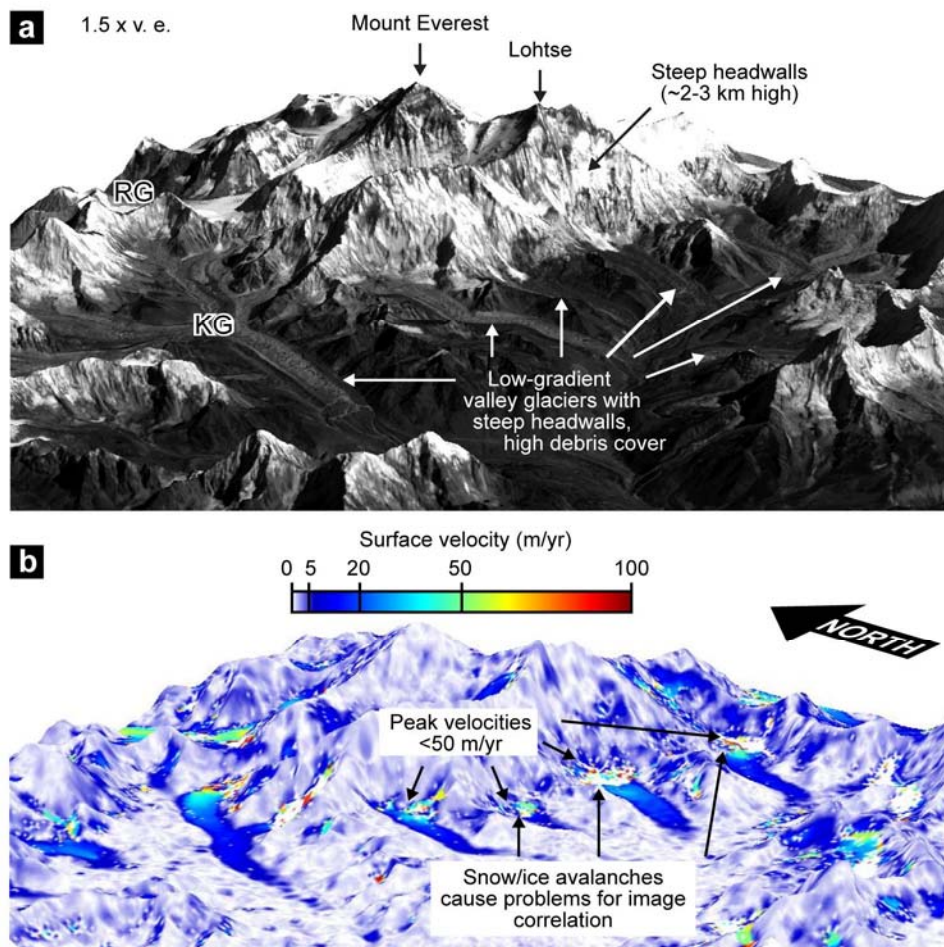
Figure 4.11: Topographic setting of glaciated landscape in the Khumbu Himal, Nepal. (a) Orthorectified ASTER image (band 3N) from Nov 10 2004, draped over a 90-m resolution SRTM DEM with 1.5 x vertical exaggeration. Note that accumulation areas are mostly confined to steep but high-reaching headwalls, from where snow and ice avalanches nourish low-gradient valley glaciers with high amounts of debris cover located below the snowline. KG and RK denote Khumbu Glacier and Rongbuk Glacier, respectively. (b) Same view as in (a), but showing mean annual surface velocities between Nov 10 2004 and Nov 29 2005. Speckled colors at the base of the headwalls indicate miscorrelations, arising from snow and ice avalanches.

4.5   Discussion

Our data provide the first comprehensive and regional assessment of glacier-surface velocities across High Asia, allowing unique insights into the patterns and magnitudes of ice flow in terrain of different complexity. In the following section, we first discuss the links between

topography, debris cover, and avalanche accumulation and then consider the influences of topography, climate, and recent climatic change on flow velocities.

4.5.1   Relationship between topography, debris cover, and avalanche accumulation

Our topographic and debris-cover analyses suggest that the amount of avalanching inferred from visual interpretation of the satellite images is related to the topographic setting of the studied glaciers and to the areal fraction of debris cover. Glaciers with high inferred amounts of avalanche accumulation tend to have steeper accumulation areas, i.e., areas above the snowline, with higher local relief and lower fractions of glacierized areas, compared to glaciers with less avalanche accumulation (Figure 4.5c-e). Our approach of determining the amount of avalanching is not suitable to capture gradual transitions and also does not decipher additional factors, such as aspect and local climate that may account for the scatter that is seen in the data. Nonetheless, it is reasonable to assume a direct relationship between avalanche accumulation, catchment relief, and fraction of glacierized area. Accordingly, the larger the areas of ice-free and sufficiently steep hillslopes (>25°; *Luckman* [1977]) protruding above the glacier surface are, the higher the amount of snow transported by avalanches onto the glacier, all other parameters equal. Furthermore, glaciers with identified high amounts of avalanche accumulation tend to have higher proportions of debris cover, supporting the notion that the principal sources of debris in these environments are the adjoining hillslopes [e.g., *Hewitt*, 1988, 2009; *Benn and Lehmkuhl*, 2000]. Snow and ice avalanches themselves may in fact be important mechanisms by which rock and debris from steep hillslopes is transferred to the glacier surface [e.g., *Rapp*, 1960; *Luckman*, 1977; *Humlum et al.*, 2007].

We note that during periods of climate warming and glacier retreat, debuttressing of hillslopes may lead to an increased frequency of slope failures and enhanced flux of debris onto the glacier surface [e.g., *Church and Slaymaker*, 1989; *Watanabe et al.*, 1998; *Ballantyne*, 2002], leading to temporarily increased, abnormal debris cover. Although such a process may serve as an important source of debris to starving glaciers, we did not observe evidence for any significant slope failures on any of the studied glaciers during the period of investigation (2000-2008).

4.5.2   Climatic and topographic controls on flow velocities

Ice flow is driven by gravitational stresses of the ice and therefore mostly depends on glacier thickness and slope [*Paterson*, 1994]. Besides geometric factors, ice temperature and basal water pressure are additional important factors controlling ice flow velocities (see Appendix B3) [*Paterson*, 1994]. Altitudinal variations in ice temperature are potentially important for glaciers covering large elevation ranges and in the distribution of cold and temperate ice. Borehole measurements from a high-altitude glacier (~6300 m asl) in the northern central Himalaya revealed basal ice temperatures of -9°C and thus, frozen-bed conditions [*Liu et al.*, 2009]. The lack of more ground-truth data hampers assessing regional gradients, but available air temperature data suggests minor regional differences of glaciers located at similar elevations, except for the West Kunlun Shan, where extreme continental conditions prevail and the glaciers may be more polar-like (see Discussion in Appendix B4) [*Ageta et al.*, 1989]. In the Hindu Kush, Karakoram, western Himalaya, and southern central Himalaya where most glaciers are located at lower elevations, precipitation and temperatures are higher [*Miehe et al.*, 2001], and significant portions of the studied glaciers may be temperate, particularly in the case of voluminous and thick glaciers.

Variations in basal water pressure depend on several factors, including variations in climate and subglacial hydrology [e.g., *Willis*, 1995], which are difficult to evaluate at the scale of our investigation. However, during our 8-year measurement period, interannual variations in basal water pressures and basal sliding most likely cancel each other out. For non-surging glaciers, downstream variations in ice thickness and slope are mostly related to the valley geometry, i.e., valley width and slope, and the glacial mass balance, and are therefore strongly influenced by climate and topography. Deciphering the contribution of downstream changes in valley geometry to changes in the surface velocity for each of the studied glaciers is beyond the scope of this study. In general, however, our observations allow pointing out the following principal characteristics regarding magnitude and distribution of ice flow along the studied glaciers:

First, velocities increase from the glacier head downstream until the approximate position of the ELA and then decrease towards the terminus. This pattern is clearer for small glaciers (<5 km) compared to larger ones, for which velocities are often additionally affected by joining tributaries and variations in valley slope and debris cover. Furthermore, the downstream distribution of velocities along the profiles is stronger skewed towards the glacier head for larger glaciers than for small glaciers (Figure 4.12). This is most likely due to hypsometric effects, with greater accumulation areas resulting in higher converging flow of larger glaciers [e.g., *Anderson et al.*, 2006], but may also be due to glacier-size related differences in mean fractional debris cover (see below), which shows a similar trend for increasing glacier-size classes of 18.3% (<5 km), 23.5% (5-10 km), 24.9% (10-15 km), 28.4% (15-20 km), and 14.9% (>20 km).
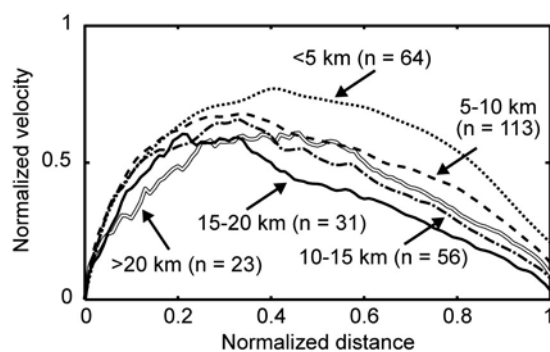
Figure 4.12: Mean normalized velocity profiles for glaciers of different lengths. Surface-velocities of all glaciers were normalized by the maximum velocity along each velocity profile.

Second, glaciers with larger accumulation areas have a greater size (by area and length) and have on average higher mean and maximum velocities along their profile than glaciers with smaller accumulation areas. However, the correlation between glacier or accumulation area size and mean or maximum velocities along the profiles are relatively weak ($R^2<0.4$), which we attribute to additional influences such as slope, basin hypsometry, tributaries, ice dynamics, and other factors. Better relationships of velocity with glacier size may be obtained when some of these effects are taken into account, for instance, when correlating mean annual ice flux per unit width with glacier area ($R^2=0.69$) or glacier length ($R^2=0.63$) (chapter 7). Using scaling analysis of the mass and momentum conservation equations, *Bahr et al.* [1997] and *Bahr* [1997] derived a power-law relationship between characteristic glacier downstream velocity divided by characteristic glacier slope and glacier surface area. These authors predict scaling exponents of 1.5 for shallow and 1.2 for steep glaciers, when assuming typical flow law parameters and a volume-area scaling exponent of 3/8 (derived from eqs. 13 and 14 in *Bahr* [1997]). We obtain a scaling exponent of ~1.2 between mean along-profile velocity divided by mean slope, and

glacier area (R²=0.68; Figure 4.13), although not all of the studied glaciers should be regarded as steep.
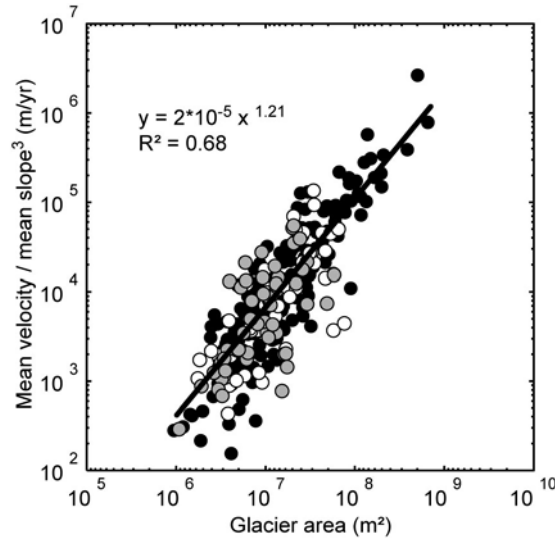
Figure 4.13: Glacier area versus mean velocity divided by mean slope to the power of 3. See text for details.

Third, local velocity peaks occur at steep segments along the glacier (cf. Figure 4.7), and if steep segments are absent the velocity profile lacks sharp peaks (cf. Figure 4.9).

Fourth, where tributary glaciers join, velocities increase, decrease, or remain unchanged (Figure 4.7-Figure 4.9). We relate this to variations in valley width and the effects on ice thickness. If valley width remains uniform across a confluence, and the additional ice flux from the tributary is not balanced by melting, ice discharge per unit width, and thus velocities increase. In those cases where velocities do not change, the joining tributary either contributes only minor amounts of ice or the valley width changes so that ice thickness remains constant. In a number of cases, we observed that velocities decreased at confluences (case study 2; Figure 4.8) and we think that the negligible contribution of ice discharge from the associated tributaries allows lateral spreading of the ice from the main glacier branch, leading to a reduced thickness and thus velocity. This may be related to the confluence occurring in a part of the glacier, where its lateral margins are formed by easily deformed moraines that may be adjusted to a higher ice flux.

Fifth, for higher fractions of debris-covered areas, the studied glaciers tend to have their peak velocities shifted to the upper part of the velocity profiles, where they have higher mean velocities compared to their lower parts, leading to more asymmetric velocity profiles (Figure 4.14). We attribute this to the effects of debris cover on glacial mass balances and recent climate change. Mass balance measurements from avalanche-fed glaciers are difficult to obtain and presently unavailable for this region, but their mass balance should exhibit large variations downstream [e.g., *Benn and Lehmkuhl*, 2000]. When snow accumulation is confined to avalanche depositional areas at the foot of headwalls that are located partly or entirely below the snowline (cf. Figure 4.11), melt rates are high, especially when snow and ice are interspersed with dust and debris [*de Scally and Gardner*, 1990]. The ELA is located immediately downstream of the avalanche depositional areas and rapid melting concentrates debris on the glacier surface, which quickly forms a continuous layer that significantly reduces melt rates once its thickness exceeds a few centimeters [*Mattson et al.*, 1993; *Kayastha et al.*, 2000; *Mihalcea et al.*, 2006], which is usually the case for Himalayan glaciers [e.g., *Shroder et al.*, 2000; *Owen et al.*, 2003; *Heimsath and McGlynn*, 2008]. Thus, downstream gradients in ice

thickness, hence velocity, should be greatest in the uppermost part but much smaller in the debris-covered part. This inference is supported by our observations from heavily debris-covered glaciers (Figure 4.8c, Figure 4.11), and the results of simplified numerical modeling of debris-covered glaciers [*Konrad and Humphrey*, 2000].
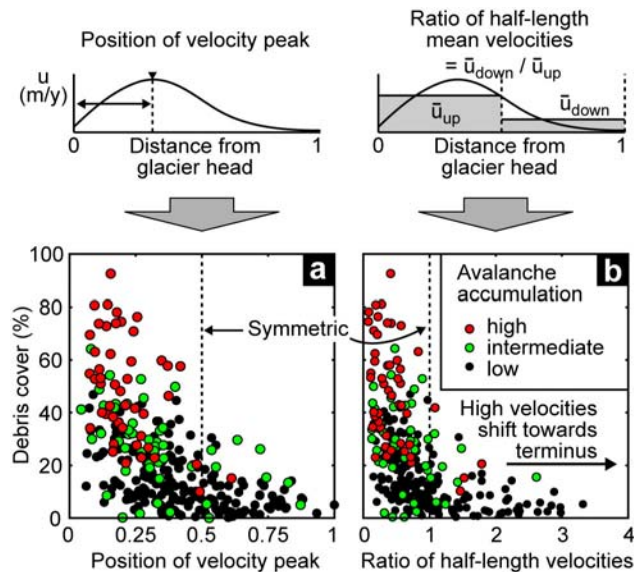
Figure 4.14: Debris cover and asymmetry of the velocity profiles. (a) Asymmetry of velocity peak vs. debris-covered area. X-axis shows position of maximum velocity in profile along normalized distance from glacier head. (b) Ratio of half-length mean velocities vs. debris-covered area. X-axis shows ratio of the mean velocities in the lower to the upper half-lengths of the velocity profiles. In both panels, farther left in the plot means that velocities are skewed towards the glacier heads and farther right means that velocities are skewed to the glacier termini.

Many Himalayan glaciers are reported to have been retreating and/or thinning during the last decades [e.g., *Berthier et al.*, 2007; *Bolch et al.*, 2008; *Raina*, 2009], and may have been doing so since ~1850 AD [*Mayewski and Jeschke*, 1979]. The insulating effect of debris cover, however, retards melting at the front, where heavily debris-covered glaciers have been observed to waste down in situ, while their fronts remain relatively stable [*Clayton*, 1964; *Kirkbride*, 1993]. Thus, heavily debris-covered glaciers may keep much of their areal extent although their thickness, slope, and velocities change (cf. Figure 4.8c, d) [*Seko et al.*, 1998; *Nakawo et al.*, 1999; *Bolch et al.*, 2008; *Scherler et al.*, 2008; *Quincey et al.*, 2007, 2009]. These effects probably lower flow velocities and shift peak velocities upstream, leading to even more pronounced asymmetries in the velocity profiles (Figure 4.14). During our study period, we did not observe any systematic decreases in flow velocities that could be related to thickness changes.

Figure 4.15 summarizes these observations in a conceptual sketch. Glaciers in low-relief areas have shallow accumulation areas, little or no debris cover, and flow velocities are evenly distributed across their length. When the topography is steeper, an increasing fraction of the accumulation is due to snow and ice avalanching from steep hillslopes, which increases the amount of debris cover on the glacier surface. Glaciers which originate from high-lying accumulation areas but descend to lower elevations show some of the highest velocities, particularly at steep segments along their flow path. Glaciers that are almost exclusively nourished by snow and ice avalanches have the highest amount of supraglacial debris cover and their flow velocities are strongly skewed towards their head.
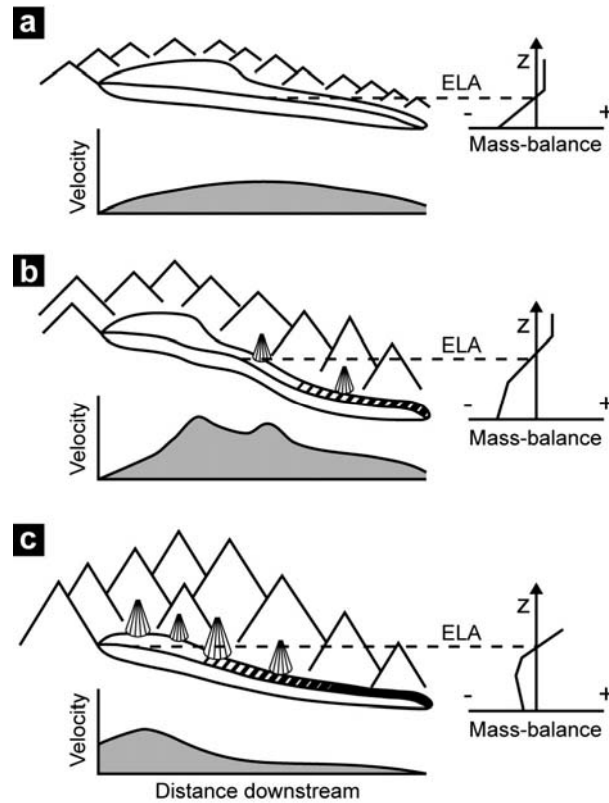
Figure 4.15: Conceptual sketch showing the effect of topography on accumulation types, debris cover, and glacier-flow velocities. (a) Glacier in a low-relief landscape, which is dominantly fed by direct snow fall and which has no debris cover (e.g., West Kunlun Shan). (b) Glacier fed by both avalanches and direct snow fall (e.g., Karakoram, western Himalaya). (c) Glacier dominantly fed by avalanches and with abundant debris cover (e.g., southern central Himalaya).

4.5.3   Regional climatic gradients and glacial topographic settings

The general topographic settings shown in Figure 4.15 and associated debris cover and glacial-flow characteristics are intimately linked with regional gradients in climate and topography and their effect on snowlines and accumulation areas (Figure 4.16). Snowlines are high above the Tibetan Plateau (>5.5 km asl, *von Wissmann* [1959], *Ohmura et al.* [1992]) and only intersect locally with topography, where it protrudes usually not more than a kilometer above the mean elevation of the Tibetan Plateau of ~5 km asl [*Fielding et al.*, 1994]. Along the margins of the Tibetan Plateau, snowlines descend due to orographic precipitation [*Ohmura et al.*, 1992]. Concomitantly, erosive dissection of the plateau margin may account for isostatic uplift [*Montgomery*, 1994], and while mean elevations are ≤5 km asl, individual massifs reach much higher elevations, particularly in the central Himalaya and Karakoram.

The areal extent of accumulation areas mostly depends on gradients in topographic relief and precipitation and the resulting changes in snowline elevation. The steep and high topography of the central Himalaya efficiently blocks moist monsoonal air from northward advection [*Bookhagen and Burbank*, 2006; *Boos and Kuang*, 2010] which results in a rapid rise of snowlines to elevations >5 km asl [*von Wissmann*, 1959]. Consequently, many accumulation areas are confined to high-reaching massifs with peaks that are typically bounded by steep, and up to ~3 km long steep hillslopes, leading to high amounts of avalanching and heavily debris-covered, slow-moving glaciers (Figure 4.11).

In the western Himalaya and Karakoram, snowline elevations are lower than farther east, most likely due to latitudinal temperature gradients and the influx of winter precipitation from the

west [*von Wissmann*, 1959]. In addition, the westerlies transport atmospheric moisture farther onto the Tibetan Plateau, which may be related to the higher tropospheric extent of the westerlies air flow [*Barry and Chorley*, 2003] that helps to overcome orographic barriers (section 7) [*Bookhagen and Burbank*, in press]. In these regions, annual precipitation of up to 2 m of snow water equivalent at high elevations where glaciers occur has been observed [*Winiger et al.*, 2005; *Wulf et al.*, 2010] or inferred from indirect methods [e.g., *Weiers*, 1994; *Bhutiyani*, 1999]. As a result, snowline elevations are <5 km asl within a broad band covering the High Himalaya and part of the Karakoram, and allow the development of sizable shallow accumulation areas on the edge of the Tibetan Plateau in which avalanching is less important (Figure 4.16). The largest glaciers in the Karakoram and within High Asia originate from these extensive low-relief accumulation areas at high altitude and flow to lower elevations through major valleys, where they reach the highest velocities (Figure 4.10).
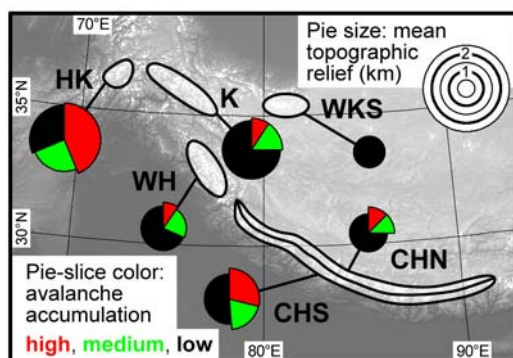
Figure 4.16: Summary of regional topographic settings. Pie slices represent fraction of glaciers with high (red), medium (green), or low (black) inferred avalanche accumulation. Pie size denotes mean topographic relief for each glacier class. Capital letters indicate geographic regions: Hindu Kush (HK), Karakoram (K), western Himalaya (WH), southern central Himalaya (CHS), northern central Himalaya (CHN), and West Kunlun Shan (WKS).

4.6   Conclusions

We presented the first comprehensive High Asian glacier synthesis of how topographic and climatic gradients affect accumulation areas, debris cover, snow avalanching, and glacial-flow velocities. The magnitude and distribution of surface velocities along the central flow line of the studied glaciers is controlled by the interplay of climate and topography. Dominant factors are the size of the accumulation area, the steepness of the bed, the joining of glacier branches, and the presence of supraglacial debris cover.

The areal fraction of supraglacial debris on the studied glaciers is closely linked with the steepness of their accumulation areas, suggesting that the main source of debris in these environments are the adjoining hillslopes. Debris cover on the glacier surface influences melt rates, hence the mass balance, and thereby the downstream-thickness evolution of the glacier and its flow velocities. Glaciers with steep accumulation areas and high amounts of snow and ice avalanching typically have their highest velocities at the glacier head but greatly reduced and slowly changing flow velocities over their debris-mantled lower parts. Glaciers in low-relief topography receive more direct snowfall, have little or no debris cover and exhibit a more symmetrical distribution of flow velocities.

Regional gradients in topography and snowlines strongly influence the size and steepness of accumulation areas and thereby glacier size, debris cover, and flow velocities. In the monsoon-dominated central Himalaya, high snowlines account for steep accumulation areas that are concentrated at the highest massifs, resulting in many avalanche-fed glaciers with high debris

cover. Most glaciers in these regions have lengths <15 km and those that are longer have high areal fractions of debris cover and relatively low velocities. In the westerlies domain, lower snowlines allow for more extensive low-relief accumulation areas where avalanching is less important and debris cover reduced. The longest and fastest glaciers are found in the Karakoram, originating from high-altitude accumulation areas with relatively low relief.

Our study documents how regional climatic and topographic gradients in High Asia affect the dominant accumulation modes and debris cover. These exert strong control on mass balances and glacier dynamics and need to be considered when studying the response of these glaciers to climate change [e.g., *Bolch et al.*, 2008; *Raina*, 2009], or when inferring past glacial episodes from dated moraines [e.g., *Scherler et al.*, 2010]. Furthermore, the along-glacier distribution of flow velocities provides first-order constraints on the spatial arrangement of glacial fluxes and thus the erosion potential of these glaciers [e.g., *Anderson et al.*, 2006].

5   Influence of debris cover on the frontal dynamics of High Asian glaciers

Abstract

The forecasted demise of mountain glaciers in High Asia involves significant impacts on the water supply in central Asia, but observations and data are controversially debated. Remotely sensed glacier-surface velocities and frontal changes of 287 glaciers from High Asia measured between 2000 and 2008 elucidate the impact of debris cover on glacier-front dynamics. Glaciers heavily covered by debris are frequent in the high-relief Hindu Kush and central Himalaya and are characterized by significant portions of non-moving, stagnant ice (up to half the glacier's length), but stable fronts and in-situ downwasting. Conversely, in the lower-relief western Himalaya and along the southern margin of the Tibetan Plateau, debris cover is reduced and the largest fraction of retreating glaciers is observed. In the Karakoram, however, more than 50% of the studied glaciers were advancing or remained stable with nearly no signs of stagnation despite significant debris cover, suggesting principle differences in recent mass-balance regimes. Thick debris mantles on the lower portions of many Himalayan glaciers effectively shield the ice from ablation and reduce the effects of atmospheric soot deposition and variations in solar radiation.

5.1   Introduction

The current state and future fate of snow and glaciers in High Asia is of central importance for the water, food, and power supply of densely populated regions in South, East, and Central Asia [*Barnett et al.*, 2005]. Due to their remoteness and difficult accessibility, detailed mass-balance studies are rare and spatially and temporally limited [e.g., *Dyurgerov and Meier*, 2005; *Berthier et al.*, 2007]. Thus, changes in glacier area or the terminus position are often used to indicate glacier condition [e.g., *Mayewski and Jeschke*, 1979; *Fujita et al.*, 1997; *Kargel et al.*, 2005; *Raina*, 2009]. A growing number of remote-sensing studies suggest that in the last decades, many Himalayan glaciers may have retreated and/or thinned [e.g., *Karma et al.*, 2003; *Berthier et al.*, 2007; *Bolch et al.*, 2008], but the rate at which this occurs is controversially debated [e.g., *Fujita et al.*, 1997; *Ageta et al.*, 2000; *Kumar et al.*, 2008; *Raina*, 2009]. Furthermore, scattered observations of glacier advance and thickening in the central Karakoram [*Hewitt*, 2005] point at regionally different glacier behavior that may be linked to disparate effects of climatic change [*Fowler and Archer*, 2006].

Many Himalayan glaciers are covered by high amounts of supraglacial debris, including the large Gangotri and Siachen glaciers that have been repeatedly cited for their frontal changes [e.g., *Kumar et al.*, 2008; *Raina*, 2009]. Debris cover of more than a few centimeters thickness shields the ice from ablation and therefore influences glacial-mass balance [e.g., *Østrem*, 1959; *Mattson et al.*, 1993] and the response of glaciers to climate change [e.g., *Ogilvie*, 1904; *Kirkbride and Warren*, 1999]. For example, repeated surveys in the Mt. Everest region indicate that surface lowering during the last five decades has been more pronounced for clean-ice compared to debris-covered glacier areas [*Nakawo et al.*, 1999; *Bolch et al.*, 2008]. Yet, the terminus of the heavily debris covered Khumbu Glacier, for instance, has not significantly

changed its position in the last ~50 years [*Bolch et al.*, 2008]. The impact of thick debris cover on glacial melting is in stark contrast to fine-layered black carbon or soot particles on glacial and snow surfaces that enhance melting [e.g., *Xu et al.*, 2009].

Limited observations of stagnant ice in the lower portions of debris-covered glaciers in the Khumbu Himal [*Scherler et al.*, 2008; *Quincey et al.*, 2007; 2009] motivated us to conduct a regional survey and examine the flow characteristics and terminus behavior of clean ice and variably debris-covered glaciers across High Asia. Here, we use remote-sensing derived glacier-surface velocities (chapter 4) and glacier frontal changes between 2000 and 2008 and shorter periods to investigate the relationship between debris cover, quasi-stagnant ice, and frontal changes. In particular, we assess stagnant glacier fronts, to decipher possible regional patterns, potentially accounting for some of the reported discrepancies in glacier behavior in High Asia [*Hewitt*, 2005; Raina, 2009].

Our study area stretches from the Hindu Kush in the west, at ~72°E, 36.5°N, to the Bhutanese Himalaya in the east, at ~90°E, 28°N. We analyzed 287 glaciers from 12 individual regions and grouped these into six geographic regions (Figure 5.1), based on similarities in climate and topography (cf. chapter 4). The study area is affected by three main atmospheric circulation regimes, the Indian and East Asian monsoons, and the mid-latitude Westerlies [*Barry and Chorley*, 2003]. The influence of the Westerlies decreases from the Hindu Kush (HK) and Karakoram (K) across the western Himalaya (WH) to the central Himalaya, while the monsoonal influence increases [*Bookhagen and Burbank*, in press]. Due to steep topographic gradients across the central Himalaya, we further distinguish glaciers located south (CHS) and north (CHN) of the main topographic divide to the Tibetan Plateau. Finally, the West Kunlun Shan (WKS) is the most continental setting, marginally influenced by the East Asian Monsoon [*Ohata et al.*, 1989].
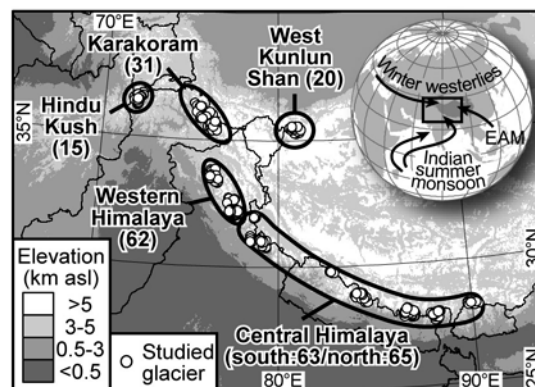
Figure 5.1: Geographic overview of the study area. Number of studied glaciers per geographic region is given in parenthesis. Inset globe depicts location of subset and main atmospheric moisture sources. EAM denotes the East Asian Monsoon.

5.2   Methods and data

We used measurements of glacier-surface velocities from 2000 to 2008, based on sub-pixel cross-correlation of optical satellite images [*Leprince et al.*, 2007; *Scherler et al.*, 2008], presented in detail in section 4. The velocity data has been obtained along the central flow line of the studied glaciers and we investigated how flow velocities at their lower ends are related to the extent of supraglacial debris cover. The extent of debris cover was determined based on digitized glacier outlines blended with the distribution of clean ice and snow at the end of the

hydrological year (section 4), obtained from thresholded Landsat Thematic Mapper (TM) band TM4/TM5-ratio images [*Paul et al.*, 2004].

We measured changes in glacier area at the terminus from the earliest and latest suitable orthorectified 15-m resolution Advanced Spaceborne Thermal Emission and Reflection Radiometer (ASTER) images that were used for the velocity measurements (section 4). Combined with glacier widths we calculated mean annual advance or retreat rates during the period of investigation (Figure 5.2). For most of the glaciers, suitable scenes separated by at least four years are available and allow determination of frontal changes during the respective observation period (Table A1).

Identifying the edges of debris-covered glaciers is not possible by standard ice and snow mapping techniques, and despite efforts for automatic mapping [e.g., *Paul et al.*, 2004] the most accurate procedure is still manual delineation by one expert investigator [*Bolch et al.*, 2008]. In our study, the high number of accurately co-registered satellite images facilitates detection of surface-area changes. Following *Bolch et al.* [2008], we estimated mapping inaccuracies by comparing several ASTER-based area changes with those obtained from 5-m resolution SPOT images. Although the periods between the available images were not identical, deviations of mean-annual frontal changes are on average ~5 m/yr and up to ~20 m/yr in the case of one heavily debris-covered glacier. For this study, we assume a uniform uncertainty of ~10 m/yr for all studied glaciers, which is likely a conservative estimate.
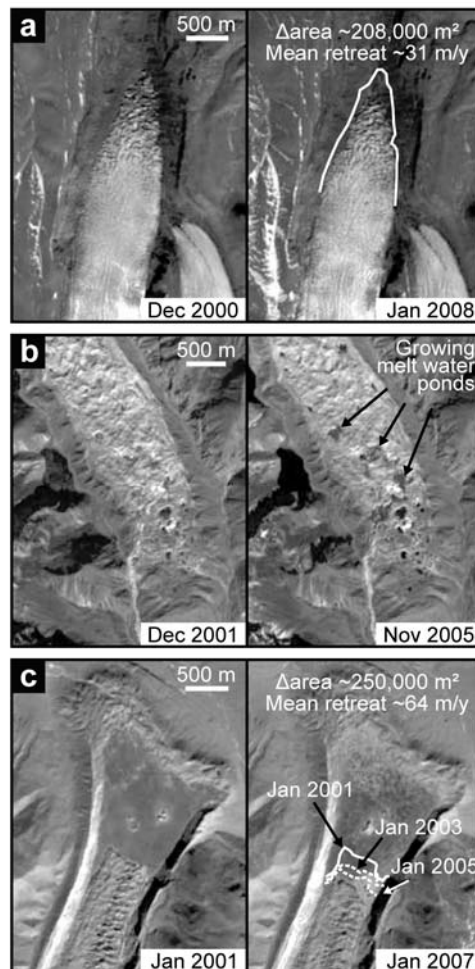
Figure 5.2: Orthorectified ASTER band 3N images with examples of glaciers with different frontal dynamics. (a) Debris-free glacier in the Manaslu region, Nepal (~28.9°N, 84.2°E). (b) Terminus region of the heavily debris-covered Ngojumba Glacier, Nepal (~27.9°N, 86.7°E). No advance or retreat of the glacier front is observed during the study period, but the enlargement of supraglacial ponds points at glacier wasting. (c) Debris-covered glacier in southern Tibet,

China, which terminates at a moraine-dammed lake (~28.3°N, 90.1°E). Date of image acquisition shown in lower right corner of each image.

5.3   Stagnant glaciers

Previous analysis of glacier-surface velocity data revealed extremely low velocities several kilometers upstream of the terminus of Himalayan glaciers [*Scherler et al.*, 2008]. In order to assess the significance and distribution of such quasi-stagnant reaches, we measured the fractions of the velocity profiles with velocities <2.5 m/yr (Figure 5.3). This particular threshold is guided by the average uncertainties in the measurements and associated limitations in discriminating between moving and stagnant ice. We tested somewhat higher and lower thresholds (0-5 m/yr), but these mostly shift the statistical moments of the distributions to higher and lower fractions, respectively, but have no effect on the relative differences.

In the Hindu Kush and the southern and northern central Himalaya, the fraction of glaciers with near-zero velocities at more than 5% of the profile lengths is ~38%, ~40%, and ~22%, respectively (Figure 5.3). With ~11%, the western Himalaya takes an intermediate position. Extreme cases are located in the southern central Himalaya, where up to the entire lower-half lengths of some glaciers are quasi-stagnant. In contrast, quasi-stagnant ice is virtually absent in the Karakoram and West Kunlun Shan. Glaciers with >5% quasi-stagnant ice have at least 10%, but mostly >20% of their areas covered with debris, with the exception of one glacier from the Karakoram and two glaciers from the West Kunlun Shan, which have no debris cover.
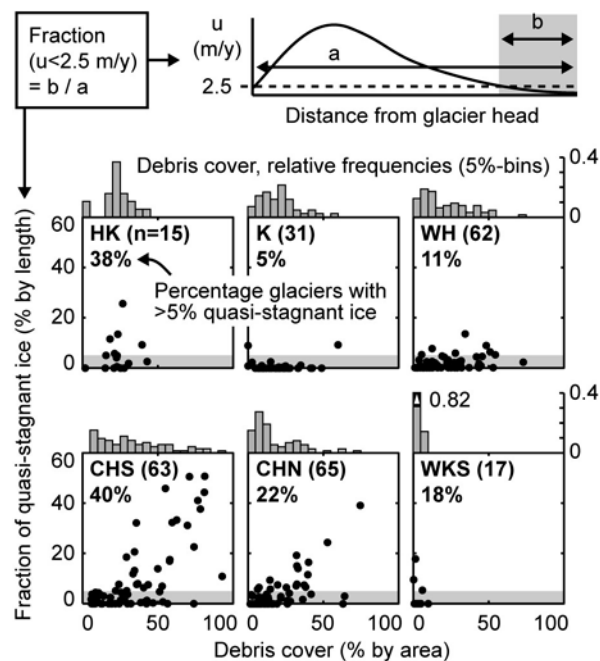
Figure 5.3: Extent of quasi-stagnant ice and debris cover for each geographic region: Hindu Kush (HK), Karakoram (K), western Himalaya (WH), southern central Himalaya (CHS), northern central Himalaya (CHN), and West Kunlun Shan (WKS). Histograms above plots give relative frequency of debris cover in 5% bins.

5.4   Frontal changes 2000-2008

Between 2000 and 2008, both retreating and advancing glaciers are observed in each geographic region, and the range in mean annual frontal changes is large (-80 to +40 m/yr) (Figure 5.4a). Glaciers in the Karakoram constitute the largest fraction of advancing glaciers compared to the other regions. In fact, 58% of the studied glaciers from the Karakoram were advancing, but mostly at slow rates with a mean velocity of ~8 m/yr. This is in contrast with all other regions,

where at least 65% of the analyzed glaciers were retreating. The highest concentration of retreating glaciers (≥80%) and also some of the highest rates (~60 m/yr) characterize the western Himalaya, the northern central Himalaya, and the West Kunlun Shan. In the southern central Himalaya, and the Hindu Kush, 65% and 73% of the studied glaciers have been retreating during the study period, respectively, but at slower rates.

In general, mean-annual frontal changes converge towards zero when an increasing fraction of the glacier terminus is quasi stagnant, i.e., flows at velocities <2.5 m/yr (Figure 5.4b). When >~10% of the glacier (by length) is quasi-stagnant, mean-annual frontal changes are statistically indistinguishable from stable glacier fronts.
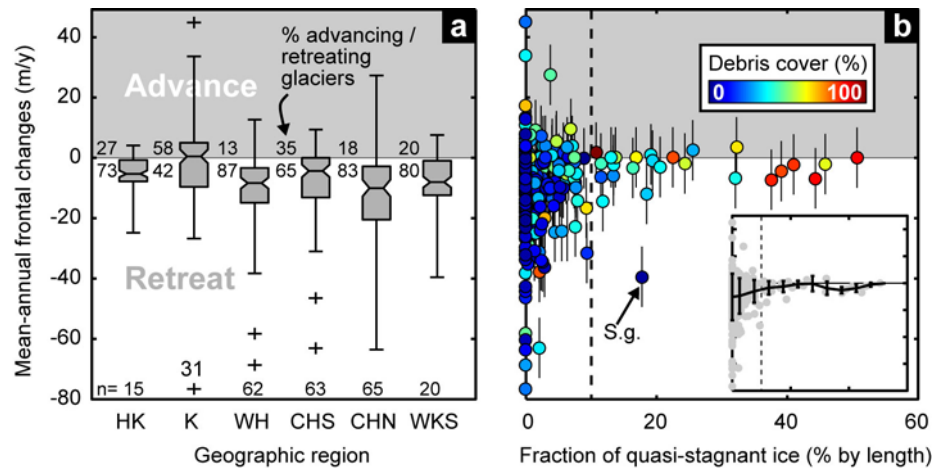
Figure 5.4: Mean-annual frontal changes between 2000 and 2008. (a) Box-and-whisker plots showing the distribution of mean-annual frontal changes for the studied regions. Boxes extend from 25th to 75th percentiles and include a bar at the median value. Notches at the side of the bars indicate 95%-confidence intervals. Whiskers extend to the last data point within 1.5 times the interquartile data range, crosses denote data points outside this range. Numbers left of boxes indicate percentage of advancing (top) and retreating (bottom) glaciers. Numbers at bottom indicate the number of glaciers per region. (b) Scatter plot of mean annual front migration rate versus fraction of velocity profile with surface velocity < 2.5 m/y. Marker-symbol colors denote the areal fraction of debris cover. Inset figure shows mean (+/-1σ) advance/retreat rates for glaciers within bins of 0.05. 's.g.' (surging glacier) refers to a glacier that presumably surged in the recent past (see discussion) and has been omitted for calculating binned means in inset.

5.5   Discussion

Our data show that stagnant, debris-covered glacier fronts are a widespread phenomenon across much of the central Himalaya, and also exist in the western Himalaya and Hindu Kush. These have been previously identified only in the Khumbu Himal, Nepal [*Quincey et al.*, 2007, 2009; *Scherler et al.*, 2008], where they are often associated with abundant and sometimes rapidly growing melt-water ponds and supraglacial lakes that reflect their present disequilibrium with climate [*Ageta et al.*, 2000; *Benn et al.*, 2000].

The insulating effect of thick debris cover significantly modifies glacial mass balances in the ablation zone of the glaciers and reduces the efficiency of radiative heat transfer to the ice [*Østrem*, 1959; *Matson et al.*, 1993]. Consequently, the mass-balance effects of decadal to centennial variations in solar radiation [e.g., *Huss et al.*, 2009] or albedo due to dust [e.g., *Oerlemans et al.*, 2009] or atmospheric soot deposition [e.g., *Xu et al.*, 2009] are reduced. Such effects may have a stronger impact on surface-radiation budgets in the accumulation areas, but these are frequently located at very high elevations, where meltwater usually refreezes in the snow pack and only evaporation removes the ice mass permanently [e.g., *Ageta et al.*, 1989; *Aizen et al.*, 2002].

The extent of stagnant glacier segments is partly coupled to the areal fraction of debris cover (Figure 5.3). Glaciers with large portions of quasi-stagnant ice tend to have higher fractions of debris cover, but not every glacier with a high fraction of debris cover has quasi-stagnant ice. The results of section 4 document that the fractional debris-covered areas of the glaciers analyzed in this study increase with mean slope angles in the accumulation areas (Figure 5.5a), suggesting that mass wasting from steep adjoining hillslopes accounts for most debris cover on the glacier surface. However, the development of stagnant, not moving glacier ice requires gravitational driving stresses to be low [*Paterson*, 1994], which is counteracted by steep glacier beds. Therefore, stagnant ice is usually found where the termini of debris-covered glaciers have shallow gradients of <8°. The largest fractions of quasi-stagnant ice occur at gradients of ~2-5° (Figure 5.5b). At glacier-surface gradients of <2° [*Reynolds*, 2000], and where lateral moraines form natural barriers, moraine-dammed melt water lakes may form, which potentially accelerate glacier wastage and retreat of the terminus position at an advanced stage of glacier wastage [*Kirkbride*, 1993]. It is difficult however, to predict the speed at which these processes occur, which likely depend on a combination of static and dynamic factors [*Kirkbride and Warren*, 1999].
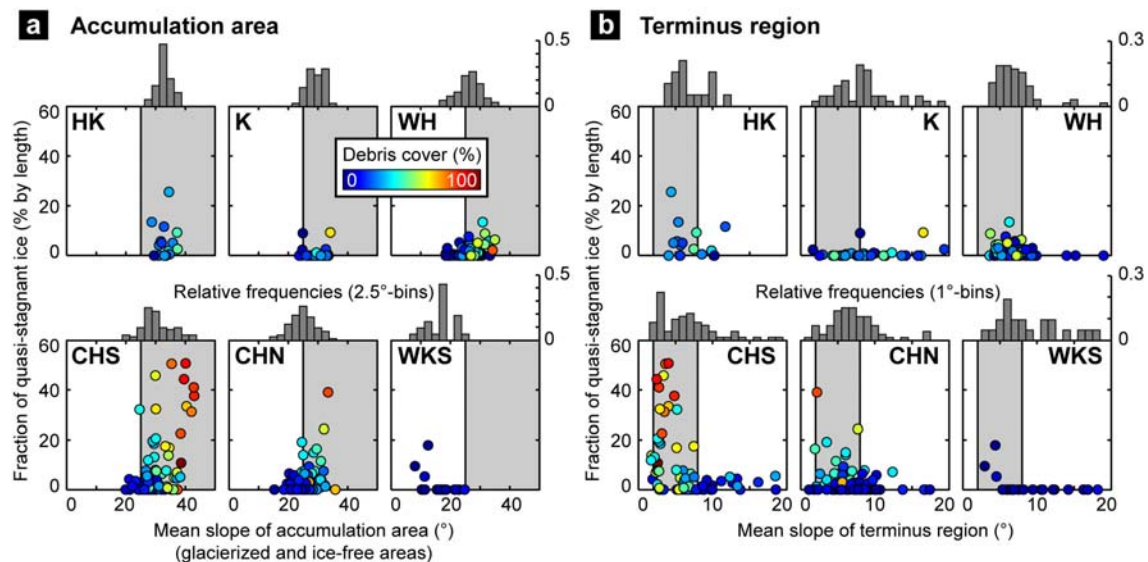
Figure 5.5: Topographic characteristics of accumulation areas and terminus regions. (a) Mean slope of accumulation areas (catchment and glacier areas above snowline) versus fraction of quasi-stagnant ice. Gray area denotes mean slope angles >25°, which promote rock falls and snow avalanches [*Luckmann*, 1977]. (b) Mean slope of terminus region (lowermost 2 km of the glaciers) versus fraction of quasi-stagnant ice. A mean slope of the terminus region between 2° and 8° promote the development of quasi-stagnant ice. Histograms above each plot show relative frequencies along the x-axis. Color-coding depicts areal fraction of debris cover.

Differences in the distribution of quasi-stagnant debris-covered glaciers between the southern and northern central Himalaya are most likely related to topographic differences. Steeper accumulation areas in the southern part account for generally more debris-covered glaciers (section 4) that are prone to in-situ decay and the development of quasi-stagnant termini (Figure 5.5a). Although glaciers in the northern part have relatively shallow termini, only few glaciers with high amounts of debris cover are characterized by quasi-stagnant ice, and on average, we observe the regionally highest retreat rates. The number of studied glaciers from the Hindu Kush is limited but indicate similar behavior as in the southern central Himalaya, with a high portion of partly debris-covered glaciers that are quasi-stagnant and which show only minor frontal changes (Figure 5.4a). Conversely, our data from the Western Himalaya suggest glacier behavior similar to the northern central Himalaya, with reduced steepness of the accumulation

areas leading to lower fractions of debris cover. Despite shallow termini, these areas have only minor amounts of quasi-stagnant ice and we observed the regionally largest fraction of retreating glaciers.

In contrast, in the West Kunlun Shan, accumulation is mostly by direct snow fall and the studied glaciers have no or very little debris covers. Consequently, there are no stagnant glaciers with thick debris mantles, and retreating glaciers dominate. However, three of the studied glaciers have quasi-stagnant portions extending ~5-20% of their lengths upstream from their terminus. Closer inspection and comparison of our ASTER imagery with Landsat MSS and TM satellite images, from 1977 and 1990 respectively, revealed that these glaciers are probably recovering from surge events in the past. In fact, our imagery documents an active surge phase of a West Kunlun Shan glacier (35°16'N, 80°48'N) between 2000 and ~2003. All other stagnant glaciers identified in this study show no signs of recent surges, but have significant areal fractions of debris cover.

In the Karakoram, accumulation areas are relatively steep (mean slope angles between 25 and 35°), debris cover and shallow termini (<8°) are frequent (Figure 5.3, Figure 5.5), but stagnant glaciers are nearly absent. Viewed together with >50% stable or advancing glacier fronts, this suggests different recent mass-balance conditions compared to their Himalayan neighbors. Based on meteorological station data from the Hindu Kush, Karakoram, and western Himalya, *Fowler and Archer* [2006] speculated that regionally disparate climatic changes, mostly in summer temperatures, may account for thickening and advance of Karakoram glaciers as reported by *Hewitt* [2005]. Although this provides a plausible explanation, our data suggest significant differences in glacier behavior between the Karakoram and the Western Himalaya and Hindu Kush, which are not compatible with the temperature records [*Fowler and Archer*, 2006].
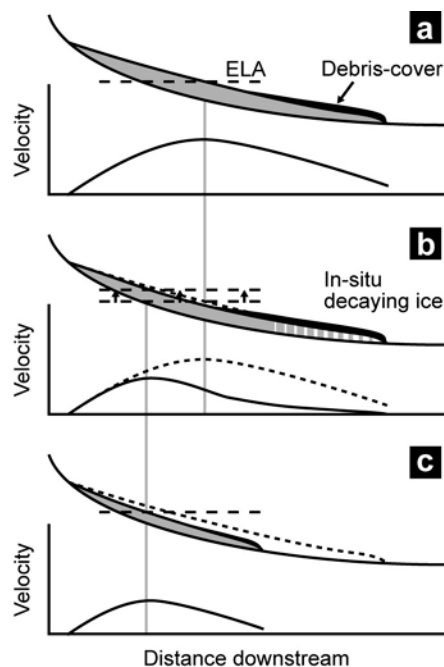
Figure 5.6: Conceptual response of a debris-covered glacier in a climate-warming scenario. In (a) and (c), the glacier is in equilibrium with climate and the surface-velocity profile has a characteristic shape with a maximum near the equilibrium line altitude (ELA), where the ice flux is highest. In (b) an upward shift of the ELA is followed by glacier thinning, particularly in debris-free areas, and rapid response of the glacier-flow velocities. The glacier's geometry takes longer to adjust due to debris cover that retards melting of the lower part, which flows at very low velocities and eventually decays in-situ.

5.6   Conclusions

In the greater Himalayan region, glaciers with quasi-stagnant portions extending several kilometers upstream from their terminus are widespread. Their formation is promoted by glacier surface gradients of ~2-5°, but requires significant supraglacial debris cover, which mostly depends on the steepness of the accumulation area. The presence of quasi-stagnant ice at glacier termini hampers changes of their fronts. Although our data on frontal changes covers only 8 years, long-term studies of Khumbu Glacier [e.g., *Bolch et al.*, 2008], for example, show that the front of a heavily-debris covered glacier can be stable for decades while the glacier is simultaneously downwasting and decaying. Consequently, observations of frontal changes from debris-covered glaciers should be interpreted with care. In particular, stable glacier fronts or changes in retreat rates on annual to decadal timescales may be unrelated to short-term climatic variations and the actual glacier condition. In such cases, glacier-surface velocity data help identify quasi-stagnant ice and glaciers with potentially complex frontal histories (Figure 5.6). Regional topographic differences largely account for the prevalance of stagnant debris-covered glaciers in the southern central Himalaya. The absence of such glaciers in the Karakoram, combined with a high fraction of advancing or stable glacier fronts, suggests regionally different mass-balance regimes.

6   Timing and extent of Late Quaternary glaciation in the western Himalaya constrained by ^{10}Be Moraine dating in Garhwal, India

Abstract

Glacial chronologies from the Himalayan region indicate various degrees of asynchronous glacial behavior. Part of this has been related to different sensitivities of glaciers situated in contrasting climatic compartments of the orogen, but so far field data in support for this hypothesis is lacking. Here, we present a new 10Be-derived glacial chronology for the upper Tons valley in western Garhwal, India, and initial results for the Pin and Thangi valleys in eastern Himachal Pradesh. These areas cover a steep gradient in orographic precipitation and allow testing for different climatic sensitivities. Our data provide a record of five glacial episodes at ~16 ka, ~11-12 ka, ~8-9 ka, ~5 ka, and <1 ka. In the Thangi valley, our results indicate a glacial episode at ~19 ka, but no data are available for younger glacial deposits in this valley. At their largest mapped extent (15-16 ka), the main glaciers in the upper Tons valley joined and descended down to ~2500 m asl, which represents a drop of ~1400 m compared to the present-day glacial extent. During the Holocene the two largest glaciers produced distinct glacial landforms that allowed us to reconstruct changes in the Equilibrium Line Altitude (ELA) over ~20 km north-south distance that is presently associated with a steep gradient in rainfall. We observe that ELA-changes have been consistently ~2 times higher for the glacier located in a presently wetter climate, pointing at different climate sensitivities, related to the amount of precipitation that they receive. At regional scale, our data is in reasonable agreement with other published glacial chronologies from the western Himalaya and suggest that glacial advances during the Holocene have been largely synchronous in this region. Comparison of glacial chronologies from the western Himalaya with other palaeoclimatic proxy data suggests that long-term changes in glacial extents are controlled by glacial-interglacial temperature oscillations related to the waxing and waning of the large northern-hemisphere ice sheets, while the timing of millennial-scale advance-and-retreat cycles are more directly related to monsoon strength.

6.1   Introduction

Information on the geographic extent and magnitude of Quaternary glaciations in the Hindu Kush, Karakoram and Himalaya (hereafter termed the HKH) region is important for understanding the climatic, erosional, and tectonic evolution of this large orogenic system. Furthermore, particularly in light of global warming, climate variability, and associated societal impacts, it is important to characterize and quantify past glacial changes for a better assessment of regional and global forcing factors of future glacier behavior. Despite a growing body of field and chronologic data, there is no general consensus concerning the timing, extent, and climatic forcing of glaciation in the Himalayan region and adjacent interior of Eurasia [e.g., *Gillespie and Molnar*, 1995; *Back et al.*, 1999; *Owen et al.*, 2008]. Previous studies have shown that glaciers in the HKH region and Tibet attained their maximum extent earlier than northern-hemisphere ice sheets during the last glacial period [e.g., *Gillespie and Molnar*, 1995; *Benn and Owen*, 1998; *Finkel et al.*, 2003; *Owen et al.*, 2005, 2008]. This has been attributed to sensitivity

of these glaciers to the strength of the Indian summer monsoon, which was reduced during the global Last Glacial Maximum (LGM), i.e., MIS 2 [*Overpeck et al.*, 1996]. Yet, differences in the timing of glacial advances even within Asia have caused some confusion. For example, *Owen et al.* [2005] proposed that glaciers in humid areas advanced due to changes in precipitation whereas glaciers in more arid areas are temperature driven and advanced synchronously with northern-hemisphere ice sheets. In contrast, *Zech et al.* [2009] recently suggested that glaciers situated in orographically shielded areas are more sensitive to changes in precipitation; whereas glaciers that receive high amounts of precipitation are more sensitive to changes in temperature. *Rupper et al.* [2009] investigated the effect of enhanced monsoon circulation during the mid Holocene on glacier-mass balance and found that increases in accumulation due to higher precipitation were presumably much smaller than reductions in ablation due to lower temperatures, as a result from increased cloudiness and evaporative cooling. Thus, despite agreement on the importance of monsoon strength for glacier behavior in the Himalayan realm, the exact mechanisms, timing, and geographic extent of monsoonal influence is debated. To resolve these discrepancies we need to better understand (1) how glaciers in different climatic compartments of an orogen, respond to climatic changes and (2) how gradients in the amount or seasonality of precipitation affect the relative sensitivity of the glacial systems.

In this study, we use field mapping and [10]Be-surface exposure dating of erratic boulders on moraines to establish a glacial chronology for the upper Tons valley in western Garhwal India (Figure 6.1). This area lies at the western end of the Bay of Bengal monsoon branch [*Barros et al.*, 2004] and marks the transition from a summer to a winter precipitation maximum farther northwest [*Wulf et al.*, 2010; *Bookhagen and Burbank*, in press]. In addition, we obtained initial results for the Pin and Thangi valleys, which lie approximately 40 km north of the high Himalayan orographic barrier and receive moisture mainly by the northern hemisphere winter westerlies (Figure 6.2). Combined with previously published glacial chronologies influenced to different extents by these two moisture regimes, we assess the impact of the moisture regime on glacial behavior in the western Himalaya.
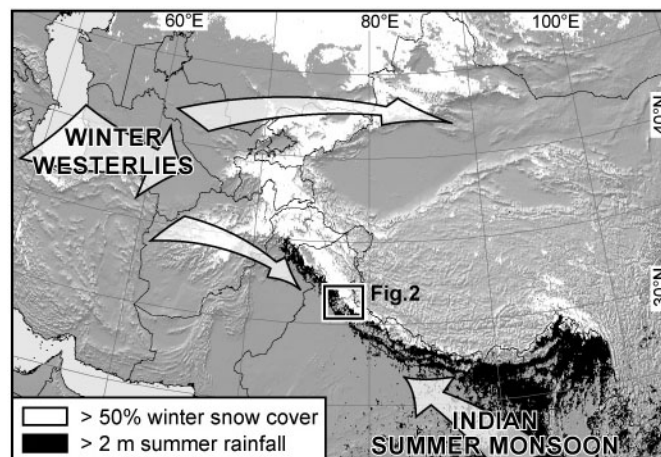
Figure 6.1: Regional setting of the study area and climatic conditions indicating the different seasonal moisture sources. The western Himalaya receives moisture from both the Indian summer monsoon and the winter westerlies, indicated by mean winter (November to April) snow cover (based on Moderate Resolution Imaging Spectroradiometer data from 2001-2008; [*Hall et al.*, 2002]) and mean summer (May to October) rainfall (based on calibrated Tropical Rainfall Measuring Mission data from 1998-2008; [*Bookhagen and Burbank*, in press]), respectively. White areas are covered >50% of the winter season by snow and black areas receive >2 m of rainfall during summer.

6.2   Climatic framework

The climate of the western Himalaya is influenced by two atmospheric circulation systems: the Indian monsoon during summer and the northern-hemisphere westerlies during winter [*Singh and Kumar*, 1997; *Barry*, 2008]. Monsoonal moisture reaches the area from June to September and originates in the Bay of Bengal, from where it is transported by north and westward-travelling mesoscale depressions [*Gadgil*, 2003; *Barros et al.*, 2004]. Snowfall during summer, when snowlines are high, is usually limited to elevations >5000 m [*Singh and Kumar*, 1997]. However, a large amount of monsoonal moisture is orographically forced out along the steep southern front of the High Himalaya at elevations <4000-5000 m, resulting in reduced quantities for the higher, glacierized regions (Figure 6.2; [*Bookhagen and Burbank*, 2006; *Wulff et al.*, 2010]). Westerlies-derived precipitation during winter and early spring is associated with low-pressure systems known as Western Disturbances (WD), which are linked to troughs in the upper tropospheric westerly jet [*Lang and Barros*, 2004; *Dimri*, 2006]. The moisture sources for winter snowfall lie in the far west, including the Mediterranean, Black, and Caspian Sea, which results in a decrease of winter snowfall eastwards. In contrast to summer rainfall, winter snowfall increases with elevation [*Barros et al.*, 2000] and reaches values of as much as 2 m snow water equivalent (swe) at elevations >4000-5000 m [*Raina et al.*, 1977]. Thus, despite large amounts of monsoon precipitation along the Himalayan front, a large part of the moisture that nourishes glaciers in the western Himalaya is associated with the winter westerlies. The climatic snowline in the western Himalaya climbs from ~4600 m at the orogenic front to ~5600 m above sea level (asl) in the orogenic interior and is therefore at a lower elevation than in the central Himalaya [*von Wissmann*, 1959] (Figure 6.2).
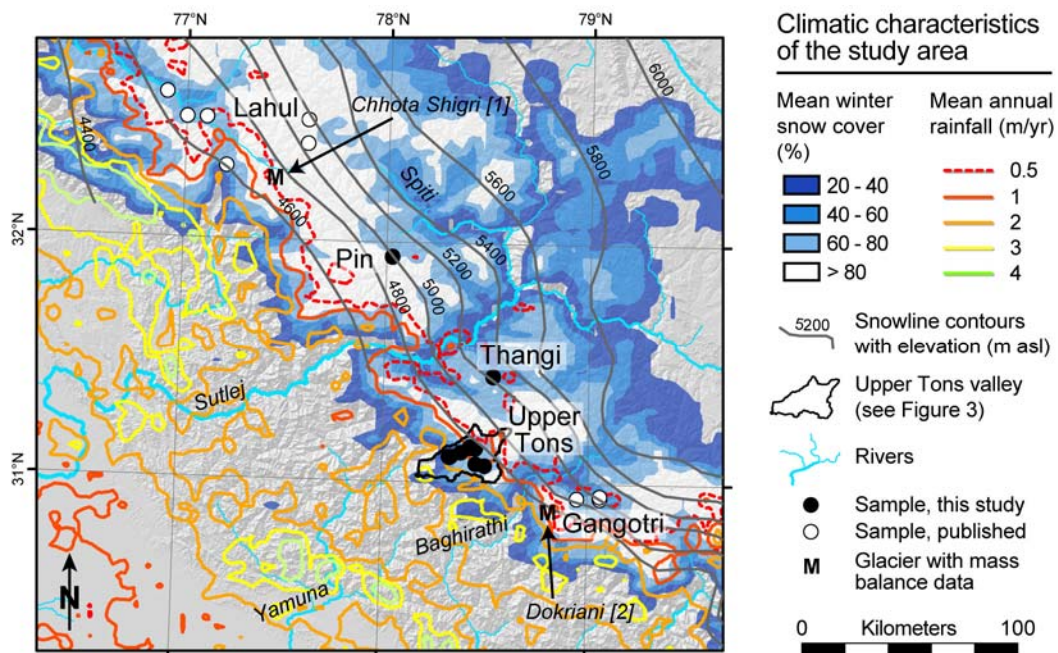
Figure 6.2: Hillshade map of the study area and surrounding regions in the western Himalaya. See Figure 1 for location. Gridded climate data after *Hall et al.* [2002] and *Bookhagen and Burbank* [in press]. The upper Tons valley is outlined by a black polygon and depicted in more detail in Figure 6.3. Regional climatic snowline elevations in gray are taken from *von Wissmann* [1959]. References to glacier mass balance studies: [1] *Wagnon et al.* [2007]; [2] *Dobhal et al.* [2008].

6.3   Study area

6.3.1   Tons valley

The Tons valley belongs to the westernmost headwaters of the Ganges River and is located in between the range-crossing Bhagirathi and Sutlej Rivers. The Tons valley receives abundant precipitation during summer from the Indian monsoon, and also considerable amounts during winter from western sources (Figure 6.2). The rocks in the glaciated part of the upper Tons valley are dominated by granites and gneisses of the High Himalaya Crystalline series. Glaciers are found north of the 6316 m high Bandarpunch peak in the Govind Pashu National Park. The two most prominent glaciers are the Jaundhar and Bandarpunch Glaciers, which presently have lengths of ~15 km and ~10 km, and terminate at ~4150 m and ~4000 m above sea level (asl), respectively (Figure 6.3). Jaundhar glacier appears to have detached just recently from the shorter glacier that flows out of the steep catchment to the south and which occupies a length of ~3 km of the Tons valley in front of Jaundhar glacier. Remote-sensing derived velocity data [*Scherler et al.*, 2008; unpublished data] from this portion of the glacier tongue show that the lower ~2 km of the ice are currently stagnant and appear to be down wasting. As these two glaciers have most likely been connected during all of the glacial stages we dated in this study, we refer these two glaciers together as Jaundhar glacier.
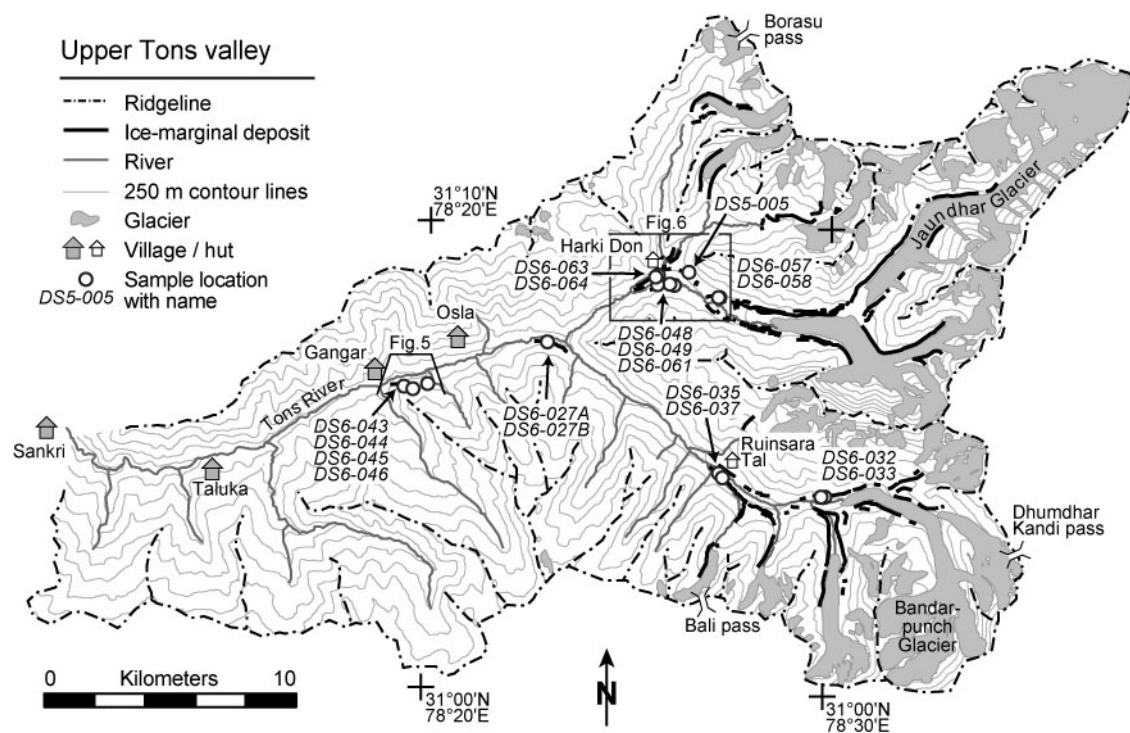
Figure 6.3: Geomorphic overview of the upper Tons valley. See Figure 6.2 for location. Sample locations are shown by white circles, present-day extent of glaciers shaded in gray.

6.3.2   Thangi and Pin valleys

The Thangi and Pin valleys are situated ~40 km and ~90 km to the north and northwest of the Tons valley, respectively (Figure 6.2). In both valleys, Higher Himalayan Crystalline granites crop out in the uppermost part of the valleys and are overlain by weakly deformed rocks of the Tethyan Himalaya that constitute the valley walls farther downstream. Both valleys are characterized by a semi-arid to arid climate. Although direct meteorological measurements from within these valleys are not available, nearby meteorological stations suggest that winter

snowfall from westerly sources accounts for most of the annual precipitation [*Wulf et al.*, in press]. The Pin valley is larger than the Thangi valley and has two main branches, the southern Pin and the northern Parahio branch that both show ample evidence for glaciations in their headwaters. We examined the southern Pin branch, and mapped and sampled moraines towards the Pin-Bhaba pass. Glaciers in the Thangi valley are generally associated with southern tributaries and the Kinner Kailash massif, whereas northern tributaries are devoid of any significant ice accumulation. Geomorphic evidence for past glacial advances is restricted to tributary valleys and indicates more restricted glacier extents compared to the Tons and Pin valleys. We examined the tributary valley south of the village Surting that leads to the Charang pass into the Baspa valley.

6.4   Materials and Methods

6.4.1   Sampling and geomorphic interpretation

We used in-situ produced cosmogenic ^{10}Be surface exposure dating of erratic boulders on lateral and terminal moraines. A detailed review of the method, the physical background, and associated uncertainties can be found in *Gosse and Phillips* [2001]. The absolute accuracy of exposure dating using terrestrial cosmogenic nuclides (TCNs) still suffers from a number of uncertainties that hamper the interpretation of ages obtained from glacial boulders, and tying glacial extents to other absolutely dated climate records [e.g., *Putkonen and Swanson*, 2003; *Owen et al.*, 2008]. In this study we follow the view that erosion and exhumation of boulders on moraines is a more likely process than prior exposure [*Hallet and Putkonen*, 1994; *Zreda and Phillips*, 1995; *Putkonen and Swanson*, 2003; *Schaefer et al.*, 2008]. This inference is supported by our field observations of boulder-rich moraine surfaces proximal to the present-day glaciers and increasingly smoothed surfaces on successively older, more distal moraines. Accordingly, the obtained ages are understood as minimum age estimates for moraines which are interpreted to record the maximum glacier extent during a glacial stage and the beginning of retreat. Thus, among a set of exposure ages derived from one or several nearby moraines that were formed during the same glacial event, we regard the oldest boulder age as the one most closely approximating the true age of the moraine. This interpretation may only be violated in cases of obvious outliers that are much older than most other ages, and therefore display either erroneous landform assignment or nuclide inheritance. Furthermore, in an undisturbed morphostratigraphic setting older moraines are associated with a greater extent of the former glacier and thus lower elevations in the catchment, where precipitation and erosion rates usually increase [*Bookhagen and Burbank*, 2006], resulting in greater potential for moraine degradation and boulder erosion. Therefore, we assume that the mismatch between the true age of the moraine and the boulder age increases with age and denudation rates. To minimize geomorphic uncertainties, we preferably sampled large boulders (>2 m height) that indicated no sign of toppling and appeared to be stably embedded in the moraine deposit. We sampled the uppermost 2-3 cm of the boulder top, but avoided surfaces that showed any evidence of exfoliation or fracturing. We recorded the geometry of the sampled boulders and their top surfaces and topographic shielding at each site. In the Tons valley, we sampled predominately granitic boulders >2 m tall, along with a few smaller gneissic boulders. In the Pin valley, exclusively quartzite was sampled (Tethyan Sediments), with generally small size (~0.5 m tall). In the Thangi valley the sampled boulders are granites and slightly taller (~1 m).

Table 6.1: Cosmogenic ^{10}Be surface exposure data of samples.

Sample ID	Valley	Lithology	Latitude (°N)	Longitude (°E)	Elevation (m asl)	Boulder dimensions (m)			Mean sample thickness (cm)	Assumed sample density (g/cm³)	Topographic shielding	10Be (atoms/g Qz) ± 1σ	
						Length	Width	Height					
DS05-05B	Tons	Granite	31.1489	78.4272	3495	2.2	2	1.5	2.5	2.65	0.98	172847	± 4260
DS6-27A	Tons	Granite	31.1246	78.3825	3010	3.5	4	2.5	2	2.65	0.96	348447	± 5442
DS6-27B	Tons	Granite	31.1246	78.3825	3010	3	3	2.5	2	2.65	0.96	352462	± 5412
DS6-32	Tons	Paragneiss	31.0715	78.4992	4071	1.2	1.5	0.6	3	2.75	0.95	12086	± 551
DS6-33	Tons	Paragneiss	31.0715	78.4977	4046	3	2	0.6	2	2.75	0.97	7688	± 873
DS6-35	Tons	Granite	31.0789	78.4548	3642	4.5	1.9	2.2	2.5	2.65	0.98	16729	± 1065
DS6-37	Tons	Granite	31.0776	78.4564	3658	2.5	1.5	1	2.5	2.65	0.98	370237	± 6273
DS6-43	Tons	Granite	31.1076	78.3233	2661	5	2.5	3.5	3	2.65	0.95	169184	± 2934
DS6-44	Tons	Granite	31.1076	78.3233	2661	2.5	1.5	2	2	2.65	0.95	337456	± 5593
DS6-45	Tons	Granite	31.1067	78.3272	2720	1.8	1	1.3	3	2.65	0.96	359096	± 5620
DS6-46	Tons	Granite	31.1087	78.3331	2725	3.5	3	2.5	2.5	2.65	0.95	393141	± 6510
DS6-48	Tons	Granite	31.1458	78.4346	3544	2.5	2.2	2	2.5	2.65	0.97	344318	± 5547
DS6-49	Tons	Granite	31.1461	78.4327	3514	2.3	2.5	2	2	2.65	0.97	321739	± 5884
DS6-57	Tons	Granite	31.1418	78.4536	3636	2.5	1.5	2.7	2.5	2.65	0.95	13695	± 538
DS6-58	Tons	Granite	31.1418	78.4531	3623	4.5	4	2.5	2.5	2.65	0.94	28171	± 821
DS6-61	Tons	Granite	31.1459	78.4278	3412	2.5	2.5	3.4	2	2.65	0.95	196900	± 4701
DS6-63	Tons	Granite	31.1493	78.4279	3516	3.5	2.5	4	2.5	2.65	0.97	173646	± 4377
DS6-64	Tons	Granite	31.1487	78.4268	3504	4	2.5	4	2.5	2.65	0.98	202168	± 5222
DS6-108	Pin	Quartzite	31.9416	78.0283	3847	1	0.5	0.5	2	2.65	0.98	875178	± 12142
DS6-109	Pin	Quartzite	31.9388	78.0282	3862	1	0.8	0.5	2	2.65	0.98	5507620	± 75309
DS6-110	Pin	Quartzite	31.9368	78.0278	3865	1.5	1.5	1	2	2.65	0.98	345129	± 6495
DS6-128	Thangi	Granite	31.4422	78.5319	4038	2	1.3	0.6	2	2.65	0.97	1057987	± 15998
DS6-129	Thangi	Granite	31.4422	78.5319	4038	2.3	1.6	1.6	2	2.65	0.94	1036104	± 14453
DS6-130	Thangi	Granite	31.4427	78.5328	4047	2.2	1.5	0.7	2	2.65	0.97	933268	± 13280

Process blanks were ~61,669 ± 13,451 10Be atoms, 1.8 ± 3.5% (1σ) of the total number of 10Be atoms in the samples. 1-σ analytical uncertainties for 10Be/9Be ratios were 2.8 ± 2.4%. Be isotope ratios were calibrated to the 07KNSTD3110 standard described in *Nishiizumi et al.* [2007]; samples normalized to 07KNSTD3110 use the revised nominal isotope ratio and revised 10Be decay constant.

Table 6.2: Exposure ages derived from different production rate-scaling models.

Sample ID	Lal(1991)/Stone(2000) Exposure age (ka) (±1σ)	Desilets et al. (2003) Exposure age (ka) (±1σ)	Dunai (2001) Exposure age (ka) (±1σ)	Lifton (2005) Exposure age (ka) (±1σ)	Lal/Stone timedep. Exposure age (ka) (±1σ)
Tons valley					
DS6-33	0.14 ± 0.02	0.17 ± 0.03	0.17 ± 0.03	0.17 ± 0.03	0.16 ± 0.02
DS6-45	14.09 ± 1.29	14.87 ± 1.79	15.13 ± 1.82	14.46 ± 1.47	13.90 ± 1.24
DS6-64	4.83 ± 0.44	5.30 ± 0.63	5.52 ± 0.66	5.28 ± 0.54	4.94 ± 0.44
DS6-32	0.22 ± 0.02	0.27 ± 0.03	0.26 ± 0.03	0.27 ± 0.03	0.25 ± 0.02
DS6-35	0.37 ± 0.04	0.45 ± 0.06	0.45 ± 0.06	0.46 ± 0.05	0.42 ± 0.04
DS6-37	8.24 ± 0.74	8.63 ± 1.02	9.10 ± 1.08	8.50 ± 0.85	8.09 ± 0.71
DS6-48	8.21 ± 0.74	8.65 ± 1.03	9.12 ± 1.08	8.53 ± 0.85	8.06 ± 0.71
DS6-57	0.31 ± 0.03	0.38 ± 0.05	0.38 ± 0.05	0.39 ± 0.04	0.36 ± 0.03
DS6-58	0.65 ± 0.06	0.76 ± 0.09	0.78 ± 0.09	0.77 ± 0.08	0.72 ± 0.07
DS6-61	5.09 ± 0.46	5.54 ± 0.66	5.78 ± 0.69	5.52 ± 0.56	5.17 ± 0.46
DS6-63	4.16 ± 0.38	4.67 ± 0.56	4.96 ± 0.59	4.66 ± 0.47	4.30 ± 0.38
DS05-05B	4.15 ± 0.38	4.66 ± 0.55	4.95 ± 0.59	4.65 ± 0.47	4.28 ± 0.38
DS6-27A	11.36 ± 1.03	12.03 ± 1.44	12.41 ± 1.48	11.73 ± 1.18	11.22 ± 1.00
DS6-27B	11.49 ± 1.04	12.16 ± 1.46	12.54 ± 1.50	11.86 ± 1.20	11.35 ± 1.01
DS6-43	6.82 ± 0.61	7.60 ± 0.90	7.95 ± 0.94	7.55 ± 0.76	6.73 ± 0.59
DS6-44	13.74 ± 1.26	14.58 ± 1.76	14.84 ± 1.79	14.18 ± 1.44	13.56 ± 1.21
DS6-46	15.54 ± 1.43	16.19 ± 1.96	16.42 ± 1.98	15.72 ± 1.61	15.23 ± 1.37
DS6-49	7.76 ± 0.70	8.21 ± 0.98	8.66 ± 1.03	8.12 ± 0.82	7.60 ± 0.67
Pin valley					
DS6-128	19.90 ± 1.85	18.76 ± 2.29	19.06 ± 2.32	18.04 ± 1.85	19.13 ± 1.73
DS6-129	20.11 ± 1.87	18.93 ± 2.31	19.23 ± 2.33	18.21 ± 1.87	19.32 ± 1.75
DS6-130	17.35 ± 1.60	16.65 ± 2.02	17.00 ± 2.05	16.07 ± 1.64	16.86 ± 1.52
Thangi valley					
DS6-108	17.56 ± 1.62	17.00 ± 2.06	17.32 ± 2.09	16.43 ± 1.67	17.08 ± 1.54
DS6-109	153.63 ± 21.06	111.66 ± 17.74	107.88 ± 16.88	104.20 ± 13.65	121.60 ± 14.78

| DS6-110 | 6.67 ± 0.60 | 7.02 ± 0.83 | 7.50 ± 0.89 | 6.96 ± 0.70 | 6.62 ± 0.59 |

Exposure-age calculations were made with the CRONUS-Earth online exposure age calculator, version 2.1, as described in *Balco et al.* [2008]. Throughout the text, we refer to exposure ages calculated with the time-dependent production rate model of *Lifton et al.* [2005] For references to production rate scaling models see *Balco et al.* [2008].

6.4.2   Laboratory procedures and age calculation

We extracted Quartz grains from the 250- to 500-µm size fraction of previously crushed and sieved rock samples, using magnetic and heavy-liquid separation. We isolated and purified the Quartz fraction following the procedure outlined by *Kohl and Nishiizumi* [1992]. Separation of the Beryllium was done according to the technique described by *von Blanckenburg et al.* [2004]. After oxidization the BeO was mixed with Niobium powder and loaded into stainless steel cathodes for determination of the ^{10}Be/^{9}Be-ratio at the Center for Accelerator Mass Spectrometry (AMS) at Lawrence Livermore National Laboratories. The reported ratios (Table 6.1) were determined relative to ICN standard 07KNSTD3110 (^{10}Be/^{9}Be = 2.85 x 10^{-12}), prepared by K. Nishiizumi [*Nishiizumi et al.*, 2007].

All TCN-derived ages presented in this study have been calculated using the CRONUS Earth online calculator (http://hess.ess.washington.edu/math/index.html; see *Balco et al.* [2008]), and applying the time-dependent production rate scaling model of *Lifton et al.* [2005]. When we compare the TCN-derived ages with other absolutely dated climate records, we provide external age uncertainties that include analytical uncertainties in the AMS measurements as well as uncertainties associated with the scaling schemes and the reference production rates [*Balco et al.*, 2008]. Production rates are corrected for skyline shielding which we measured in the field at each sample site. We calculated our final ages assuming an erosion rate of the boulder surface of 0.003 mm/yr, which is at the lower range of bedrock erosion rates reported from granites in other Alpine settings [*Small et al.*, 1997]. We did not perform any snow-cover correction as we assume that the top surfaces of tall boulders protrude above the snow blanket and that wind usually keeps these surfaces free of snow [*Ivy-Ochs et al.*, 1999]. No correction has been made for production rate changes due to surface uplift in the Himalaya. For the short time periods relevant to this study, such errors are negligible and generally very small compared to other uncertainties. The main conclusions we draw are independent of which production rate scaling method we used (Table 6.2).

To compare our results with other published TCN-based glacial chronologies from the Himalaya, we recalculated all published ages using the same scaling methods. We followed the author's notes given in the publications on which samples are reliable and which are likely affected by intense weathering, moraine disturbance, or reworking of older boulders, for example, and excluded such ages from further comparison. In rare cases, the author's interpretation of the sampled deposits as being related to glacial processes is ambiguous. For example, ~5 ka deposits near Skardu, Karakoram, have been interpreted as moraines by *Seong et al.* [2007], but identified as rock avalanche deposits by *Hewitt* [1999], were consequently excluded. Table C1 provides all published and recalculated data used in this study.

6.4.3   Glacier and ELA reconstruction

We identified moraines with orthorectified and co-registered Système Pour l'Observation de la Terre (SPOT) and Advanced Spaceborne Thermal Emission and reflection Radiometer (ASTER) satellite images that have a ground resolution of 2.5-5 m and 15 m, respectively and validated glacial features during field work. The mapped and dated moraines enabled us to reconstruct former glacier extents. We focused on the large Jaundhar and Bandarpunch glaciers

that generated abundant moraines and for some of which we obtained exposure ages. We also attempted a reconstruction of the tributary glaciers, which proved more difficult due to the lack of age control (Figure 6.3). Additional uncertainties are associated with the ice surfaces of the former glaciers, which we obtained by linear interpolation of the reconstructed glacier margin elevations that were taken from the 90-m digital elevation model (DEM) from the Shuttle Radar Topography Mission (SRTM). To allow comparison with the reconstructed former glacier surfaces, we interpolated the present-day glacier surfaces in the same way and used these as our present-day reference. Comparison of the present-day interpolated surface with that derived from the DEM indicates that elevation differences are mostly found in the upper accumulation area and are on average -6 ± 27 (1σ) m and 2 ± 36 m for Bandarpunch and Jaundhar glacier, respectively.

From the reconstructed glacier surfaces, we estimated the equilibrium line altitude (ELA) by means of the accumulation-area ratio (AAR) and the toe-to-headwall altitude ratio (THAR) methods [*Meier and Post*, 1962; *Meierding*, 1982]. Both methods are sensitive to the existence of debris cover, with the result that a wide range of ratios is used [*Clark et al.*, 1994; *Benn and Lehmkuhl*, 2000]. In general, it is thought that glaciers with high amounts of debris cover that reduces ablation have lower AARs as compared to clean-ice glaciers, for which an AAR of 0.65 is usually applied [*Benn and Lehmkuhl*, 2000]. Recent glaciological studies on the nearby Chhota Shigri [*Wagnon et al.*, 2007] and Dokriani glaciers [*Dobhal et al.*, 2008] (Figure 6.2), which are of similar length but carry less debris cover, suggest zero net-mass balance AARs of ~0.7 and an associated ELA of ~4800 m and ~5000 m, respectively. Mass balance studies on debris-covered glaciers in the adjoining Baspa catchment, on the other hand, revealed zero net-mass balance AARs of ~0.45 and ELAs of ~5100-5150 m [*Kulkarni*, 1992]. No mass balance measurements are available for the investigated glaciers and thus steady state ELAs and the corresponding AARs are unknown. Therefore it is not clear which AAR is best applied and we compared ELA-estimates derived from AARs of 0.45, 0.55, and 0.65, and THARs of 0.5 and 0.6.

6.5   Results

6.5.1   Tons valley

We identified five distinct moraine sequences in the upper Tons valley (Table 6.4). Each former ice extent is established on the basis of lateral and terminal moraines (Figure 6.3). The valley floors are generally covered with sediments and we did not find any glacially polished bedrock surfaces suitable for dating. It is possible that earlier glacier advances were more extensive and reached lower elevations, but that subsequent erosion removed any evidence for this.

The lowermost moraine we found is at an elevation of ~2700 m asl, and ~200 m above the present-day valley floor, near the village of Gangar. The lateral moraine is identified as a valley-parallel ridge, which is separated by a 20-30 m wide depression from the hillslope (Figure 6.4B). We sampled two meter-sized boulders on this ridge (DS06-43, -44), which are surrounded by dense, bushy vegetation up to 3 m tall. Without correcting for shielding from vegetation we obtained a minimum model age for these boulders of 7.5 (±0.8) ka and 14.2 (±1.4) ka. The moraine ridge rapidly descends in elevation downstream, indicating the proximity to the former glacier terminus (Figure 6.5). The preservation of this moraine can be attributed to the small contributing area uphill and the convex-outward hillslope, leading to divergent material flux, which both account for limited influx of hillslope material. Continuation of this moraine up valley is indicated by low-sloping portions on the valley walls,

which we interpret as hillslope deposits that formed on kame terraces between the moraine ridge and the adjoining hillslope. We sampled two more boulders from the outermost moraine remnants (DS06-45, -46). As the erosional degradation of the moraine appears to be much stronger, we sampled only very tall granite boulders (>3 m) that are clearly sourced in upstream sectors. These samples yielded minimum exposure ages of 14.5 (±1.5) ka and 15.7 (±1.6) ka. As three of the four sampled boulders from this moraine yielded exposure ages >10 ka, we interpret the much younger age from sample DS06-43 to result from moraine degradation, and boulder exhumation or tipping. Our minimum model age for glacier retreat is therefore ~15.7 (±1.6) ka.
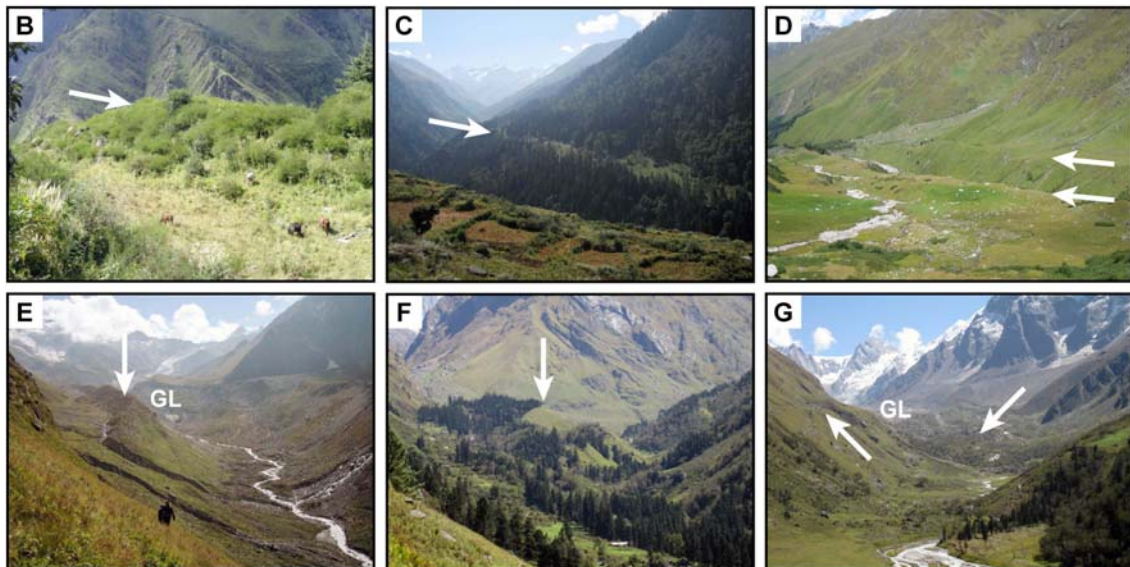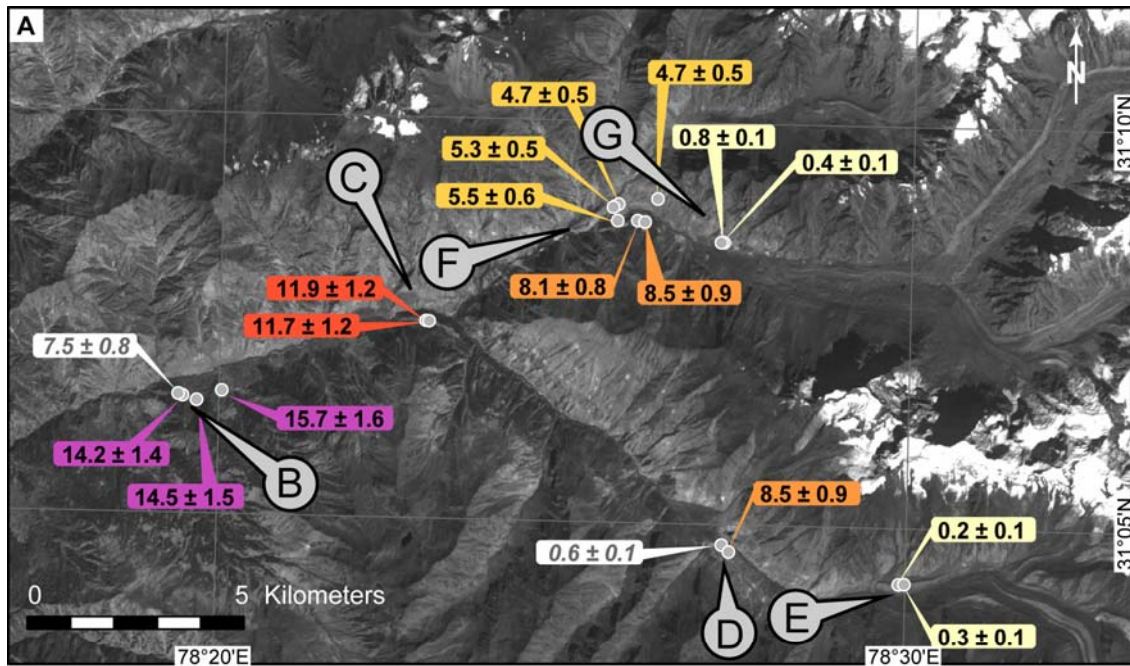
Figure 6.4: Section of the upper Tons valley with geomorphic evidence for glaciation. (A) Orthorectified ASTER satellite image (band 3) with sample locations, and surface-exposure ages of glacial boulders obtained in this study. Letters (B-G) in callouts depict the viewing directions of the photos shown below: (B) latero-terminal moraine near village of Gangar (compare with Figure 6.5). (C) lateral moraine near village of Osla. (D) lateral moraine near lake Ruinsara Tal. (E) Young, inferred Little Ice Age moraines. Note the snout of Bandarpunch glacier in the distance (GL). (F) Moraine complex at Harki Don (compare with Figure 6.6). (G) A series of young recessional moraines in front of the present-day glacier terminus. White arrows in B-G indicate geomorphic features and moraines; a 'GL' indicates the terminus of the present-day glaciers.

The next well identifiable lateral moraine is found ~6 km up valley near the village of Osla at the confluence of the meltwater-rich streams sourced from the Jaundhar and Bandar Punch Glaciers (Figure 6.4B). The moraine is marked by a well defined ridge with numerous tall granite boulders and is separated from the valley wall by a ~100-150 m wide depression. As with the previous moraine deposit, the excellent preservation of this moraine along a length of ~1.5 km can be explained by a small contributing area with divergent material flux. In the center, the moraine ridge is found ~100 m above the present-day river. At its down-valley end, the moraine is only ~70 m above the river which suggests that the former terminus was not far away. We sampled two granite boulders from this moraine (DS06-27A, B), which yielded ages of 11.7 (±1.2) ka and 11.9 (±1.2) ka. The morphology of the moraine suggests that is was formed when ice was exiting the southeastern valley. Most likely, another glacier joined from the upstream north-eastern valley at the same time, as suggested by several other dated moraine deposits nearby (see below). It should be noted that we cannot entirely exclude that other glacial advances formed moraines between deposition of the moraines near Gangar and Osla and which were subsequently removed by erosion.
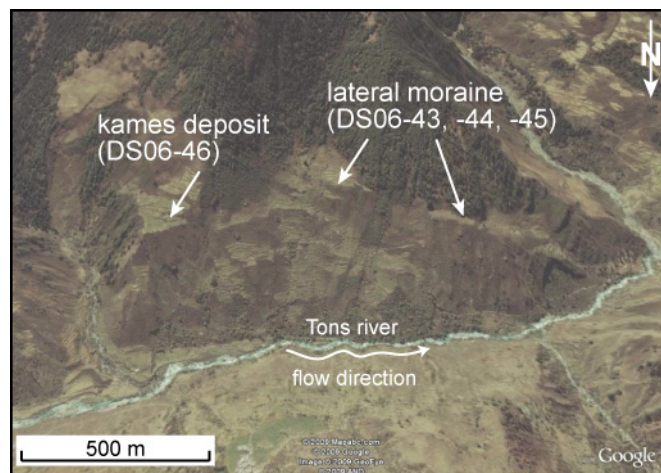
Figure 6.5: Oblique south-directed aerial view of the moraine near the village of Gangar. See Figure 6.3 for location. The Tons River flows in the foreground from east to west (left to right). Note the downstream decrease in elevation of the lateral moraine, indicating proximity of the former glacier terminus. Kame terraces in between the former moraines and the hillslope are presently used for farming. High-resolution satellite image is taken from Google Earth.

A major confluence of three valleys is located ~5 km up the north-eastern valley, at the site of Harki-Don, which also marks a transition in valley morphology from relatively narrow to wide with an anastomosing river system (Figure 6.4E). This transition is associated with a tall ridge of bouldery material that stretches for ~1.5 km along the northern side of the valley before it narrows toward the valley center (Figure 6.6). We interpret this landform as a medial moraine that initially formed due to the confluence of ice from the smaller northern two, and the larger eastern valley. After retreat of the northern glaciers beyond the valley junction, the larger Jaundhar Glacier continued depositing material on this ridge, which then became a lateral moraine. Two large boulders (>3 m) yielded exposure ages of 4.7 (±0.5) ka (DS06-63) and 5.3 (±0.5) ka (DS06-64). From these sample locations, the moraine ridge can be traced farther upstream and we sampled another boulder (DS5-005) on the northern wall of the Jaundhar Glacier valley, i.e., immediately before the junction with the two northern valleys, which yielded an age of 4.7 (±0.5) ka. On the opposite side of the valley, lateral moraines are preserved at three different levels (Figure 6.6). We dated a boulder from the lowermost moraine at 5.5 (±0.6) ka (DS06-61), and two boulders from the intermediate moraine, which provide exposure ages of 8.1 (±0.8) ka (DS06-49), and 8.5 (±0.9) ka (DS06-48). These data suggest that

Jaundhar Glacier terminated near the south-western end of the large medial-lateral moraine ridge at ~5 ka, but extended farther downvalley at ~8 ka. Another 2-3 km upstream, the valley floor remains broad and flat before a series of terminal moraines that are breached only locally by melt water streams indicate proximity to the glacier (Figure 6.4F). Multiple arcuate moraine ridges are found over a distance of ~1.5 km before heavily debris-covered ice becomes visible. Two boulders from the outermost of the series of lateral moraines yield exposure ages of 0.4 (±0.1) ka (DS06-57) and 0.8 (±0.1) ka (DS06-58).
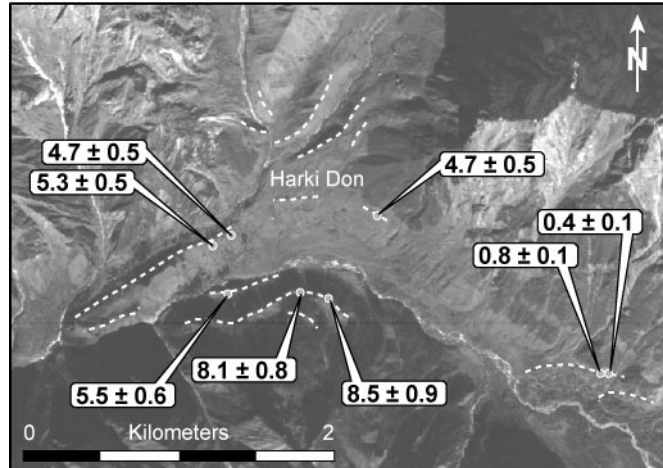
Figure 6.6: Orthorectified SPOT satellite image of the Harki Don moraine complex. See Figure 6.3 for location. The Tons River flows from the lower right corner through the image center to the lower left. White dashed lines indicate moraine ridges. Sample locations are depicted by gray circles and labels show the surface exposure ages in ka. Note the elongated glacial deposits that shift the confluence of the Tons River and the tributaries coming from the northern catchments by ~1.5 km downvalley. See text for geomorphic interpretations.

The southern branch of the upper Tons valley, which leads to Bandar Punch Glacier (Figure 6.3), features a large and prominent lateral moraine that terminates at an elevation of ~3500 m near the lake Ruinsara (Figure 6.4D). The moraine is well preserved and indicates a sustained stable position of Bandarpunch Glacier at this site. We sampled two boulders from the southern side of the moraine, which yield exposure ages of 0.6 (±0.1) ka (DS06-35) and 8.5 (±0.9) ka (DS06-37). The younger age is derived from a boulder located at the lower end of the moraine where moraine degradation and disturbance by rock falls from a steep catchment on the northern side of the valley is possible. In fact, the debris fan associated with this steep tributary catchment is the cause for valley impoundment and formation of lake Ruinsara, which prevented us from sampling the northern moraine ridge. Therefore, we have more confidence in the older age, which also agrees very well with two ages from the less extensive lateral moraine near Harki Don. From this early-Holocene ice extent, the next pronounced moraine farther upstream is found at a distance of ~2 km from the present-day terminus of Bandar Punch Glacier (Figure 6.4D). Two boulders from this moraine yield ages of 0.3 (±0.1) ka (DS06-32) and 0.2 (±0.1) ka (DS06-33), approximately similar to the youngest moraine that we dated in the valley of Jaundhar Glacier. In between this moraine and the Ruinsara stage moraine, no other distinct moraine can be found which could be correlated with the ~5 ka moraine near Harki Don, although some small moraine-like ridges occur in the large ~8.5 ka Ruinsara Tal moraine.

6.5.2   Thangi valley

In the examined tributary of the Thangi valley, the lowermost identified moraine lies at an elevation of ~4000 m, approximately 80 m above the present-day river (Figure 6.7). We

sampled three granite boulders that yielded ages of 18.0 (±1.9) ka (DS06-128), 18.2 (±1.9) ka (DS06-129), and 16.1 (±1.6) ka (DS06-130). We identified at least one, more likely two more lateral moraines in close proximity (<2 km) to the dated moraine. However, these deposits are partly eroded by a stream from a tributary catchment (Figure 6.7). Farther up the valley, the next morphologically clearly discernible glacial landform is a ~1.2 km long terminal moraine that occupies the entire valley width. Immediately behind the moraine is a small melt-water lake with a surface area of ~18,000 m². From here it is another ~3 km until the present-day glaciers are found. Interestingly, no further terminal moraine is found in between. While two ice lobes of the main glacier in this valley clearly terminate above a bedrock knob that marks a step in the longitudinal valley profile, another ice lobe farther south, flows across the bedrock knob and submerges in coarse debris that blankets the valley. Analysis of SPOT satellite imagery suggests that some heavily debris-covered ice still exists close to the steep southwestern valley walls, where it is topographically shielded from direct solar radiation.
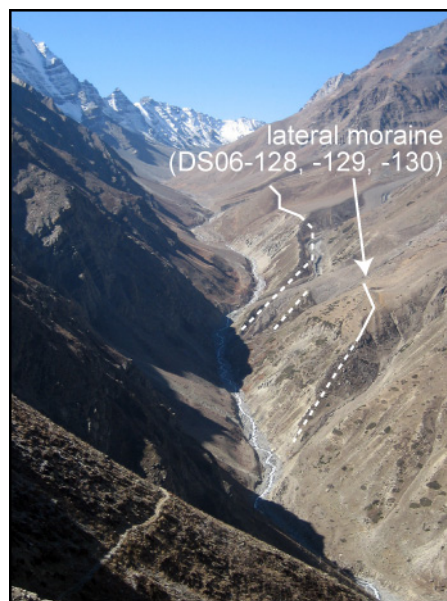
Figure 6.7: Southwest-directed view of the investigated tributary of the Thangi valley. See Figure 6.2 for location. White lines indicate the trace of moraine ridges. We sampled the farthest downstream moraine ridge. The present-day glacier terminus is located approximately 6.5 km upstream.

6.5.3   Pin valley

Former glaciation of the Pin valley was more extensive compared to the Thangi valley. The lowermost glacial deposits constitute impressive long lateral moraines that terminate near the village of Mud, at an elevation of ~3900 m and at a distance of ~20 km from the largest glaciers upstream. In several places, the moraine has been degraded by fluvial erosion or covered by landslide deposits and debris from the hillslopes. We sampled three quartzite boulders on a stretch of moraine which is separated by a ~500-m-wide depression from the nearest hillslope and which yielded ages of 16.4 (±1.5) ka (DS06-108), 104.2 (±13.7) ka (DS06-109), and 7.0 (±0.7) ka (DS06-110). We attribute part of the age scatter to the small size (~0.5 m height) of the boulders, strong foliation and high fissility, which all increase the possibility of enhanced exhumation and erosion affecting the surface exposure history. Due to these age uncertainties we do not consider our results from the Pin valley to be reliable indicators of the local glacial history and refrain from discussing them in detail. From the Mud stage moraine, the next set of moraines is found ~10 km upstream at a river confluence called Paldar (~3960 m asl). More evidence for glaciation exists ~3 km upstream at the next confluence (~4050 m asl). Between

this location and the Pin-Bhaba pass, we did not observe any additional glacial landforms, but instead abundant hillslope deposits forming debris cones and fans on both valley sides that merge in the valley center.

6.5.4   Reconstruction of glacial extents and Equilibrium Line Altitudes (ELAs)

We reconstructed the former glacial extents in the upper Tons and Thangi valleys to determine estimates for former equilibrium line altitudes (Figure 6.8). Our reconstructions in the Tons valley result in a relatively uniform decrease in glacial extents over the last ~16 ka, although the fastest retreat occurred between ~16 ka and 8-9 ka. The retreat of Bandar Punch glacier between ~11-12 ka and ~8-9 ka appears exceptionally large (Figure 6.8), and could be related to the disconnection of several tributaries in between these two glacial stages. An alternative hypothesis that we deem to be less likely, however, is that this glacier did not reach all the way to the ~11-12 ka moraine near Osla, but terminated somewhere in between, where we did not find any moraine remnants. However, the geometry of the Osla moraine suggests that Bandarpunch glacier descended to the confluence at the time of moraine formation (see above).
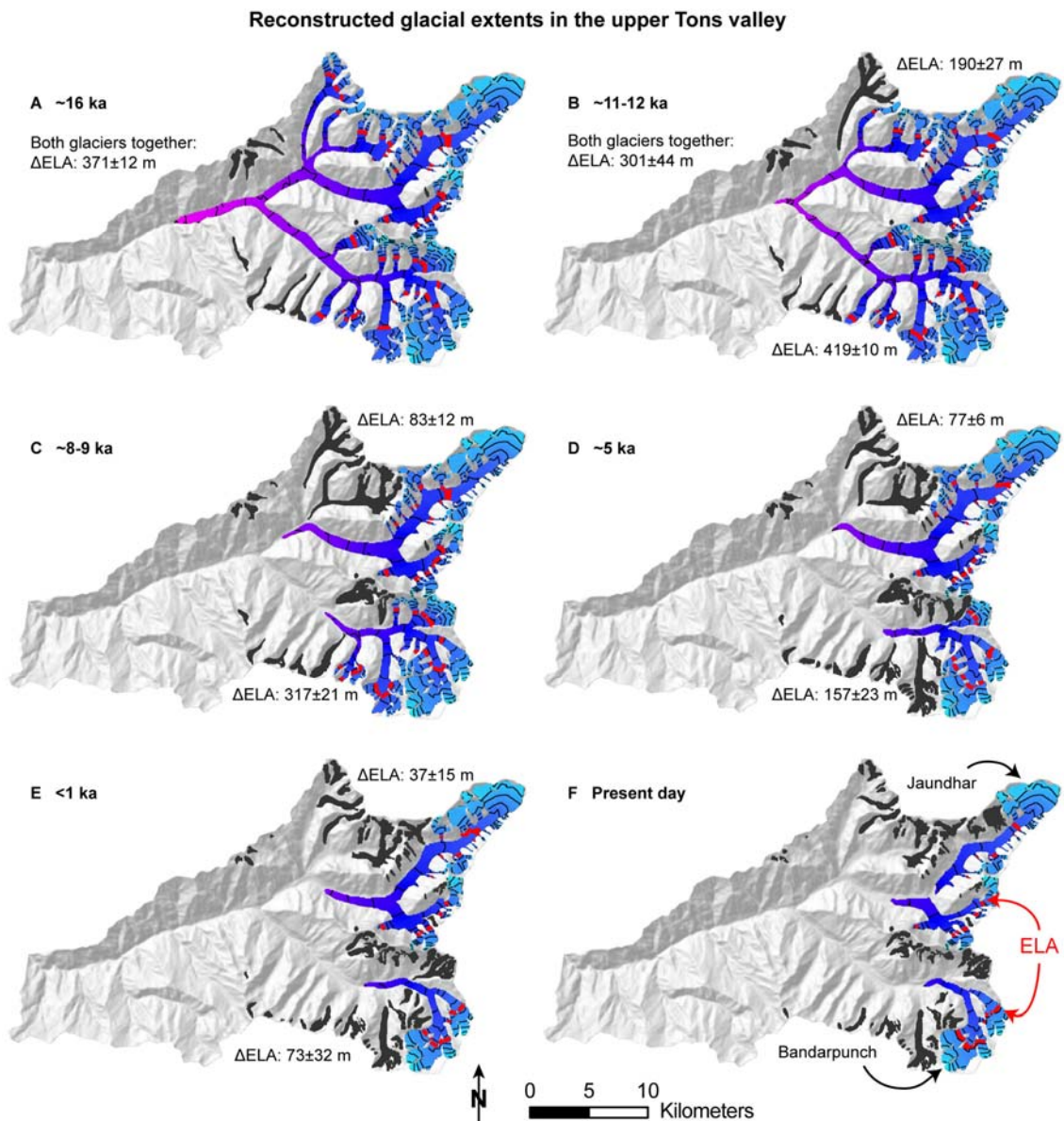
Figure 6.8: Reconstructed glacial extents in the upper Tons valley. Subsets A-F show glacial extents for each moraine sequence dated in this study. Contour lines on the glaciers are in 200 m intervals. Red bold line indicates the

equilibrium line altitude (ELA) derived from the reconstructed glacier surface and an AAR of 0.55. Details of the reconstruction are in the text.
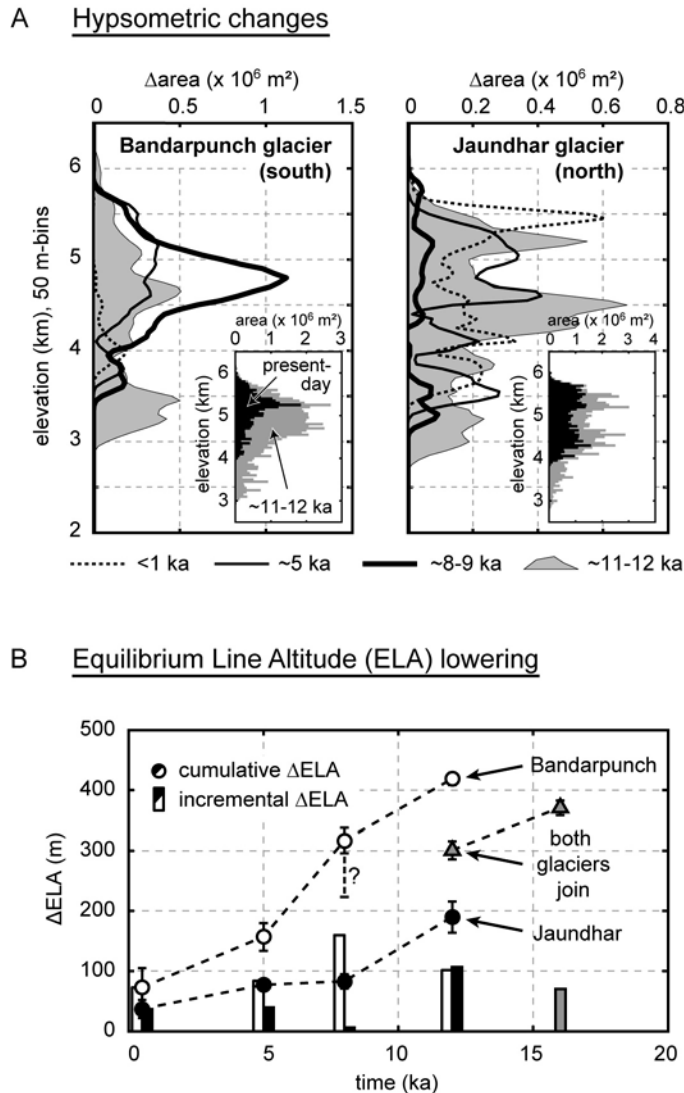
Figure 6.9: Hypsometric and equilibrium line altitude (ELA) changes. (A) Changes in the hypsometry of Bandarpunch and Jaundhar glaciers between present-day and ~11-12 ka, (B) changes of the associated equilibrium line altitudes. The insets in (A) show the hypsometries in 50-m elevation bins. Note the different scales on the axes of the inset diagrams. Although the Jaundhar glacier is aerially larger than the Bandarpunch glacier, the relative changes in area are smaller. The ΔELA-values in (B) represent the average (± 1σ) of the values obtained with the AAR-method (see Table 6.3). Both glaciers formed one glacier system at ~16 ka and most likely already at ~11-12 ka. Note that the relative changes in the ELA are always higher for Bandarpunch than for Jaundhar glacier.

The most difficult part in the reconstruction of glacial extents concerns the timing when tributary glaciers joined the main valley glaciers. This leads to some ambiguity in the stepwise evolution of the glacier hypsometry between some of the glacial stages, and accordingly the derived changes in the equilibrium line altitude (ΔELA). For example, between ~5 ka and ~8-9 ka the ΔELA for Bandarpunch glacier is exceptionally high (Figure 6.9B), because of the large gain in areas at intermediate elevations (Figure 6.9A), which is due to the confluence of two tributary glaciers from southern catchments (Figure 6.8). Yet, if the timing of confluence with the tributary glaciers is incorrect and the derived ΔELA is too high, then the overestimated ΔELA would have to be included in an earlier or later shift in the ELA. The ΔELA-difference between the two glaciers was most likely not that large at ~8-9 ka, but possibly somewhat larger at ~11-12 ka. Thus, it seems that changes in the ELA over the entire period were consistently

higher for Bandarpunch as compared to Jaundhar glacier. The areal distribution of the largest extent at ~16 ka, however, appears relatively robust, because numerous well-preserved moraines suggest that most of the larger tributary glaciers were connected with the main valley glaciers at some time in the past (Figure 6.3).

Table 6.3: Past equilibrium line altitudes (ELAs).

	Present-day	<1 ka	ΔELA	~5 ka	ΔELA	~8 ka	ΔELA	~12 ka	ΔELA	~16 ka	ΔELA
Jaundhar											
Area [km²]	37.1	46.3		54.9		56.9		72.2			
Headwall [m]	5600	5600		5600		5600		5600			
Toe [m][a]	3850	3550		3340		3150		2780			
ELA [m]											
AAR 0.45	5075	5055	20	4995	80	4985	90	4875	200		
AAR 0.55	4845	4805	40	4765	80	4755	90	4635	210		
AAR 0.65	4635	4585	50	4565	70	4565	70	4475	160		
Mean AAR			37±15		77±6		83±12		190±26		
THAR 0.5	4725	4575	150	4470	255	4375	350	4190	535		
THAR 0.6	4900	4780	120	4696	204	4620	280	4472	428		
Bandarpunch											
Area [km²]	19.7	21.2		30.5		49.0		63.3			
Headwall [m]	5500	5500		5500		5500		5500			
Toe [m]	3980	3740		3650	[b]	3510		2800			
ELA [m]											
AAR 0.45	5324	5214	110	5154	170	4984	340	4895	429		
AAR 0.55	5154	5104	50	5024	130	4844	310	4745	409		
AAR 0.65	5024	4964	60	4854	170	4724	300	4605	419		
Mean AAR			73±32		157±23		317±21		419±10		
THAR 0.5	4740	4620	120	4575	164	4505	235	4150	590		
THAR 0.6	4892	4796	96	4760	132	4704	188	4420	472		
Jaundhar and Bandarpunch											
Area [km²]	56.8							135.5		152.4	
Headwall [m]	5550	[c]						5550		5550	[c]
Toe [m]a	3915	[c]						2780		2370	
ELA [m]											
AAR 0.45	5200							4885	315	4815	385
AAR 0.55	5000							4695	305	4635	365
AAR 0.65	4830							4545	285	4465	365
Mean AAR									301±15		371±12
THAR 0.5	4733							4165	568	3960	773
THAR 0.6	4896							4442	454	4278	618

Former ELAs are derived from the accumulation-area-ratio (AAR) method and the toe-to-headwall-ratio (THAR) method. The AAR-derived estimates are based on surface-reconstructions of the glaciers shown in Figure 6.8.. [a] The present-day terminus of Jaundhar glacier refers to that of its southern and largest tributary. [b] The elevation of Bandarpunchs toe at w5 ka is not well constrained. [c] Headwall and toe altitudes are taken as the mean of both glaciers.

The absolute elevation of the ELA is sensitive to the AAR-ratio that is used and varies by ~100-200 m for each 0.1 AAR step (Table 6.3). If we consider an AAR of ~0.45-0.55 for the heavily-debris covered Jaundhar glacier, which is more similar to the adjoining Gara, Gor-Garang, and Shaune Garang glaciers [*Kulkarni*, 1992; *Kulkarni et al.*, 2004], and an AAR of ~0.65 for Bandarpunch glacier, which has a greater affinity to the nearby Chhota Shigri and Dokriani glaciers [*Wagnon et al.*, 2007; *Dobhal et al.*, 2008], we obtain steady-state ELAs of ~4900-5000 m and ~5000-5100 m, respectively.

We attempted to quantify the impact of hypsometric effects, i.e., the confluence of tributary glaciers and associated expansion of the glacier area on ΔELA values by applying the THAR method, which is insensitive to hypsometric changes. In general, the differences in ΔELA between the THAR and AAR methods, and thus the influence of hypsometry effects are larger for Jaundhar as compared to Bandarpunch glacier (Table 6.3). In fact, the ΔELA values

obtained with both methods are quite similar for the Bandarpunch glacier but at larger ELA depressions, different THARs result in ΔELAs over a large range of values.

We also reconstructed glacial extents in the Thangi valley. Due to the limited data, we did this only for the extent at ~18.2 ka and the morphologically pronounced moraine close to the present-day glaciers (Figure 6.10). Although we do not have any ages for this moraine, the lack of any moraines in between, the inferred presence of dead ice, and the unweathered appearance of large amounts of debris without any indication of fluvial modification, suggest that this moraine is rather young (< ~1 ka). Compared to the glaciers of the upper Tons valley, the Thangi valley glacier is smaller and has a simpler geometry. As the true glacier terminus is difficult to locate, we conducted a conservative mapping and restricted the present-day glacier area to the clearly visible, debris-free part, taking into consideration, however that this is an underestimation. The associated ELA we obtained lies at ~5300 m asl, assuming an AAR of 0.65. The ΔELA associated with the next older glacier size is already ~260 m and with the glaciers at ~18.2 ka, it is ~400 m. We suggest that the true present-day ELA is located somewhere between ~5300 and ~5040 m asl and that the ΔELA at ~18.2 ka was therefore most likely <300 m lower.
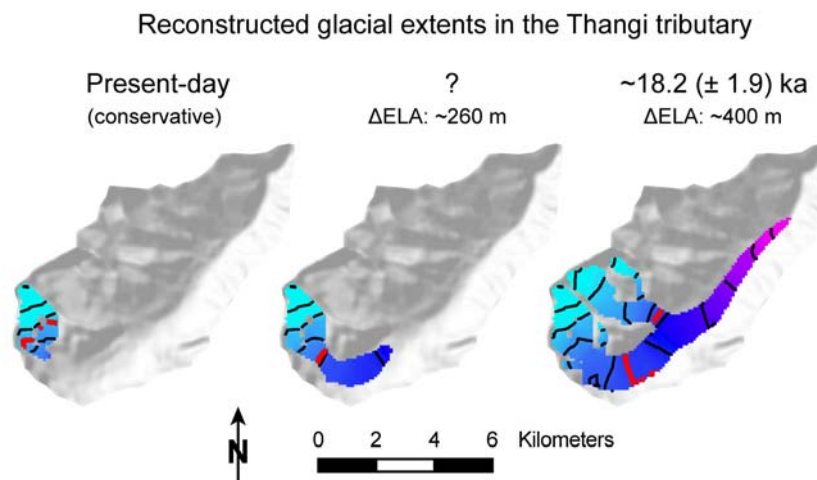
Figure 6.10: Reconstructed glacial extent for the investigated part of the Thangi valley. See Figure 6.2 for location. Contour lines on the glaciers are in 200 m intervals. The red thick contour line indicates the equilibrium line altitude (ELA) derived from the reconstructed glacier surface and an AAR of 0.65. See text for details on the reconstruction.

6.6   Discussion

6.6.1   Late Pleistocene-Holocene glacial history of the western Himalaya

Our new glacial chronology from the Tons valley provides a detailed record of glacial episodes during the end of the last glacial period of the Pleistocene and throughout the Holocene, and thus allows assessing potential climatic forcing mechanisms in this sensitive region of the orogen. However, we are aware that sample numbers for some of the studied moraines and glacial stages are limited, which somewhat complicates assessing the precise timing of moraine formation. Nevertheless, we took great care in choosing sample locations and the scatter among the ages is generally low, providing confidence in our sampling strategy and the obtained results. Confidence in the validity of our data is further strengthened by reasonable agreement with existing data from nearby Lahul [*Owen et al.*, 2001], Gangotri [*Barnard et al.*, 2004], the Nun Kun area in the western Himalaya [*Röthlisberger and Geyh*, 1985], and Nanga Parbat in the far northwestern Himalaya [*Phillips et al.*, 2000]. At least five glacial events can be

recognized that have been dated in at least two different areas of the western Himalaya (Figure 6.11). Boulder ages of ~15-16 ka have been reported from the Bhagirathi valley, ~50 km farther east [*Barnard et al.*, 2004], and Lahul, ~150 km farther northwest of our study area [*Owen et al.*, 2001] (Table 6.4). In addition, *Röthlisberger and Geyh* [1985] dated a glacier advance that took place before ~12,750 ± 190 ^{14}C yr BP in the Nun Kun area. Our boulder ages from the Thangi valley are similar to the oldest ages found in Lahul, where *Owen et al.* [2001] dated boulders from moraines produced by different glaciers in different climatic settings (Figure 6.2), which may explain the large scatter of the ages (Figure 6.11). Thus, an earlier, distinct glacial event in the Thangi valley and Lahul areas is possible, but age uncertainties and the limited amount of data do not yet allow a firm conclusion to be drawn.

Our new ages and existing data from Nanga Parbat [*Phillips et al.*, 2000] provide evidence for a glacial event at ~11-12 ka. However, we could obtain only two ages and the data from Nanga Parbat is subject to significant internal, i.e., analytical uncertainties (Figure 6.11). More data is thus needed to better constrain the timing of this event. The next younger prominent glacial event observed in our study occurred during the early Holocene, and is supported by data from the Bhagirathi valley [*Barnard et al.*, 2004] and the Nanga Parbat area [*Phillips et al.*, 2000]. *Röthlisberger and Geyh* [1985; for calibrated ages see *Owen*, 2008] also dated a major glacier advance at ~8-8.5 ka in the Nun Kun area, but no ages are so far available for moraines of inferred Holocene age in Lahul [*Owen et al.*, 2001]. The ~5 ka moraine at Harki Don in the Tons valley agrees well with the ~5 ka Shivling stage from the Bhagirathi valley, defined by two OSL-ages from aeolian deposits on a lateral moraine [*Sharma and Owen*, 1996] and with Radiocarbon dates from moraines in the Nun Kun area [*Röthlisberger and Geyh*, 1985]. Moraines that are close to the present-day glaciers are ubiquitous but usually not the main target for TCN-dating studies [e.g., *Owen et al.*, 2008]. *Röthlisberger and Geyh* [1985] reported ^{14}C-ages of a large number of glacial fluctuations over the last ~5 kyr in the Nun Kun area. However, evidence in form of well developed moraines is generally more restricted and comprises one (this study) or two (Gangotri; [*Barnard et al.*, 2004]) distinct glacial advances during the last ~3 kyr.

Table 6.4: Glacial episodes in the western Himalaya.

Tons	Gangotri	Lahul
<1 ka	<0.5 ka (Bhujbas)	n/a
~5 ka	~5 ka (Shivling)	n/a
~8 ka	~7-8 ka (Kedar)	n/a
~12 ka	n/a	~11-14 ka (Kulti)
~15-16 ka	n/a	~14-18 ka (Batal)

Data are from the Tons valley (this study), Gangotri [*Barnard et al.*, 2004], and Lahul [*Owen et al.*, 2001]. Glacial stage names assigned by the authors are given in brackets.

The currently available data from the western Himalaya indicates significant glacier retreat between 15 and 20 ka, which was roughly coeval with increasing global temperatures as reflected in ice cores from Antarctica [*Stenni et al.*, 2001], Greenland [*Cuffey and Clow*, 1997], and northwestern Tibet [*Thompson et al.*, 1997]. At the end of the deglacial temperature rise, however, the glaciers still had considerable lengths (Figure 6.8), which contrasts with many other regions on Earth, where glacial extents were at a minimum during the early to mid-Holocene [e.g., *Nesje and Dahl*, 1993; *Nesje*, 2009; *Menounos et al.*, 2009; *Ivy-Ochs et al.*, 2009]. The reason for this may be seen in strengthening of monsoon circulation coeval with globally increasing temperatures [e.g., *Wang et al.*, 2001; *Fleitmann et al.*, 2003; *Dykoski et al.*, 2005; *Herzschuh*, 2006]. While the accumulation effect of more precipitation is obvious, it has

recently been proposed that associated increases in cloudiness and evaporation account for additional cooling at that time, which may even have a more far-reaching effect on glacier-mass balances by reducing ablation [*Rupper et al.*, 2009]. Thus, enhanced monsoon circulation has most likely offset part of the negative mass balance effect of globally increasing temperatures during the Pleistocene-Holocene transition.
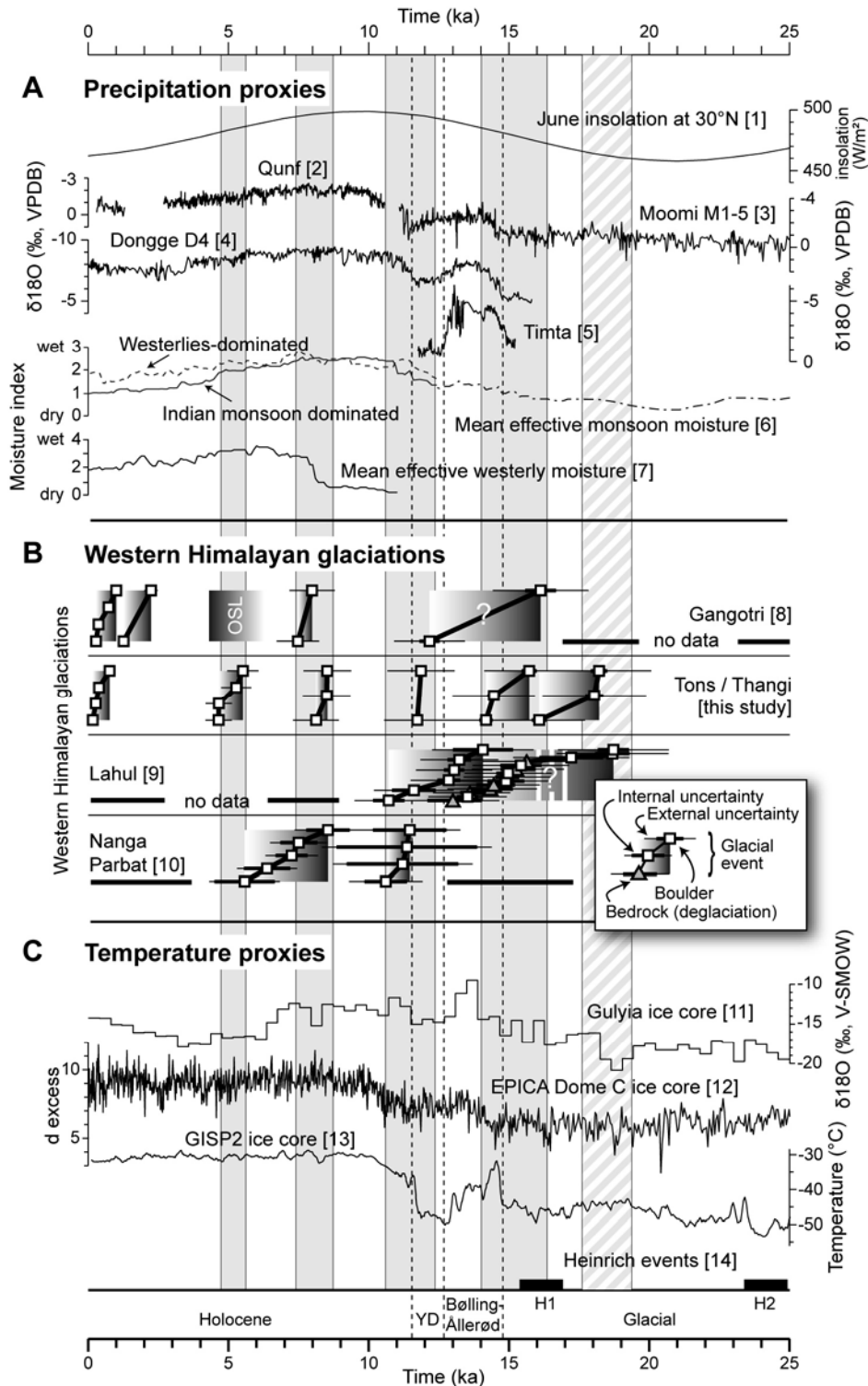
Figure 6.11: Compilation of western Himalayan glacial chronologies in a regional and global climatic context. (A) Records that depict changes in precipitation in the monsoon domain based on a variety of proxies ([1] *Berger and Loutre*, 1991; [2] *Fleitmann et al.*, 2003; [3] *Shakun et al.*, 2007; [4] *Yuan et al.*, 2004; [5] *Sinha et al.*, 2005; [6] *Herzschuh*, 2006; [7] *Chen et al.*, 2008). (B) Compilation of glacial studies in the western Himalaya ([8] *Barnard et al.*, 2004; *Sharma and Owen*, 1996; [9] *Owen et al.*, 2001; [10] *Phillips et al.*, 2000), including this study. Rectangles with

horizontal grayscale-gradient indicate that we regard the oldest cosmogenic nuclide-derived age (dark grey) from ages that belong to the same glacial event as the one closest to the true age of the glacial event. See text for more detailed discussion of the glacial chronologies. (C) Records that depict primarily changes in temperature ([11] *Thompson et al.*, 1997; [12] *Stenni et al.*, 2001; [13] *Cuffey and Clow*, 1997). The black bars at the bottom denote and Heinrich events H1 and H2 ([14] *Bond et al.*, 1992).

Relatively constant or decreasing global temperatures during the mid to late Holocene, however, do not explain further glacial retreat, which may suggest that monsoonal dynamics become more important (Figure 6.11). Several lake records from northwestern India [*Wasson et al.*, 1984; *Enzel et al.*, 1999; *Demske et al.*, 2009] and western Tibet [*Van Campo and Gasse*, 1993; *Gasse et al.*, 1996] indicate relatively humid conditions prevailing until the mid Holocene. Yet, part of this prolonged wet period has been linked to a strengthening of winter precipitation from the early to mid Holocene [*Prasad and Enzel*, 2006; *Chen et al.*, 2008], coeval with a decline in summer rainfall in the same time period [*Fleitmann et al.*, 2003; *Wang, et al.*, 2001; *Dykoski et al.*, 2005]. This could also explain the pronounced negative shift of $\delta^{18}O$-values in the Gulyia ice core at ~7 ka [*Thompson et al.*, 1997] (Figure 6.11), because winter snowfall associated with the westerlies has a much lower $\delta^{18}O$-signature than summer precipitation in this area [*Aizen et al.*, 2009]. Therefore, stepwise departure from more humid conditions in the early to mid-Holocene could serve to explain the steadily decreasing glacial extents. Finally, the youngest dated boulders of <1 ka may tentatively be linked to glacier readvances related to the Little Ice Age [*Röthlisberger and Geyh*, 1985; *Barnard et al.*, 2004].

The western Himalaya is located at the western end of the Bay of Bengal monsoon branch and the relative importance of monsoonal versus westerlies-derived moisture supply for this area has most likely changed over time [e.g., *Bookhagen et al.*, 2005a; *Herzschuh*, 2006; *Demske et al.*, 2009]. *Rupper et al.* [2009] suggested that the mass balance effect of climatic changes during the early to mid-Holocene was positive for monsoonal areas but negative for non-monsoonal areas, such as those influenced by the westerlies. The apparently larger glaciers over much of the western Himalaya at that time may therefore indicate that monsoon influence has been regionally more extensive than today. However, multiple Holocene glacial advances and more extended glaciers in the early Holocene have also been reported from areas like the Chinese Pamir [*Seong et al.*, 2009], which are far from monsoon influence and where the study by *Rupper et al.* [2009] predicts higher early to mid Holocene ELAs than today. Thus, more data from the western areas of the HKH region will hopefully better constrain the extent and timing of monsoonal versus westerlies-influence and their effect on glacial mass balances.

In summary, the currently available data from the western Himalaya show reasonable agreement in the timing of glacial events, at least for the Holocene. At present, however, it is not possible to firmly assess potential systematic differences in the timing of glacial advances for older periods or between more humid or arid areas [*Owen et al.*, 2005; *Zech et al.*, 2009]. First, the response of glaciers to changes in temperatures and precipitation depends on a number of factors, including climate sensitivity and hypsometry of the glacier, as well as local climatic effects. Hence, some differences in the timing of glacial events may be quite common. Second, locations in the more arid orogenic interior of the western Himalaya, receive most moisture during winter from the westerlies as compared to valleys along the southern orogenic front, for which monsoon precipitation dominates the moisture budget [*Singh and Kumar*, 1997; *Bookhagen and Burbank*, 2006; *Wulf et al.*, 2010]. Therefore, the north-south precipitation gradient in the western Himalaya is superimposed by a longitudinal gradient in moisture supply (Figure 6.2) resulting in disparate effects of climatic change [*Rupper et al.*, 2009]. Third, geomorphic uncertainties usually increase with exposure duration and may also vary between

climatic zones [*Owen et al.*, 2005]. In this regard, longer exposure of sampled boulders may be associated with higher degrees of fracturing and exfoliation and thus greater ambiguities in the obtained ages [*Chevalier et al.*, 2008].

6.6.2   Rapid global climatic changes and glacier response in the Hindu Kush-Karakoram-Himalayan (HKH) region

The deglacial and Holocene evolution of ELAs and glacial extents, as observed in the Tons valley and other areas in the western Himalaya are clearly a regional phenomenon that can be explained by long term, orbitally-controlled changes in temperature and precipitation in the greater HKH region. This scenario does not preclude discrete rapid climatic changes to be the cause for distinct glacier readvances as proposed by others [*Phillips et al.*, 2000; *Barnard et al.*, 2004; *Seong et al.*, 2009]. If global, rapidly occuring climatic changes were indeed driving glacial advances in the Himalaya, the identified glacial events in the western Himalaya could be related to the Younger Dryas (YD) at ~11-12 ka, the 8.2-ka event [*Alley et al.*, 1997], and the 4.2-ka cold event [e.g., *Weiss et al.*, 1993]. However, the TCN-derived ages are not accurate enough to unambiguously support this correlation and we doubt that this issue can be resolved by acquiring more TCN-derived glacial chronological data, because the geomorphic uncertainties in exposure histories will remain. Yet, in order to correctly interpret glacial records it is crucial to understand, if and which glacial advances in the Himalaya are related to rapid or gradual temperature or precipitation changes. In this section we focus on evidence for or against glacier response to global rapid climatic changes.
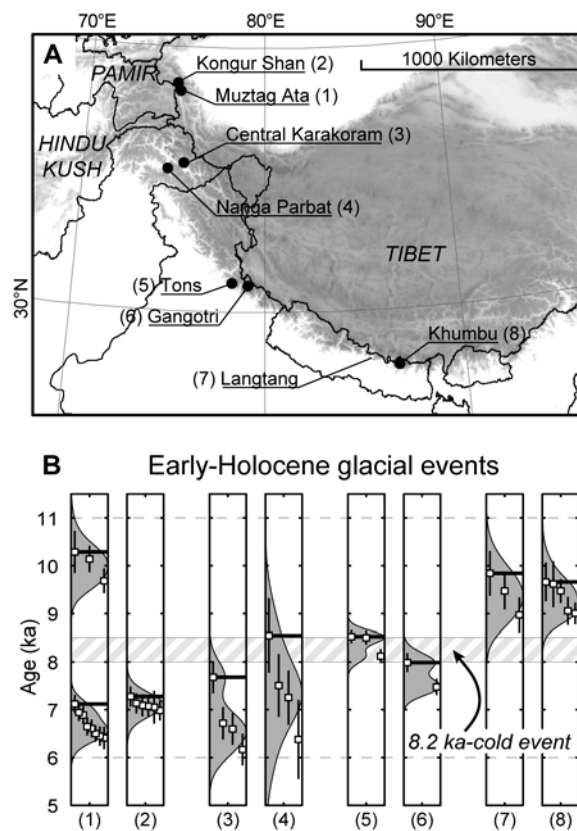
Figure 6.12: Spatiotemporal extent of early Holocene glacial events in the Himalaya. (A) Map of Central Asia, the Himalaya, and Tibetan Plateau for the locations shown in B. (B) Probability density functions of TCN-samples >6 ka and <11 ka that document an early Holocene glacial event in different glacial chronologies. Samples within this age range that are clearly related to older or younger glacial stages have been omitted. The error bars on the data points denote internal uncertainties as all samples have been recalculated using the same production-rate scaling model after *Lifton et al.* [2005]. Horizontal bars extend from the oldest of a group of samples. Neither the oldest nor the mean ages from

these glacial episodes show clear alignment with the 8.2 ka-cold event. Data sources: (1,2,3) *Seong et al.* [2009]; (4) *Phillips et al.* [2000]; (5) this study; (6) *Barnard et al.* [2004]; (7) *Abramowski* [2004]; (8) *Finkel et al.* [2003].

Many glacial chronologies from the HKH region provide evidence for a pronounced early Holocene glacial event [e.g., *Röthlisberger and Geyh*, 1985; *Phillips et al.*, 2000; *Finkel et al.*, 2003; *Seong et al.*, 2009]. In Figure 6.12, we compiled TCN-derived glacial exposure ages from the time period 6-11 ka. For compatibility with our data we recalculated all ages using the Lifton et al. (2005) production-rate scaling model and 0.003 mm/yr erosion of the sampled surfaces using the CRONUS calculator [*Balco et al.*, 2008]. The along-strike comparison demonstrates that an early Holocene glacial event is widespread in the Himalaya but differs in timing by as much as ~3 kyr between east and west. This diachronous behavior provides some evidence against the influence of the 8.2-ka cold event in forcing these glacial events. The lack of evidence for glacier response to this event could be either due to an insufficient impact on glacial mass balances in this region or more extensive subsequent advances that destroyed evidence for this event. It is also notable that no glacial chronology in the Himalaya has so far provided conclusive evidence for regional glacier advances during the YD cold reversal, which has arguably been the most pronounced rapid cooling event of the last 20 kyr.

We suggest that mass balance perturbations in the Himalaya associated with rapid climatic changes which most likely originated [e.g., *Clark et al.*, 2002] or were amplified [e.g., *Seager and Battisti*, 2007] in the North Atlantic, were small and did not cause any pronounced glacier advances due to coeval and opposing effects of temperature and precipitation changes. Several studies suggest that the dramatic decrease in temperatures during the YD was primarily due to decreased winter temperatures and associated with the spread of sea-ice [*Atkinson et al.*, 1987; *Isarin and Renssen*, 1999; *Denton et al.*, 2005]. For most glaciers, however, changes in winter temperature have only minor effects on mass balance [e.g., *Oerlemans and Reichert*, 2000; *Fujita and Ageta*, 2000]. In addition, many monsoon records show a reduction in monsoon strength and precipitation during the YD and also the 8.2-ka event [e.g., *Schulz et al.*, 1998; *Staubwasser et al.*, 2002; *Fleitmann et al.*, 2003; *Sinha et al.*, 2005; *Dykoski et al.*, 2005] (Figure 6.11). This has been linked by *Denton et al.* [2005] to processes in the North Atlantic region through a proposed negative effect of Eurasian snow cover on monsoon strength [*Blanford*, 1884]. Accordingly, long and cold winters are associated with reduced monsoon precipitation in the following summer season [*Hahn and Shukla*, 1976; *Barnett et al.*, 1988], which results in a negative glacial mass balance perturbation. Furthermore, lower winter temperatures reduce the capacity of air to hold moisture, which would directly affect moisture transport by the winter westerlies. Eventually, we expect an overall negligible positive or, more likely, a negative mass balance perturbation of glaciers in the HKH region during rapid climatic changes that are linked to processes in the North Atlantic.

In summary, current data does not support widespread glacial advances during the YD and the different timing of early Holocene glacial periods contradicts the notion of glacier response to an abrupt cold event at ~8.2 ka. This could be explained by low sensitivity of high-altitude Himalayan glaciers to temperature changes that are largely restricted to winter, and the opposing effect of coeval changes in monsoon precipitation.

6.6.3   Equilibrium Line Altitude changes (ΔELA) across a precipitation gradient

The glacial history in the upper Tons valley is characterized by significant changes in glacial cover (Figure 6.8), but the associated depression of the ELA is only ~400 m for Bandarpunch glacier and even less for Jaundhar glacier (Figure 6.9B). The comparison of ΔELAs derived

with the THAR and AAR method points at significant hypsometric effects, particularly for Jaundhar glacier, and highlights the problems associated with simple 'glacier elevation indices' such as THAR to derive former ELAs for complex glacial systems [*Benn and Lehmkuhl*, 2000; *Owen and Benn*, 2005].

An important observation from the reconstructions is that generally ΔELA values have been higher for Bandarpunch than for Jaundhar glacier. This implies that either the magnitude of climatic change or the response to a given climatic perturbation was different for these two glaciers. Numerical glacier models have shown that among climatic factors, only the amount of precipitation systematically influences the sensitivity of a glacier to changes in temperature or precipitation [e.g., *Oerlemans and Fortuin*, 1992; *Oerlemans*, 2005]. Reliable precipitation measurements from glacierized elevations in the Himalaya are scarce [e.g., *Putkonen*, 2004] and no data is available for the upper Tons valley. However, rainfall derived from the Tropical Rainfall Measuring Mission (TRMM), and calibrated to weather station data by *Bookhagen and Burbank* [2006] and *Bookhagen and Burbank* [in press], indicate a steep north-south gradient in precipitation across the upper Tons valley (Figure 6.13). Rainfall decreases from 2-4 m/yr in the upper Yamuna valley, south of the upper Tons valley, to 1-2 m/yr over Bandarpunch glacier, and to 0.5-1.5 m/yr over Jaundhar glacier. Present-day rainfall is <0.5 m/yr in the Thangi valley, where the glacier reconstruction indicates ΔELA of <300 m at ~18.2 ka. Although the Thangi data refers to a slightly earlier time and is less well constrained, it still fits into the expectation of further decrease in ΔELA towards the drier parts of the orogen.
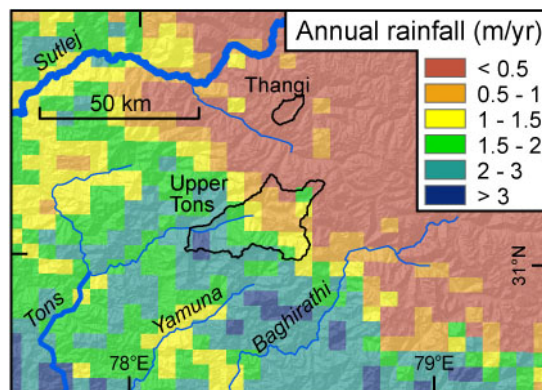
Figure 6.13: Annual rainfall over the study area derived from calibrated TRMM-data (1998-2008). Data is from *Bookhagen and Burbank* [2006, in press]. The upper Tons and the studied tributary in the Thangi catchment are delimited by a solid black line. Note the steep southwest-northeast gradient in rainfall across the upper Tons valley.

The magnitude of ELA depression in the upper Tons and Thangi valleys during the last ~15-20 kyr differs from other places in the Himalaya. *Gayer et al.* [2006] reconstructed former ELAs for a small glacier located at the southern front of the High Himalaya in central Nepal which is exposed to high amounts of monsoon precipitation. The authors found that the ELA was depressed by ~400 m during the early Holocene at ~8 ka and apparently more than 700 m during the latest Pleistocene. In contrast, *Owen et al.* [2009] reconstructed ELAs for the Khumbu and Rongbuk glaciers, located in eastern Nepal, south and north of Mount Everest, respectively, and find generally lower ΔELA values. At ~16-17 ka, the ELA was depressed by only ~100 m at Rongbuk and ~270 m at Khumbu glacier. During the early and mid Holocene ELA depressions were only ~50 m. These very low values are certainly related to the drier climate conditions in these places, with annual precipitation ≤ 0.5 m /yr at present [*Bolasina et al.*, 2002; *Owen et al.*, 2009 and references therein]. Thus, the depression of the ELA as reconstructed for various places along the Himalaya seems to be a consequence of the climate

sensitivity of the respective glaciers. This, in turn is mostly influenced by the amount of annual precipitation that they receive. It is unknown how the precipitation gradient has been during episodes of changed monsoon strength. However, precipitation in the Himalaya is strongly affected by orography [*Bookhagen and Burbank*, 2006], and presently observed precipitation gradients most likely persisted to some degree during the younger geologic past, although probably at a different level [*Bookhagen et al.*, 2005a].

6.7   Conclusions

Our study of the glacial history in the upper Tons valley provides new insights into the late Pleistocene and Holocene climate variability and associated glacial changes in the western Himalaya:

At least five glacial events occurred during the last ~16 kyr in the upper Tons valley. These are in reasonable agreement with existing chronologies from the western Himalaya and suggest broadly synchronous glacial behavior in this region during the Holocene. However, as the geomorphic uncertainties usually increase with exposure duration and may also vary between climatic zones, our ability to unambiguously assess synchronous or asynchronous prior glacial behavior is limited.

The glaciers in the upper Tons valley show marked differences in Equilibrium Line Altitude (ELA)-lowering over distances of only ~20 km. We explain this by an orographically induced, steep north-south gradient in precipitation that results in different climatic sensitivities of these glaciers. This conclusion is supported by other ELA reconstructions in the Himalaya and highlights the influence of orographic barriers on regional and local glacial dynamics.

Continuously decreasing glacial extents over the last ~16 kyr are best explained by coeval changes in temperature and precipitation. In contrast to many other regions in the northern hemisphere, the Tons glaciers had still considerable extents during the early Holocene, which can be related to enhanced monsoon precipitation that subsequently decreased. The early Holocene glacial event is most likely not related to the 8.2 ka cold event as shown by comparison of glacial chronologies along strike of the orogen and considering the mass-balance effects on Himalayan glaciers during this event.

Comparison of glacial chronologies from the western Himalaya with other palaeoclimatic proxy data suggests that long-term changes in glacial extents are controlled by glacial-interglacial temperature oscillations related to the waxing and waning of the large northern-hemisphere ice sheets, while the timing of millennial-scale advance-and-retreat cycles are more directly related to monsoon strength and associated variability in moisture regime.

7   Contrasting atmospheric moisture sources and glacial-erosion potential in the Himalaya

High Asia hosts some of the world's largest valley glaciers [von Wissmann, 1959], but their erosional impact is ambiguous [*Brozovic et al.*, 1997; *Burbank et al.*, 2003; *Harper and Humphrey*, 2003; *Korup and Montgomery*, 2008; *Van der Beek et al.*, 2009; *Whipple*, 2009]. Systematic changes of precipitation characteristics, morphology, and satellite-derived flow velocities of 265 analyzed glaciers across the southern and western edges of the Tibetan Plateau help elucidate the role of glacial erosion on Himalayan landscape evolution. In this region glacier-surface velocities peak near the equilibrium-line altitude (ELA), and the associated ice flux per unit width, a proxy for glacial-erosion potential, increases linearly with glacier area (length) to the power of ~1.3 (~0.9). Snowlines below the mean elevation of the Tibetan Plateau in the westerlies-influenced part of the orogen result in extensive accumulation areas that feed large, high ice-flux valley glaciers. In the steep central Himalaya, however, the seasonality and tropospheric structure of the monsoon circulation account for high and rapidly northward rising snowlines that greatly limit snow accumulation areas, even during the Last Glacial Maximum. This may be related to the sensitivity of the monsoon to glacial periods [*Prell and Kutzbach*, 1992]. These conditions confine glacial erosion in the central Himalaya to regions largely above the mean elevation of the Tibetan Plateau, and helps maintain a steep southern margin, in contrast to a widely dissected margin in the west [*Van der Beek et al.*, 2009].

Current hypotheses [*Brozovic et al.*, 1997; *Berger and Spotila*, 2008; *Egholm et al.*, 2009] suggest that glacial erosion controls the upper limit of topography, irrespective of tectonic forcing, and peaks at or near the long-term ELA, which is approximately equal to the climatic snowline [*von Wissmann*, 1959]. Outside the tropics, the main controls on snowline elevations are summer temperatures and annual snowfall [*Ohmura et al.*, 1992]. Consequently, snowlines are highest near the subtropical high-pressure belt [*von Wissmann*, 1959; *Egholm et al.*, 2009; *Ohmura et al.*, 1992], where also the two highest and largest orogenic plateaus, the Altiplano/Puna and the Tibetan Plateau (TP), are located. In light of feedbacks between erosion and tectonic deformation of orogens [*Whipple*, 2009; *Willett*, 1999; *Tomkin and Roe*, 2007], this raises the question whether the protracted existence of such highlands is limited by their intersection with the snowline and associated glacial erosion that matches rock uplift [*Montgomery et al.*, 2001]. Although the evolution of orogenic plateaus is intensely researched [*Strecker et al.*, 2007], their erosional decay has received little attention [*Korup and Montgomery*, 2008; *Van der Beek et al.*, 2009; *Masek et al.*, 1994]. In particular, the effects of different atmospheric-circulation regimes on snowline variations, glacial erosion, and plateau evolution, have not been considered so far. The Himalaya, which forms the southern and western margin of the TP, is a perfect setting to study such potential feedbacks, as moisture sources and the timing of seasonal snow accumulation vary considerably along the orogen. While the central Himalaya receives most precipitation from the Indian summer monsoon, the western part of the orogen is dominated by the mid-latitude westerlies during winter (Figure 7.1) [*Barry and Chorley*, 2003].

Here, we study the climatic controls of High Asian glaciers and their erosional footprint using satellite-derived glacier-surface velocities from 265 glaciers across the southern and western margin of the TP. This is an established method [*Scambos et al.*, 1992], routinely used on fast-flowing Greenland and Antarctic glaciers, but its broader application in high and steep terrain has been limited. Our velocity measurements provide ice-flux estimates near the ELA as a proxy for glacial erosion potential [*Hallet et al.*, 1996]. For the first time this allows to directly identify zones of high glacial-erosion potential across large areas, which has hitherto only been inferred indirectly from topographic characteristics [*Brozovic et al.*, 1997; *Egholm et al.*, 2009].
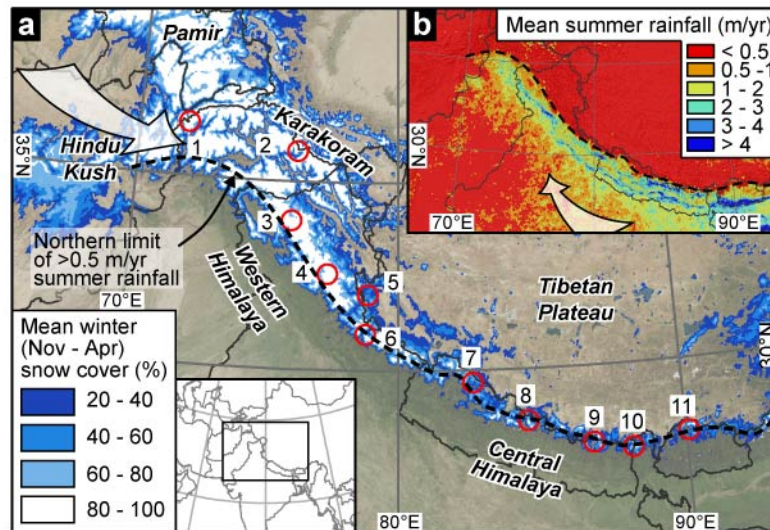
Figure 7.1: Moisture sources and precipitation patterns in High Asia. (a) Mean winter-snow cover (2000-2008) [*Hall et al.*, 2007]. (b) Mean annual rainfall (1998-2006) [*Bookhagen and Burbank*, 2006]. Arrows indicate influx of westerlies precipitation during winter (a) and monsoon precipitation during summer (b). Red circles show areas where glacier velocities were obtained (number of glaciers in brackets): 1 Hindu Kush (13), 2 Karakoram (40), 3 Zanskar (27), 4 Lahul (37), 5 Leo Pargil (7), 6 Garhwal (22), 7 Gurla Mandatha (7), 8 Manaslu (26), 9 Khumbu (38), 10 Kanchenjunga (26), 11 Bhutan (18). Regions 3-4 constitute the western Himalaya and regions 5-11 the central Himalaya in Figure 2.

Altitudinal distributions of glacier-surface velocities along the central flow line show that glaciers flow fastest in an elevation band of ~1-1.5 km vertical extent, approximately centered on the hypsometric maximum of their catchments (Figure 7.2). This band is lowest in the westerlies-influenced Hindu Kush, Karakoram, and western Himalaya at ~4.9 ± 0.7 km asl (±2σ). In the monsoon-dominated central Himalaya it is located at ~5.4 ± 0.8 km asl to the south, and rises to 5.8 ± 0.5 km asl north of the topographic divide. Generally, velocities are highest near the ELA, in accordance with theoretical predictions of glacier flow [*Paterson*, 1994]. Furthermore, estimated ice flux per unit width near the ELA increases with glacier area to a power of ~1.29 (R^2=0.7) or length to a power of ~0.93 (R^2=0.67) (Figure D3). It is assumed that glacial erosion is proportional to basal sliding [*Berger and Spotila*, 2008; *Egholm et al.*, 2009; *Tomkin and Roe*, 2007; *Hallet et al.*, 1996], which however, is difficult to measure, especially on a regional scale [*Hallet et al.*, 1996; *Paterson*, 1994]. Under the simplifying assumption of similar ratios of basal sliding to internal deformation in the study area, glacial erosion potential is approximately proportional to our estimates of ice flux per unit width. This assumption would be violated if regional trends in ice temperatures lead to significant cold based non-sliding ice [*Paterson*, 1994]. Due to the absence of data on basal-glacier conditions, we analyzed climate data and found similar annual air temperatures at the locations of the studied glaciers (Figure D8), suggesting approximately similar ice temperatures and no

significant differences in the glacier-sliding-to-deformation ratio. Thus, our data indicate that to first order, glacial-erosion potential in the study area increases with glacier size.
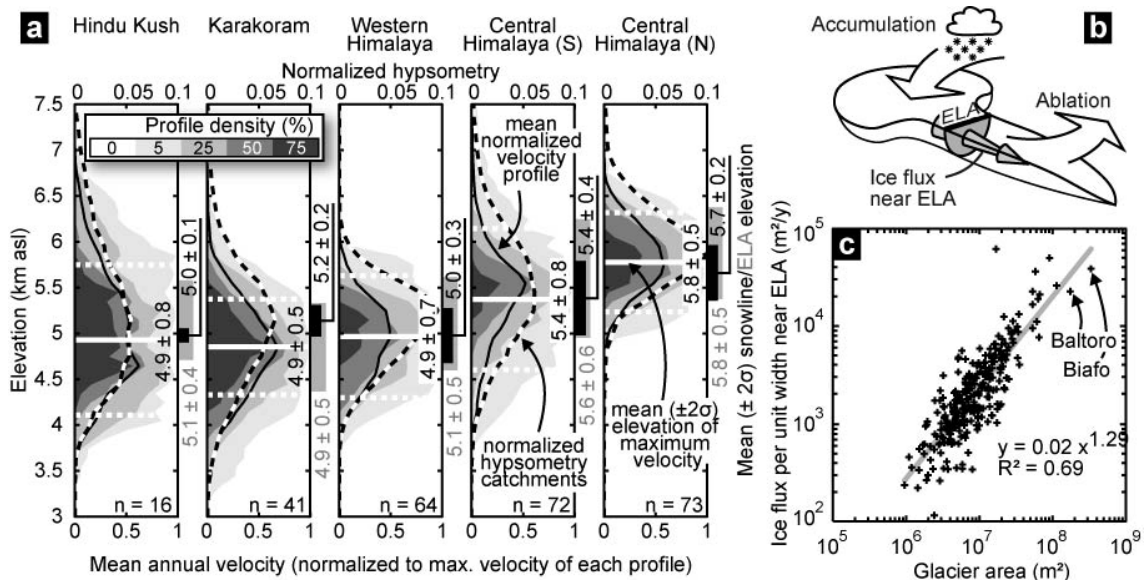
Figure 7.2: Altitudinal concentration of ice flux and relationship with glacier size. (a) Altitudinal distribution of normalized glacier-surface velocities in five geographic regions. Central Himalayan glaciers are divided with respect to their location south (S) or north (N) of the main topographic divide. Profile density is defined as the percentage of profiles reaching certain normalized velocities within 0.1-km-elevation bins. Hypsometry of catchments is regionally aggregated. Black and grey bars right of the velocity plots indicate the mean (±2σ) elevation of satellite-derived ELA estimates and regional climatic-snowline elevations [*von Wissmann*, 1959], respectively. (b) Glacier sketch showing ice flux at ELA. (c) Scatter plot depicting power-law relationship between estimated ice flux per unit width near the ELA and glacier area for 265 glaciers from High Asia.

The principle factor controlling the size of glaciers is the amount and seasonal distribution of snowfall and the size of the accumulation area [*von Wissmann*, 1959]. Snowfall data from High Asia is scarce and unavailable for the entire region, but remotely-sensed snow cover [*Hall et al.*, 2007] suggests a westward increase in snowfall due to the influx of westerlies-derived moisture (Figure 7.1). To examine how accumulation areas vary spatially and temporally, we reconstructed Quaternary glacial landscapes across High Asia based on the similarity between remotely-sensed ELAs and published records of regional climatic-snowline elevations [*von Wissmann*, 1959] (Figure 7.2a, Figure D4-Figure D6). Lowering of the ELA (or snowline) to its Last Glacial Maximum (LGM) position, results in extensive accumulation areas between the Hindu Kush, Karakoram, and western Himalaya (Figure 7.3). Conversely, in the central Himalaya accumulation areas remained small, even under full glacial conditions. In central and eastern Nepal, where topography is very steep, absolute and relative area changes are minimal.

The east-west differences in accumulation areas are mainly due to westward-decreasing snowlines, which likely result from differences in annual air temperatures (~4 K; Figure D7) and snowfall [*Ohmura et al.*, 1992]. Furthermore, snowlines in the west remain low and intersect topography across large areas in the orogen interior (Figure 7.4). We relate this to the high tropospheric extent of westerly air flow [*Barry and Chorley*, 2003] enabling moisture to migrate farther into the orogen. In the central Himalaya, where ELAs are higher, advection of monsoonal moisture during summer occurs at lower tropospheric levels [*Barry and Chorley*, 2003] with the bulk of moisture precipitating at elevations below ~4-5 km [*Bookhagen and Burbank*, 2006]. Here, intense rainfall accounts for vigorous fluvial incision and mass wasting, resulting in steep hillslopes [*Burbank et al.*, 2003; *Bookhagen and Burbank*, 2003]. North of the orographic barrier of the High Himalaya, hillslopes are less steep, topography and relief are

lower, and precipitation greatly reduced, causing even higher ELAs (>5.5 km; Figure 7.2). Consequently, high-elevation sites in the monsoon-dominated central Himalaya are either too steep with only small areas above the ELA, or lack precipitation to support extensive valley glaciers. This assessment agrees with glacier-modeling results [*Harper and Humphrey*, 2003].
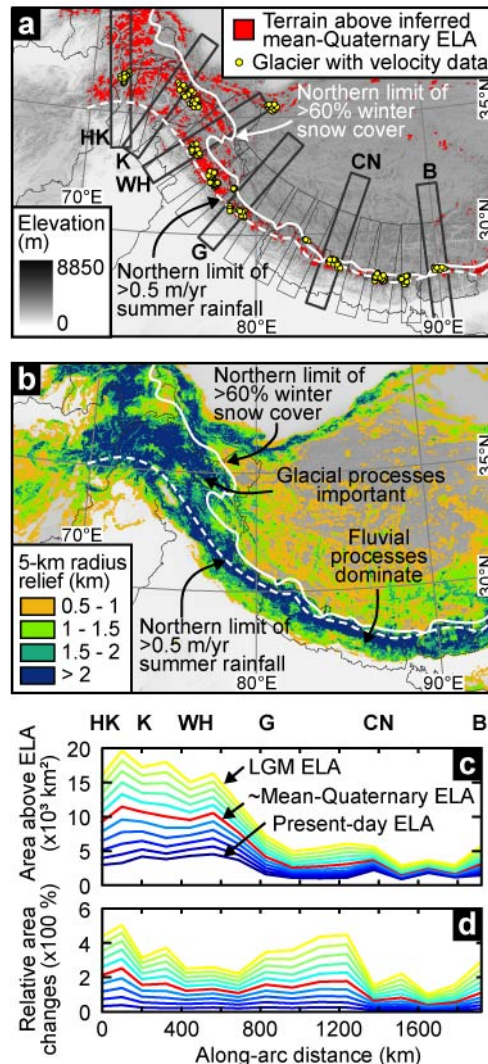
Figure 7.3: Quaternary growth of glacial environments across High Asia. (a) Land surface above inferred mean-Quaternary ELA. Thin rectangles indicate location of 500 km long and 100 km wide swath profiles. Bold rectangles are 700-km long swaths shown in Figure 7.4. (b) 5-km radius relief. (c) Areas above the ELA and (d) relative area changes, measured within the 500-km long swath profiles, as the ELA descends in 10-% steps from its present-day position (dark blue) towards its LGM-position (yellow). Along-arc distance refers to swath centers.

Steep topography and monsoonal climate in the central Himalaya also affected the growth of accumulation areas during the Pleistocene. First, in steep terrain, ELA lowering results in smaller accumulation-area changes compared to gentle terrain [*Brozovic et al.*, 1997]. Second, the amount of ELA-lowering results from climatic changes partly related to variations in summer insolation and monsoon strength on >103-year time scales [*Prell and Kutzbach*, 1992]. When insolation is high, strong monsoons increase precipitation and penetrate deeper into the orogen, which has been inferred from higher palaeo-lake levels and pollen spectra indicative of increased moisture availability [*Herzschuh*, 2006]. However, during increased insolation, temperatures are also higher compared to full glacial conditions when insolation reached a minimum and monsoons were weaker [*Prell and Kutzbach*, 1992; *Herzschuh*, 2006]. Thus, higher insolation may partly offset the positive glacial mass-balance effect of stronger

monsoons, reflected by limited ELA depressions and associated glacier advances [*Scherler et al.*, 2010; *Owen et al.*, 2009; *Shi*, 2002].
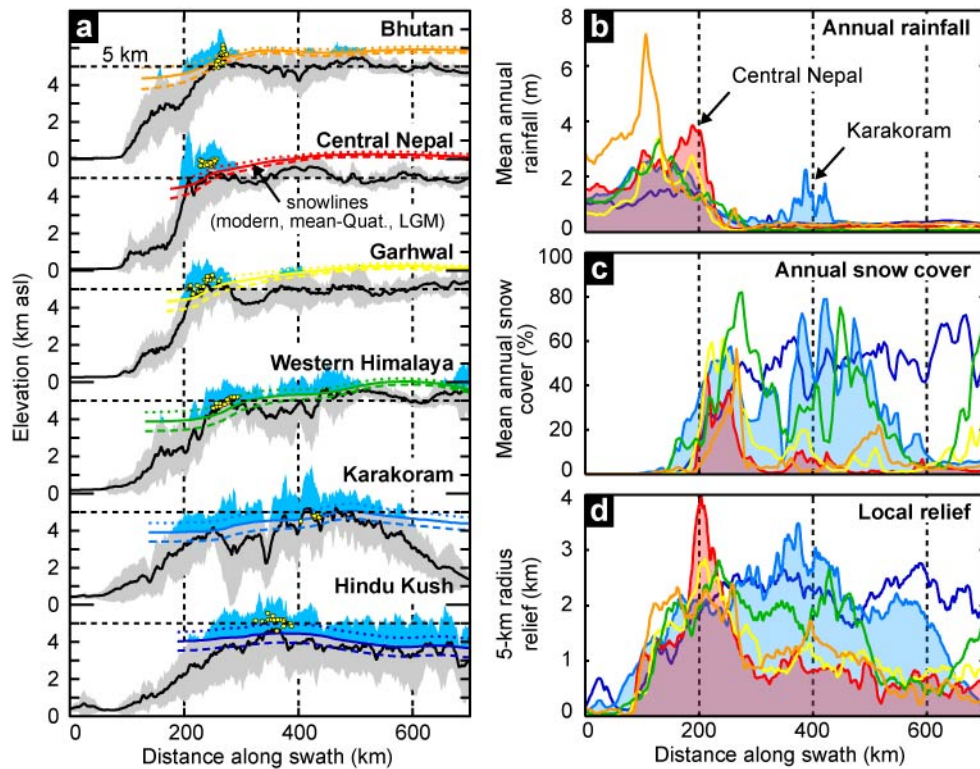
Figure 7.4: Topographic and climatic east-west gradients. (a) Selected swath profiles showing mean (black solid line) +/- 2σ-envelope (gray polygon) of topographic elevations. Colored lines indicate modern (dotted), mean-Quaternary (solid) and LGM (dashed) snowlines [*von Wissmann*, 1959; *Shi*, 2002]. Yellow points refer to the present-day ELAs of studied glaciers that lie within the swaths (see Figure 7.3 for their location). (b) Mean annual rainfall, (c) mean annual snow cover, and (d) mean 5-km radius local relief measured across swaths.

In summary, present and past climatic and topographic conditions along the monsoon-influenced central Himalaya do not favor large, high-ice flux valley glaciers, such as in the westerlies-influenced regions, and thus result in limited glacial erosion. The highest relief in the central Himalaya occurs in the transition between the monsoon-impacted Lesser and Greater Himalaya, where our glacier-velocity data indicate present-day glacial erosion focused at ~5.4 ± 0.8 km asl, lowered by approximately 0.5-0.8 km during the LGM [*Shi*, 2002] (Figure D7). Farther north, on the edge of the TP, glacial erosion is focused at ~5.8 ± 0.5 km asl, lowered by <0.5 km during the LGM [*Shi*, 2002]. This is insufficient to promote incision of the plateau with mean elevations of ~5 km asl [*Fielding et al.*, 1994], reflected by a rapid northward decrease in relief (Figure 7.4). The uniform long-wavelength mean elevation of the TP at ~5 km asl is interpreted to reflect the crustal limit to sustain high topography [*Fielding et al.*, 1994]. Mean elevations of ~5 km also prevail across the southern plateau margin and into the Greater Himalaya, where erosional unloading-induced uplift has been proposed to account for the world's highest peaks next to the deepest gorges [*Masek et al.*, 1994; *Burbank*, 1992]. In these environments, river incision most likely paces out glacial erosion, hence decreasing accumulation areas [*Masek et al.*, 1994] and restricting glaciers to high elevations, where hillslopes are too steep to support extensive glaciation [*Harper and Humphrey*, 2003]. Thus, the effective upper-topographic limit may be controlled by crustal properties instead of glacial erosion [*Brozovic et al.*, 1997; *Egholm et al.*, 2009].

West of ~78°E the decrease in snowline elevations and greater lowering of Pleistocene ELAs increases the terrain susceptible for glaciation as winter-snow cover is high, but rainfall low (Figure 7.3). The approximate coincidence of mean surface elevations with the mean position of the ELA during the Quaternary, which we assume lies halfway between the modern and the LGM ELA [*Brozovic et al.*, 1997], may reflect efficient glacial erosion limiting topography [*Brozovic et al.*, 1997; *Egholm et al.*, 2009]. This contradicts the notion of slowly eroding, low-relief landscapes at high elevation, interpreted as remnants of a formerly more extensive TP [*Van der Beek et al.*, 2009]. However, higher exhumation at the edges of such plateau remnants [*Van der Beek et al.*, 2009] documents their topographic disequilibrium and erosional decay. Given efficient glacial erosion at the ELA, we find it more surprising to see extensive high-relief areas above the ELA, such as in the Karakoram (Figure 7.4). This could be related to significant amounts of non erosive cold-based ice at high elevations but can also be reconciled with glacier-size dependency of glacial erosion, as suggested by our data. In order for glacial erosion to keep pace with high rock-uplift rates, glaciers need to be sufficiently large, which requires greater accumulation areas above the ELA [*Brozovic et al.*, 1997]. However, focused erosion by large valley glaciers results in deeply incised valleys amidst high peaks and thus high relief [*Brocklehurst and Whipple*, 2007], as in the Karakoram. If topographic growth in these regions is indeed matched by glacial erosion [*Brozociv et al.*, 1997; *Egholm et al.*, 2009], then this mechanism would suggest that relief and glacier size, all other parameters being equal, are positively correlated with rock-uplift [*Brocklehurst and Whipple*, 2007].

Our study documents the limited erosional potential of monsoon-influenced glaciers. On time scales of 106-years, this characteristic may have helped preserve Earth's largest continental plateau as a geomorphic entity, ultimately keeping this region at an elevation controlled by geodynamics [*Fielding et al.*, 1994], instead of glacial erosion [*Egholm et al.*, 2009]. The demise of continental plateaus can be achieved by tectonic denudation or by precipitation, runoff, and erosive power. The high reaching westerly-air flow and snowlines below the mean elevation of the TP provide perfect conditions for glacial dissection of the western plateau margin [*Brozovic et al.*, 1997], creating pathways for moisture-bearing winds into the orogen and accelerating headward fluvial erosion [*Bookhagen et al.*, 2005a]. Conversely, in the central Himalaya, glaciers remain relatively small and focus erosion above the mean elevation of the TP, resulting in limited dissection and maintaining of an orographic barrier that impedes headward erosion and capture of northward draining rivers. Although oscillating glacier activity may even block incising rivers [*Korup and Montgomery*, 2008], the key limiting factor remains the availability of precipitation to generate runoff and erosion [*Masek et al.*, 1994]. In this respect, the particular seasonal and tropospheric structure of monsoon precipitation, concentrating fluvial erosion at low-to-moderate, but limiting glacial erosion at high elevations, helps maintain a steep plateau margin [*Masek et al.*, 1994]. As circulation characteristics are similar in other monsoonal regions, this glacial inefficiency may have a more general relevance for the fate of orogenic plateaus at subtropical latitudes [*Montgomery et al.*, 2001; *Strecker et al.*, 2007; *Masek et al.*, 1994].

Methods summary

Glacier-surface velocities were determined by correlation of >300 optical satellite images from the years 2000-2008. We measured velocities along the central flow line of 265 glaciers from the high Hindu Kush in the west to the Bhutanese Himalaya in the east. We estimated the ice-flux as close to the equilibrium line altitude (ELA) as possible, which we identified using late-summer satellite images. In cases where the ELA was found located in complex glacial terrain, e.g., broad accumulation basins, we chose the next suitable location downstream, where a parabolic channel form is likely. In these locations, the ice-flux estimates rely on (1) measured glacier widths and center-line surface velocities; (2) thickness estimates assuming constant driving-stresses [*Paterson*, 1994]; and (3) shape factors to derive the cross-sectional flux from the above quantities for given widths and depths. For topographic analysis we used a 90-m resolution SRTM digital elevation model (DEM), provided by NASA. To investigate how changes in the ELA affected the growth and extent of glaciers during the Quaternary, we used the DEM together with snowline elevations [*von Wissmann*, 1959] as a proxy for the ELA [*Brozovic et al.*, 1997; *Egholm et al.*, 2009], and a map of ELA-depressions during the last glacial maximum [*Shi*, 2002]. We obtained the distribution of mean annual rainfall from calibrated Tropical Rainfall Measuring Mission (TRMM) data from 1998-2006 at 5-km resolution [*Bookhagen and Burbank*, 2006]. Reliable estimates of snow-water equivalent in mountainous terrain are rare and unavailable for the study region. Thus we use the 0.05°-resolution data on fractional snow cover of the MODerate resolution Imaging Spectroradiometer (MODIS) collected between 2000 and 2008 [*Hall et al.*, 2007] as a proxy for snowfall.

8   Conclusions

In this study, I examined various aspects of glacial dynamics in High Asia, using a combination of remote-sensing techniques, cosmogenic nuclide surface-exposure dating, and topographic and climatic analysis. The studied glacial processes occur on time scales ranging from 10^0 to 10^6 years but are intimately linked with each other and result in complex, spatially and temporally disparate glacial behavior. Correlation of optical satellite imagery proved as a cost efficient method to obtain accurate glacier-surface velocities over large regions and at high temporal and spatial resolution. The thus obtained flow velocities from widely differing glaciers across High Asia provide unique insight into the topographic and climatic control on flow and frontal dynamics.

Accumulation areas of glaciers in high-relief areas along the margin of the Tibetan Plateau largely occupy steep topography, and snow and ice avalanching are important processes that contribute to transferring large amounts of rock debris to the glacier surface. This results in supraglacial-debris cover, which usually exceeds a few centimeters thickness, shields the underlying ice from melting, and thus affects the downstream evolution of glacial mass balance and flow velocities. Debris-covered glaciers that occupy shallow sloping valleys (<8°), are prone to in-situ decay, with the development of glacier karst and stagnant glacier termini. This frontal behavior contrasts with that of debris-free glaciers, which are situated in lower-relief areas, are mainly nourished by direct snow fall, and have moving termini. Such differences in glacier behavior mostly depend on the topographic characteristics of their accumulation areas but also on climatic gradients, mediated by variations in snowline elevations. In the monsoon-influenced central Himalaya, snowlines are generally high and the glacierized zone is relatively narrow and confined to the highest peaks and massifs. Steep across-strike gradients in climate and relief are accompanied by a rapid northward decrease of debris cover and associated changes in flow characteristics and frontal dynamics. Towards the western end of High Asia, influence of the mid-latitude westerlies increases, which shifts the accumulation season to late winter and early spring, and results in lower snowline elevations. In addition, the upper-level westerlies jet transports atmospheric moisture into summer-arid, internal sectors of the orogen in the western Himalaya and Karakoram, where accumulation areas have gentler slopes, and consequently the amount of debris cover reduced. The glacial flow velocities combined with observations of frontal changes reveal pronounced differences in present-day terminus behavior between the Karakoram, and the Himalaya and Hindu Kush that are best explained by climate-controlled differences in glacial mass balances. Importantly, previously reported, but poorly constrained advancing and stable glacier termini in the Karakoram are clearly observed in the 8-yr record of frontal changes and unrelated to the effects of debris cover on frontal dynamics.

Climatic and topographic gradients and their impact on glacial behavior are also important for millennial scale advances of High Asian glaciers due to natural climate variations during the Quaternary. A new cosmogenic nuclide-based glacial chronology from western Garhwal, in the transitional zone from the central to the western Himalaya, documents at least five glacial advances since ~16 ka. Orographic interception of monsoonal moisture at the front of the

Himalaya induces a steep gradient in precipitation, which is tracked by climate-related equilibrium line altitude (ELA) changes. Although the available data from the western Himalaya indicates largely synchronous glacial advances during the late glacial and Holocene, the superposition of different climatic and topographic gradients result in contrasting glacial dynamics that can lead to asynchronous glacial chronologies, which are observed in other parts of High Asia. At present, it is not entirely clear how High Asian glaciers respond to rapid global climatic changes, such as the Younger Dryas or the 8.2-ka cold events, but the available chronological data, and palaeoclimatic and glacial mass balance arguments, suggest that these episodes had little effects in the Himalaya. Instead, gradual glacial-interglacial temperature changes, superimposed with orbital-scale changes in monsoon strength seem to account for most of the observed glacial variability. However, past changes in westerlies-derived precipitation are poorly constrained and part of the along-strike differences in glacial advances could be related to variations in the strength of the westerlies, asynchronous with monsoon changes.

On 10^5-10^7-year time scales, the interaction of climate and topography is conditioned by the erosive effects of glaciers and their impact on landscape evolution. With the remotely sensed glacier-velocity data, I obtained annual ice-flux estimates near the ELA, which document glacial-erosion potential increasing with glacier size. Thus, higher topography and lower snowlines, allow for the development of more extensive glaciers with greater ability to erode. This provides a positive feedback mechanism for glacial erosion to adjust to different rock uplift rates, which is required for the hypothesis that glacial erosion limits topographic growth. The climatic and topographic analysis further demonstrates that east-west gradients in snowline elevations result in westward increasing accumulation areas, hence glacier sizes and erosion potentials prevailing during the Pleistocene. These data suggest that the glacial impact on topography and significant amounts of relief-production along the western margin of the Tibetan Plateau is due to westerlies-driven glacial erosion, and creates pathways for moisture-bearing winds into the orogen, which accelerate headward fluvial erosion. Conversely, glacial erosion in the monsoonal central Himalaya has largely been confined to elevations >5 km asl, i.e., above the mean elevation of the Tibetan Plateau. Because monsoon strength is reduced during full glacial conditions, and rapid northward decreases in ELA-lowering prevent the development of large and erosive glaciers in the central Himalaya, monsoonal climate is only a weak driver of glacial erosion, helping to preserve an orographic barrier and protecting the Tibetan Plateau margin from lateral incision and destruction.

9   Bibliography

Abramowski, U., A. Bergau, D. Seebach, R. Zech, B. Glaser, P. Sosin, P. W. Kubik, and W. Zech (2006), Pleistocene glaciations of Central Asia: results from ^{10}Be surface exposure ages of erratic boulders from the Pamir (Tajikistan), and the Alay–Turkestan range (Kyrgyzstan), *Quat. Sci. Rev.*, 25, 1080-1096.

Ageta, Y., and K. Higuchi (1984), Estimation of mass balance components of a summer-accumulation type glacier in the Nepal Himalaya, *Geogr. Ann., Ser. A, Phys. Geogr.*, 66, 249-255.

Ageta, Y., W. Zhang, and M. Nakawo (1989), Mass balance studies on Chongce Ice Cap in the West Kunlun Mountains, *Bull. Glacier Res.*, 7, 37-43.

Ageta Y., S. Iwata, H. Yabuki, N. Naito, A. Sakai, C. Narama and Karma (2000), Expansion of glacier lakes in recent decades in the Bhutan Himalayas, in: *Debris-covered glaciers*, edited by M. Nakawo, C. F. Raymond, and A. Fountain, pp. 165-175, IAHS Publication no. 264., Wallingford, UK.

Aizen, V. B., E. M. Aizen, and V. N. Nikitin (2002), Glacier regime on the northern slope of the Himalaya (Xixibangma glaciers), *Quat. Int.*, 97-98, 27-39.

Aizen, V. B., V. A. Kuzmichenok, A. B. Surazakov, and E. M. Aizen (2007), Glacier changes in the Tien Shan as determined from topographic and remotely sensed data, *Global Planet Change*, 56(3-4), 328-340.

Aizen, V. B., P. A. Mayewski, E. M. Aizen, D. R. Joswiak, A. B. Surazakov, S. Kaspari, B. Grigholm, M. Krachler, M. Handley, and A. Finaev (2009), Stable-isotope and trace element time series from Fedchenko glacier (Pamirs) snow/firn cores, *J. Glaciol.*, 55, 275-291.

Allégre, C. J., V. Courtillot, P. Tapponnier, A. Hirn, M. Mattauer, C. Coulon, J. J. Jaeger, J. Achache, U. Schärer, J. Marcoux, J. P. Burg, J. Girardeau, R. Armijo, C. Gariépy, C. Göpel, L. Tindong, X. Xuchang, C. Chenfa, L. Guangqin, L. Baoyu, T. Jiwen, W. Naiwen, C. Guoming, H. Tonglin, W. Xibin, D. Wanming, S. Huaibin, C. Yougong, Z. Ji, Q. Hongrong, B. Peisheng, W. Songchan, W. Bixiang, Z. Yaoxiu and R. Xu. (1984), Structure and Evolution of the Himalaya-Tibet Orogenic Belt, *Nature*, 307 (5946), 17–22.

Alley, R. B., A. Mayewski, T. Sowers, M. Stuiver, K. C. Taylor, and P. U. Clark (1997), Holocene climate instability: a prominent, widespread event 8200 yr ago, *Geology*, 25, 483–486.

Anderson, R. S., P. Molnar, and M. A. Kessler (2006), Features of glacial valley profiles simply explained, *J. Geophys. Res.*, 111 doi:10.1029/2005JF000344.

Anderson, R. S., S. P. Anderson, K. R. MacGregor, E. D. Waddington, S. O'Neel, C. A. Riihimaki, and M. G. Loso (2004), Strong feedbacks between hydrology and sliding of a small alpine glacier, *J. Geophys. Res.*, 109, F03005, doi:10.1029/2004JF000120.

Asahi, K. (2010), Equilibrium-line altitudes of the present and Last Glacial Maximum in the eastern Nepal Himalayas and their implications for SW monsoon climate, *Quat. Int.*, 212, 26-34, doi:10.1016/j.quaint.2008.08.004.

Atkinson, T. C., K. R. Briffa, and G. R. Coope (1987), Seasonal temperatures in Britain during the past 22,000 years, reconstructed using beetle remains, *Nature*, 325, 587–592.

Avouac, J. P., and E. G. Burov (1996), Erosion as a driving mechanism of intracontinental growth?, *J. Geopys. Res.*, 101, 17747-17769.

Avouac, J.-P., F. Ayoub, S. Leprince, O. Konca, and D. V. Helmberger, (2006), The 2005, Mw 7.6 Kashmir earthquake: sub-pixel correlation of ASTER images and seismic waveform analysis, *Earth Planet. Sci. Lett.*, 249(3–4), 514−528.

Back, S., M. D. Batist, M. R. Strecker, and P. Vanhauwaert (1999), Quaternary Depositional Systems in Northern Lake Baikal, Siberia, *J. Geol.*, 107, 1-12.

Bahr, D. B. (1997), Global distributions of glacier properties: A stochastic scaling paradigm, *Water Resour. Res.*, 33(7), 1669–1679.

Bahr, D. B., M. F. Meier, and S. D. Peckham (1997), The physical basis of glacier volume-area scaling, *J. Geophys. Res.*, 102(B9), 20,355-20,362.

Balco, G., J. O. Stone, N. A. Lifton, and T. J. Dunai (2008), A complete and easily accessible means of calculating surface exposure ages or erosion rates from ^{10}Be and ^{26}Al measurements, *Quat. Geochron.*, 8, 174–195.

Ballantyne, C. K. (2002), Paraglacial geomorphology, *Quat. Science. Rev.*, 21, 1935-2017.

Barnard, P. L., L. A. Owen, and R. C. Finkel (2004), Style and timing of glacial and paraglacial sedimentation in a monsoonal influenced high Himalayan environment, the upper Bhagirathi Valley, Garhwal Himalaya, *Sed. Geol.*, 165, 199–221.

Barnett, T. P., J. C. Adam, and D. P. Lettenmaier (2005), Potential impacts of a warming climate on water availability in snow-dominated regions, *Nature*, 439, 303-309, doi:10.1038/nature04141.

Barnett, T., L. Dümenil, U. Schleseand, and E. Roeckner (1988), The effect of Eurasian snow cover on global climate, *Science*, 239, 504–507.

Barrand, N. E., and T. Murray (2006), Multivariate Controls on the Incidence of Glacier Surging in the Karakoram Himalaya, *Arct., Antarct., Alp. Res.*, 38(4), 489–498.

Barros, A. P., G. Kim, and E. Williams (2004), Probing orographic controls in the Himalayas during the monsoon using satellite imagery, *Nat. Hazards Earth Syst. Sci.*, 4, 29–51.

Barros, A. P., M. Joshi, J. Putkonen, and D. W. Burbank (2000), A study of the 1999 monsoon rainfall in a mountainous region in central Nepal using TRMM products and rain gauge observations, *Geophys. Res. Let.*, 27, 3683-3686.

Barry, R. (2008), *Mountain Weather and Climate*, 512 pp., Cambridge University Press, Cambridge, UK.

Barry, R. G., and R. J. Chorley (2003), *Atmosphere, Weather and Climate*, 472 pp., Routledge, London, UK.

Bartholomaus, T. C., R. S. Anderson, and S. P. Anderson (2008), Response of glacier basal motion to transient water storage, *Nature Geosci.*, 1, 33-37.

Beaumont, C., P. Fullsack, and J. Hamilton (1992), Erosional control of active compressional orogens, in *Thrust tectonics*, edited by K. R. McClay, pp. 1-18, Chapman and Hall, London.

Beaumont, C., R. A. Jamieson, M. H. Nguyen, and B. Lee (2001), Himalayan tectonics explained by extrusion of a low-viscosity crustal channel coupled to focussed surface denudation, *Nature*, 414, 738-742.

Benn, D. I., and D. J. E. Evans (1998), *Glaciers and Glaciation*, 734 pp., Arnold, London.

Benn, D. I., and L. A. Owen (1998), The role of the Indian summer monsoon and the midlatitude westerlies in Himalayan glaciation: review and speculative discussion, *J. Geol. Soc., London*, 155, 353–363.

Benn, D. I., and F. Lehmkuhl (2000), Mass balance and equilibrium-line altitudes of glaciers in high-mountain environments, *Quat. Int.*, 65/66, 15-29.

Benn, D. I., S. Wiseman, and C. R. Warren (2000), Rapid growth of a supraglacial lake, Ngozumpa Glacier, Khumbu Himal, Nepal, in: *Debris-covered glaciers*, edited by M. Nakawo, C. F. Raymond, and A. Fountain, pp. 177-185, IAHS Publication no. 264., Wallingford, UK.

Benn, D. I., M. P. Kirkbride, L. A. Owen, and V. Brazier (2003), Glaciated valley landsystems, in *Glacial Landsystems*, edited by D. J. A. Evans, pp. 372-404, Hodder Arnold , London, UK.

Berger, A., and M. F. Loutre (1991), Insolation values for the climate of the last 10 million years, *Quat. Sci. Rev.*, 10, 297-317.

Berger, A. L., and J. A. Spotila (2008), Denudation and deformation in a glaciated orogenic wedge: The St. Elias orogen, Alaska, *Geology*, 36, 7, 523–526, doi:10.1130/G24883A.

Berger, A., S. P. S. Gulick, J. A. Spotila, P. Upton, J. A. Jaeger, J. B. Chapman, L. A. Worthington, T. L. Pavlis, K. D. Ridgway, B. A. Willems, and R. J. McAleer (2008), Quaternary tectonic response to intensified glacial erosion in an orogenic wedge, *Nature Geosci.*, 1, 793-799.

Berthier, E., Y. Arnaud, R. Kumar, S. Ahmad, P. Wagnon, and P. Chevallier (2007). Remote sensing estimates of glacier mass balances in the Himachal Pradesh (Western Himalaya, India), *Remote Sens. Environ.*, 108, 327−338.

Berthier, E., H. Vadon, D. Baratoux, Y. Arnaud, C. Vincent, K. L. Feigl, F. Rémy, and B. Legrésy (2005), Surface motion of mountain glaciers derived from satellite optical imagery, *Remote Sens. Environ.*, 95, 14-28.

Bhutiyani, M. R. (1999), Mass-balance studies on Siachen Glacier in the Nubra valley, Karakoram Himalaya, India, *J. Glaciol.*, 45(149), 112-118.

Bindschadler, R. A. (1998), Monitoring ice sheet behavior from space, *Rev. Geophys.*, 36, 79-104.

Bindschadler, R. A. and T. A. Scambos (1991), Satellite-Image-Derived Velocity Field of an Antarctic Ice Stream, *Science*, 252(5003), 242-252.

Bindschadler, R., W. D. Harrison, C. F. Raymond, and R. Crosson (1977), Geometry and dynamics of a surge-type glacier, *J. Glaciol.*, 18(79), 181-194.

Bindschadler, R. A., P. L. Vornberger, D. D. Blankenship, T. A. Scambos, and R. Jacobel (1996), Surface velocity and mass balance of Ice Streams D and W, West Antarctica, *J. Glaciol.*, 42(142), 461-475.

Blanford, H. F. (1884), On the connection of the Himalayan snowfall with dry winds and seasons of drought in India, *Proc. Roy. Soc. London*, 37, 3–22.

Bolch, T., M. Buchroitner, T. Pieczonka, and A. Kunert (2008), Planimetric and volumetric glacier changes in the Khumbu Himal, Nepal, since 1962 using Corona, Landsat TM and ASTER data, *J. Glaciol.*, 94, 592-600.

Bollasina, M., L. Bertolani, G. Tartari (2002), Meteorological observations in the Khumbu Valley, Nepal Himalayas, 1994–1999, *Bull. Glacier Res.*, 19, 1–11.

Bond, G., H. Heinrich, W. Broecker, L. Labeyrie, J. McManus, J. Andrews, S. Huon, R. Jantschik, S. Clasen, C. Simet, K. Tedesco, M. Klas, G. Bonani, and S. Ivy (1992), Evidence for massive discharges of icebergs into the North Atlantic ocean during the last glacial period, *Nature*, 360, 245-249.

Bookhagen, B., and D. W. Burbank (2006), Topography, relief, and TRMM-derived rainfall variations along the Himalaya, *Geophys. Res. Lett.*, 33, L08405, doi:10.1029/2006GL026037.

Bookhagen, B., and D. W. Burbank (in press), Towards a complete Himalayan hydrologic budget: The spatiotemporal distribution of snow melt and rainfall and their impact on river discharge, *J. Geophys. Res.*, doi:10.1029/2009jf001426.

Bookhagen, B., R. C. Thiede, and M. R. Strecker (2005a), Late Quaternary intensified monsoon phases control landscape evolution in the northwest Himalaya, *Geology*, 33, 149-152, doi:10.1130/G20982.1.

Bookhagen, B., R. C. Thiede, and M. R. Strecker (2005b), Abnormal Monsoon years and their control on erosion and sediment flux in the high, arid northwest Himalaya, *Earth Planet. Sci. Let.*, 231, 131-146.

Boos, W. R., and Z. Kuang (2010), Dominant control of the South Asian monsoon by orographic insulation versus plateau heating, *Nature*, 463, 218-222, doi:10.1038/nature08707.

Boulton, G. S., and N. Eyles (1979), Sedimentation by valley glaciers: a model and genetic classification, in *Moraines and Varves*, edited by C. Schluchter, pp. 11-23, Balkena, Rotterdam.

Bourgine, B. and N. Baghdadi (2005), Assessment of C-band SRTM DEM in a dense equatorial forest zone, *C. R. Geoscience*, 337(14), 1225-1234.

Broccoli, A. J., and S. Manabe (1992), The effects of orography on midlatitude Northern Hemisphere dry climates, *J. Climate*, 5, 1181-1201.

Brocklehurst, S. H., and K. X. Whipple (2002), Glacial erosion and relief production in the Eastern Sierra Nevada, California, *Geomorphology*, 42(1-2), 1-24.

Brocklehurst, S. H.,and K. X. Whipple (2007), Response of glacial landscapes to spatial variations in rock uplift rate, *J. Geophys. Res.*, 112, F02035, doi:10.1029/2006JF000667.

Brozovic, N., D. W. Burbank, and A. J. Meigs (1997), Climatic limits on landscape development in the northwestern Himalaya, *Science*, 276, 571–574.

Budd, W. F., and I. F. Allison (1975), An empirical scheme for estimating the dynamics of unmeasured glaciers, *IAHS-AISH Publication*, 104, 246-256.

Budd, W. F., P. L. Kreage, and N. A., Blundy (1979), Empirical studies of ice sliding, *J. Gaciol.*, 23(89), 157-170.

Bull, W. B. (1991), *Geomorphic Responses to Climatic Change*, pp. 326, Oxford University Press, New York, USA.

Burbank, D. W. (1992), Causes of recent Himalayan uplift deduced from deposited patterns in the Ganges basin, *Nature*, 357, 680-683.

Burbank, D. W., A. E. Blythe, J. Putkonen, B. Pratt-Sitaula, E. Gabet, M. Oskin, A. Barros, and T. P. Ojha (2003), Decoupling of erosion and precipitation in the Himalayas, *Nature*, 426, 652-655.

Cenderelli, D. A. and E. E. Wohl (2001), Peak discharge estimates of glacial-lake outburst floods and "normal" climatic floods in the Mount Everest region, Nepal, *Geomorphology*, 40, 57-90.

Chen, F., Z. Yu, M. Yanag, E. Ito, S. Wang, D. B. Madsen, X. Huang, Y. Zhao, T. Sato, J. B. Birks, I. Boomen, J. Chen, C. An, and B. Wünnemann (2008), Holocene moisture evolution in arid central Asia and its out-of-phase relationship with Asian monsoon history, *Quat. Sci. Rev.*, 27, 351–364.

Chen, F.-H., J.-H. Chen, J. Holmes, I. Boomer, P. Austin, J. B. Gates, N.-L. Wang, S. J. Brooks, and J.-W. Zhang (2010), Moisture changes over the last millennium in arid central Asia: a review, synthesis and comparison with monsoon region, *Quat. Sci. Rev.*, 29, 1055-1068, doi:10.1016/j.quascirev.2010.01.005.

Cheng, H., R. L. Edwards, W. S. Broecker, G. H. Denton, X. Kong, Y. Wang, R. Zhang, and X. Wang (2009), Ice Age Termination, *Science*, 326(248), DOI: 10.1126/science.1177840.

Chevalier, M. L., G. E. Hilley, J. Liu-Zeng, P. Tapponnier, and J. Van Der Woerd (2008), Surface-exposure cosmogenic dating of Southern Tibet moraines reveal glaciations coincident with the Northern Hemisphere, *Eos Trans. AGU*, 89(53), Fall Meet. Suppl., Abstract GC21A-0723.

Church, M., and O. Slaymaker (1989), Disequilibrium of Holocene sediment yield in glaciated British Columbia, *Nature*, 337, 452–454.

Clark, D. H., M. M. Clark, and A. R. Gillespie (1994), Debris-covered glaciers in the Sierra Nevada, California, and their implications for snowline reconstructions, *Quat. Res.*, 41, 139-153.

Clark, P. U., N. G. Pisias, T. F. Stocker, and A. J. Weaver (2002), The role of the thermohaline circulation in abrupt climate change, *Nature*, 415, 863-869.

Clayton, L. (1964), Karst topography on stagnant glaciers, *J. Glaciol.*, 5, 107-112.

Crippen, R. E., S. J. Hook, and E. J. Fielding (2007), Nighttime ASTER thermal imagery as an elevation surrogate for filling SRTM DEM voids, *Geophys. Res. Let.*, 34, L01302, doi:10.1029/2006GL028496.

Cruz, R.V., H. Harasawa, M. Lal, S. Wu, Y. Anokhin, B. Punsalmaa, Y. Honda, M. Jafari, C. Li and N. Huu Ninh (2007), Asia, in: *Climate Change 2007: Impacts, Adaptation and Vulnerability. Contribution of Working Group II to the Fourth Assessment Report of the Intergovernmental Panel on Climate Change*, edited by M.L. Parry, O.F. Canziani, J.P. Palutikof, P.J. van der Linden and C.E. Hanson, Eds., pp. 469-506, Cambridge University Press, Cambridge, UK.

Cuffey, K. M., and G. D. Clow (1997), Temperature, accumulation, and ice sheet elevation in central Greenland through the last deglacial transition, *J. Geophys. Res.*, 102, 26,383-26,396.

Damm, B. (2006), Late Quaternary glacier advances in the upper catchment area of the Indus River (Ladakh and Western Tibet), *Quat. Int.*, 154–155, 87–99, doi:10.1016/j.quaint.2006.02.013.

de Scally, F. A. (1997), Deriving lapse rates of slope air temperature for meltwater runoff modeling in subtropical mountains: an example from the Punjab Himalaya, Pakistan, *Mt. Res. Dev.*, 17, 353-362.

de Scally, F. A., and J. F. Gardner (1990), Ablation of Avalanched and Undisturbed snow, Himalaya Mountains, Pakistan, *Water Resour. Res.*, 26(11), 2757-2767.

Demske, D., P. E. Tarasov, B. Wünnemann, and F. Riedel (2009), Late glacial and Holocene vegetation, Indian monsoon and westerly circulation in the Trans-Himalaya recorded in the lacustrine pollen sequence from Tso Kar, Ladakh, NW India, *Palaeogeogr., Palaeocl., Palaeoecol.*, 279, 172–185.

Denton, G. H., R. B. Alley, G. C. Comer, and W. S. Broecker (2005), The role of seasonality in abrupt climate change, *Quat. Sci. Rev.*, 24, 1159–1182.

Dimri, A. P. (2006), The Contrasting Features of Winter Circulation During Surplus and Deficient Precipitation Over Western Himalayas, *Pure Appl. Geophys.*, 162, 2215-2237.

Dobhal, D. P., J. T. Gergan, and R. J. Thayyen (2008), Mass balance studies of the Dokriani Glacier from 1992 to 2000, Garhwal Himalaya, India, *Bull. Glaciol. Res.*, 25, 9-17.

Duncan, C. C, A. J. Klein, J. G. Masek, and B. L. Isacks (1998), Comparison of Late Pleistocene and Modern Glacier Extents in Central Nepal Based on Digital Elevation Data and Satellite Imagery, *Quat. Res.*, 49, 241–254.

Dykoski, C. A., R. L. Edwards, H. Cheng, D. Yuan, Y. Cai, M. Zhang, Y. Lin, J. Qing, Z. An, and J. Revenaugh (2005), A high-resolution, absolute-dated Holocene and deglacial Asian monsoon record from Dongge Cave, China, *Earth Planet. Sci. Let.*, 233, 71–86.

Dyurgerov, M. B., and M. F. Meier (2005), *Glaciers and the changing Earth system: A 2004 snapshot*, Occas. Pap., 58, 117 pp., Inst. of Arct. And Alp. Res., Boulder, Colo. (Available at http://instaar.colorado.edu/other/download/OP58_dyurgerov_meier.pdf).

Eckert, S., T. Kellenberger, and K. Itten (2005), Accuracy assessment of automatically derived digital elevation models from aster data in mountainous terrain, *Int. J. Remote Sens.*, 26(9), 1943-1957.

Egholm, D. L., S. B. Nielsen, V. K. Pedersen, and J.-E. Lesemann (2009), Glacial effects limiting mountain height, *Nature Geosci.*, 460, 884-887, doi:10.1038/nature08263.

Enzel, Y., L. L. Ely, S. Mishra, R. Ramesh, R. Amit, B. Lazar, S. N. Rajaguru, V. R. Baker, and A. Sandler (1999), High-resolution Holocene environmental changes in the Thar Desert, northwestern India, *Science*, 284, 125–128.

Farr, T. G., P. A. Rosen, E. Caro, R. Crippen, R. Duren, S. Hensley, M. Kobrick, M. Paller, E. Rodriguez, L. Roth, D. Seal, S. Shaffer, J. Shimada, J. Umland, M. Werner, M. Oskin, D. Burbank, and D. Alsdorf5 (2007), The Shuttle Radar Topography Mission, *Rev. Geophys.*, 45, RG2004, doi:10.1029/2005RG000183.

Fielding, E., B. Isacks, M. Barazangi, and C. Duncan (1994), How flat is Tibet?, *Geology*, 22, 163-167.

Finkel, R. C., L. A. Owen, P. L. Barnard, and M. W. Caffee (2003), Beryllium-10 dating of Mount Everest moraines indicates a strong monsoonal influence and glacial synchroneity throughout the Himalaya, *Geology*, 31, 561–564.

Fleitmann, D., S. J. Burns, M. Mudelsee, U. Neff, J. Kramers, A. Mangini, and A. Matter (2003), Holocene Forcing of the Indian Monsoon Record in a Stalagmite from the Southern Oman, *Science*, 300, 1737–1739.

Flint, R. F. (1942), Glacier thinning during deglaciation. Part II. Glacier thinning inferred from geological data, *Am. Jour. Sci.*, 240(2), 113-136.

Flohn H. (1956), Zum Klima der Hochgebirge Zentralasiens II, *Meteorol. Rdsch.,* 9, 85-88.

Flohn, H. (1957), Large-scale aspects of the "summer monsoon" in south and East Asia, *J. Meteor. Soc. Japan*, 75, 180–186.

Fountain, A. C. and J. S. Walder (1998), Water flow through temperate glaciers, *Rev. Geophys.*, 36(3), 299-328.

Fowler, A. C. and D. A. Larson (1978), On the Flow of Polythermal Glaciers. I. Model and preliminary analysis, *P. Roy. Soc. Lond A Mat.*, 363(1713), 217-242.

Fowler, H. J., and D. R. Archer (2006), Conflicting signals of climatic change in the upper Indus Basin, *J. Clim.*, 19, 4276-4293.

Fuchs, G. (1975), Contributions to the geology of the North-Western Himalayas*, Abh. Geol. Bundesanst. Vienna/A*, 32, pp. 59.

Fujisada, H., G. B. Bailey, G. G. Kelly, S. Hara, and M. J. Abrams (2005), ASTER DEM Performance, *IEEE T. Geosci. Remote*, 43(12), 2707-2714.

Fujita, K., and Y. Ageta (2000), Effect of summer accumulation on glacier mass balance on the Tibetan Plateau revealed by mass balance model, *J. Glaciol.*, 46, 244-252.

Fujita, K., N. Takeuchi, and K. Seko (1998), Glaciological observations of Yala Glacier, in Langtang valley, Nepal Himalayas, 1994 and 1996, *Bull. Glacier Res.*, 16, 75-81.

Fujita, K., F. Nakazawa, and B. Rana (2001), Glaciological observations on Rikha Samba Glacier, Hidden Valley, Nepal Himalayas, 1989 and 199, *Bull. Glacier Res.*, 18, 31-35.

Fujita, K., M. Nakawo, Y. Fujii, and P. Paudyal (1997), Changes in glaciers in Hidden Valley, Mukut Himal, Nepal Himalayas, from 1974 to 1994, *J. Glaciol.*, 43, 583-588.

Fujita, K., Y. Ageta, P. Jianchen, and Y. Tandong (2000), Mass balance of Xiao Dongkemadi glacier on the central Tibetan Plateau, *Ann. Glaciol.*, 31, 159-163.

Gadgil, S. (2003), The Indian Monsoon and Its Variability, *Ann. Rev. Earth Planet. Sci.*, 31, 429–67, doi:10.1146/annurev.earth.31.100901.141251

Gansser, A. (1964), *Geology of the Himalayas*, pp. 289, Interscience, London, UK.

Gasse, F., J. Ch. Fontes, E. Van Campo, and K. Wei (1996), Holocene environmental changes in Bangong Co basin (western Tibet). Part 4: discussions and conclusions, *Palaeogeogr., Palaeocl., Palaeoecol.*, 120, 79–82.

Gayer, E., J. Lavé, R. Pik, and C. France-Lanord (2006), Monsoonal forcing of Holocene glacier fluctuations in Ganesh Himal (Central Nepal) constrained by cosmogenic 3He exposure ages of garnets, *Earth Planet. Sci. Let.*, 252, 275–288, doi:10.1016/j.epsl.2006.09.040.

Gillespie, A., and P. Molnar (1995), Asynchronous maximum advances of mountain and continental glaciers, *Rev. Geophys.*, 33, 311–364.

Goldstein, R. M., H. Engelhardt, B. Kamb, and R. M. Frolich (1993), Satellite Radar Interferometry for Monitoring Ice Sheet Motion: Application to an Antarctic Ice Stream, *Science*, 262(5139), 1525-1530.

Gorokhovich, Y. and A. Voustianiouk (2006), Accuracy assessment of the processed SRTM-based elevation data by CGIAR using field data from USA and Thailand and its relation to the terrain characteristics, *Remote Sens. Environ.*, 104, 409-415.

Gosse, J. C., and F. M. Phillips (2001), Terrestrial in situ cosmogenic nuclides: theory and application, *Quat. Sci. Rev.*, 20, 1475–1560.

Goswami, B. N., V. Venugopal, D. Sengupta, M. S. Madhusoodanan, and P. Xavier (2006), Increasing trend of extreme rain events over India in a warming environment, *Science*, 314(5804), 1442-1445.

Gudmundsson, G. H., A. Bassi, M. Vonmoos, A. Bauder, U. H. Fischer, and M. Funk (2000), High-resolution measurements of spatial and temporal variations in surface velocities of Unteraargletscher, Bernese Alps, Switzerland, *Ann. Glaciol.*, 31, 63-68.

Haeberli, W., Cihlar, J., Barry, R.G. (2000). Glacier monitoring within the global climate observing system. *Ann. Glaciol.*, 31, 241-246.

Haeberli, W., M. Hoelzle, F. Paul, and M. Zemp (2007), Integrated monitoring of mountain glaciers as key indicators of global climate change: the European Alps, *Ann. Glaciol.*, 46, 150-160.

Hahn, D. G. and S. Manabe (1975), The role of mountains in the south Asian monsoon circulation, *J. Atmos. Sci.*, 32, 1515-1541.

Hahn, D. G., and J. Shukla (1976), An Apparent Relationship between Eurasian Snow Cover and Indian Monsoon Rainfall, *J. Atmos. Sci.*, 33, 2461-2462.

Hall, D. K., G. A. Riggs, and V. V. Salomonson (2007), *MODIS/Aqua Snow Cover Daily L3 Global 0.05deg CMG V005*, [March 2000 – March 2008]. Boulder, Colorado USA: National Snow and Ice Data Center. Digital media, updated daily.

Hallet, B., and J. Putkonen (1994), Surface dating of dynamic landforms: young boulders on aging moraines, *Science*, 265, 937–940.

Hallet, B., L. Hunter, and J. Bogen (1996), Rates of eosion and sediment evacuation by glaciers: A review of field data and their implications, *Global Planet. Change*, 12, 213-235.

Harper, J. T., and N. F. Humphrey (2003), High altitude Himalayan climate inferred from glacial ice flux, *Geophys. Res. Let.*, 30(14), 1764-1769, doi:1710.1029/2003GL017329.

Harper, J. T., N. F. Humphrey, W. T. Pfeffer, B. Lazar (2007), Two modes of accelerated glacier sliding related to water, *Geophys. Res. Let.*, 34, L12503, doi:10.1029/2007GL030233.

Harrison, T. M., P. Copeland, W. S. F. Kidd, and A. Yin (1992), Raising Tibet, *Science*, 255, 1663-1670.

Hays, J. D., J. Imbrie, and N. J. Shackleton (1976), Variations in the Earth's Orbit: Pacemaker of the Ice Ages, *Science*, 194(4270), 1121-1132.

Hedin, S. (1900), *Die Geographisch-wissenschaftlichen Ergebnisse meiner Reisen in Zentralasien*, 1894-1897, pp. 399, Gotha, Perthes.

Heimsath, A. M. and R. S. McGlynn (2008), Quantifying headwall retreat rates in the Nepal High Himalaya, *Geomorphology*, 97(1-2), 5-23.

Herzschuh, U. (2006), Paleo-moisture evolution in monsoonal Central Asia during the last 50,000 years, *Quat. Sci. Rev.*, 25, 163–178.

Hewitt, K. (1988), Catastrophic landslide deposits in the Karakoram Himalaya, *Science*, 242, 64-67.

Hewitt, K. (1999), Quaternary moraines vs. catastrophic avalanches in the Karakoram Himalaya, northern Pakistan, *Quat. Res.*, 51, 220–237.

Hewitt, K. (2005), The Karakoram anomaly? Glacier expansion and the 'elevation effect,' Karakoram Himalaya, *Mt. Res. Dev.*, 25, 332–340.

Hewitt, K. (2007), Tributary glacier surges: an exceptional concentration at Panmah Glacier, Karakoram Himalaya. *J. Glaciol.*, 53, 181-188.

Hewitt, K. (2009), Catastrophic rock slope failures and late Quaternary developments in the Nanga Parbat–Haramosh Massif, Upper Indus basin, northern Pakistan, *Quat. Sci. Rev.*, 28 , 1055–1069.

Hodges, K. V. (2000), Tectonics of the Himalaya and southern Tibet from two perspectives, *Geol. Soc. Am., Bull.*, 112, 324-350.

Hoskins, B. J. and K. I. Hodges (2002), New Perspectives on the Northern Hemisphere Winter Storm Tracks, *J. Atmos. Sci.*, 59, 1041-1061.

Howat, I. M., I. Jougin, and T. A. Scambos (2007), Rapid Changes in Ice Discharge from Greenland Outlet Glaciers, *Science*, 315, 1559-1561.

Hubbard, B. and N. F. Glasser (2005), *Field Techniques in Glaciology and Glacial Geomorphology,* pp. 412, Wiley, Chichester, UK.

Humlum, O., H. H. Christiansen, and H. Juliussen (2007), Avalanche-derived Rock Glaciers in Svalbard, *Permafrost Periglac. Proc.*, 18(1), 75-88.

Huss, M., M. Funk, and A. Ohmura (2009), Strong Alpine glacier melt in the 1940s due to enhanced solar radiation, *Geophys. Res. Let.*, 36, L23501, doi:10.1029/2009GL040789.

Imbrie, J., and K. P. Imbrie (1979), *Ice Ages: Solving the Mystery*, pp. 224, Harvard University press, Cambridge, USA.

Inoue, J. (1977), Mass budget of Khumbu Glacier, *Seppyo*, 39 (Special Issue), 15-19.

IPCC (2007a). *Climate Change 2007: The Physical Science Basis. Contribution of Working Group I to the Fourth Assessment Report of the Intergovernmental Panel on Climate Change* edited by S. Solomon, D. Qin, M. Manning, Z. Chen, M. Marquis, K. B. Averyt, M. Tignor, and H. L. Miller, Cambridge University Press, Cambridge, UK.

IPCC (2007b). *Climate Change 2007: Impacts, Adaption and Vulnerability. Contribution of Working Group II to the Fourth Assessment Report of the Intergovernmental Panel on Climate Change* , edited by M. L. Parry, O. F. Canziani, J. P. Palutikof, P. J. van der Linden, and C. E. Hanson, Cambridge University Press, Cambridge, UK.

Isarin, R. F. B., and H. Renssen (1999), Reconstructing and modeling Late Weichselian climates: the Younger Dryas in Europe as a case study, *Earth Sci. Rev.*, 48, 1–38.

Ivy-Ochs, S., C. Schlüchter, P. W. Kubik, G. H. Denton (1999), Moraine Exposure Dates Imply Synchronous Younger Dryas Glacier Advances in the European Alps and in the Southern Alps of New Zealand, *Geogr. Ann., Ser. A, Phys. Geogr.*, 81, 313-323.

Ivy-Ochs, S., H. Kerschner, M. Maisch, M. Christl, P. W. Kubik, C. Schlüchter (2009), Latest Pleistocene and Holocene glacier variations in the European Alps, *Quat. Sci. Rev.*, 28, 2137-2149, doi:10.1016/j.quascirev.2009.03.009.

Jain, S. K, A. Goswami, and A. K. Saraf (2008), Determination of land surface temperature and its lapse rate in the Satluj River basin using NOAA data, *Int. J. Remote Sens.*, 29, 3091–3103.

Joughin, I. (2002), Ice-sheet velocity mapping: a combined interferometric and speckle-tracking approach, *Annals of Glaciology*, 34, 195-201.

Joughin, I., R. Kwok, and M. Fahnestock (1996), Estimation of ice-sheet motion using satellite radar interferometry: method and error analysis with application to Humboldt Glacier, Greenland, *J. Glaciol.*, 42(142), 564-575.

Joughin, I., W. Abdalati, and M. Fahnestock (2004), Large fluctuations in speed on Greenland's Jakobshavn Isbrae glacier, *Nature*, 432(7017), 608-610.

Joughin, I., T. Slawek, R. Bindschadler, and S. F. Price (2002), Changes in west Antarctic ice stream velocities: Observation and analysis, *J. Geophys. Res.*, 107(B11), 2289, doi:10.1029/2001JB001029.

Kääb, A. (2002), Monitoring high-mountain terrain deformation from repeated air- and spaceborne optical data: examples using digital aerial imagery and ASTER data. *ISPRS J. Photogramm.*, 57, 39-52.

Kääb, A. (2005), Combination of SRTM3 and repeat ASTER data for deriving alpine glacier flow velocities in the Bhutan Himalaya, *Remote Sens. Environ.*, 94, 463-474.

Kääb, A., C. Huggel, L. Fischer, S. Guex, F. Paul, I. Roer, N. Salzmann, S. Schlafli, K. Schmutz, T. Strozzi, and Y. Weidmann (2005), Remote sensing of glacier- and permafrost-related hazards in high mountains: an overview, *Nat. Hazards Earth Sys.*, 5, 527–554.

Kale, V. S., and P. S. Hire (2004), Effectiveness of monsoon floods on the Tapi River, India: role of channel geometry and hydrologic regime, *Geomorphology*, 57, 275–291.

Kalnay, E., M. Kanamitsu, R. Kistler, W. Collins, D. Deavon, L. Gandin, M. Iredell, S. Saha, G. White, J. Woollen, Y. Zhu, M. Chelliah, W. Ebisuzaki, W. Higgens, J. Janowiak, K. C. Mo, C. Ropelewski, J. Wang, A. Leetmaa, R. Reynolds, R. Jenne, and D. Joseph (1996), The NCEP/NCAR 40-year reanalysis project, *Bull. Amer. Meteor. Soc.*, 77, 437-470.

Kargel, J. S., M. J. Abrams, M. P. Bishop, A. Bush, G. Hamilton, H. Jiskoot, A. Kääb, H. H. Kieffer, E. M. Lee, F. Paul, F. Rau, B. Raup, J. F. Shroder, D. Soltesz, D. Stainforth, L. Stearns, R. Wessels (2005), Multispectral imaging contributions to global land ice measurements from space, *Remote Sens. Environ.*, 99, 187-219.

Karim, A., and J. Veizer (2002), Water balance of the Indus River Basin and moisture source in the Karakoram and western Himalaya: Implications from hydrogen and oxygen isotopes in river water. *J. Geophys. Res.*, 107(D18), 4362, doi:10.1029/2000JD000253.

Karma, Y. Ageta, N. Naito, S. Iwata, H. Yabuki (2003), Glacier distribution in the Himalayas and glacier shrinkage from 1963-1993 in the Bhutan Himalayas, *Bull. Glac. Res.*, 20, 29-40.

Kattelmann, R. (2003), Glacial Lake Outburst Floods in the Nepal Himalaya: A Manageable Hazard? *Natural Hazards*, 28, 145-154.

Kayastha, R. B., Y. Takeuchi, M. Nakawo, and Y. Ageta (2000), Practical prediction of ice melting beneath various thickness of debris cover on Khumbu glacier, Nepal, using a positive degree-day factor, in *Debris-covered glaciers*, edited by M. Nakawo, C. F. Raymond, and A. Fountain, pp.71-82, IAHS Publication no. 264, Wallingford, UK.

Kehrwald, N. M., L. G. Thompson, Y. Tandong, E. Mosley-Thompson, U. Schotterer, V. Alfimov, J. Beer, J. Eikenberg, and M. E. Davis (2008), Mass loss on Himalayan glacier endangers water resources, *Geophys. Res. Lett.*, 35, L22503, doi:10.1029/2008GL035556.

Khalsa, S. J. S., M. B. Dyurgerov, T. Khromova, B. H. Raup, R. G. Barry (2004), Space-Based Mapping of Glacier Changes Using ASTER and GIS Tools. *IEEE T. Geosci. Remote Sens.*, 42(19), 2177-2183.

Kirkbride, M. P. (1993), The temporal significance of transitions from melting to calving termini at glaciers in the central Southern Alps of New Zealand, *Holocene*, 3(3), 232-240, doi: 10.1177/095968369300300305.

Kirkbride, M. (1995), Ice Flow Vectors on the Debris-Mantled Tasman Glacier, 1957-1986, *Geogr. Ann., Ser. A, Phys. Geogr.*, 77(3), 147-157.

Kirkbride, M. P., and C. R. Warren (1999), Tasman Glacier, New Zealand: Twentieth-century thinning and predicted calving retreat, *Global Planet. Change*, 22, 11-28.

Kohl, C. P., and K. Nishiizumi (1992), Chemical isolation of quartz for measurement of in situ produced cosmogenic nuclides, *Geochim. Cosmochim. Ac.* 56, 3583–3587.

Konrad, S. K. and N. F. Humphrey (2000), Steady-state flow model of debris-covered glaciers (rock glaciers), in *Debris-covered glaciers*, edited by M. Nakawo, C. F. Raymond, and A. Fountain, pp. 255-263 , IAHS Publication no. 264., Wallingford, UK.

Korup, O., and D. R. Montgomery (2008), Tibetan plateau river incision inhibited by glacial stabilization of the Tsangpo gorge, *Nature*, 455, 786-789, doi:10.1038/nature07322.

Kulkarni, A. V. (1992), Mass balance of Himalayan glaciers using AAR and ELA methods, *J. Glaciol.*, 38(128), 101−104.

Kulkarni, A. V., B. P. Rathore, and S. Alex (2004), Monitoring of glacial mass balance in the Baspa basin using accumulation area ratio method, Current Science 86, 185-190.

Kulkarni, A. V., B. P. Rathore, S. Mahajan, P. Mathur (2005). Alarming retreat of Parbati glacier, Beas basin, Himachal Pradesh. *Curr. Sci. India*, 88(11), 1844-1850.

Kutzbach, J. E. (1981), Monsoon Climate of the Early Holocene: Climate Experiment with the Earth's Orbital Parameters for 9000 Years Ago, *Science*, 214, 59-61.

Lang, T. J., and A. P. Barros (2004), Winter Storms in the Central Himalayas, *J. Meteorol. Soc. Japan*, 82, 829-844.

Leprince, S., P. Musé, and J.-P. Avouac (2008), In-flight CCD distortion calibration for pushbroom satellites based on subpixel correlation, *IEEE Trans. Geosci. Remote Sens.*, 46, 2675–2683, doi:10.1109/TGRS.2008.918649.

Leprince, S., S. Barbot, F. Ayoub, and J.-P. Avouac (2007), Automatic and precise orthorectification, coregistration, and subpixel correlation of satellite images, application to ground deformation measurements, *IEEE Trans. Geosci. Remote Sens.*, 45(6), 1529-1558, doi: 10.1109/TGRS.2006.888937.

Leprince, S., E. Berthier, F. Ayoub, C. Delacourt, and J.-P. Avouac (2008), Monitoring Earth surface dynamics with optical imagery, *EOS Transactions*, 89(1), 1−2.

Lifton, N. A., J. W. Bieber, J. M. Clem, M. L. Duldig, P. Evenson, J. E. Humble, R. Pyle (2005), Addressing solar modulation and long-term uncertainties in scaling secondary cosmic rays for in situ cosmogenic nuclide applications, *Earth Planet. Sci. Let.*, 239, 140–161.

Liu, S., Z. Xie, G. Song, L. Ma, and Y. Ageta (1996), Mass-balance of Kangwure (flat-top) Glacier, on the north side of Mt. Xixiabangma, China, *Bull. Glacier Res.*, 14, 37-43.

Liu, S., D. Shangguan, Y. Ding, H. Han, C. Xie, Y. Zhang, J. Li, J. Wang, and G. Li (2006), Glacier changes during the past century in the Gangrigabo mountains, southeast Qinghai-Xizang (Tibetan) Plateau, China, *Ann. Glaciol.*, 43, 187-193.

Liu, Y., S. Hou, Y. Wang, and L. Song (2009), Distribution of Borehole Temperature at Four High-altitude Alpine Glaciers in Central Asia, *J. Mt. Sci.*, 6, 221–227, doi: 10.1007/s11629-009-0254-9

Lucchita, B. K. And H. M. Ferguson (1986), Antarctica: Measuring Glacier Velocity from Satellite Images, *Science*, 234(4779), 1105-1108.

Luckman, A., D. Quincey, and S. Bevan (2007), The potential of satellite radar interferometry and feature tracking for monitoring flow rates of Himalayan glaciers, *Remote Sens. Environ.*, 111, 172-181.

Luckman, B. H. (1977), The Geomorphic Activity of Snow Avalanches, *Geogr. Ann., Ser. A, Phys. Geogr.*, 59(1/2), 31-48.

Luedeling, E., S. Siebert, and A. Buerkert (2007), Filling the voids in the SRTM elevation model – A TIN-based delta surface approach, *ISPRS J. Photogramm. Remote Sens.*, 62(4), 283-294.

Masek, J. G., B. L. Isacks, T. L. Gubbels, E. J. Fielding (1994), Erosion and tectonics at the margins of continental plateaus, *J. Geophys. Res.*, 99(B7), 13,941-13,956.

Massonet, D. and K. L. Feigl (1998), Radar interferometry and its application to changes in the Earth's surface. *Rev. Geophys.*, 36(4), 441-500.

Mattson, L. E., J. S. Gardner, and G.J. Young (1993), Ablation on debris covered glaciers: an example from the Rakhiot Glacier, Punjab, Himalaya, in *Snow and Glacier Hydrology*, edited by G. J. Young, pp. 289.296, IAHS Publication no. 218, Wallingford, UK.

Mayewski, P. A., and P. A. Jeschke (1979), Himalayan and Trans-Himalayan Glacier Fluctuations Since AD 1812, *Arct. Alp. Res.*, 11(3), 267-287.

Meehl, G. A., and W. M. Washington (1993), South Asian Summer Monsoon Variability in a Model with Doubled Atmospheric Carbon Dioxide Concentration, *Science*, 260(5111), 1101-1104.

Meier, M. F., and A. S. Post (1962), Recent variations in mass net budgets of glaciers in western North America, *IAHS Publication*, 58, 63-77.

Meierding, T. C. (1982), Late Pleistocene glacial equilibrium-line in the Colorado Front Range: a comparison of methods, *Quat. Res.*, 18, 289–310.

Menounos, B., G. Osborn, J. J. Clague, and B. H. Luckman (2009), Latest Pleistocene and Holocene glacier fluctuations in western Canada, *Quat. Sci. Rev.*, 28, 2049-2074, doi:10.1016/j.quascirev.2008.10.018.

Meyer, M. C., Ch.-Ch. Hofmann, A. M. D. Gemmell, E. Haslinger, H. Häusler, and D. Wangda (2009), Holocene glacier fluctuations and migration of Neolithic yak pastoralists into the high valleys of northwest Bhutan, *Quat. Sci. Rev.*, 28, 1217-1237, doi:10.1016/j.quascirev.2008.12.025.

Michel, R. and E. Rignot (1999), Flow of Glacier Moreno, Argentina, from repeat-pass Shuttle Imaging Radar images: Comparison of the phase correlation method with radar interferometry, *J. Glaciol.*, 45(149), 93-100.

Miehe, G., M. Winiger, J. Böhner, and Z. Yili (2001), The Climatic Diagram Map of High Asia. Purpose and Concepts, *Erdkunde*, 55, 94-97.

Mihalcea, C., C. Myer, G. Diolaiuti, A. Lambrecht, C. Smiraglia,, and G. Tartari (2006), Ice ablation and meteorological conditions on the debris-covered area of Baltoro glacier, Karakoram, Pakistan, *Ann. Glaciol.*, 43, 292-300.

Mitchell, S. G., and D. R. Montgomery (2006), Influence of a glacial buzzsaw on the height and morphology of the Washington Cascade Range, Washington State, USA, *Quat. Res.*, 65(1), 96-107.

Molnar, P. and P. Tapponnier (1975), Cenozoic tectonics of Asia: Effects of a continental collision, *Science*, 189, 419-426.

Molnar, P., and P. England (1990), Late Cenozoic uplift of mountain ranges and global climate change: chicken or egg?, *Nature*, 346, 29-34.

Montgomery, D. R. (1994), Valley Incision and the uplift of mountain peaks, *J. Geophys. Res.*, 99(B7), 13,913-13,921.

Montgomery, D. R., G. Balco, and S. D. Willett (2001), Climate, tectonics, and the morphology of the Andes, *Geology*, 29, 7, 579-582.

Müller, F. (1980) Present and late Pleistocene equilibrium line altitudes in the Mt Everest region – an application of the glacier inventory data, *IAHS-AISH Publ.*, 126, 75-94.

Nakawo, M., H. Yabuki and A. Sakai (1999), Characteristics of Khumbu Glacier, Nepal Himalaya: recent changes in the debris covered area, *Ann. Glaciol.*, 28, 118–122.

National Snow and Ice Data Center (2009), *World glacier inventory*, World Glacier Monitoring Service and National Snow and Ice Data Center/World Data Center for Glaciology. Boulder, CO. Digital media available online at http://nsidc.org/data/g01130.html, updated 2009.

Nesje, A. (2009), Latest Pleistocene and Holocene alpine glacier fluctuations in Scandinavia, *Quat. Sci. Rev.*, 28, 2119-2136, doi:10.1016/j.quascirev.2008.12.016

Nesje, A., S. O. Dahl (1993), Lateglacial and Holocene glacier fluctuations and climate variations in western Norway: a review, *Quat. Sci. Rev.*, 12, 255–261.

New, M., D. Lister, M. Hulme, and I. Makin (2002), A high-resolution data set of surface climate over global land areas, *Clim. Res.*, 21, 1–25.

Nishiizumi, K., E. L. Winterer, C. P. Kohl, D. Lal, J. R. Arnold, J. Klein, and R. Middleton (1989), Cosmic ray production rates of ^{10}Be and ^{26}Al in quartz from glacially polished rocks, *J. Geophys. Res.*, 94, 17,907-17,915.

Nye, J. F. (1959), A method of determining the strain-rate tensor at the surface of a glacier, *J. Glaciol.*, 3(25), 409-419.

Nye, J. F. (1965), The flow of a glacier in a channel of rectangular, elliptic or parabolic cross-section, *J. Glaciol.*, 5 (41), 661-690.

O'Callaghan, J. F., and D. M. Mark (1984), The extraction of drainage networks from digital elevation data, *Comput. Vision Graph.*, 28, 323-344.

Odell, N. E. (1925), Observations on the Rocks and Glaciers of Mount Everest, *Geogr. J.*, 66(4), 289-313.

Oerlemans, J. (1994), Quantifying global warming from the retreat of glaciers, *Science*, 264(5156), 243-245.

Oerlemans, J. (2001), *Glaciers and Climate Change*, 148 pp., Balkema, Lisse, Netherlands.

Oerlemans, J. (2005), Extracting a Climate Signal from 169 Glacier Records, *Science*, 308, 675-677.

Oerlemans, J., and J. P. F. Fortuin (1992), Sensitivity of small glaciers and ice caps to greenhouse warming, *Science*, 258, 115-117.

Oerlemans, J., and B. K. Reichert (2000), Relating glacier mass balance to meteorological data by using a seasonal sensitivity characteristic, *J. Glaciol.*, 46, 1-6.

Oerlemans, J., R. H. Giesen, and M. R. Van den Broeke (2009),Retreating alpine glaciers: increase melt rates due to accumulation of dust (Vadret da Morteratsch, Switzerland), *J. Glaciol.*, 55(192), 729-736.

Ogilvie, I. H. (1904), The Effect of Superglacial Débris on the Advance and Retreat of Some Canadian Glaciers, *J. Geol.*, 12(8), 722-743.

Ohata, T., S. Takahashi, and X. Kang (1989), Meteorological conditions of the West Kunlun Mountains in the summer of 1987, *Bull. Glac. Res.*, 7, 67-76.

Ohmura, A., P. Kasser, and M. Funk (1992), Climate at the equilibrium line of glaciers, *J. Glaciol.*, 38(130), 397-411.

Østrem, G. (1959), Ice melting under a thin layer of moraine, and the existence of ice cores in moraine ridges, *Geogr. Ann.*, 41(4), 228-230.

Overpeck, J., D. Anderson, S. Trumbore, W. Prell (1996), The southwest Indian monsoon over the last 18000 years, *Clim. Dynam.*, 12, 213–225.

Owen, L. A. (2009), Latest Pleistocene and Holocene glacier fluctuations in the Himalaya and Tibet, *Quat. Sci. Rev.*, 28 , 2150–2164, doi:10.1016/j.quascirev.2008.10.020.

Owen, L. A., Benn, D. I. (2005), Equilibrium-line altitudes of the Last Glacial Maximum for the Himalaya and Tibet: an assessment and evaluation of results. *Quat. Int.*, 138–139, 55–78, doi:10.1016/j.quaint.2005.02.006.

Owen. L. A., E. Derbyshire, and C. H. Scott (2003), Contemporary sediment production and transfer in high-altitude glaciers, *Sed. Geol.*, 155, 13–36.

Owen, L. A., U. Kamp, J. Q. Spencer, and K. Haserodt (2002), Timing and style of Late Quaternary glaciation in the eastern Hindu Kush, Chitral, northern Pakistan: a review and revision of the glacial chronology based on new optically stimulated luminescence dating, *Quat. Int.*, 97–98, 41–55.

Owen, L. A., M. W. Caffee, R. C. Finkel, B. Y. Seong (2008), Quaternary glaciations of the Himalayan-Tibetan orogen, *J. Quat. Sci.*, 23, 513–532.

Owen, L. A., L. Gualtieri, R. C. Finkel, M. W. Caffee, D. I. Benn, and M. C. Sharma (2001), Cosmogenic radionuclide dating of glacial landforms in the Lahul Himalaya, northern India: defining the timing of Late Quaternary glaciation, *J. Quat. Sci.*, 16, 555–563.

Owen, L. A., R. C. Finkel, P. L. Barnard, M. Haizhou, K. Asahi, M. W. Caffee, and E. Derbyshire (2005), Climatic and topographic controls on the style and timing of Late Quaternary glaciation throughout Tibet and the Himalaya defined by [10]Be cosmogenic radionuclide surface exposure dating, *Quat. Sci. Rev.*, 24, 1391–1411.

Owen, L. A., R. Robinson, D. I. Benn, R. C. Finkel, N. K. Davis, C. Yi, J. Putkonen, D. Li, and A. S. Murray (2009), Quaternary glaciation of Mount Everest, *Quat. Sci. Rev.*, 28, 1412–1433, doi:10.1016/j.quascirev.2009.02.010.

Paterson, W. S. B. (1994), *The Physics of Glaciers*, 480 pp., Elsevier, New York.

Paul, F., C. Huggel, and A. Kääb (2004), Combining satellite multispectral image data and a digital elevation model for mapping debris-covered glaciers, *Remote Sens. Environ.*, 89, 510–518.

Paul, F., A. Kääb., M. Maisch, T. Kellenberger, and W. Haeberli (2002), The new remote-sensing-derived Swiss glacier inventory: I. Methods, *Ann. Glaciol.*, 34, 355-361.

Penck, A., and E. Brückner (1909), *Die Alpen im Eiszeitalter*, pp. 1199, Tauchnitz, Leipzig, Germany.

Phillips, W. M., V. F. Sloan, J. F. Shroder Jr., P. Sharma, M. L. Clarke, and H. M. Rendell (2000), Asynchronous glaciation at Nanga Parbat, northwestern Himalaya Mountains, Pakistan, *Geology*, 28, 431–434.

Porter, S. C. (1970) Quaternary Glacial Record in Swat Kohistan, West Pakistan, *Geol. Soc. Am. Bull.*, 81, 1421-1446.

Prasad, S., and Y. Enzel (2006), Holocene paleoclimates of India, *Quat. Res.*, 66, 442–453.

Pratt-Sitaula, B. (2005), *Glaciers, climate, and topography in the Nepalese Himalaya*, Unpublished PhD Thesis, University of California, Santa Barbara. 144 pp.

Prell, W. L., and J. E. Kutzbach (1992), Sensitivity of the Indian monsoon to forcing parameters and implications for its evolution, *Nature*, 360, 647–652.

Putkonen, J. K. (2004) Continuous snow and rain data at 500 to 4400 m altitude near Annapurna, Nepal, 1999–2001, *Arct., Antarct., Alp. Res.*, 36, 244–248.

Putkonen, J., and T. Swanson (2003), Accuracy of cosmogenic ages for moraines, *Quat. Res.*, 59, 255–261.

Quincey, D. J., A. Luckman, and D. I. Benn (2009), Quantification of Everest region glacier velocities between 1992 and 2002, using satellite radar interferometry and feature tracking, *J. Glaciol.*, 55, 596-606.

Quincey, D. J., S. D. Richardson, A. Luckman, and R. M. Lucas (2007), Early recognition of glacial lake hazards in the Himalaya using remote sensing datasets, *Global Planet. Change*, 56(1-2), 137-152.

Rabatel, A., J.-P. Dedieu, and C. Vincent (2005), Using remote-sensing data to determine equilibrium-line altitude and mass-balance time series: validation on three French glaciers, 1994-2002, *J. Glaciol.*, 51(175), 539-546.

Raina, V. K., M. K. Kaul, and S. Singh (1977), Mass balance studies of Gara-glacier, *J. Glaciol.*, 19, 123-139.

Raina, V. K. (2009), *Himalayan Glaciers*. A State-of-Art Review of Glacial Studies, Glacial Retreat and Climate Change, 60 pp., Ministry of Environment and Forests, India (available online at http://moef.nic.in/downloads/public-information/MoEF%20Discussion%20Paper%20_him.pdf).

Rapp, A. (1960), Recent development of mountain slopes in Karkevagge and surroundings, northern Scandinavia, *Geogr. Ann., Ser. A, Phys. Geogr.*, 42, 65–200.

Raymo, M. E., and W. F. Ruddiman (1992), Tectonic forcing of late Cenozoic climate, *Nature*, 359, 117-122.

Raymo, M. E., W. F. Ruddiman, and P. N. Froelich (1988), Influence of late Cenozoic mountain building on ocean geochemical cycles, *Geology*, 16, 649-653.

Reeh, N., J. J. Mohr, S. N. Madsen, H. Oerter, and N. S. Gundestrup (2003), Three-dimensional surface velocities of Storstrømmen glacier, Greenland, derived from radar interferometry and ice-sounding radar measurements, *J. Glaciol.*, 49(165), 201-209.

Ren, D., and D. J. Karoly (2008), Predicting the response of seven Asian glaciers to future climate scenarios using a simple linear glacier model, *J. Geophys. Res.*, 113, D05103, doi:10.1029/2007JD008997.

Reynolds, J. M. (2000), On the formation of supraglacial lakes on debris-covered laciers, in *Debris-covered glaciers*, edited by M. Nakawo, C. F. Raymond, and A. Fountain, pp. 153-161 , IAHS Publication no. 264., Wallingford, UK.

Richardson, S. D. and J. M. Reynolds (2000), An overview of glacial hazards in the Himalayas, *Quat. Int.*, 65-66, 31–47.

Rignot, E., and P. Kanagaratnam (2006), Changes in the Velocity Structure of the Greenland Ice Sheet, *Science*, 311(5763), 986-990.

Rodwell M. J., and B. J. Hoskins (1996), Monsoons and the dynamics of deserts, *Quart. J. Roy. Meteor. Soc.*, 122, 1385-1404.

Röthlisberger, F., and M. Geyh (1985), Glacier variations in Himalayas and Karakoram, *Z. Gletscherk. Glazialgeol.*, 21, 237–249.

Rupper, S. and G. Roe (2008), Glacier Changes and Regional Climate: A Mass and Energy Balance Approach, *J. Climate*, 21, 5384-5401.

Rupper, S., G. Roe, and A. Gillespie (2009), Spatial patterns of Holocene glacier advance and retreat in Central Asia, *Quat. Res.*, 72, 337-346.

Russell, I. C. (1895), The Influence of Debris on the Flow of Glaciers, *J. Geol.*, 3(7), 823-832.

Scambos, T. A., M. J. Dutkiewicz, J. C. Wilson, and R. A. Bindschadler (1992), Application of image cross-correlation to the measurement of glacier velocity using satellite image data, *Remote Sens. Environ.*, 42, 177−186.

Schaefer, J. M., P. Oberholzer, Z. Zhao, S. Ivy-Ochs, R. Wieler, H. Baur, P. W. Kubik, and C. Schlüchter (2008), Cosmogenic beryllium-10 and neon-21 dating of late Pleistocene glaciations in Nyalam, monsoonal Himalayas, *Quat. Sci. Rev.*, 27, 295–311, doi:10.1016/j.quascirev.2007.10.014.

Scherler, D., Leprince, S., and M. R. Strecker (2008), Glacier-surface velocities in alpine terrain from optical satellite imagery - accuracy improvement and quality assessment, *Remote Sens. Environ.*, 112, 3806–3819, doi:10.1016/j.rse.2008.05.018.

Scherler, D., B. Bookhagen, M. R. Strecker, F. von Blanckenburg, and D. Rood (2010), Timing and extent of late Quaternary glaciation in the western Himalaya constrained by 10Be moraine dating in Garhwal, India, *Quat. Sci. Rev.*, 29, 815-831, doi:10.1016/j.quascirev.2009.11.031.

Schlagintweit, H. (1871), *Reisen in Indien und Hochasien, Zweiter Band, Hochasien 1: Der Himálaya von Bhután bis Kashmir*, 468 pp., Costenoble, Gotha, Germany.

Schulz, H., U. von Rad, and H. Erlenkeuser (1998), Correlation between Arabian Sea and Greenland climate oscillations of the past 110,000 years, *Nature*, 393, 54–57.

Schumm, S. A., and R. W. Lichty (1965), Time, space and causality in geomorphology, *Am. J. Sci.*, 263, 110-19.

Seager, R. and D. S. Battisti (2007), Challenges to our understanding of the general circulation: Abrupt climate change, in *The General Circulation of the Atmosphere*, edited by T. P. Schneider and A. S. Sobel, pp. 331.371, Princeton University Press, Princton, USA.

Seko, K. (1987), Seasonal variation of altitudinal dependence of precipitation in Langtang Valley, Nepal Himalayas, *Bull. Glacier Res.*, 5, 41-47.

Seko, K., H. Yabuki, M. Nakawo, A. Sakai, T. Kadota, and Y. Yamada (1998), Changing surface features of Khumbu Glacier, Nepal Himalayas revealed by SPOT images, *Bull. Glacier Res.*, 16, 33-41.

Seong, Y. B., L. A, Owen, C. Yi, and R. C. Finkel (2009), Quaternary glaciation of Muztag Ata and Kongur Shan: evidence for glacier response to rapid climate changes throughout the Late Glacial and Holocene in westernmost Tibet, *Geol. Soc. Am. Bull.*, 121, 348–365.

Seong, Y. B. L. A. Owen, M. P. Bishop, A. Bush, P. Clendon, L. Copland, R. Finkel, U. Kamp, and J. F. Shroder Jr. (2007), Quaternary glacial history of the Central Karakoram, *Quat. Sci. Rev.*, 26, 3384–3405, doi:10.1016/j.quascirev.2007.09.015.

Shakun, J. D., S. J. Burns, D. Fleitmann, J. Kramers, A. Matter, and A. Al-Subary (2007), A high-resolution, absolute-dated deglacial speleothem record of Indian Ocean climate from Socotra Island, Yemen, *Earth Planet. Sci. Let.*, 259, 442-456.

Sharma, M. C., L. A. Owen (1996), Quaternary glacial history of the Garhwal Himalaya, India, *Quat. Sci. Rev.*, 15, 335–365.

Shi, Y. (2002), Characteristics of late Quaternary monsoonal glaciation on the Tibetan Plateau and in East Asia, *Quat. Int.*, 97–98, 79–91.

Shi, Y. and X. Zhang (1984), Some studies of the Batura glacier in the Karakoram Mountains, in *The International Karakoram Project, vol. I*, edited by K. J. Miller, pp. 51-63, Cambridge University Press, Great Britain.

Shroder, J. F., M. P. Bishop, L. Copland, and V. F. Sloan (2000), Debris-covered glaciers and rock glaciers in the Nanga Parbat Himalaya, Pakistan, *Geogr. Ann., Ser. A, Phys. Geogr.*, 82(1), 17-31.

Singh, P., and N. Kumar (1997), Effect of orography on precipitation in the western Himalayan region, *J. Hydrol.*, 199, 183-206.

Singh, P., U. K. Haritashya, and N. Kumar (2007), Meteorological study for Gangotri Glacier and its comparison with other high altitude meteorological stations in central Himalayan region, *Nord. Hydrol.*, 38(1), 59-77.

Singh, P., U. K. Haritashya, N. Kumar, and Y. Singh (2006), Hydrological characteristics of the Gangotri Glacier, central Himalayas, India, *J. Hydrol.*, 327(1-2), 55-67.

Sinha, A. K. G. Cannariato, L. D. Stott, H.-C. Li, C.-F. You, H. Cheng, R. L. Edwards, and I. B. Singh (2005), Variability of Southwest Indian summer monsoon precipitation during the Bølling-Ållerød, *Geology*, 33, 813–816.

Small, E. E., R. S. Anderson, J. L. Repka, and R. C. Finkel (1997), Erosion rates of alpine bedrock summit surfaces deduced from in situ ^{10}Be and ^{26}Al, *Earth Planet. Sci. Let.*, 150, 413–425.

Sobel, E. R., G. E. Hilley, and M. R. Strecker (2003), Formation of internally drained contractional basins by aridity-limited bedrock incision, *J. Geophys. Res.*, 108, B7, 2344, doi:10.1029/2002JB001883,

Staubwasser, M., F. Sirocko, P. M. Grootes, H. Erlenkeuser (2002), South Asian monsoon climate change and radiocarbon in the Arabian Sea during early and middle Holocene, *Paleoceanography*, 17, doi:10.1029/2000PA000608.

Stearns, L. and G. Hamilton (2005), A new velocity map for Byrd Glacier, East Antarctica, from sequential ASTER satellite imagery, *Ann. Glaciol.*, 41, 71-76.

Stenni, B., V. Masson-Delmotte, S. Johnsen, J. Jouzel, A. Longinelli, E. Monnin, R. Röthlisberger, and E. Selmo (2001), An Oceanic Cold Reversal during the last deglaciation, *Science*, 293, 2074-2077.

Strecker, M. R., R. N. Alonso, B. Bookhagen, B. Carrapa, G. E. Hilley, E. R. Sobel, and M. H. Trauth (2007), Tectonics and Climate of the Southern Central Andes, *Annu. Rev. Earth Planet. Sci.*, 35, 747–87, doi:10.1146/annurev.earth.35.031306.140158.

Strozzi, T., A. Luckman, T. Murray, U. Wegmüller, C. L. Werner (2002), Glacier Motion Estimation Using SAR Offset-Tracking Procedures, *IEEE T. Geosci. Remote Sens.*, 40(11), 2384-2391.

Teshima, Y., and A. Iwasaki (2008), Correction of Attitude Fluctuation Terra Spacecraft Using ASTER/SWIR Imagery With Parallax Observation, *IEEE T. Geosci. Remote Sens.*, 46(1), 222-227.

Thayyen, R. J., J. T. Gergan, and D. P. Dobhal (2005), Slope lapse rates of temperature in Din Gad (Dokriani GIacier) catchment, Garhwal Himalaya, lndia, *Bull. Glaciol. Res.*, 22, 31-37.

Thiede, R., B. Bookhagen, J. R. Arrowsmith, E. Sobel, and M. Strecker (2004), Climatic control on rapid exhumation along the Southern Himalayan Front, *Earth Planet. Sci. Lett.*, 222, 791 – 806, doi:10.1016/j.epsl.2004.03.015.

Thiede, R. C., J. R. Arrowsmith, B. Bookhagen, M. O. McWilliams, E. R. Sobel, and M. R. Strecker (2005), From tectonically to erosionally controlled development of the Himalayan orogen, *Geology*, 33, 689– 692, doi:10.1130/G21483.1.

Thompson, L. G., T. Yao, M. E. Davis, K. A. Henderson, E. Mosley-Thompson, P-N. Lin, J. Beer, H. A. Synal, J. Cole-Dai, and F. F. Bolzan (1997), Tropical climate instability: the last glacial cycle from a Qinghai–Tibetan ice core, *Science*, 276, 1821–1825.

Tomkin, J. H., and G. H. Roe (2007), Climate and tectonic controls on glaciated critical-taper orogens, *Earth Planet. Sci. Let.*, 262, 385–397, doi:10.1016/j.epsl.2007.07.040.

Toutin, T. (2002a), Impact of terrain slope and aspect on radargrammetric DEM accuracy, *ISPRS J. Photogramm. Remote Sens.*, 57(3), 228-240.

Toutin, T. (2002b), Three-Dimensional Topographic Mapping With ASTER Stereo Data in Rugged Topography, *IEEE T. Geosc. Remote Sens.*, 40(10), 2241-2247.

Toutin, T. (2004), Review article: Geometric processing of remote sensing images: models, algorithms and methods, *Int. J. Remote Sens.*, 25(10), 1893-1924.

Trouvé, E., G. Vasile, M. Gay, L. Bombrun, P. Grussenmeyer, T. Landes, J.-M. Nicolas, P. Bolon, I. Petillot, A. Julea, L. Valet, J. Chanussot, and M. Koehl (2007), Combining Airborne Photographs and Spaceborne SAR Data to Monitor Temperate Glaciers: Potentials and Limits, *IEEE T. Geosci. Remote Sens.*, 45(4), 905-924.

Tucker, G. E. (2004), Drainage basin sensitivity to tectonic and climatic forcing: implications of a stochastic model for the role of entrainment and erosion thresholds, *Earth Surf. Proc. Landforms*, 29, 185–205.

Van Campo, E., and F. Gasse (1993), Pollen- and diatom-inferred climatic and hydrological changes in Sumxi Co basin (western Tibet) since 13,000 yr. BP, *Quat. Res.*, 39, 300-313.

Van der Beek, P., J. Van Melle, S. Guillot, A. Pêcher, P. W. Reiners, S. Nicolescu, and M. Latif (2009), Eocene Tibetan plateau remnants preserved in the northwest Himalaya, *Nature Geosci.*, 2, 364-368, doi:10.1038/ngeo503.

Van Puymbroeck, N., R, Michel, R. Binet, J.-P. Avouac, and J. Taboury (2000), Measuring earthquakes from optical satellite images, *Appl. Optics*, 39(20), 3486-3494.

von Blanckenburg, F., T. Hewawasam, P. W. Kubik (2004), Cosmogenic nuclide evidence for low weathering and denudation in the wet, tropical highlands of Sri Lanka, *J. Geophys. Res.*, 109, F03008, doi:10.1029/2003JF000049,

Von Wissmann. H. (1959), Die heutige Vergletscherung und Schneegrenze in Hochasien mit Hinweisen auf die Vergletscherung der letzten Eiszeit, *Akad. Wiss. u. Lit. Mainz, Abh. Math.-Naturw. Kl.*, 14, 1101-1431.

Wagnon, P., A. Linda, Y. Arnaud, R. Kumar, P. Sharma, C. Vincent, J. G. Pottakkal, E. Berthier, A. Ramanathan, S. I. Hasnain, and P. Chevallier (2007), Four years of mass balance on Chhota Shigri Glacier, Himachal Pradesh, India, a new benchmark glacier in the western Himalaya, *J. Glaciol.*, 53(18), 603-611.

Wang, P., S. Clemens, L. Beaufort, P. Braconnot, G. Ganssen, Z. Jian, P. Kershaw, and M. Sarntheim (2005), Evolution and variability of the Asian monsoon system: State of the art and outstanding issues, *Quat. Sci. Rev.*, 24, 595–629.

Wang, Y. J., H. Cheng, R. L. Edwards, Z. S. An, J. Y. Wu, C.-C. Shen, and J. A. Dorale (2001), A High-Resolution Absolute-Dated Late Pleistocene Monsoon Record from Hulu Cave, China; *Science*, 294, 2345-2348.

Wasson, R. J., G. I. Smith, and D. P. Agrawal (1984), Late Quaternary sediments, minerals, and inferred geochemical history of Didwana lake, Thar desert India, *Palaeogeogr. Palaeocl. Palaeoecol.*, 46, 345–372.

Watanabe, T., L. Dali, and T. Shiraiwa (1998), Slope denudation and the supply of debris to cones in Langtang Himal, Central Nepal Himalaya, *Geomorphology*, 26, 185-197.

Weiers, S. (1994), Zur Klimatologie des NW-Karakoram und angrenzender Gebiete, 169 pp., *Bonner Geographische Abhandlungen*, 92, Bonn, Germany.

Weiss, H., M.-A. Courty, W. Wetterstrom, F. Guichard, L. Senior, R. Meadow, and A. Curnow (1993), The Genesis and Collapse of Third Millennium North Mesopotamian Civilization, *Science*, 261, 995-1004.

Wessels, R. L., J. S. Kargel, and H. H. Kieffer (2002), ASTER measurement of supraglacial lakes in the Mount Everest region of the Himalaya, *Ann. Glaciol.*, 34, 399-408.

WGMS (2008), *Global Glacier Changes: facts and figures*, edited by M. Zemp, I. Roer, A. Kääb, M. Hoelzle, F. Paul, and W. Haeberli, UNEP, World Glacier Monitoring Service, Zurich, Switzerland, 88 pp.

Whipple, K. X. (2009), The influence of climate on the tectonic evolution of mountain belts, *Nature Geosci.*, 2, 97-104, doi:10.1038/ngeo413.

Willett, S. D. (1999), Orogeny and orography: The effects of erosion on the structure of mountain belts, *J. Geophys. Res.*, 104(B12), 28,957-28,98.

Willett, S. D., F. Schlunegger, and V. Picotti (2006), Messinian climate change and erosional destruction of the central European Alps, Geology, 34(8), 613–616, doi:10.1130/G22280.1.

Willis, I. C. (1995), Intra-annual variations in glacier motion: a review, *Prog. Phys. Geog.*, 19(1), 61-106, doi: 10.1177/030913339501900104.

Winiger, M., M. Gumpert, and H. Yamout (2005), Karakorum–Hindukush–western Himalaya, assessing high-altitude water resources, *Hydrol. Process.*, 19, 2329–2338.

Wobus, C. W., K. V. Hodges, and K. X. Whipple (2003), Has focused denudation sustained active thrusting at the Himalayan topographic front? *Geology*, 31(10), 861-864.

Wobus, C. W., A. M. Heimsath, K. X. Whipple, and K. V. Hodges (2005), Active out-of-sequence thrust faulting in the central Nepalese Himalaya, *Nature*, 434, 1008-1011.

Wulf, H., B. Bookhagen, and D. Scherler (in press), Seasonal precipitation gradients and their impact on fluvial sediment flux in the Northwest Himalaya, *Geomorphology*, doi:10.1016/j.geomorph.2009.12.003.

Xu, B., J. Cao, J. Hansen, T. Yao, D. R. Joswia, N. Wang, G. Wu, M. Wang, H. Zhao, W. Yang, X. Liu, and J. He (2009), Black soot and the survival of Tibetan glaciers, *Proc. Natl. Acad. Sci. USA*, 106(52), 22114-22118, doi: 10.1073/pnas.0910444106.

Yadav, R. K., K. R. Kumar, and M. Rajeevan (2009), Increasing influence of ENSO and decreasing influence of AO/NAO in the recent decades over northwest India winter precipitation, *J. Geophys. Res.*, 114, D12112, doi:10.1029/2008JD011318.

Yasunari, T. (1976), Seasonal Weather Variations in Khumbu Himal, *Seppyo*, 38, 74-83.

Yasunari, T., and J. Inoue (1978), Characteristics of Monsoonal Precipitation around Peaks and Ridges in Shorong and Khumbu Himal, *Seppyo*, 40, 26-32.

Yin, A. (2006), Cenozoic tectonic evolution of the Himalayan orogen as constrained by along-strike variation of structural geometry, exhumation history, and foreland sedimentation, *Earth-Sci. Rev.*, 76, 1–131.

Yuan, D., H. Cheng, R. L. Edwards, C. A. Dykoski, M. J. Kelly, M. Zhang, J. Qing, Y. Lin, Y. Wang, J. Wu, J. A. Dorale, Z. An, and Y. Cai. (2004), Timing, duration, and transitions of the last interglacial Asian monsoon, *Science*, 304, 575-578.

Zachos, J., M. Pagani, L. Sloan, E. Thomas, and K. Billup (2001), Trends, Rhythms, and Aberrations in Global Climate 65 Ma to Present, Science, 292, 686-693.

Zech, R., M. Zech, P. W. Kubik, K. Kharki, and W. Zech (2009), Deglaciation and landscape history around Annapurna, Nepal, based on [10]Be surface exposure dating, *Quat. Sci. Rev.*, 28, 1106–1118.

Zeitler, P. K., A. S. Meltzer, P. O. Koons, D. Craw, B. Hallet, C. P. Chamberlain, W. S. F. Kidd, S. K. Park, L. Seeber, M. Bishop, and J. Shroder (2001), Erosion, Himalayan Geodynamics, and the Geomorphology of Metamorphism, *Geol. Soc. Am. Today*, 11, 4-9.

Zreda, M. G., and F. M. Phillips (1995), Insights into alpine moraine development from cosmogenic [36]C1 buildup dating, *Geomorphology*, 14, 149-156.

9 Bibliography

Appendix A: Satellite images and correlation details

Table A1: List of all ASTER satellite images used in this study.

No.	Geographic region	ASTER Granule ID	Acquisition date	Incidence angle [°]	Cloud cover [%]
1	Bhutan	ASTL1A 0101200458520109050995	20.01.2001	-0.019	60
2	Bhutan	ASTL1A 0111040451360111170671	04.11.2001	-2.832	19
3	Bhutan	ASTL1A 0111200451120111300272	20.11.2001	-0.022	33
4	Bhutan	ASTL1A 0212090448280212220388	09.12.2002	-2.873	42
5	Bhutan	ASTL1A 0301100447490304130278	10.01.2003	-2.873	63
6	Bhutan	ASTL1A 0501060452260501170201	06.01.2005	8.580	70
7	Bhutan	ASTL1A 0501150446180501260416	15.01.2005	-2.826	79
8	Bhutan	ASTL1A 0509280446010509300440	28.09.2005	-0.028	27
9	Bhutan	ASTL1A 0601180445230601230029	18.01.2006	0.022	81
10	Bhutan	ASTL1A 0602100451590602120700	10.02.2006	8.586	80
11	Bhutan	ASTL1A 0602260452140603010086	26.02.2006	8.586	48
12	Bhutan	ASTL1A 0612200446380612250005	20.12.2006	-1.448	73
13	Bhutan	ASTL1A 0701050446530701080251	05.01.2007	-2.832	61
14	Bhutan	ASTL1A 0701210447050701240139	21.01.2007	-0.022	80
15	Bhutan	ASTL1A 0702220447190702270059	22.02.2007	-0.022	51
16	Bhutan	ASTL1A 0703260447200703290416	26.03.2007	-0.017	32
17	Bhutan	ASTL1A 0704020453290704040588	02.04.2007	8.588	52
18	Bhutan	ASTL1A 0705040453140705070028	04.05.2007	8.586	53
19	Bhutan	ASTL1A 0705130446560705170311	13.05.2007	-2.873	41
20	Bhutan	ASTL1A 0705290446510706020317	29.05.2007	-2.870	14
21	Bhutan	ASTL1A 0710110453130710130457	11.10.2007	8.580	43
22	Bhutan	ASTL1A 0712140453090712180402	14.12.2007	8.580	72
23	Kanchenjunga	ASTL1A 0010070507170106171024	07.10.2000	0.022	36
24	Kanchenjunga	ASTL1A 0012010512050107290690	01.12.2000	8.588	64
25	Kanchenjunga	ASTL1A 0012010512140107290691	01.12.2000	8.588	57
26	Kanchenjunga	ASTL1A 0102280504430312150721	28.02.2001	-0.011	74
27	Kanchenjunga	ASTL1A 0104080509330312050170	08.04.2001	8.594	39
28	Kanchenjunga	ASTL1A 0104080509420312050171	08.04.2001	8.594	71
29	Kanchenjunga	ASTL1A 0110260458250111100014	26.10.2001	-5.727	51
30	Kanchenjunga	ASTL1A 0111110457430112140260	11.11.2001	-5.666	38
31	Kanchenjunga	ASTL1A 0111270457290402220471	27.11.2001	0.019	37
32	Kanchenjunga	ASTL1A 0112130456420112270108	13.12.2001	0.019	37
33	Kanchenjunga	ASTL1A 0201050502070201300923	05.01.2002	8.588	64
34	Kanchenjunga	ASTL1A 0201050502160201300924	05.01.2002	8.588	28
35	Kanchenjunga	ASTL1A 0201300455400202170317	30.01.2002	-0.028	77
36	Kanchenjunga	ASTL1A 0204040454430204150209	04.04.2002	-5.727	63
37	Kanchenjunga	ASTL1A 0205130500520205230702	13.05.2002	8.586	18
38	Kanchenjunga	ASTL1A 0205130501010205230703	13.05.2002	8.586	27
39	Kanchenjunga	ASTL1A 0210290454280211121103	29.10.2002	-2.870	51
40	Kanchenjunga	ASTL1A 0408150452490408280597	15.08.2004	0.022	47
41	Kanchenjunga	ASTL1A 0412050452090412170068	05.12.2004	-2.870	62
42	Kanchenjunga	ASTL1A 0502140458310502240663	14.02.2005	8.588	89
43	Kanchenjunga	ASTL1A 0502140458400502240664	14.02.2005	8.588	76
44	Kanchenjunga	ASTL1A 0611090452420611120038	09.11.2006	-2.873	76
45	Kanchenjunga	ASTL1A 0611250452450611290423	25.11.2006	-2.873	70
46	Kanchenjunga	ASTL1A 0711030459100711060158	03.11.2007	5.729	80
47	Kanchenjunga	ASTL1A 0711120452550711150090	12.11.2007	-2.867	82
48	Kanchenjunga	ASTL1A 0711190459030711220179	19.11.2007	8.525	69
49	Kanchenjunga	ASTL1A 0711190459120711220180	19.11.2007	8.525	35
50	Kanchenjunga	ASTL1A 0712300453230801020215	30.12.2007	-2.870	65

Appendix A: Satellite images and correlation details

No.	Geographic region	ASTER Granule ID	Acquisition date	Incidence angle [°]	Cloud cover [%]
51	Khumbu	ASTL1A 0009280513430312080380	28.09.2000	-2.870	25
52	Khumbu	ASTL1A 0009280513510312080381	28.09.2000	-2.870	63
53	Khumbu	ASTL1A 0010140513180106251045	14.10.2000	0.022	37
54	Khumbu	ASTL1A 0010140513270106251046	14.10.2000	0.022	70
55	Khumbu	ASTL1A 0010300512460107110671	30.10.2000	-0.025	27
56	Khumbu	ASTL1A 0112200502200201111046	20.12.2001	0.025	60
57	Khumbu	ASTL1A 0112200502290201111047	20.12.2001	0.025	43
58	Khumbu	ASTL1A 0210040500290210261258	04.10.2002	-2.829	21
59	Khumbu	ASTL1A 0210040500380210261259	04.10.2002	-2.829	49
60	Khumbu	ASTL1A 0211210500340212070707	21.11.2002	-0.041	36
61	Khumbu	ASTL1A 0301080500070303170125	08.01.2003	-0.030	77
62	Khumbu	ASTL1A 0301080500160303170126	08.01.2003	-0.030	48
63	Khumbu	ASTL1A 0310230459200311050562	23.10.2003	0.019	18
64	Khumbu	ASTL1A 0310230459290311050563	23.10.2003	0.019	25
65	Khumbu	ASTL1A 0410090458300410220102	09.10.2004	0.022	31
66	Khumbu	ASTL1A 0410090458390410220103	09.10.2004	0.022	72
67	Khumbu	ASTL1A 0410250458150411040497	25.10.2004	-2.873	63
68	Khumbu	ASTL1A 0410250458240411040498	25.10.2004	-2.873	77
69	Khumbu	ASTL1A 0411100458100411210130	10.11.2004	-1.480	70
70	Khumbu	ASTL1A 0411100458190411210131	10.11.2004	-1.480	55
71	Khumbu	ASTL1A 0511130458410511190111	13.11.2005	0.022	47
72	Khumbu	ASTL1A 0511290458400512020077	29.11.2005	-0.019	45
73	Khumbu	ASTL1A 0512060504390512090572	06.12.2005	8.588	76
74	Khumbu	ASTL1A 0512150458320512180055	15.12.2005	0.016	43
75	Khumbu	ASTL1A 0602010458090602040117	01.02.2006	-2.876	40
76	Khumbu	ASTL1A 0701190459250701220147	19.01.2007	-2.867	90
77	Khumbu	ASTL1A 0701190459340701220148	19.01.2007	-2.867	67
78	Khumbu	ASTL1A 0801060459270801090347	06.01.2008	0.014	87
79	Khumbu	ASTL1A 0801060459360801090348	06.01.2008	0.014	48
80	Manaslu	ASTL1A 0010120525320106240667	12.10.2000	0.025	38
81	Manaslu	ASTL1A 0011290524260107270734	29.11.2000	0.019	34
82	Manaslu	ASTL1A 0011290524350107270735	29.11.2000	0.019	21
83	Manaslu	ASTL1A 0012150524110108090592	15.12.2000	-0.017	29
84	Manaslu	ASTL1A 0012150524200108090593	15.12.2000	-0.017	21
85	Manaslu	ASTL1A 0102170523210112070649	17.02.2001	2.873	47
86	Manaslu	ASTL1A 0105010515320105140485	01.05.2001	-8.589	55
87	Manaslu	ASTL1A 0210020512460210241099	02.10.2002	0.025	12
88	Manaslu	ASTL1A 0210020512550210241100	02.10.2002	0.025	14
89	Manaslu	ASTL1A 0211030512410211170128	03.11.2002	5.721	57
90	Manaslu	ASTL1A 0211030512490211170129	03.11.2002	5.721	29
91	Manaslu	ASTL1A 0310050511250310180496	05.10.2003	-0.022	14
92	Manaslu	ASTL1A 0310050511330310180497	05.10.2003	-0.022	8
93	Manaslu	ASTL1A 0402100512150402290204	10.02.2004	-0.022	45
94	Manaslu	ASTL1A 0403130511570404015542	13.03.2004	5.729	30
95	Manaslu	ASTL1A 0403130512060404015543	13.03.2004	5.729	44
96	Manaslu	ASTL1A 0409050510550409170312	05.09.2004	2.881	70
97	Manaslu	ASTL1A 0410230510300411020192	23.10.2004	5.729	47
98	Manaslu	ASTL1A 0410230510390411020193	23.10.2004	5.729	32
99	Manaslu	ASTL1A 0411170504130412100771	17.11.2004	-5.727	46
100	Manaslu	ASTL1A 0412030504190412140490	03.12.2004	-5.729	34
101	Manaslu	ASTL1A 0412260510440501090793	26.12.2004	5.732	75
102	Manaslu	ASTL1A 0607020505040607050249	02.07.2006	-8.591	40
103	Manaslu	ASTL1A 0611070504450611100030	07.11.2006	-8.586	59
104	Manaslu	ASTL1A 0611070504540611100031	07.11.2006	-8.586	58
105	Manaslu	ASTL1A 0704070511510704100125	07.04.2007	2.873	59
106	Manaslu	ASTL1A 0704070512000704100126	07.04.2007	2.873	44
107	Manaslu	ASTL1A 0704230511440704260183	23.04.2007	2.870	80
108	Manaslu	ASTL1A 0801040511390801070124	04.01.2008	2.878	69
109	Manaslu	ASTL1A 0801040511480801070125	04.01.2008	2.878	29
110	Gurla Mandatha	ASTL1A 0110310516020111120765	31.10.2001	-8.583	48
111	Gurla Mandatha	ASTL1A 0201030514170201290966	03.01.2002	-8.589	80

Appendix A: Satellite images and correlation details

No.	Geographic region	ASTER Granule ID	Acquisition date	Incidence angle [°]	Cloud cover [%]
112	Gurla Mandatha	ASTL1A 0212280518390301140465	28.12.2002	0.016	88
113	Gurla Mandatha	ASTL1A 0302140518300303100587	14.02.2003	2.832	99
114	Gurla Mandatha	ASTL1A 0302230512170303310409	23.02.2003	-8.583	58
115	Gurla Mandatha	ASTL1A 0306150511380307011009	15.06.2003	-8.591	22
116	Gurla Mandatha	ASTL1A 0309260517080310070441	26.09.2003	1.925	14
117	Gurla Mandatha	ASTL1A 0510100510300510130020	10.10.2005	-8.580	57
118	Gurla Mandatha	ASTL1A 0612230517090612270410	23.12.2006	1.398	77
119	Gurla Mandatha	ASTL1A 0704140517420704170217	14.04.2007	-0.022	48
120	Gurla Mandatha	ASTL1A 0707190517410707230025	19.07.2007	0.022	37
121	Gurla Mandatha	ASTL1A 0711150523170711180135	15.11.2007	8.580	60
122	Garhwal (Gangotri)	ASTL1A 0011090549040303210003	09.11.2000	8.578	55
123	Garhwal (Gangotri)	ASTL1A 0109090542130109210888	09.09.2001	5.699	52
124	Garhwal (Gangotri)	ASTL1A 0111210533440112050016	21.11.2001	-8.589	39
125	Garhwal (Gangotri)	ASTL1A 0122230532340202250746	23.12.2001	-8.586	48
126	Garhwal (Gangotri)	ASTL1A 0201080532060202020960	08.01.2002	-8.586	45
127	Garhwal (Gangotri)	ASTL1A 0205160531070205250344	16.05.2002	-8.583	32
128	Garhwal (Gangotri)	ASTL1A 0310100529250310220539	10.10.2003	-5.727	44
129	Garhwal (Gangotri)	ASTL1A 0310100529340310220540	10.10.2003	-5.727	13
130	Garhwal (Gangotri)	ASTL1A 0407240529140408100758	24.07.2004	-8.586	40
131	Garhwal (Gangotri)	ASTL1A 0508190534580508220145	19.08.2005	5.729	87
132	Garhwal (Gangotri)	ASTL1A 0510150528360510180881	15.10.2005	-8.583	69
133	Garhwal (Gangotri)	ASTL1A 0609230535100609260202	23.09.2006	2.878	52
134	Garhwal (Gangotri)	ASTL1A 0610090534580610120384	09.10.2006	5.729	62
135	Garhwal (Gangotri)	ASTL1A 0610180528400610210283	18.10.2006	-5.727	76
136	Garhwal (Gangotri)	ASTL1A 0611100535050611130259	10.11.2006	2.873	57
137	Garhwal (Gangotri)	ASTL1A 0705050535450705080221	05.05.2007	2.876	81
138	Garhwal (Gangotri)	ASTL1A 0711060529070711090209	06.11.2007	-8.580	54
139	Garhwal (Gangotri)	ASTL1A 0711060529160711090210	06.11.2007	-8.580	30
140	Garhwal (Gangotri)	ASTL1A 0711220529160711250112	22.11.2007	-8.580	63
141	Garhwal (Gangotri)	ASTL1A 0711220529250711250113	22.11.2007	-8.580	17
142	Garhwal (Tons)	ASTL1A 0111210533440112050016	21.11.2001	-8.589	39
143	Garhwal (Tons)	ASTL1A 0112070533200112220027	07.12.2001	-8.589	53
144	Garhwal (Tons)	ASTL1A 0112300538430201260386	30.12.2001	0.016	30
145	Garhwal (Tons)	ASTL1A 0205160531070205250344	16.05.2002	-8.583	32
146	Garhwal (Tons)	ASTL1A 0304240536010305040110	24.04.2003	0.019	12
147	Garhwal (Tons)	ASTL1A 0310010535290310120326	01.10.2003	-0.025	13
148	Garhwal (Tons)	ASTL1A 0403090536090403230332	09.03.2004	-0.030	59
149	Garhwal (Tons)	ASTL1A 0404260535430405070040	26.04.2004	-0.022	46
150	Garhwal (Tons)	ASTL1A 0409100535020409120470	01.09.2004	-0.030	69
151	Garhwal (Tons)	ASTL1A 0411040534340411120657	04.11.2004	-0.022	23
152	Garhwal (Tons)	ASTL1A 0510150528360510180881	15.10.2005	-8.583	69
153	Garhwal (Tons)	ASTL1A 0510220534470510250071	22.10.2005	-0.017	30
154	Garhwal (Tons)	ASTL1A 0704030536000704060191	03.04.2007	2.876	29
155	Garhwal (Tons)	ASTL1A 0706060535380706110246	06.06.2007	-0.017	22
156	Garhwal (Tons)	ASTL1A 0711130535190711160126	13.11.2007	0.016	41
157	Garhwal (Tons)	ASTL1A 0712310535460801030198	31.12.2007	0.025	47
158	Leo Pargil	ASTL1A 0103170546010201070780	17.03.2001	-2.870	18
159	Leo Pargil	ASTL1A 0111210533260112050014	21.11.2001	-8.589	45
160	Leo Pargil	ASTL1A 0111210533350112050015	21.11.2001	-8.589	29
161	Leo Pargil	ASTL1A 0304240535430305040108	24.04.2003	0.019	10
162	Leo Pargil	ASTL1A 0310010535020310120323	01.10.2003	-0.025	33
163	Leo Pargil	ASTL1A 0310010535110310120324	01.10.2003	-0.025	27
164	Leo Pargil	ASTL1A 0310170535220310290241	17.10.2003	-2.870	67
165	Leo Pargil	ASTL1A 0311020535240311160279	02.11.2003	-2.870	29
166	Leo Pargil	ASTL1A 0409100534450409120468	01.09.2004	-0.030	33
167	Leo Pargil	ASTL1A 0411040534070411120654	04.11.2004	-0.022	89
168	Leo Pargil	ASTL1A 0411040534160411120655	04.11.2004	-0.022	71
169	Leo Pargil	ASTL1A 0509040534310509080554	04.09.2005	2.867	13
170	Leo Pargil	ASTL1A 0510220534300510250069	22.10.2005	-0.017	64
171	Leo Pargil	ASTL1A 0611010540540611040102	01.11.2006	8.588	60
172	Leo Pargil	ASTL1A 0706060535210706110244	06.06.2007	-0.017	30

Appendix A: Satellite images and correlation details

No.	Geographic region	ASTER Granule ID	Acquisition date	Incidence angle [°]	Cloud cover [%]
173	Leo Pargil	ASTL1A 0711060528490711090207	06.11.2007	-8.580	80
174	Leo Pargil	ASTL1A 0711130535010711160124	13.11.2007	0.016	88
175	Leo Pargil	ASTL1A 0711220528580711250110	22.11.2007	-8.580	99
176	Leo Pargil	ASTL1A 0712310535290801030196	31.12.2007	0.025	89
177	Lahul (South)	ASTL1A 0207010543130208150812	01.07.2002	5.729	39
178	Lahul (South)	ASTL1A 0210300536330211130402	30.10.2002	-8.589	50
179	Lahul (South)	ASTL1A 0310080541190310210182	08.10.2003	2.873	28
180	Lahul (South)	ASTL1A 0310080541280310210183	08.10.2003	2.873	38
181	Lahul (South)	ASTL1A 0310240541340311110443	24.10.2003	0.022	52
182	Lahul (South)	ASTL1A 0409080540560409190507	08.09.2004	-0.011	16
183	Lahul (South)	ASTL1A 0409170534440409280460	17.09.2004	-8.580	58
184	Lahul (South)	ASTL1A 0511070534350511100073	07.11.2005	-8.583	61
185	Lahul (South)	ASTL1A 0609300540580610030214	30.09.2006	-0.022	28
186	Lahul (South)	ASTL1A 0610160540360610190142	16.10.2006	0.022	59
187	Lahul (South)	ASTL1A 0610160540450610190143	16.10.2006	0.022	26
188	Lahul (South)	ASTL1A 0611170541010611200053	17.11.2006	1.423	73
189	Lahul (South)	ASTL1A 0705210535140705240094	21.05.2007	-8.591	68
190	Lahul (South)	ASTL1A 0711200541090711230108	20.11.2007	2.873	77
191	Lahul (South)	ASTL1A 0711200541180711230109	20.11.2007	2.873	53
192	Lahul (South)	ASTL1A 0712150535230712190552	15.12.2007	-8.569	54
193	Lahul (North)	ASTL1A 0006250556410205200667	25.06.2000	-0.025	30
194	Lahul (North)	ASTL1A 0008280556270212310499	28.08.2000	0.019	28
195	Lahul (North)	ASTL1A 0210050542310210260531	05.10.2002	-2.873	15
196	Lahul (North)	ASTL1A 0210280548370211110725	28.10.2002	8.586	53
197	Lahul (North)	ASTL1A 0210280548450211110726	28.10.2002	8.586	20
198	Lahul (North)	ASTL1A 0210300536330211130402	30.10.2002	-8.589	50
199	Lahul (North)	ASTL1A 0310080541190310210182	08.10.2003	2.873	28
200	Lahul (North)	ASTL1A 0310240541250311110442	24.10.2003	0.022	50
201	Lahul (North)	ASTL1A 0409080540470409190506	08.09.2004	-0.011	24
202	Lahul (North)	ASTL1A 0409170534350409280459	17.09.2004	-8.580	22
203	Lahul (North)	ASTL1A 0409170534440409280460	17.09.2004	-8.580	58
204	Lahul (North)	ASTL1A 0510290540340511070136	29.10.2005	0.030	55
205	Lahul (North)	ASTL1A 0511070534260511100072	07.11.2005	-8.583	88
206	Lahul (North)	ASTL1A 0511070534350511100073	07.11.2005	-8.583	61
207	Lahul (North)	ASTL1A 0609300540500610030213	30.09.2006	-0.022	43
208	Lahul (North)	ASTL1A 0610160540360610190142	16.10.2006	0.022	59
209	Lahul (North)	ASTL1A 0706130541260706160194	13.06.2007	-2.873	41
210	Lahul (North)	ASTL1A 0711200541090711230108	20.11.2007	2.873	77
211	Lahul (North)	ASTL1A 0712150535230712190552	15.12.2007	-8.569	54
212	Jammu	ASTL1A 0210120548170210310211	12.10.2002	2.87	57
213	Jammu	ASTL1A 0303050547540303220353	5.3.2003	0.02	58
214	Jammu	ASTL1A 0310310547150311140751	31.10.2003	-0.022	32
215	Jammu	ASTL1A 0503260546510503290271	26.03.2005	2.87	13
216	Jammu	ASTL1A 0510130540230510170292	13.10.2005	-5.73	65
217	Jammu	ASTL1A 0510200546250510220487	20.10.2005	2.884	62
218	Jammu	ASTL1A 0610070546370610100198	07.10.2006	2.870	55
219	Jammu	ASTL1A 0610230546320610260139	23.10.2006	2.88	56
220	Jammu	ASTL1A 0712220541100712260233	22.12.2007	-8.53	52
221	Karakoram (Baltoro)	ASTL1A 0009110607520301210381	11.09.2000	8.580	61
222	Karakoram (Baltoro)	ASTL1A 0108290600030109100540	29.08.2001	8.586	51
223	Karakoram (Baltoro)	ASTL1A 0210030554040210250577	03.10.2002	8.586	46
224	Karakoram (Baltoro)	ASTL1A 0309200552270310020633	20.09.2003	5.672	24
225	Karakoram (Baltoro)	ASTL1A 0310060552460310190240	06.10.2003	8.588	32
226	Karakoram (Baltoro)	ASTL1A 0310220552540311040573	22.10.2003	8.591	44
227	Karakoram (Baltoro)	ASTL1A 0403300552550404130517	30.03.2004	8.588	47
228	Karakoram (Baltoro)	ASTL1A 0408140546140408280137	14.08.2004	-2.873	24
229	Karakoram (Baltoro)	ASTL1A 0409150546040409260541	15.09.2004	-2.873	46
230	Karakoram (Baltoro)	ASTL1A 0502220545470508180153	22.02.2005	0.022	22
231	Karakoram (Baltoro)	ASTL1A 0506210552100506270657	21.06.2005	8.588	47
232	Karakoram (Baltoro)	ASTL1A 0506300546030507040533	30.06.2005	-2.870	78
233	Karakoram (Baltoro)	ASTL1A 0509250551550509280072	25.09.2005	8.583	88

Appendix A: Satellite images and correlation details

No.	Geographic region	ASTER Granule ID	Acquisition date	Incidence angle [°]	Cloud cover [%]
234	Karakoram (Baltoro)	ASTL1A 0607260552400607290068	26.07.2006	5.680	20
235	Karakoram (Biafo Gyang)	ASTL1A 0009110607520301210381	11.09.2000	8.580	61
236	Karakoram (Biafo Gyang)	ASTL1A 0103060603530201020311	06.03.2001	5.729	33
237	Karakoram (Biafo Gyang)	ASTL1A 0105180556200105280799	18.05.2001	-5.727	14
238	Karakoram (Biafo Gyang)	ASTL1A 0108290600030109100540	29.08.2001	8.586	51
239	Karakoram (Biafo Gyang)	ASTL1A 0305310553080306200218	31.05.2003	5.677	30
240	Karakoram (Biafo Gyang)	ASTL1A 0309200552270310020633	20.09.2003	5.672	24
241	Karakoram (Biafo Gyang)	ASTL1A 0411020545360411110367	02.11.2004	-5.677	37
242	Karakoram (Biafo Gyang)	ASTL1A 0504020552210504050375	02.04.2005	5.727	30
243	Karakoram (Biafo Gyang)	ASTL1A 0504020552300504050376	02.04.2005	5.727	12
244	Karakoram (Biafo Gyang)	ASTL1A 0511050545540511080468	05.11.2005	-8.591	40
245	Karakoram (Biafo Gyang)	ASTL1A 0603130545580603160141	13.03.2006	-5.729	18
246	Karakoram (Biafo Gyang)	ASTL1A 0603290546060604010104	29.03.2006	-5.727	50
247	Karakoram (Biafo Gyang)	ASTL1A 0604050552110604080006	05.04.2006	2.837	66
248	Karakoram (Biafo Gyang)	ASTL1A 0604050552200604080007	05.04.2006	2.837	45
249	Karakoram (Biafo Gyang)	ASTL1A 0605160546060605190122	16.05.2006	-5.729	21
250	Karakoram (Biafo Gyang)	ASTL1A 0606170546180606200585	17.06.2006	-8.583	21
251	Karakoram (Biafo Gyang)	ASTL1A 0606240552240606270217	24.06.2006	5.729	18
252	Karakoram (Biafo Gyang)	ASTL1A 0606240552320606270218	24.06.2006	5.729	22
253	Karakoram (Biafo Gyang)	ASTL1A 0607260552310607290067	26.07.2006	5.680	19
254	Karakoram (Biafo Gyang)	ASTL1A 0607260552400607290068	26.07.2006	5.680	20
255	Karakoram (Biafo Gyang)	ASTL1A 0609050546220609080110	05.09.2006	-5.666	56
256	Karakoram (Biafo Gyang)	ASTL1A 0609120552210609150241	12.09.2006	-0.019	44
257	Karakoram (Biafo Gyang)	ASTL1A 0609280552110610010266	28.09.2006	2.837	37
258	Karakoram (Biafo Gyang)	ASTL1A 0610300552040611020126	30.10.2006	-0.022	38
259	Karakoram (Biafo Gyang)	ASTL1A 0611080546070611110148	08.11.2006	-5.735	16
260	Karakoram (Biafo Gyang)	ASTL1A 0612100546110612130029	10.12.2006	-5.729	80
261	Karakoram (Biafo Gyang)	ASTL1A 0701020552370701050476	02.01.2007	5.677	74
262	Karakoram (Biafo Gyang)	ASTL1A 0701020552460701050477	02.01.2007	5.677	40
263	Karakoram (Biafo Gyang)	ASTL1A 0701110546430701140142	11.01.2007	-5.727	74
264	Karakoram (Biafo Gyang)	ASTL1A 0701270546530701300158	27.01.2007	-5.666	36
265	Karakoram (Biafo Gyang)	ASTL1A 0703070553070703100401	07.03.2007	5.727	42
266	Karakoram (Biafo Gyang)	ASTL1A 0703070553160703100402	07.03.2007	5.727	29
267	Karakoram (Biafo Gyang)	ASTL1A 0703230553070703270137	23.03.2007	5.672	18
268	Karakoram (Biafo Gyang)	ASTL1A 0703230553160703270138	23.03.2007	5.672	20
269	Karakoram (Biafo Gyang)	ASTL1A 0706110552450706140125	11.06.2007	5.727	24
270	Karakoram (Biafo Gyang)	ASTL1A 0706110552540706140126	11.06.2007	5.727	20
271	Karakoram (Biafo Gyang)	ASTL1A 0706270552520706300203	27.06.2007	5.721	21
272	Karakoram (Biafo Gyang)	ASTL1A 0706270553010706300204	27.06.2007	5.721	25
273	Karakoram (Biafo Gyang)	ASTL1A 0711270546320711300252	27.11.2007	-8.580	17
274	Karakoram (Hispar)	ASTL1A 0109300558330110131083	30.09.2001	0.022	15
275	Karakoram (Hispar)	ASTL1A 0109300558420110131084	30.09.2001	0.022	19
276	Karakoram (Hispar)	ASTL1A 0310290558540311120339	29.10.2003	8.588	22
277	Karakoram (Hispar)	ASTL1A 0409130558170409250097	13.09.2004	8.588	18
278	Karakoram (Hispar)	ASTL1A 0409290558120410090296	29.09.2004	8.583	91
279	Karakoram (Hispar)	ASTL1A 0511050545540511080468	05.11.2005	-8.591	40
280	Karakoram (Hispar)	ASTL1A 0511050545450511080467	05.11.2005	-8.591	53
281	Karakoram (Hispar)	ASTL1A 0603110558100603140060	11.03.2006	8.580	1
282	Karakoram (Hispar)	ASTL1A 0604050552110604080006	05.04.2006	2.837	66
283	Karakoram (Hispar)	ASTL1A 0604210552130604240319	21.04.2006	-0.030	59
284	Karakoram (Hispar)	ASTL1A 0606170546180606200585	17.06.2006	-8.583	21
285	Karakoram (Hispar)	ASTL1A 0609120552210609150241	12.09.2006	-0.019	44
286	Karakoram (Hispar)	ASTL1A 0609120553000609150242	12.09.2006	-0.019	40
287	Karakoram (Hispar)	ASTL1A 0609280552110610010266	28.09.2006	2.837	37
288	Karakoram (Hispar)	ASTL1A 0610300552040611020126	30.10.2006	-0.022	38
289	Karakoram (Hispar)	ASTL1A 0705010559020705040176	01.05.2007	8.588	68
290	Karakoram (Hispar)	ASTL1A 0711270546320711300252	27.11.2007	-8.580	17
291	Hindu Kush (North)	ASTL1A 0008310626110301030420	31.08.2000	8.580	10
292	Hindu Kush (North)	ASTL1A 0110050616490110190607	05.10.2001	5.699	31
293	Hindu Kush (North)	ASTL1A 0110140610390110260251	14.10.2001	-0.442	38
294	Hindu Kush (North)	ASTL1A 0207040612490208050489	04.07.2002	8.580	39

Appendix A: Satellite images and correlation details

No.	Geographic region	ASTER Granule ID	Acquisition date	Incidence angle [°]	Cloud cover [%]
295	Hindu Kush (North)	ASTL1A 020922061236021015 0796	22.09.2002	8.583	19
296	Hindu Kush (North)	ASTL1A 021008061207021029 0273	08.10.2002	5.732	27
297	Hindu Kush (North)	ASTL1A 060816061054060819 0236	16.08.2006	8.588	54
298	Hindu Kush (North)	ASTL1A 060901061049060904 0147	01.09.2006	8.586	93
299	Hindu Kush (North)	ASTL1A 070515061105070520 0121	15.05.2007	8.580	17
300	Hindu Kush (North)	ASTL1A 070727060515070730 0190	27.07.2007	0.022	32
301	Hindu Kush (North)	ASTL1A 070819061127070823 0087	19.08.2007	8.580	34
302	Hindu Kush (South)	ASTL1A 000831062620030103 0421	31.08.2000	8.580	10
303	Hindu Kush (South)	ASTL1A 010624061319010701 0540	24.06.2001	-2.829	25
304	Hindu Kush (South)	ASTL1A 010928061101011012 0232	28.09.2001	-0.838	15
305	Hindu Kush (South)	ASTL1A 011014061048011026 0252	14.10.2001	-0.442	30
306	Hindu Kush (South)	ASTL1A 020704061258020805 0490	04.07.2002	8.580	10
307	Hindu Kush (South)	ASTL1A 020922061245021015 0797	22.09.2002	8.583	9
308	Hindu Kush (South)	ASTL1A 021008061215021029 0274	08.10.2002	5.732	29
309	Hindu Kush (South)	ASTL1A 030614060521030630 0523	14.06.2003	0.019	15
310	Hindu Kush (South)	ASTL1A 031020060506031101 0292	20.10.2003	-0.022	28
311	Hindu Kush (South)	ASTL1A 040515060512040527 0448	15.05.2004	0.022	17
312	Hindu Kush (South)	ASTL1A 040616060457040629 0312	16.06.2004	0.022	21
313	Hindu Kush (South)	ASTL1A 040920060427041001 0164	20.09.2004	-2.873	50
314	Hindu Kush (South)	ASTL1A 060816061102060819 0237	16.08.2006	8.588	35
315	Hindu Kush (South)	ASTL1A 070515061114070520 0122	15.05.2007	8.580	18
316	Hindu Kush (South)	ASTL1A 070727060524070730 0191	27.07.2007	0.022	28
317	Hindu Kush (South)	ASTL1A 070819061136070823 0088	19.08.2007	8.580	43
318	West Kunlun Shan	ASTL1A 000510054350020412 0475	10.05.2000	0.027	40
319	West Kunlun Shan	ASTL1A 000510054359020412 0476	10.05.2000	0.027	36
320	West Kunlun Shan	ASTL1A 010310053913020104 0563	10.03.2001	-5.729	39
321	West Kunlun Shan	ASTL1A 010326053849020209 0556	26.03.2001	-0.019	58
322	West Kunlun Shan	ASTL1A 010326053858020209 0557	26.03.2001	-0.019	70
323	West Kunlun Shan	ASTL1A 020216053557020301 0929	16.02.2002	8.575	78
324	West Kunlun Shan	ASTL1A 020313052927020329 0309	13.03.2002	-0.022	68
325	West Kunlun Shan	ASTL1A 020313052936020329 0310	13.03.2002	-0.022	55
326	West Kunlun Shan	ASTL1A 021014053523021103 1149	14.10.2002	5.699	23
327	West Kunlun Shan	ASTL1A 030408053503030419 0316	08.04.2003	8.588	61
328	West Kunlun Shan	ASTL1A 030722052726030805 0112	22.07.2003	0.022	14
329	West Kunlun Shan	ASTL1A 031010052815031022 0531	10.10.2003	-5.727	36
330	West Kunlun Shan	ASTL1A 040318052829040404 0357	18.03.2004	-0.030	49
331	West Kunlun Shan	ASTL1A 040318052838040404 0358	18.03.2004	-0.030	36
332	West Kunlun Shan	ASTL1A 041206053313041218 0063	06.12.2004	8.580	53
333	West Kunlun Shan	ASTL1A 041206053322041218 0064	06.12.2004	8.580	79
334	West Kunlun Shan	ASTL1A 050116052730050127 0399	16.01.2005	-0.022	85
335	West Kunlun Shan	ASTL1A 050116052739050127 0400	16.01.2005	-0.022	67
336	West Kunlun Shan	ASTL1A 050201052727050212 0308	01.02.2005	-0.019	87
337	West Kunlun Shan	ASTL1A 050201052736050212 0309	01.02.2005	-0.019	60
338	West Kunlun Shan	ASTL1A 050312053344050318 0318	12.03.2005	8.578	95
339	West Kunlun Shan	ASTL1A 051006053326051008 0508	06.10.2005	8.580	62
340	West Kunlun Shan	ASTL1A 051006053335051008 0509	06.10.2005	8.580	53
341	West Kunlun Shan	ASTL1A 060204052654060207 0254	04.02.2006	0.022	94
342	West Kunlun Shan	ASTL1A 060204052703060207 0255	04.02.2006	0.022	67
343	West Kunlun Shan	ASTL1A 060211053312060214 0125	11.02.2006	8.572	51
344	West Kunlun Shan	ASTL1A 060211053321060214 0126	11.02.2006	8.572	76
345	West Kunlun Shan	ASTL1A 070412052827070415 0324	12.04.2007	-0.022	48
346	West Kunlun Shan	ASTL1A 070412052836070415 0325	12.04.2007	-0.022	43
347	West Kunlun Shan	ASTL1A 071129053412071202 0139	29.11.2007	8.594	49
348	West Kunlun Shan	ASTL1A 071129053421071202 0140	29.11.2007	8.594	80
349	West Kunlun Shan	ASTL1A 071208052807071211 0194	08.12.2007	0.022	89
350	West Kunlun Shan	ASTL1A 071208052816071211 0195	08.12.2007	0.022	80
351	West Kunlun Shan	ASTL1A 080125052827080128 0093	25.01.2008	0.025	71

Appendix A: Satellite images and correlation details

Table A 2: List of all SPOT satellite images used in this study.

Instrument and Sensor	Processing level	Column (K)	Row (J)	Date	Incidence angle (°)
SPOT 4 HRVIR 1	L1A	208	288	22.09.2001	2.50
SPOT 5 HRG 1	L1A	208	288	17.12.2002	2.03
SPOT 5 HRG 1	L1A	208	288	11.07.2004	1.72
SPOT 5 HRG 2	L1A	208	288	31.08.2005	2.17
SPOT 5 HRG 2	L1A	208	288	06.10.2005	14.44
SPOT 5 HRG 1	L1A	208	288	17.11.2005	2.17

Table A 3: List of all LANDSAT satellite images used in this study.

Instrument and Sensor	Processing level	Path	Row	Date
LANDSAT 5 TM	Orthorectified	148	39	29.06.1990
LANDSAT 5 TM	Orthorectified	142	40	11.10.1990
LANDSAT 5 TM	Orthorectified	145	39	15.11.1990
LANDSAT 5 TM	Orthorectified	145	35	15.11.1990
LANDSAT 5 TM	Orthorectified	145	36	17.10.1991
LANDSAT 5 TM	Orthorectified	140	41	17.11.1992
LANDSAT 7 ETM+	Orthorectified	150	35	16.09.1999
LANDSAT 7 ETM+	Orthorectified	147	37	29.09.2000
LANDSAT 7 ETM+	Orthorectified	143	39	10.03.2000
LANDSAT 7 ETM+	Orthorectified	146	38	10.08.2000
LANDSAT 7 ETM+	Orthorectified	147	38	15.10.2000
LANDSAT 7 ETM+	Orthorectified	147	37	15.10.2000
LANDSAT 7 ETM+	Orthorectified	148	37	22.10.2000
LANDSAT 7 ETM+	Orthorectified	151	35	27.10.2000
LANDSAT 7 ETM+	Orthorectified	138	40	17.11.2000
LANDSAT 7 ETM+	Orthorectified	139	41	26.12.2000
LANDSAT 7 ETM+	Orthorectified	149	35	30.09.2001
LANDSAT 7 ETM+	Orthorectified	138	41	20.11.2001

Table A4: Image correlation details.

No.	Geographic region	Date [yyyy-mm-dd] Scene 1	Scene 2	Time span [years]	Incidence angle diff. [°]	Residual offset [m] East-West Mean	SD	North-South Mean	SD	Total displacement uncertainty [m] Mean	SD	Velocity uncertainty [m/yr] Mean	SD
1	Bhutan	20.01.2001	04.11.2001	0.789	2.8	0.031	2.629	-0.028	2.638	0.042	3.725	0.053	4.721
2	Bhutan	20.01.2001	20.11.2001	0.833	0.0	0.044	2.518	0.054	2.483	0.069	3.537	0.083	4.246
3	Bhutan	20.01.2001	10.01.2003	1.973	2.9	-0.044	2.587	-0.068	2.663	0.081	3.713	0.041	1.882
4	Bhutan	20.01.2001	15.01.2005	3.989	2.8	-0.085	2.568	-0.028	2.613	0.089	3.664	0.022	0.919
5	Bhutan	20.01.2001	18.01.2006	4.997	0.0	-0.071	2.826	0.025	2.891	0.075	4.043	0.015	0.809
6	Bhutan	20.01.2001	20.12.2006	5.918	1.4	0.004	3.250	-0.069	3.576	0.069	4.832	0.012	0.817
7	Bhutan	20.01.2001	22.02.2007	6.093	0.0	0.041	3.327	-0.217	3.645	0.221	4.935	0.036	0.810
8	Bhutan	04.11.2001	09.12.2002	1.096	0.0	-0.006	2.469	-0.065	2.686	0.065	3.649	0.060	3.330
9	Bhutan	04.11.2001	10.01.2003	1.184	0.0	-0.005	2.982	-0.132	3.156	0.132	4.342	0.111	3.669
10	Bhutan	20.11.2001	09.12.2002	1.052	2.9	-0.092	2.192	-0.009	2.436	0.093	3.277	0.088	3.115
11	Bhutan	20.11.2001	10.01.2003	1.140	2.9	-0.106	2.786	-0.249	2.906	0.270	4.026	0.237	3.532
12	Bhutan	20.11.2001	06.01.2005	3.132	8.6	-0.295	3.229	-0.074	2.749	0.304	4.241	0.097	1.354
13	Bhutan	20.11.2001	15.01.2005	3.156	2.8	-0.060	2.595	-0.022	2.619	0.064	3.686	0.020	1.168
14	Bhutan	20.11.2001	18.01.2006	4.164	0.0	-0.038	2.883	-0.016	2.838	0.041	4.045	0.010	0.971
15	Bhutan	20.11.2001	20.12.2006	5.085	1.4	-0.046	3.407	-0.022	3.717	0.051	5.042	0.010	0.992
16	Bhutan	10.01.2003	15.01.2005	2.016	0.0	-0.042	2.452	0.209	2.648	0.213	3.609	0.106	1.790
17	Bhutan	10.01.2003	28.09.2005	2.718	2.8	-0.068	3.197	0.151	3.262	0.166	4.567	0.061	1.681
18	Bhutan	10.01.2003	18.01.2006	3.025	2.9	-0.101	2.850	0.054	2.987	0.115	4.129	0.038	1.365
19	Bhutan	10.01.2003	05.01.2007	3.989	0.0	-0.029	2.608	0.059	2.831	0.066	3.849	0.017	0.965
20	Bhutan	10.01.2003	21.01.2007	4.033	2.9	-0.016	2.602	0.010	2.699	0.019	3.749	0.005	0.930
21	Bhutan	10.01.2003	22.02.2007	4.121	2.9	0.065	3.033	-0.317	3.328	0.323	4.503	0.078	1.093
22	Bhutan	06.01.2005	10.02.2006	1.096	0.0	0.086	2.856	-0.094	2.925	0.127	4.088	0.116	3.730
23	Bhutan	06.01.2005	26.02.2006	1.140	0.0	-0.003	2.775	0.027	2.792	0.027	3.937	0.024	3.454

No.	Geographic region	Date [yyyy-mm-dd]		Time span [years]	Inci-dence angle diff. [°]	Residual offset [m]				Total displacement uncertainty [m]		Velocity uncertainty [m/yr]	
						East-West		North-South					
		Scene 1	Scene 2			Mean	SD	Mean	SD	Mean	SD	Mean	SD
24	Bhutan	06.01.2005	14.12.2007	2.937	0.0	0.014	2.523	0.043	2.489	0.045	3.545	0.015	1.207
25	Bhutan	15.01.2005	28.09.2005	0.701	2.8	-0.141	2.931	0.199	2.918	0.243	4.136	0.347	5.897
26	Bhutan	15.01.2005	18.01.2006	1.008	2.8	-0.065	2.546	0.090	2.501	0.111	3.568	0.110	3.539
27	Bhutan	15.01.2005	10.02.2006	1.071	11.4	-0.066	3.218	-0.020	3.075	0.069	4.451	0.065	4.155
28	Bhutan	15.01.2005	26.02.2006	1.115	11.4	-0.150	3.456	-0.101	3.154	0.181	4.679	0.163	4.196
29	Bhutan	15.01.2005	20.12.2006	1.929	1.4	-0.250	3.033	-0.240	3.330	0.347	4.504	0.180	2.335
30	Bhutan	15.01.2005	05.01.2007	1.973	0.0	-0.024	2.495	0.062	2.669	0.067	3.654	0.034	1.852
31	Bhutan	15.01.2005	21.01.2007	2.016	2.8	0.131	2.471	-0.128	2.527	0.183	3.534	0.091	1.752
32	Bhutan	15.01.2005	22.02.2007	2.104	2.8	0.211	3.176	-0.227	3.496	0.310	4.723	0.147	2.245
33	Bhutan	15.01.2005	13.05.2007	2.323	0.0	0.082	3.319	0.031	3.707	0.088	4.976	0.038	2.142
34	Bhutan	15.01.2005	29.05.2007	2.367	0.0	-0.023	3.145	0.023	3.717	0.033	4.870	0.014	2.057
35	Bhutan	15.01.2005	14.12.2007	2.912	11.4	-0.079	3.232	0.074	2.680	0.108	4.198	0.037	1.442
36	Bhutan	28.09.2005	18.01.2006	0.307	0.1	0.046	3.167	0.004	3.265	0.046	4.549	0.151	14.824
37	Bhutan	28.09.2005	20.12.2006	1.227	1.4	0.134	3.784	0.192	4.158	0.234	5.623	0.190	4.581
38	Bhutan	28.09.2005	05.01.2007	1.271	2.8	0.154	3.296	-0.241	3.310	0.286	4.671	0.225	3.674
39	Bhutan	28.09.2005	21.01.2007	1.315	0.0	0.203	3.277	-0.008	3.318	0.203	4.663	0.155	3.546
40	Bhutan	28.09.2005	22.02.2007	1.403	0.0	0.189	3.757	-0.092	3.933	0.210	5.440	0.150	3.878
41	Bhutan	28.09.2005	26.03.2007	1.490	0.0	0.256	3.360	-0.047	3.446	0.260	4.813	0.174	3.229
42	Bhutan	28.09.2005	29.05.2007	1.666	2.8	0.084	2.559	-0.040	2.758	0.094	3.762	0.056	2.259
43	Bhutan	18.01.2006	20.12.2006	0.921	1.5	0.144	3.427	-0.154	3.726	0.211	5.062	0.229	5.499
44	Bhutan	18.01.2006	05.01.2007	0.964	2.9	0.158	2.897	-0.124	2.942	0.200	4.129	0.208	4.281
45	Bhutan	18.01.2006	21.01.2007	1.008	0.0	0.056	2.620	-0.045	2.665	0.072	3.738	0.072	3.707
46	Bhutan	18.01.2006	22.02.2007	1.096	0.0	0.214	3.480	-0.274	3.837	0.348	5.180	0.317	4.727
47	Bhutan	18.01.2006	26.03.2007	1.184	0.0	0.159	3.153	-0.124	3.425	0.201	4.655	0.170	3.933
48	Bhutan	26.02.2006	21.01.2007	0.901	8.6	0.197	3.434	0.085	2.937	0.215	4.519	0.238	5.013
49	Bhutan	26.02.2006	22.02.2007	0.989	8.6	0.406	3.829	-0.019	3.513	0.406	5.196	0.411	5.254
50	Bhutan	26.02.2006	26.03.2007	1.077	8.6	0.296	3.651	-0.019	3.191	0.296	4.849	0.275	4.504
51	Bhutan	26.02.2006	14.12.2007	1.797	0.0	-0.256	3.187	0.139	3.276	0.291	4.571	0.162	2.543
52	Bhutan	20.12.2006	14.12.2007	0.984	10.0	-0.044	3.666	0.183	3.152	0.188	4.834	0.191	4.915
53	Bhutan	05.01.2007	14.12.2007	0.940	11.4	-0.095	3.378	0.195	2.968	0.217	4.497	0.231	4.785
54	Bhutan	21.01.2007	14.12.2007	0.896	8.6	-0.202	3.406	0.214	2.977	0.294	4.524	0.328	5.050
55	Kanchenjunga	07.10.2000	27.11.2001	1.140	0.0	-0.012	3.101	0.039	3.105	0.041	4.388	0.036	3.850
56	Kanchenjunga	07.10.2000	13.12.2001	1.184	0.0	0.070	3.103	0.030	3.146	0.076	4.419	0.064	3.734
57	Kanchenjunga	07.10.2000	30.01.2002	1.315	0.1	-0.027	3.812	-0.091	3.673	0.095	5.293	0.072	4.025
58	Kanchenjunga	07.10.2000	29.10.2002	2.060	2.9	-0.033	3.074	0.074	3.144	0.081	4.397	0.039	2.134
59	Kanchenjunga	07.10.2000	15.08.2004	3.858	0.0	0.051	3.338	-0.221	3.464	0.227	4.811	0.059	1.247
60	Kanchenjunga	01.12.2000	27.11.2001	0.989	8.6	0.007	3.913	-0.236	3.214	0.236	5.064	0.238	5.120
61	Kanchenjunga	01.12.2000	13.12.2001	1.033	8.6	0.050	3.902	-0.023	3.207	0.055	5.051	0.053	4.890
62	Kanchenjunga	01.12.2000	05.01.2002	1.096	0.0	-0.223	2.736	0.076	2.550	0.236	3.740	0.215	3.413
63	Kanchenjunga	01.12.2000	30.01.2002	1.164	8.6	0.258	4.364	-0.265	3.626	0.370	5.673	0.317	4.872
64	Kanchenjunga	28.02.2001	29.10.2002	1.666	2.9	-0.076	3.288	0.218	3.414	0.230	4.740	0.138	2.846
65	Kanchenjunga	08.04.2001	13.05.2002	1.096	0.0	-0.075	3.526	0.041	3.454	0.086	4.936	0.078	4.504
66	Kanchenjunga	26.10.2001	04.04.2002	0.438	0.0	0.274	3.387	-0.498	3.599	0.568	4.943	1.296	11.275
67	Kanchenjunga	26.10.2001	29.10.2002	1.008	2.9	-0.137	2.317	0.114	2.342	0.178	3.295	0.176	3.268
68	Kanchenjunga	11.11.2001	29.10.2002	0.964	2.8	-0.018	2.649	-0.068	2.906	0.070	3.932	0.073	4.077
69	Kanchenjunga	11.11.2001	05.12.2004	3.068	2.8	-0.084	2.636	0.252	2.762	0.266	3.818	0.087	1.244
70	Kanchenjunga	27.11.2001	29.10.2002	0.921	2.9	0.104	2.960	-0.111	3.041	0.153	4.244	0.166	4.610
71	Kanchenjunga	27.11.2001	05.12.2004	3.025	2.9	-0.053	3.028	0.105	2.906	0.117	4.197	0.039	1.388
72	Kanchenjunga	27.11.2001	25.11.2006	4.997	2.9	-0.044	3.706	-0.133	3.695	0.140	5.234	0.028	1.047
73	Kanchenjunga	13.12.2001	29.10.2002	0.877	2.9	0.127	3.001	-0.192	3.081	0.230	4.301	0.262	4.906
74	Kanchenjunga	13.12.2001	05.12.2004	2.981	2.9	0.026	2.724	-0.133	2.752	0.135	3.872	0.045	1.299
75	Kanchenjunga	05.01.2002	29.10.2002	0.814	11.5	0.043	3.981	-0.212	3.078	0.216	5.032	0.266	6.184
76	Kanchenjunga	30.01.2002	29.10.2002	0.745	2.8	-0.108	3.653	0.097	3.604	0.145	5.131	0.195	6.886
77	Kanchenjunga	30.01.2002	05.12.2004	2.849	2.8	-0.101	3.718	0.346	3.569	0.360	5.154	0.126	1.809
78	Kanchenjunga	29.10.2002	05.12.2004	2.104	0.0	-0.087	2.977	0.294	3.048	0.306	4.261	0.146	2.025
79	Kanchenjunga	29.10.2002	30.12.2007	5.173	0.0	-0.108	3.133	0.194	3.146	0.222	4.440	0.043	0.858
80	Kanchenjunga	05.12.2004	09.11.2006	1.929	0.0	0.070	3.507	-0.093	3.688	0.116	5.089	0.060	2.638
81	Kanchenjunga	05.12.2004	25.11.2006	1.973	0.0	0.069	3.214	-0.145	3.397	0.161	4.677	0.081	2.371
82	Kanchenjunga	05.12.2004	12.11.2007	2.937	0.0	0.042	3.412	-0.118	3.405	0.125	4.821	0.043	1.641

Appendix A: Satellite images and correlation details

No.	Geographic region	Date [yyyy-mm-dd] Scene 1	Date [yyyy-mm-dd] Scene 2	Time span [years]	Incidence angle diff. [°]	Residual offset [m] East-West Mean	SD	North-South Mean	SD	Total displacement uncertainty [m] Mean	SD	Velocity uncertainty [m/yr] Mean	SD
83	Kanchenjunga	05.12.2004	30.12.2007	3.068	0.0	-0.313	2.899	0.278	2.867	0.419	4.077	0.136	1.329
84	Kanchenjunga	09.11.2006	12.11.2007	1.008	0.0	-0.008	3.205	0.093	3.284	0.094	4.589	0.093	4.551
85	Kanchenjunga	25.11.2006	12.11.2007	0.964	0.0	0.017	3.254	0.093	3.284	0.095	4.623	0.098	4.794
86	Khumbu (South)	28.09.2000	20.12.2001	1.227	2.9	0.289	3.654	-0.449	3.681	0.534	5.186	0.435	4.225
87	Khumbu (South)	28.09.2000	04.10.2002	2.016	0.0	-0.044	2.892	-0.228	3.124	0.232	4.257	0.115	2.111
88	Khumbu (South)	28.09.2000	09.10.2004	4.033	2.9	-0.036	3.003	0.031	3.072	0.047	4.296	0.012	1.065
89	Khumbu (South)	28.09.2000	25.10.2004	4.077	0.0	0.106	3.258	-0.040	3.195	0.113	4.564	0.028	1.119
90	Khumbu (South)	14.10.2000	20.12.2001	1.184	0.0	-0.005	3.312	-0.112	3.361	0.113	4.719	0.095	3.987
91	Khumbu (South)	14.10.2000	04.10.2002	1.973	2.9	-0.048	2.862	-0.173	2.842	0.179	4.034	0.091	2.045
92	Khumbu (South)	14.10.2000	21.11.2002	2.104	0.1	0.110	3.137	-0.063	3.488	0.127	4.692	0.061	2.230
93	Khumbu (South)	14.10.2000	08.01.2003	2.236	0.1	0.161	3.508	-0.175	3.603	0.238	5.029	0.106	2.249
94	Khumbu (South)	14.10.2000	23.10.2003	3.025	0.0	-0.007	2.978	-0.003	3.037	0.008	4.253	0.003	1.406
95	Khumbu (South)	14.10.2000	09.10.2004	3.989	0.0	0.056	3.107	-0.070	2.969	0.090	4.297	0.022	1.077
96	Khumbu (South)	14.10.2000	25.10.2004	4.033	2.9	-0.089	3.133	-0.064	3.093	0.110	4.402	0.027	1.092
97	Khumbu (South)	14.10.2000	10.11.2004	4.077	1.5	-0.036	2.970	0.055	3.066	0.066	4.268	0.016	1.047
98	Khumbu (South)	20.12.2001	04.10.2002	0.789	2.9	-0.090	3.021	-0.106	3.294	0.139	4.469	0.177	5.664
99	Khumbu (South)	20.12.2001	21.11.2002	0.921	0.1	0.151	2.502	0.076	2.827	0.169	3.775	0.184	4.101
100	Khumbu (South)	20.12.2001	08.01.2003	1.052	0.1	0.030	2.811	-0.234	3.061	0.236	4.156	0.224	3.950
101	Khumbu (South)	20.12.2001	23.10.2003	1.841	0.0	-0.012	2.599	-0.116	2.730	0.116	3.769	0.063	2.047
102	Khumbu (South)	20.12.2001	10.11.2004	2.893	1.5	0.045	2.591	-0.094	2.682	0.104	3.729	0.036	1.289
103	Khumbu (South)	20.12.2001	13.11.2005	3.901	0.0	0.033	2.596	-0.077	2.604	0.084	3.678	0.021	0.943
104	Khumbu (South)	20.12.2001	29.11.2005	3.945	0.0	0.003	2.438	-0.104	2.526	0.104	3.510	0.026	0.890
105	Khumbu (South)	20.12.2001	15.12.2005	3.989	0.0	-0.054	2.406	-0.017	2.442	0.057	3.428	0.014	0.859
106	Khumbu (South)	20.12.2001	01.02.2006	4.121	2.9	-0.030	2.525	-0.090	2.522	0.095	3.569	0.023	0.866
107	Khumbu (South)	20.12.2001	19.01.2007	5.085	2.9	-0.064	2.568	-0.152	2.622	0.166	3.670	0.033	0.722
108	Khumbu (South)	04.10.2002	08.01.2003	0.263	2.8	0.215	3.186	-0.111	3.264	0.242	4.561	0.919	17.343
109	Khumbu (South)	04.10.2002	23.10.2003	1.052	2.8	0.192	2.788	0.060	2.735	0.201	3.906	0.191	3.712
110	Khumbu (South)	04.10.2002	09.10.2004	2.016	2.9	-0.052	2.704	0.119	2.683	0.130	3.809	0.064	1.889
111	Khumbu (South)	04.10.2002	10.11.2004	2.104	1.3	-0.102	2.955	-0.210	3.219	0.233	4.370	0.111	2.077
112	Khumbu (South)	04.10.2002	13.11.2005	3.112	2.9	0.031	2.984	0.007	3.169	0.031	4.353	0.010	1.399
113	Khumbu (South)	04.10.2002	29.11.2005	3.156	2.8	0.139	3.194	0.452	3.306	0.473	4.597	0.150	1.457
114	Khumbu (South)	04.10.2002	15.12.2005	3.200	2.8	-0.031	3.244	-0.029	3.401	0.043	4.700	0.013	1.469
115	Khumbu (South)	04.10.2002	19.01.2007	4.296	0.0	-0.018	3.263	-0.113	3.374	0.114	4.694	0.027	1.093
116	Khumbu (South)	21.11.2002	23.10.2003	0.921	0.1	-0.019	2.469	-0.125	2.605	0.126	3.589	0.137	3.899
117	Khumbu (South)	21.11.2002	10.11.2004	1.973	1.4	0.011	2.299	-0.086	2.347	0.087	3.285	0.044	1.665
118	Khumbu (South)	21.11.2002	29.11.2005	3.025	0.0	-0.136	2.399	0.247	2.507	0.282	3.470	0.093	1.147
119	Khumbu (South)	08.01.2003	09.10.2004	1.753	0.1	-0.048	3.693	0.132	3.571	0.141	5.137	0.080	2.930
120	Khumbu (South)	08.01.2003	10.11.2004	1.841	1.5	-0.051	2.881	0.037	2.955	0.063	4.127	0.034	2.242
121	Khumbu (South)	08.01.2003	13.11.2005	2.849	0.1	-0.199	3.158	0.082	3.210	0.215	4.504	0.075	1.581
122	Khumbu (South)	08.01.2003	29.11.2005	2.893	0.0	-0.124	2.915	0.127	3.028	0.177	4.203	0.061	1.453
123	Khumbu (South)	08.01.2003	15.12.2005	2.937	0.0	-0.006	2.859	0.149	3.017	0.150	4.156	0.051	1.415
124	Khumbu (South)	08.01.2003	19.01.2007	4.033	2.8	-0.081	2.822	-0.044	3.022	0.092	4.134	0.023	1.025
125	Khumbu (South)	23.10.2003	09.10.2004	0.964	0.0	0.017	2.880	0.037	2.921	0.041	4.102	0.042	4.253
126	Khumbu (South)	23.10.2003	10.11.2004	1.052	1.5	0.025	2.430	0.108	2.534	0.111	3.511	0.106	3.338
127	Khumbu (South)	23.10.2003	13.11.2005	2.060	0.0	-0.075	2.630	0.136	2.680	0.155	3.755	0.075	1.822
128	Khumbu (South)	23.10.2003	29.11.2005	2.104	0.0	-0.103	2.491	0.125	2.534	0.162	3.553	0.077	1.689
129	Khumbu (South)	23.10.2003	15.12.2005	2.148	0.0	-0.029	2.596	0.026	2.625	0.039	3.692	0.018	1.719
130	Khumbu (South)	23.10.2003	01.02.2006	2.279	2.9	-0.042	2.538	0.073	2.467	0.084	3.540	0.037	1.553
131	Khumbu (South)	09.10.2004	19.01.2007	2.279	2.9	-0.032	3.158	-0.144	3.215	0.147	4.507	0.065	1.977
132	Khumbu (South)	25.10.2004	13.11.2005	1.052	2.9	-0.147	3.035	0.247	3.060	0.288	4.310	0.274	4.097
133	Khumbu (South)	25.10.2004	29.11.2005	1.096	2.9	-0.083	3.119	-0.064	3.156	0.105	4.437	0.096	4.048
134	Khumbu (South)	25.10.2004	15.12.2005	1.140	2.9	-0.167	3.293	0.020	3.314	0.169	4.672	0.148	4.099
135	Khumbu (South)	25.10.2004	19.01.2007	2.236	0.0	-0.018	3.287	-0.106	3.461	0.108	4.774	0.048	2.135
136	Khumbu (South)	10.11.2004	13.11.2005	1.008	1.5	-0.089	2.338	0.003	2.527	0.089	3.442	0.088	3.414
137	Khumbu (South)	10.11.2004	29.11.2005	1.052	1.5	-0.129	2.416	0.002	2.520	0.129	3.491	0.123	3.318
138	Khumbu (South)	10.11.2004	15.12.2005	1.096	1.5	-0.133	2.548	-0.009	2.619	0.134	3.654	0.122	3.335
139	Khumbu (South)	10.11.2004	01.02.2006	1.227	1.4	-0.097	2.655	-0.038	2.654	0.104	3.754	0.085	3.059
140	Khumbu (South)	10.11.2004	19.01.2007	2.192	1.4	-0.104	2.690	-0.042	2.687	0.112	3.802	0.051	1.735
141	Khumbu (South)	15.12.2005	19.01.2007	1.096	2.9	-0.060	2.409	-0.293	2.431	0.299	3.422	0.272	3.122

Appendix A: Satellite images and correlation details

No.	Geographic region	Date [yyyy-mm-dd] Scene 1	Scene 2	Time span [years]	Inci-dence angle diff. [°]	Residual offset [m] East-West Mean	SD	North-South Mean	SD	Total displacement uncertainty [m] Mean	SD	Velocity uncertainty [m/yr] Mean	SD
142	Khumbu (South)	01.02.2006	19.01.2007	0.964	0.0	-0.022	2.372	-0.234	2.532	0.235	3.470	0.244	3.598
143	Khumbu (North)	28.09.2000	04.10.2002	2.016	0.0	0.035	2.017	0.063	2.007	0.072	2.845	0.036	1.411
144	Khumbu (North)	28.09.2000	09.10.2004	4.033	2.9	-0.008	2.215	0.084	2.231	0.084	3.144	0.021	0.780
145	Khumbu (North)	28.09.2000	25.10.2004	4.077	0.0	0.043	2.604	0.090	2.702	0.100	3.752	0.024	0.920
146	Khumbu (North)	28.09.2000	10.11.2004	4.121	1.4	0.068	2.541	0.056	2.603	0.088	3.637	0.021	0.883
147	Khumbu (North)	28.09.2000	19.01.2007	6.312	0.0	0.101	2.908	0.009	2.861	0.101	4.080	0.016	0.646
148	Khumbu (North)	14.10.2000	20.12.2001	1.184	0.0	0.026	2.221	-0.019	2.227	0.032	3.145	0.027	2.657
149	Khumbu (North)	14.10.2000	04.10.2002	1.973	2.9	-0.003	1.731	0.016	1.725	0.016	2.444	0.008	1.239
150	Khumbu (North)	14.10.2000	08.01.2003	2.236	0.1	0.124	2.998	-0.106	2.905	0.163	4.175	0.073	1.868
151	Khumbu (North)	14.10.2000	23.10.2003	3.025	0.0	0.013	1.929	0.052	1.879	0.054	2.693	0.018	0.890
152	Khumbu (North)	14.10.2000	09.10.2004	3.989	0.0	-0.002	1.985	0.018	1.964	0.018	2.793	0.004	0.700
153	Khumbu (North)	14.10.2000	25.10.2004	4.033	2.9	-0.026	2.307	0.026	2.297	0.037	3.256	0.009	0.807
154	Khumbu (North)	14.10.2000	10.11.2004	4.077	1.5	-0.010	2.100	0.064	2.085	0.064	2.959	0.016	0.726
155	Khumbu (North)	30.10.2000	20.12.2001	1.140	0.1	0.009	1.901	0.030	1.866	0.031	2.664	0.028	2.338
156	Khumbu (North)	30.10.2000	04.10.2002	1.929	2.8	-0.007	1.837	0.012	1.859	0.014	2.614	0.007	1.355
157	Khumbu (North)	30.10.2000	08.01.2003	2.192	0.0	0.088	3.060	-0.203	3.015	0.221	4.296	0.101	1.960
158	Khumbu (North)	30.10.2000	23.10.2003	2.981	0.0	0.008	1.664	-0.003	1.709	0.008	2.385	0.003	0.800
159	Khumbu (North)	30.10.2000	09.10.2004	3.945	0.0	-0.020	1.904	-0.058	2.052	0.061	2.800	0.015	0.710
160	Khumbu (North)	30.10.2000	10.11.2004	4.033	1.5	-0.026	2.019	0.009	2.004	0.028	2.845	0.007	0.705
161	Khumbu (North)	30.10.2000	19.01.2007	6.225	2.8	0.009	2.286	0.047	2.088	0.048	3.096	0.008	0.497
162	Khumbu (North)	20.12.2001	04.10.2002	0.789	2.9	-0.011	2.049	0.053	2.130	0.054	2.956	0.069	3.746
163	Khumbu (North)	20.12.2001	08.01.2003	1.052	0.1	0.082	2.699	-0.382	2.855	0.391	3.928	0.371	3.734
164	Khumbu (North)	20.12.2001	23.10.2003	1.841	0.0	0.023	1.817	0.003	1.872	0.023	2.609	0.012	1.417
165	Khumbu (North)	20.12.2001	09.10.2004	2.805	0.0	0.001	2.098	0.019	2.118	0.019	2.981	0.007	1.063
166	Khumbu (North)	20.12.2001	10.11.2004	2.893	1.5	-0.009	1.964	-0.017	1.958	0.019	2.774	0.007	0.959
167	Khumbu (North)	20.12.2001	19.01.2007	5.085	2.9	-0.034	1.959	-0.030	1.811	0.045	2.667	0.009	0.525
168	Khumbu (North)	04.10.2002	23.10.2003	1.052	2.8	0.037	1.658	0.054	1.636	0.065	2.329	0.062	2.214
169	Khumbu (North)	04.10.2002	09.10.2004	2.016	2.9	-0.007	1.767	0.026	1.792	0.027	2.517	0.014	1.248
170	Khumbu (North)	04.10.2002	25.10.2004	2.060	0.0	0.020	2.153	0.024	2.206	0.031	3.083	0.015	1.496
171	Khumbu (North)	04.10.2002	10.11.2004	2.104	1.3	-0.003	2.049	0.035	2.194	0.035	3.002	0.017	1.427
172	Khumbu (North)	04.10.2002	19.01.2007	4.296	0.0	-0.039	2.572	-0.026	2.646	0.047	3.690	0.011	0.859
173	Khumbu (North)	08.01.2003	23.10.2003	0.789	0.0	-0.096	2.936	0.171	2.901	0.196	4.127	0.248	5.231
174	Khumbu (North)	08.01.2003	09.10.2004	1.753	0.1	-0.170	3.052	0.185	3.005	0.251	4.283	0.143	2.443
175	Khumbu (North)	08.01.2003	10.11.2004	1.841	1.5	-0.069	2.739	0.129	2.750	0.146	3.882	0.079	2.108
176	Khumbu (North)	23.10.2003	09.10.2004	0.964	0.0	0.000	1.597	-0.006	1.599	0.006	2.260	0.006	2.343
177	Khumbu (North)	23.10.2003	10.11.2004	1.052	1.5	-0.008	1.721	0.015	1.724	0.016	2.436	0.016	2.316
178	Khumbu (North)	23.10.2003	19.01.2007	3.244	2.9	-0.037	2.093	0.020	1.929	0.042	2.847	0.013	0.878
179	Khumbu (North)	09.10.2004	19.01.2007	2.279	2.9	0.028	2.243	0.009	2.236	0.029	3.167	0.013	1.389
180	Khumbu (North)	25.10.2004	19.01.2007	2.236	0.0	0.062	2.548	0.117	2.560	0.133	3.612	0.059	1.616
181	Khumbu (North)	10.11.2004	19.01.2007	2.192	1.4	-0.020	2.123	0.072	2.141	0.075	3.015	0.034	1.376
182	Manaslu	29.11.2000	02.10.2002	1.841	0.0	-0.188	3.142	0.043	3.178	0.193	4.469	0.105	2.427
183	Manaslu	29.11.2000	05.10.2003	2.849	0.0	-0.160	3.005	0.056	3.087	0.169	4.308	0.059	1.512
184	Manaslu	29.11.2000	10.02.2004	3.200	0.0	0.011	3.624	-0.083	3.707	0.084	5.184	0.026	1.620
185	Manaslu	15.12.2000	02.10.2002	1.797	0.0	0.108	2.727	0.074	2.960	0.131	4.024	0.073	2.239
186	Manaslu	15.12.2000	05.10.2003	2.805	0.0	-0.004	2.577	-0.011	2.707	0.011	3.738	0.004	1.332
187	Manaslu	17.02.2001	05.10.2003	2.630	2.9	-0.147	4.045	0.157	3.900	0.215	5.619	0.082	2.136
188	Manaslu	17.02.2001	10.02.2004	2.981	2.9	0.035	3.717	0.109	3.858	0.115	5.357	0.038	1.797
189	Manaslu	17.02.2001	07.04.2007	6.137	0.0	0.059	3.609	-0.133	3.773	0.145	5.221	0.024	0.851
190	Manaslu	02.10.2002	05.10.2003	1.008	0.0	-0.019	2.145	0.021	2.260	0.028	3.116	0.028	3.091
191	Manaslu	03.11.2002	23.10.2004	1.973	0.0	-0.004	2.941	-0.015	2.831	0.015	4.082	0.008	2.069
192	Manaslu	03.11.2002	26.12.2004	2.148	0.0	0.033	2.886	-0.016	2.815	0.037	4.032	0.017	1.877
193	Manaslu	13.03.2004	23.10.2004	0.614	0.0	-0.014	3.255	0.084	3.366	0.086	4.682	0.139	7.629
194	Manaslu	13.03.2004	17.11.2004	0.682	11.5	-0.253	4.269	0.166	3.448	0.303	5.487	0.444	8.044
195	Manaslu	13.03.2004	03.12.2004	0.726	11.5	0.088	4.501	0.196	3.410	0.214	5.647	0.295	7.778
196	Manaslu	13.03.2004	07.04.2007	3.068	2.9	0.052	3.050	0.125	2.978	0.135	4.262	0.044	1.389
197	Manaslu	13.03.2004	04.01.2008	3.814	2.9	-0.127	3.388	0.231	3.410	0.264	4.807	0.069	1.260
198	Manaslu	23.10.2004	07.11.2006	2.041	14.3	-0.029	3.905	-0.013	2.886	0.032	4.856	0.016	2.379
199	Manaslu	23.10.2004	07.04.2007	2.455	2.9	-0.033	3.666	-0.032	3.649	0.046	5.172	0.019	2.107
200	Manaslu	23.10.2004	04.01.2008	3.200	2.9	-0.189	3.029	0.201	2.965	0.276	4.239	0.086	1.325

Appendix A: Satellite images and correlation details

No.	Geographic region	Date [yyyy-mm-dd] Scene 1	Scene 2	Time span [years]	Inci-dence angle diff. [°]	Residual offset [m] East-West Mean	SD	North-South Mean	SD	Total displacement uncertainty [m] Mean	SD	Velocity uncertainty [m/yr] Mean	SD
201	Manaslu	03.12.2004	07.11.2006	1.929	2.9	0.095	3.198	0.040	2.966	0.103	4.362	0.053	2.262
202	Manaslu	26.12.2004	07.11.2006	1.866	14.3	0.024	3.718	-0.016	3.060	0.029	4.815	0.016	2.581
203	Manaslu	26.12.2004	04.01.2008	3.025	2.9	-0.024	2.558	-0.017	2.541	0.029	3.606	0.010	1.192
204	Manaslu	07.11.2006	04.01.2008	1.159	11.5	-0.140	4.123	0.058	2.930	0.152	5.058	0.131	4.364
205	Manaslu	07.04.2007	04.01.2008	0.745	0.0	-0.120	3.544	0.179	3.696	0.216	5.120	0.289	6.871
206	Gurla Mandatha	31.10.2001	28.12.2002	1.159	8.6	-0.270	3.413	-0.198	2.854	0.336	4.450	0.289	3.839
207	Gurla Mandatha	31.10.2001	26.09.2003	1.904	10.5	-0.382	3.304	-0.062	2.654	0.387	4.238	0.203	2.226
208	Gurla Mandatha	03.01.2002	28.12.2002	0.984	8.6	-0.282	3.790	0.216	3.239	0.355	4.986	0.361	5.069
209	Gurla Mandatha	03.01.2002	23.12.2006	4.973	10.0	-0.054	3.509	0.287	3.090	0.292	4.676	0.059	0.940
210	Gurla Mandatha	28.12.2002	26.09.2003	0.745	1.9	-0.025	2.581	0.088	2.702	0.092	3.736	0.124	5.014
211	Gurla Mandatha	28.12.2002	10.10.2005	2.786	8.6	0.090	3.532	0.010	3.158	0.090	4.737	0.032	1.700
212	Gurla Mandatha	28.12.2002	23.12.2006	3.989	1.4	0.030	3.689	-0.110	4.162	0.114	5.562	0.029	1.394
213	Gurla Mandatha	14.02.2003	23.12.2006	3.858	1.4	0.086	2.522	-0.034	2.777	0.093	3.751	0.024	0.972
214	Gurla Mandatha	23.02.2003	23.12.2006	3.833	10.0	-0.004	3.600	-0.368	3.368	0.368	4.930	0.096	1.286
215	Gurla Mandatha	26.09.2003	10.10.2005	2.041	10.5	0.530	3.005	-0.063	2.351	0.534	3.815	0.261	1.869
216	Gurla Mandatha	26.09.2003	23.12.2006	3.244	0.5	-0.044	4.241	0.581	4.427	0.583	6.130	0.180	1.890
217	Gurla Mandatha	23.12.2006	14.04.2007	0.307	1.4	-0.089	3.351	-0.374	3.937	0.385	5.170	1.254	16.849
218	Gurla Mandatha	23.12.2006	19.07.2007	0.570	1.4	-0.041	4.225	-0.312	4.288	0.315	6.020	0.552	10.563
219	Gurla Mandatha	23.12.2006	15.11.2007	0.896	7.2	-0.076	4.035	0.200	3.645	0.214	5.438	0.239	6.070
220	Gurla Mandatha	14.04.2007	19.07.2007	0.263	0.0	-0.229	3.891	0.263	4.107	0.348	5.658	1.324	21.511
221	Gurla Mandatha	14.04.2007	15.11.2007	0.589	8.6	-0.349	3.972	0.538	3.889	0.641	5.558	1.088	9.436
222	Garhwal (Gangotri)	09.11.2000	09.09.2001	0.833	2.9	0.144	3.354	0.457	3.374	0.479	4.757	0.575	5.712
223	Garhwal (Gangotri)	09.11.2000	10.10.2003	2.918	14.3	0.004	5.376	0.100	3.679	0.100	6.515	0.034	2.233
224	Garhwal (Gangotri)	10.11.2000	19.08.2005	4.775	2.8	0.183	3.891	0.098	4.020	0.208	5.595	0.044	1.172
225	Garhwal (Gangotri)	11.11.2000	09.10.2006	5.912	2.8	-0.297	3.490	-0.041	3.079	0.300	4.655	0.051	0.787
226	Garhwal (Gangotri)	09.09.2001	10.10.2003	2.085	11.4	0.003	3.487	-0.007	2.811	0.008	4.479	0.004	2.148
227	Garhwal (Gangotri)	09.09.2001	24.07.2004	2.874	14.3	0.299	3.268	-0.218	3.269	0.370	4.622	0.129	1.608
228	Garhwal (Gangotri)	09.09.2001	23.09.2006	5.041	2.8	0.267	3.098	-0.096	2.864	0.284	4.219	0.056	0.837
229	Garhwal (Gangotri)	09.09.2001	09.10.2006	5.085	0.0	0.145	3.297	0.014	2.935	0.146	4.414	0.029	0.868
230	Garhwal (Gangotri)	09.09.2001	10.11.2006	5.173	2.8	-0.016	3.334	-0.062	3.213	0.064	4.630	0.012	0.895
231	Garhwal (Gangotri)	21.11.2001	10.10.2003	1.885	2.9	0.181	3.114	0.013	2.729	0.181	4.141	0.096	2.197
232	Garhwal (Gangotri)	21.11.2001	24.07.2004	2.674	0.0	0.316	3.759	-0.051	3.919	0.320	5.430	0.120	2.031
233	Garhwal (Gangotri)	21.11.2001	15.10.2005	3.901	0.0	0.454	3.235	-0.075	3.174	0.460	4.532	0.118	1.162
234	Garhwal (Gangotri)	23.12.2001	10.10.2003	1.797	2.9	-0.389	4.298	0.169	3.780	0.424	5.724	0.236	3.185
235	Garhwal (Gangotri)	23.12.2001	06.11.2007	5.874	0.0	0.060	4.076	-0.181	3.733	0.191	5.527	0.032	0.941
236	Garhwal (Gangotri)	23.12.2001	22.11.2007	5.918	0.0	0.075	3.628	-0.090	3.552	0.117	5.077	0.020	0.858
237	Garhwal (Gangotri)	08.01.2002	10.10.2003	1.753	2.9	-0.022	4.051	0.289	3.933	0.290	5.646	0.165	3.220
238	Garhwal (Gangotri)	08.01.2002	15.10.2005	3.770	0.0	-0.028	3.799	0.079	3.972	0.084	5.496	0.022	1.458
239	Garhwal (Gangotri)	10.10.2003	24.07.2004	0.789	2.9	0.116	3.366	0.308	3.276	0.329	4.697	0.416	5.953
240	Garhwal (Gangotri)	11.10.2003	18.08.2005	1.855	11.5	0.230	4.842	0.385	4.251	0.448	6.444	0.242	3.474
241	Garhwal (Gangotri)	11.10.2003	15.10.2005	2.014	2.9	0.228	3.208	0.227	2.878	0.322	4.309	0.160	2.140
242	Garhwal (Gangotri)	11.10.2003	23.09.2006	2.953	8.6	1.165	4.791	-0.462	3.564	1.254	5.972	0.425	2.022
243	Garhwal (Gangotri)	12.10.2003	09.10.2006	2.995	11.5	0.135	4.449	0.107	3.275	0.172	5.525	0.058	1.845
244	Garhwal (Gangotri)	24.07.2004	19.08.2005	1.071	14.3	-0.074	4.070	0.191	3.179	0.204	5.165	0.191	4.821
245	Garhwal (Gangotri)	24.07.2004	15.10.2005	1.227	0.0	0.039	3.489	-0.016	3.600	0.042	5.013	0.034	4.084
246	Garhwal (Gangotri)	24.07.2004	09.10.2006	2.211	14.3	-0.124	5.202	-0.037	3.683	0.129	6.373	0.058	2.883
247	Garhwal (Gangotri)	24.07.2004	10.11.2006	2.299	11.5	0.069	5.283	0.059	4.180	0.091	6.737	0.040	2.931
248	Garhwal (Gangotri)	19.08.2005	23.09.2006	1.096	2.9	-0.070	3.499	-0.038	3.732	0.079	5.115	0.072	4.668
249	Garhwal (Gangotri)	19.08.2005	18.10.2006	1.164	11.5	0.101	5.177	0.250	4.167	0.269	6.646	0.231	5.707
250	Garhwal (Gangotri)	19.08.2005	10.11.2006	1.227	2.9	-0.104	3.682	-0.221	3.989	0.244	5.428	0.199	4.423
251	Garhwal (Gangotri)	15.10.2005	23.09.2006	0.940	11.5	0.045	4.614	-0.021	3.591	0.050	5.847	0.053	6.222
252	Garhwal (Gangotri)	15.10.2005	09.10.2006	0.984	14.3	0.122	4.330	0.081	3.426	0.147	5.521	0.149	5.614
253	Garhwal (Gangotri)	15.10.2005	18.10.2006	1.008	2.9	0.010	3.525	0.242	2.859	0.242	4.539	0.240	4.502
254	Garhwal (Gangotri)	15.10.2005	10.11.2006	1.071	11.5	-0.008	4.428	0.226	3.423	0.226	5.596	0.211	5.224
255	Garhwal (Gangotri)	23.09.2006	09.10.2006	0.044	2.9	-0.049	2.417	0.142	2.261	0.151	3.310	3.438	75.502
256	Garhwal (Gangotri)	23.09.2006	10.11.2006	0.132	0.0	0.165	2.957	0.301	3.063	0.343	4.258	2.608	32.376
257	Garhwal (Gangotri)	18.10.2006	06.11.2007	1.052	2.9	-0.218	3.769	-0.016	3.405	0.218	5.080	0.207	4.828
258	Garhwal (Tons)	07.12.2001	01.10.2003	1.816	8.6	-0.087	3.854	0.073	3.546	0.114	5.237	0.063	2.883
259	Garhwal (Tons)	07.12.2001	22.10.2005	3.877	8.6	0.194	3.691	0.082	3.200	0.210	4.885	0.054	1.260

Appendix A: Satellite images and correlation details

No.	Geographic region	Date [yyyy-mm-dd] Scene 1	Scene 2	Time span [years]	Incidence angle diff. [°]	Residual offset [m] East-West Mean	SD	North-South Mean	SD	Total displacement uncertainty [m] Mean	SD	Velocity uncertainty [m/yr] Mean	SD
260	Garhwal (Tons)	30.12.2001	01.10.2003	1.753	0.0	-0.058	2.879	0.066	3.353	0.088	4.420	0.050	2.521
261	Garhwal (Tons)	30.12.2001	09.03.2004	2.192	0.0	0.064	3.146	-0.102	3.336	0.121	4.585	0.055	2.092
262	Garhwal (Tons)	30.12.2001	04.11.2004	2.849	0.0	-0.002	2.296	0.008	2.525	0.008	3.413	0.003	1.198
263	Garhwal (Tons)	30.12.2001	22.10.2005	3.814	0.0	0.117	2.687	0.047	2.913	0.126	3.963	0.033	1.039
264	Garhwal (Tons)	01.10.2003	09.03.2004	0.438	0.0	0.177	3.602	-0.572	4.122	0.598	5.474	1.365	12.488
265	Garhwal (Tons)	01.10.2003	01.09.2004	0.921	0.0	-0.025	2.859	0.218	3.153	0.220	4.257	0.239	4.624
266	Garhwal (Tons)	01.10.2003	04.11.2004	1.096	0.0	0.296	2.518	-0.115	2.923	0.317	3.858	0.289	3.520
267	Garhwal (Tons)	01.10.2003	22.10.2005	2.060	0.0	0.117	2.057	0.109	2.334	0.159	3.111	0.077	1.510
268	Garhwal (Tons)	01.10.2003	13.11.2007	4.121	0.0	-0.006	2.501	0.000	2.932	0.006	3.854	0.002	0.935
269	Garhwal (Tons)	09.03.2004	04.11.2004	0.658	0.0	-0.019	3.327	0.140	3.629	0.142	4.924	0.215	7.488
270	Garhwal (Tons)	09.03.2004	13.11.2007	3.682	0.0	-0.057	3.575	-0.120	4.023	0.133	5.382	0.036	1.462
271	Garhwal (Tons)	01.09.2004	04.11.2004	0.175	0.0	0.046	3.409	0.459	4.155	0.461	5.375	2.630	30.652
272	Garhwal (Tons)	01.09.2004	13.11.2007	3.200	0.0	0.020	3.549	-0.213	4.090	0.214	5.415	0.067	1.692
273	Garhwal (Tons)	04.11.2004	22.10.2005	0.964	0.0	-0.024	2.071	0.051	2.295	0.056	3.091	0.058	3.205
274	Garhwal (Tons)	04.11.2004	13.11.2007	3.025	0.0	-0.044	2.097	0.070	2.260	0.083	3.083	0.027	1.019
275	Garhwal (Tons)	22.10.2005	13.11.2007	2.060	0.0	-0.024	2.066	-0.018	2.220	0.030	3.033	0.015	1.472
276	Leo Pargil	17.03.2001	24.04.2003	2.104	2.9	0.147	2.597	0.039	2.927	0.152	3.913	0.072	1.860
277	Leo Pargil	17.03.2001	01.10.2003	2.542	2.8	-0.134	2.707	0.448	2.931	0.467	3.990	0.184	1.569
278	Leo Pargil	17.03.2001	17.10.2003	2.586	0.0	0.021	2.987	1.015	3.210	1.015	4.385	0.392	1.695
279	Leo Pargil	17.03.2001	04.11.2004	3.638	2.8	0.013	2.698	-0.004	3.150	0.013	4.147	0.004	1.140
280	Leo Pargil	17.03.2001	31.12.2007	6.795	2.9	-0.018	2.648	0.114	2.938	0.115	3.955	0.017	0.582
281	Leo Pargil	21.11.2001	04.11.2004	2.956	8.6	-0.146	3.016	-0.165	2.322	0.220	3.806	0.075	1.287
282	Leo Pargil	21.11.2001	22.10.2005	3.921	8.6	0.089	3.506	-0.088	2.955	0.125	4.585	0.032	1.170
283	Leo Pargil	24.04.2003	04.11.2004	1.534	0.0	-0.249	3.738	0.300	4.019	0.390	5.488	0.254	3.577
284	Leo Pargil	24.04.2003	22.10.2005	2.499	0.0	-0.228	3.875	0.304	4.279	0.380	5.772	0.152	2.310
285	Leo Pargil	01.10.2003	01.09.2004	0.921	0.0	0.077	1.753	-0.040	1.957	0.087	2.627	0.094	2.854
286	Leo Pargil	01.10.2003	04.11.2004	1.096	0.0	0.147	2.404	0.218	2.497	0.263	3.466	0.240	3.163
287	Leo Pargil	01.10.2003	22.10.2005	2.060	0.0	0.146	1.969	0.176	2.304	0.229	3.031	0.111	1.471
288	Leo Pargil	01.10.2003	01.11.2006	3.088	8.6	-0.129	2.819	0.063	2.096	0.143	3.513	0.046	1.138
289	Leo Pargil	01.10.2003	06.06.2007	3.682	0.0	0.296	2.646	-0.369	3.178	0.473	4.136	0.129	1.123
290	Leo Pargil	01.10.2003	13.11.2007	4.121	0.0	0.191	2.716	0.130	2.781	0.231	3.888	0.056	0.943
291	Leo Pargil	01.10.2003	31.12.2007	4.252	0.1	0.302	3.227	-0.220	3.276	0.373	4.598	0.088	1.081
292	Leo Pargil	02.11.2003	31.12.2007	4.164	2.9	0.193	3.055	-0.466	3.209	0.504	4.431	0.121	1.064
293	Leo Pargil	01.09.2004	22.10.2005	1.140	0.0	0.013	2.335	0.259	2.541	0.260	3.451	0.228	3.028
294	Leo Pargil	01.09.2004	06.06.2007	2.762	0.0	0.314	2.696	-0.411	2.912	0.518	3.968	0.187	1.437
295	Leo Pargil	04.11.2004	22.10.2005	0.964	0.0	-0.052	2.015	-0.054	2.210	0.075	2.990	0.078	3.101
296	Leo Pargil	04.11.2004	13.11.2007	3.025	0.0	0.029	2.353	-0.002	2.417	0.029	3.373	0.009	1.115
297	Leo Pargil	04.11.2004	31.12.2007	3.156	0.0	0.123	2.857	0.229	3.056	0.260	4.183	0.082	1.325
298	Leo Pargil	22.10.2005	06.06.2007	1.622	0.0	0.285	2.941	-0.212	3.525	0.355	4.590	0.219	2.830
299	Leo Pargil	22.10.2005	13.11.2007	2.060	0.0	0.090	2.548	0.031	2.660	0.095	3.683	0.046	1.788
300	Leo Pargil	22.10.2005	31.12.2007	2.192	0.0	0.195	3.098	0.063	3.397	0.205	4.597	0.093	2.098
301	Lahul (South)	01.07.2002	08.10.2003	1.271	2.9	-0.176	4.108	0.222	4.467	0.283	6.069	0.223	4.774
302	Lahul (South)	30.10.2002	08.10.2003	0.940	11.5	0.064	4.047	-0.118	3.397	0.134	5.284	0.143	5.623
303	Lahul (South)	30.10.2002	24.10.2003	0.984	8.6	-0.010	3.931	0.059	3.221	0.060	5.082	0.061	5.167
304	Lahul (South)	30.10.2002	17.09.2004	1.885	0.0	-0.063	3.704	-0.201	3.984	0.211	5.440	0.112	2.886
305	Lahul (South)	30.10.2002	07.11.2005	3.025	0.0	-0.398	2.868	0.166	2.828	0.431	4.028	0.142	1.332
306	Lahul (South)	30.10.2002	30.09.2006	3.921	8.6	0.365	4.275	0.066	3.557	0.371	5.561	0.095	1.419
307	Lahul (South)	30.10.2002	16.10.2006	3.964	8.6	0.055	3.865	-0.083	3.009	0.100	4.898	0.025	1.235
308	Lahul (South)	30.10.2002	17.11.2006	4.052	10.0	0.101	4.259	1.045	4.042	1.050	5.872	0.259	1.449
309	Lahul (South)	30.10.2002	20.11.2007	5.060	11.5	0.119	3.950	0.205	3.156	0.237	5.056	0.047	0.999
310	Lahul (South)	30.10.2002	15.12.2007	5.129	0.0	-0.089	3.950	0.061	3.853	0.108	5.518	0.021	1.076
311	Lahul (South)	08.10.2003	08.09.2004	0.921	2.9	0.036	2.532	0.038	2.696	0.052	3.698	0.057	4.018
312	Lahul (South)	08.10.2003	17.09.2004	0.945	11.5	0.054	3.936	0.103	3.190	0.116	5.067	0.123	5.360
313	Lahul (South)	08.10.2003	07.11.2005	2.085	11.5	-0.116	3.957	0.181	3.348	0.215	5.184	0.103	2.486
314	Lahul (South)	08.10.2003	30.09.2006	2.981	2.9	-0.017	2.491	-0.071	2.504	0.073	3.532	0.024	1.185
315	Lahul (South)	08.10.2003	16.10.2006	3.025	2.9	0.011	2.996	0.173	3.134	0.173	4.336	0.057	1.434
316	Lahul (South)	08.10.2003	17.11.2006	3.112	1.5	-0.188	4.018	0.650	3.898	0.677	5.599	0.217	1.799
317	Lahul (South)	08.10.2003	21.05.2007	3.619	11.5	0.853	4.677	-0.470	4.753	0.974	6.668	0.269	1.843
318	Lahul (South)	08.10.2003	20.11.2007	4.121	0.0	-0.010	3.265	0.099	3.292	0.100	4.637	0.024	1.125

Appendix A: Satellite images and correlation details

No.	Geographic region	Date [yyyy-mm-dd] Scene 1	Scene 2	Time span [years]	Inci-dence angle diff. [°]	Residual offset [m] East-West Mean	SD	North-South Mean	SD	Total displacement uncertainty [m] Mean	SD	Velocity uncertainty [m/yr] Mean	SD
319	Lahul (South)	08.10.2003	15.12.2007	4.189	11.4	-0.204	4.361	0.130	3.758	0.242	5.757	0.058	1.374
320	Lahul (South)	24.10.2003	08.09.2004	0.877	0.0	0.043	2.688	-0.251	3.174	0.255	4.159	0.290	4.744
321	Lahul (South)	24.10.2003	30.09.2006	2.937	0.0	0.055	2.499	-0.190	2.692	0.198	3.673	0.067	1.251
322	Lahul (South)	24.10.2003	16.10.2006	2.981	0.0	0.207	2.727	-0.058	2.811	0.215	3.916	0.072	1.314
323	Lahul (South)	24.10.2003	20.11.2007	4.077	2.9	-0.126	3.013	0.108	3.171	0.166	4.374	0.041	1.073
324	Lahul (South)	08.09.2004	07.11.2005	1.164	8.6	0.215	4.090	0.197	3.775	0.291	5.566	0.250	4.780
325	Lahul (South)	08.09.2004	30.09.2006	2.060	0.0	-0.079	1.981	0.127	2.251	0.150	2.998	0.073	1.455
326	Lahul (South)	08.09.2004	16.10.2006	2.104	0.0	-0.008	2.769	0.082	3.097	0.083	4.155	0.039	1.975
327	Lahul (South)	17.09.2004	07.11.2005	1.140	0.0	-0.014	3.840	0.136	3.801	0.137	5.403	0.120	4.741
328	Lahul (South)	17.09.2004	30.09.2006	2.036	8.6	-0.013	4.256	0.072	3.381	0.073	5.436	0.036	2.670
329	Lahul (South)	17.09.2004	16.10.2006	2.079	8.6	-0.122	4.082	0.170	3.605	0.209	5.447	0.100	2.619
330	Lahul (South)	17.09.2004	17.11.2006	2.167	10.0	-0.193	4.663	0.254	4.723	0.319	6.637	0.147	3.063
331	Lahul (South)	17.09.2004	21.05.2007	2.674	0.0	0.414	4.482	-0.745	4.669	0.852	6.472	0.319	2.420
332	Lahul (South)	17.09.2004	20.11.2007	3.175	11.5	-0.048	4.104	-0.209	3.709	0.215	5.531	0.068	1.742
333	Lahul (South)	17.09.2004	15.12.2007	3.244	0.0	-0.007	4.210	0.103	4.011	0.103	5.815	0.032	1.793
334	Lahul (South)	07.11.2005	30.09.2006	0.896	8.6	-0.053	4.156	-0.479	3.466	0.482	5.412	0.538	6.041
335	Lahul (South)	07.11.2005	16.10.2006	0.940	8.6	0.039	3.763	0.011	3.140	0.040	4.901	0.043	5.215
336	Lahul (South)	07.11.2005	17.11.2006	1.027	10.0	-0.166	3.908	0.346	3.331	0.384	5.135	0.374	4.998
337	Lahul (South)	07.11.2005	21.05.2007	1.534	0.0	0.443	4.341	-0.455	4.626	0.635	6.344	0.414	4.135
338	Lahul (South)	07.11.2005	20.11.2007	2.036	11.5	0.015	3.705	0.113	2.942	0.114	4.731	0.056	2.324
339	Lahul (South)	07.11.2005	15.12.2007	2.104	0.0	-0.055	3.723	0.195	3.729	0.203	5.269	0.096	2.504
340	Lahul (South)	16.10.2006	20.11.2007	1.096	2.9	-0.041	2.936	0.164	3.058	0.169	4.240	0.154	3.869
341	Lahul (South)	16.10.2006	15.12.2007	1.164	8.6	-0.096	4.460	0.088	3.832	0.130	5.880	0.112	5.050
342	Lahul (South)	17.11.2006	20.11.2007	1.008	1.5	-0.165	2.686	0.311	3.053	0.352	4.067	0.349	4.033
343	Lahul (North)	25.06.2000	28.08.2000	0.175	0.0	-0.227	3.138	0.147	3.352	0.270	4.591	1.541	26.186
344	Lahul (North)	28.08.2000	24.10.2003	3.156	0.0	0.180	3.423	-0.009	3.443	0.180	4.855	0.057	1.538
345	Lahul (North)	28.08.2000	08.09.2004	4.033	0.0	0.131	2.636	-0.053	2.547	0.142	3.666	0.035	0.909
346	Lahul (North)	28.08.2000	17.09.2004	4.058	8.6	-0.263	3.606	0.102	3.040	0.282	4.716	0.070	1.162
347	Lahul (North)	28.08.2000	29.10.2005	5.173	0.0	0.206	3.393	0.015	3.382	0.207	4.791	0.040	0.926
348	Lahul (North)	08.10.2003	08.09.2004	0.921	2.9	-0.030	2.964	0.042	3.078	0.052	4.273	0.056	4.642
349	Lahul (North)	08.10.2003	17.09.2004	0.945	11.5	-0.079	3.956	0.062	2.924	0.101	4.920	0.107	5.205
350	Lahul (North)	08.10.2003	29.10.2005	2.060	2.8	-0.046	2.973	0.297	3.055	0.301	4.263	0.146	2.069
351	Lahul (North)	08.10.2003	07.11.2005	2.085	11.5	-0.190	3.885	0.217	3.114	0.288	4.979	0.138	2.388
352	Lahul (North)	08.10.2003	30.09.2006	2.981	2.9	-0.098	2.783	-0.077	2.971	0.125	4.071	0.042	1.366
353	Lahul (North)	08.10.2003	16.10.2006	3.025	2.9	-0.131	2.874	0.169	2.975	0.214	4.137	0.071	1.368
354	Lahul (North)	24.10.2003	08.09.2004	0.877	0.0	-0.040	2.910	0.017	3.068	0.044	4.228	0.050	4.823
355	Lahul (North)	24.10.2003	17.09.2004	0.901	8.6	0.216	2.867	0.314	2.973	0.382	4.130	0.423	4.582
356	Lahul (North)	24.10.2003	07.11.2005	2.041	8.6	0.232	2.844	-0.156	3.174	0.280	4.262	0.137	2.088
357	Lahul (North)	24.10.2003	16.10.2006	2.981	0.0	0.001	3.059	-0.187	3.104	0.187	4.358	0.063	1.462
358	Lahul (North)	08.09.2004	17.09.2004	0.025	8.6	0.044	2.942	0.150	3.006	0.157	4.207	6.352	170.606
359	Lahul (North)	08.09.2004	07.11.2005	1.164	8.6	0.272	2.499	0.229	2.772	0.356	3.732	0.305	3.205
360	Lahul (North)	08.09.2004	16.10.2006	2.104	0.0	0.066	3.131	0.374	3.289	0.380	4.541	0.180	2.158
361	Lahul (North)	17.09.2004	29.10.2005	1.115	8.6	0.137	3.899	0.038	3.303	0.142	5.110	0.127	4.583
362	Lahul (North)	17.09.2004	07.11.2005	1.140	0.0	0.027	3.302	0.075	3.308	0.080	4.674	0.070	4.101
363	Lahul (North)	17.09.2004	30.09.2006	2.036	8.6	0.024	3.539	0.115	2.776	0.118	4.498	0.058	2.209
364	Lahul (North)	17.09.2004	16.10.2006	2.079	8.6	0.144	3.838	0.191	3.190	0.239	4.991	0.115	2.400
365	Lahul (North)	29.10.2005	30.09.2006	0.921	0.1	0.127	2.860	-0.029	3.142	0.130	4.249	0.141	4.615
366	Lahul (North)	29.10.2005	16.10.2006	0.964	0.0	0.276	3.010	-0.128	2.991	0.304	4.244	0.315	4.400
367	Lahul (North)	29.10.2005	20.11.2007	2.060	2.8	0.003	3.027	0.173	3.189	0.173	4.396	0.084	2.134
368	Lahul (North)	07.11.2005	30.09.2006	0.896	8.6	0.022	3.959	-0.068	3.327	0.071	5.171	0.079	5.772
369	Lahul (North)	07.11.2005	16.10.2006	0.940	8.6	0.166	3.782	-0.074	3.174	0.182	4.938	0.194	5.254
370	Lahul (North)	07.11.2005	20.11.2007	2.036	11.5	0.027	4.040	0.040	2.997	0.049	5.030	0.024	2.471
371	Lahul (North)	30.09.2006	16.10.2006	0.044	0.0	0.027	2.590	0.459	2.981	0.459	3.949	10.477	90.078
372	Lahul (North)	30.09.2006	20.11.2007	1.140	2.9	0.091	3.146	-0.247	3.354	0.263	4.599	0.231	4.035
373	Lahul (North)	30.09.2006	15.12.2007	1.208	8.5	-0.240	4.638	0.162	3.707	0.290	5.938	0.240	4.914
374	Lahul (North)	16.10.2006	20.11.2007	1.096	2.9	0.070	3.105	0.402	3.246	0.408	4.492	0.372	4.099
375	Lahul (North)	16.10.2006	15.12.2007	1.164	8.6	-0.178	4.744	0.018	3.977	0.179	6.190	0.154	5.317
376	Jammu	12.10.2002	05.03.2003	0.395	2.9	0.048	3.866	-0.058	4.027	0.075	5.582	0.191	14.149
377	Jammu	12.10.2002	31.10.2003	1.052	2.9	-0.067	3.266	0.158	3.242	0.171	4.602	0.163	4.374

Appendix A: Satellite images and correlation details

No.	Geographic region	Date [yyyy-mm-dd] Scene 1	Scene 2	Time span [years]	Inci-dence angle diff. [°]	Residual offset [m] East-West Mean	SD	North-South Mean	SD	Total displacement uncertainty [m] Mean	SD	Velocity uncertainty [m/yr] Mean	SD
378	Jammu	12.10.2002	26.03.2005	2.455	0.0	-0.056	3.752	-0.019	4.006	0.059	5.489	0.024	2.236
379	Jammu	12.10.2002	13.10.2005	3.005	8.6	0.818	5.158	0.162	3.609	0.833	6.296	0.277	2.095
380	Jammu	12.10.2002	20.10.2005	3.025	0.0	-0.134	3.046	0.306	2.949	0.334	4.240	0.110	1.402
381	Jammu	05.03.2003	31.10.2003	0.658	0.0	-0.205	3.473	0.251	3.924	0.324	5.240	0.492	7.970
382	Jammu	05.03.2003	26.03.2005	2.060	2.9	0.040	2.835	-0.043	2.652	0.059	3.882	0.028	1.884
383	Jammu	05.03.2003	20.10.2005	2.630	2.9	0.035	3.536	0.267	3.757	0.270	5.159	0.103	1.962
384	Jammu	05.03.2003	07.10.2006	3.595	2.8	0.171	3.473	0.103	3.649	0.199	5.037	0.055	1.401
385	Jammu	05.03.2003	23.10.2006	3.638	2.9	0.055	3.579	0.103	3.816	0.116	5.232	0.032	1.438
386	Jammu	31.10.2003	26.03.2005	1.403	2.9	0.117	3.748	-0.123	4.007	0.170	5.486	0.121	3.911
387	Jammu	31.10.2003	20.10.2005	1.973	2.9	0.318	2.948	0.052	2.858	0.323	4.106	0.164	2.082
388	Jammu	31.10.2003	07.10.2006	2.937	2.9	0.088	2.971	-0.084	3.030	0.121	4.244	0.041	1.445
389	Jammu	31.10.2003	23.10.2006	2.981	2.9	0.152	2.841	-0.104	2.741	0.185	3.947	0.062	1.324
390	Jammu	26.03.2005	20.10.2005	0.570	0.0	-0.038	3.453	0.290	3.811	0.292	5.142	0.513	9.024
391	Jammu	26.03.2005	07.10.2006	1.534	0.0	0.018	3.361	0.184	3.607	0.185	4.930	0.121	3.213
392	Jammu	26.03.2005	23.10.2006	1.578	0.0	0.056	3.592	0.155	3.771	0.165	5.208	0.104	3.300
393	Jammu	26.03.2005	22.12.2007	2.742	11.4	-0.160	4.449	0.108	3.595	0.193	5.720	0.070	2.086
394	Jammu	13.10.2005	07.10.2006	0.984	8.6	-0.228	4.938	-0.173	3.665	0.286	6.150	0.291	6.253
395	Jammu	13.10.2005	23.10.2006	1.027	8.6	-0.241	4.819	0.125	3.351	0.272	5.870	0.265	5.713
396	Jammu	20.10.2005	07.10.2006	0.964	0.0	-0.066	2.693	-0.031	2.692	0.073	3.808	0.076	3.949
397	Jammu	20.10.2005	23.10.2006	1.008	0.0	0.104	2.726	0.215	2.835	0.239	3.933	0.237	3.901
398	Jammu	20.10.2005	22.12.2007	2.173	11.4	-0.358	4.476	0.232	3.659	0.427	5.782	0.196	2.661
399	Jammu	07.10.2006	22.12.2007	1.208	11.4	-0.240	4.345	0.115	3.488	0.266	5.572	0.220	4.612
400	Jammu	23.10.2006	22.12.2007	1.164	11.4	-0.394	4.551	0.234	3.773	0.459	5.912	0.394	5.077
401	Karakorum (Baltoro)	11.09.2000	29.08.2001	0.964	0.0	0.069	3.535	-0.002	3.451	0.069	4.941	0.072	5.123
402	Karakorum (Baltoro)	11.09.2000	03.10.2002	2.060	0.0	-0.169	3.657	0.140	3.011	0.220	4.737	0.107	2.299
403	Karakorum (Baltoro)	11.09.2000	20.09.2003	3.025	2.9	-0.495	3.881	0.079	2.928	0.501	4.862	0.166	1.607
404	Karakorum (Baltoro)	11.09.2000	06.10.2003	3.068	0.0	-0.921	4.077	0.545	3.380	1.070	5.296	0.349	1.726
405	Karakorum (Baltoro)	11.09.2000	22.10.2003	3.112	0.0	-0.186	4.128	0.096	3.203	0.210	5.225	0.067	1.679
406	Karakorum (Baltoro)	11.09.2000	15.09.2004	4.014	11.5	0.211	5.558	-0.019	4.075	0.212	6.892	0.053	1.717
407	Karakorum (Baltoro)	29.08.2001	03.10.2002	1.096	0.0	-0.158	3.984	-0.227	3.507	0.277	5.307	0.252	4.843
408	Karakorum (Baltoro)	29.08.2001	20.09.2003	2.060	2.9	-0.542	3.889	-0.181	3.102	0.572	4.975	0.278	2.415
409	Karakorum (Baltoro)	29.08.2001	06.10.2003	2.104	0.0	-0.188	4.013	0.007	3.506	0.189	5.329	0.090	2.533
410	Karakorum (Baltoro)	29.08.2001	22.10.2003	2.148	0.0	-0.063	4.109	-0.218	3.534	0.227	5.420	0.105	2.523
411	Karakorum (Baltoro)	03.10.2002	20.09.2003	0.964	2.9	-0.049	3.306	-0.093	3.170	0.105	4.580	0.109	4.749
412	Karakorum (Baltoro)	03.10.2002	06.10.2003	1.008	0.0	-0.001	2.865	0.280	2.947	0.280	4.110	0.278	4.077
413	Karakorum (Baltoro)	03.10.2002	22.10.2003	1.052	0.0	-0.223	3.095	0.031	2.947	0.225	4.274	0.214	4.062
414	Karakorum (Baltoro)	03.10.2002	30.03.2004	1.490	0.0	0.116	3.618	-0.458	3.558	0.473	5.075	0.317	3.405
415	Karakorum (Baltoro)	20.09.2003	06.10.2003	0.044	2.9	0.191	2.850	0.193	2.749	0.271	3.959	6.187	90.321
416	Karakorum (Baltoro)	20.09.2003	22.10.2003	0.088	2.9	0.063	3.181	0.271	3.042	0.278	4.401	3.175	50.203
417	Karakorum (Baltoro)	20.09.2003	30.03.2004	0.526	2.9	0.076	3.406	-0.374	3.411	0.382	4.820	0.726	9.164
418	Karakorum (Baltoro)	20.09.2003	14.08.2004	0.901	8.5	-0.042	5.278	-0.084	3.775	0.094	6.489	0.104	7.199
419	Karakorum (Baltoro)	20.09.2003	21.06.2005	1.753	2.9	0.207	3.977	-0.006	4.369	0.207	5.907	0.118	3.369
420	Karakorum (Baltoro)	20.09.2003	25.09.2005	2.016	2.9	0.230	3.859	-0.097	3.622	0.250	5.293	0.124	2.625
421	Karakorum (Baltoro)	20.09.2003	26.07.2006	2.849	0.0	-0.013	3.086	0.177	2.964	0.177	4.279	0.062	1.502
422	Karakorum (Baltoro)	06.10.2003	30.03.2004	0.482	0.0	0.050	3.223	-0.359	3.262	0.362	4.586	0.751	9.511
423	Karakorum (Baltoro)	06.10.2003	14.08.2004	0.858	11.5	0.268	5.530	-0.398	4.246	0.479	6.972	0.559	8.130
424	Karakorum (Baltoro)	06.10.2003	22.02.2005	1.384	8.6	0.598	5.676	0.019	4.009	0.599	6.949	0.433	5.023
425	Karakorum (Baltoro)	06.10.2003	21.06.2005	1.710	0.0	0.107	3.932	-0.060	3.888	0.123	5.530	0.072	3.235
426	Karakorum (Baltoro)	06.10.2003	25.09.2005	1.973	0.0	0.094	3.690	-0.207	3.603	0.227	5.157	0.115	2.615
427	Karakorum (Baltoro)	22.10.2003	30.03.2004	0.438	0.0	0.202	3.372	-0.425	3.408	0.470	4.794	1.073	10.937
428	Karakorum (Baltoro)	22.10.2003	21.06.2005	1.666	0.0	0.093	3.987	-0.090	4.019	0.129	5.661	0.078	3.399
429	Karakorum (Baltoro)	22.10.2003	25.09.2005	1.929	0.0	0.271	3.770	-0.111	3.747	0.292	5.315	0.152	2.756
430	Karakorum (Baltoro)	30.03.2004	22.02.2005	0.901	8.6	-0.315	5.562	-0.003	3.928	0.315	6.809	0.350	7.554
431	Karakorum (Baltoro)	30.03.2004	25.09.2005	1.490	0.0	-0.037	3.956	-0.050	3.893	0.063	5.550	0.042	3.724
432	Karakorum (Baltoro)	30.03.2004	26.07.2006	2.323	2.9	-0.046	3.668	0.101	3.498	0.111	5.069	0.048	2.182
433	Karakorum (Baltoro)	14.08.2004	15.09.2004	0.088	0.0	-0.021	2.883	-0.196	2.854	0.197	4.056	2.249	46.266
434	Karakorum (Baltoro)	14.08.2004	22.02.2005	0.526	2.9	0.170	4.226	-0.218	3.836	0.277	5.707	0.526	10.850
435	Karakorum (Baltoro)	14.08.2004	30.06.2005	0.877	0.0	-0.165	4.690	0.036	3.884	0.168	6.089	0.192	6.945
436	Karakorum (Baltoro)	15.09.2004	22.02.2005	0.438	2.9	0.315	4.316	-0.024	4.119	0.316	5.966	0.721	13.610

126

Appendix A: Satellite images and correlation details

No.	Geographic region	Date [yyyy-mm-dd] Scene 1	Scene 2	Time span [years]	Inci-dence angle diff. [°]	Residual offset [m] East-West Mean	SD	North-South Mean	SD	Total displacement uncertainty [m] Mean	SD	Velocity uncertainty [m/yr] Mean	SD
437	Karakorum (Baltoro)	15.09.2004	25.09.2005	1.027	11.5	0.235	5.556	-0.059	4.372	0.242	7.070	0.236	6.881
438	Karakorum (Baltoro)	25.09.2005	26.07.2006	0.833	2.9	-0.312	4.089	0.101	3.899	0.328	5.650	0.393	6.783
439	Karakorum (Biafo Gyang)	11.09.2000	18.05.2001	0.682	14.3	-0.490	4.349	-0.043	3.485	0.492	5.573	0.722	8.169
440	Karakorum (Biafo Gyang)	11.09.2000	29.08.2001	0.964	0.0	-0.278	3.302	0.040	2.989	0.281	4.454	0.291	4.618
441	Karakorum (Biafo Gyang)	11.09.2000	20.09.2003	3.025	2.9	0.047	3.581	0.055	2.765	0.072	4.524	0.024	1.496
442	Karakorum (Biafo Gyang)	06.03.2001	18.05.2001	0.200	11.5	-0.120	4.513	0.019	3.928	0.122	5.983	0.609	29.915
443	Karakorum (Biafo Gyang)	06.03.2001	31.05.2003	2.236	0.1	-0.050	3.579	-0.077	3.416	0.092	4.948	0.041	2.213
444	Karakorum (Biafo Gyang)	06.03.2001	02.11.2004	3.663	11.4	-0.225	4.502	0.153	3.754	0.272	5.862	0.074	1.600
445	Karakorum (Biafo Gyang)	18.05.2001	31.05.2003	2.036	11.4	0.091	4.186	-0.066	3.263	0.113	5.307	0.055	2.607
446	Karakorum (Biafo Gyang)	18.05.2001	20.09.2003	2.342	11.4	0.346	4.187	0.477	3.692	0.590	5.582	0.252	2.383
447	Karakorum (Biafo Gyang)	18.05.2001	02.11.2004	3.463	0.1	-0.120	3.363	0.290	3.603	0.314	4.928	0.091	1.423
448	Karakorum (Biafo Gyang)	18.05.2001	16.05.2006	4.997	0.0	0.060	2.991	-0.080	2.790	0.100	4.090	0.020	0.818
449	Karakorum (Biafo Gyang)	29.08.2001	20.09.2003	2.060	2.9	0.087	3.645	0.112	2.878	0.142	4.644	0.069	2.254
450	Karakorum (Biafo Gyang)	31.05.2003	16.05.2006	2.962	11.4	-0.135	4.112	0.102	3.212	0.169	5.218	0.057	1.762
451	Karakorum (Biafo Gyang)	31.05.2003	24.06.2006	3.068	0.1	0.054	3.339	0.093	3.198	0.108	4.624	0.035	1.507
452	Karakorum (Biafo Gyang)	31.05.2003	26.07.2006	3.156	0.0	0.129	3.720	0.096	3.443	0.160	5.069	0.051	1.606
453	Karakorum (Biafo Gyang)	20.09.2003	02.11.2004	1.121	11.3	-0.374	4.310	0.169	3.720	0.411	5.694	0.367	5.081
454	Karakorum (Biafo Gyang)	20.09.2003	02.04.2005	1.534	0.1	0.040	3.438	-0.214	3.398	0.217	4.834	0.142	3.151
455	Karakorum (Biafo Gyang)	20.09.2003	16.05.2006	2.655	11.4	0.049	4.456	-0.483	4.181	0.486	6.110	0.183	2.302
456	Karakorum (Biafo Gyang)	20.09.2003	24.06.2006	2.762	0.1	0.081	3.389	-0.115	3.441	0.140	4.830	0.051	1.749
457	Karakorum (Biafo Gyang)	20.09.2003	26.07.2006	2.849	0.0	-0.113	3.081	0.062	3.013	0.128	4.310	0.045	1.512
458	Karakorum (Biafo Gyang)	02.11.2004	05.11.2005	1.008	2.9	-0.268	2.872	0.262	2.831	0.375	4.033	0.372	4.000
459	Karakorum (Biafo Gyang)	02.11.2004	13.03.2006	1.359	0.1	0.185	3.600	-0.224	3.719	0.291	5.176	0.214	3.809
460	Karakorum (Biafo Gyang)	02.11.2004	29.03.2006	1.403	0.1	0.233	3.457	-0.281	3.622	0.365	5.007	0.260	3.570
461	Karakorum (Biafo Gyang)	02.11.2004	05.04.2006	1.422	8.5	-0.117	4.637	-0.328	3.878	0.348	6.045	0.245	4.251
462	Karakorum (Biafo Gyang)	02.11.2004	16.05.2006	1.534	0.1	0.122	3.580	-0.171	3.821	0.210	5.236	0.137	3.413
463	Karakorum (Biafo Gyang)	02.11.2004	17.06.2006	1.622	2.9	0.181	3.671	-0.132	3.892	0.224	5.350	0.138	3.299
464	Karakorum (Biafo Gyang)	02.11.2004	24.06.2006	1.641	11.4	0.160	4.522	-0.393	4.165	0.424	6.148	0.258	3.746
465	Karakorum (Biafo Gyang)	02.11.2004	26.07.2006	1.729	11.4	0.069	4.625	-0.261	4.100	0.270	6.181	0.156	3.575
466	Karakorum (Biafo Gyang)	02.11.2004	05.09.2006	1.841	0.0	0.112	3.577	-0.110	3.535	0.157	5.029	0.085	2.732
467	Karakorum (Biafo Gyang)	02.11.2004	28.09.2006	1.904	8.5	0.179	4.613	-0.307	3.927	0.355	6.058	0.187	3.182
468	Karakorum (Biafo Gyang)	02.11.2004	08.11.2006	2.016	0.1	-0.109	3.020	0.264	3.093	0.286	4.323	0.142	2.144
469	Karakorum (Biafo Gyang)	02.11.2004	10.12.2006	2.104	0.1	0.052	3.832	-0.074	3.848	0.090	5.431	0.043	2.581
470	Karakorum (Biafo Gyang)	02.11.2004	11.01.2007	2.192	0.1	-0.017	3.526	-0.050	3.602	0.053	5.041	0.024	2.300
471	Karakorum (Biafo Gyang)	02.11.2004	27.01.2007	2.236	0.0	0.065	3.343	-0.092	3.378	0.112	4.753	0.050	2.126
472	Karakorum (Biafo Gyang)	02.11.2004	07.03.2007	2.342	11.4	0.077	4.425	-0.305	3.744	0.315	5.796	0.134	2.474
473	Karakorum (Biafo Gyang)	02.11.2004	23.03.2007	2.386	11.3	0.151	4.537	-0.264	3.914	0.304	5.992	0.128	2.511
474	Karakorum (Biafo Gyang)	02.11.2004	27.11.2007	3.068	2.9	-0.061	3.258	0.259	3.172	0.266	4.547	0.087	1.482
475	Karakorum (Biafo Gyang)	02.04.2005	13.03.2006	0.945	11.5	-0.156	4.341	0.232	3.481	0.279	5.564	0.296	5.886
476	Karakorum (Biafo Gyang)	02.04.2005	29.03.2006	0.989	11.5	-0.054	4.085	0.291	3.143	0.296	5.154	0.300	5.211
477	Karakorum (Biafo Gyang)	02.04.2005	05.04.2006	1.008	2.9	-0.016	2.773	0.151	2.564	0.151	3.777	0.150	3.746
478	Karakorum (Biafo Gyang)	02.04.2005	16.05.2006	1.121	11.5	0.285	4.694	-0.127	4.039	0.312	6.193	0.279	5.526
479	Karakorum (Biafo Gyang)	02.04.2005	24.06.2006	1.227	0.0	-0.083	3.711	-0.030	3.716	0.089	5.251	0.072	4.278
480	Karakorum (Biafo Gyang)	02.04.2005	28.09.2006	1.490	2.9	-0.224	3.801	0.391	3.677	0.451	5.288	0.302	3.548
481	Karakorum (Biafo Gyang)	02.04.2005	02.01.2007	1.753	0.1	-0.135	3.728	-0.090	3.595	0.163	5.179	0.093	2.954
482	Karakorum (Biafo Gyang)	02.04.2005	07.03.2007	1.929	0.0	-0.069	2.972	0.159	2.930	0.173	4.174	0.090	2.164
483	Karakorum (Biafo Gyang)	02.04.2005	23.03.2007	1.973	0.1	-0.079	2.854	0.130	2.832	0.152	4.021	0.077	2.038
484	Karakorum (Biafo Gyang)	05.11.2005	13.03.2006	0.351	2.9	0.317	3.857	0.055	3.733	0.322	5.368	0.918	15.308
485	Karakorum (Biafo Gyang)	05.11.2005	16.05.2006	0.526	2.9	0.189	3.765	-0.044	3.836	0.194	5.375	0.368	10.218
486	Karakorum (Biafo Gyang)	05.11.2005	17.06.2006	0.614	0.0	0.185	3.829	-0.173	3.990	0.253	5.530	0.413	9.011
487	Karakorum (Biafo Gyang)	05.11.2005	28.09.2006	0.896	11.4	0.098	4.784	-0.235	3.802	0.255	6.111	0.284	6.821
488	Karakorum (Biafo Gyang)	05.11.2005	30.10.2006	0.984	8.6	-0.393	4.765	-0.179	3.771	0.432	6.077	0.439	6.178
489	Karakorum (Biafo Gyang)	05.11.2005	08.11.2006	1.008	2.9	-0.058	2.918	0.012	3.364	0.059	4.453	0.059	4.417
490	Karakorum (Biafo Gyang)	05.11.2005	11.01.2007	1.184	2.9	-0.102	3.843	-0.044	3.555	0.111	5.235	0.094	4.423
491	Karakorum (Biafo Gyang)	05.11.2005	27.01.2007	1.227	2.9	-0.030	3.467	-0.054	3.431	0.062	4.878	0.050	3.974
492	Karakorum (Biafo Gyang)	05.11.2005	07.03.2007	1.334	14.3	-0.364	4.583	-0.259	3.540	0.447	5.791	0.335	4.340
493	Karakorum (Biafo Gyang)	05.11.2005	27.11.2007	2.060	0.0	-0.155	3.349	0.071	3.151	0.170	4.598	0.083	2.232
494	Karakorum (Biafo Gyang)	13.03.2006	07.03.2007	0.984	11.5	-0.006	4.272	0.109	3.589	0.109	5.579	0.111	5.672
495	Karakorum (Biafo Gyang)	13.03.2006	23.03.2007	1.027	11.4	0.111	4.198	-0.249	3.506	0.272	5.469	0.265	5.324

Appendix A: Satellite images and correlation details

No.	Geographic region	Date [yyyy-mm-dd]		Time span [years]	Inci-dence angle diff. [°]	Residual offset [m]				Total displacement uncertainty [m]		Velocity uncertainty [m/yr]	
						East-West		North-South					
		Scene 1	Scene 2			Mean	SD	Mean	SD	Mean	SD	Mean	SD
496	Karakorum (Biafo Gyang)	13.03.2006	27.11.2007	1.710	2.9	-0.052	3.917	0.129	4.027	0.140	5.618	0.082	3.286
497	Karakorum (Biafo Gyang)	29.03.2006	27.01.2007	0.833	0.1	-0.035	3.301	-0.083	3.488	0.090	4.802	0.108	5.765
498	Karakorum (Biafo Gyang)	29.03.2006	07.03.2007	0.940	11.5	0.039	4.180	0.080	3.496	0.089	5.449	0.095	5.799
499	Karakorum (Biafo Gyang)	29.03.2006	23.03.2007	0.984	11.4	0.054	4.429	0.003	3.469	0.055	5.626	0.055	5.720
500	Karakorum (Biafo Gyang)	29.03.2006	27.11.2007	1.666	2.9	-0.101	3.870	0.111	3.845	0.150	5.456	0.090	3.275
501	Karakorum (Biafo Gyang)	05.04.2006	07.03.2007	0.921	2.9	0.001	3.064	0.167	2.953	0.167	4.255	0.182	4.622
502	Karakorum (Biafo Gyang)	05.04.2006	23.03.2007	0.964	2.8	0.071	3.126	0.181	3.055	0.195	4.371	0.202	4.532
503	Karakorum (Biafo Gyang)	05.04.2006	27.11.2007	1.647	11.4	-0.248	4.687	0.165	4.142	0.298	6.255	0.181	3.799
504	Karakorum (Biafo Gyang)	16.05.2006	17.06.2006	0.088	2.9	0.135	2.757	-0.147	2.659	0.199	3.830	2.274	43.685
505	Karakorum (Biafo Gyang)	16.05.2006	08.11.2006	0.482	0.0	0.104	3.780	0.452	4.203	0.464	5.652	0.962	11.722
506	Karakorum (Biafo Gyang)	16.05.2006	27.01.2007	0.701	0.1	0.133	3.865	0.087	4.088	0.159	5.626	0.227	8.021
507	Karakorum (Biafo Gyang)	16.05.2006	27.06.2007	1.115	11.5	-0.129	4.457	0.159	3.728	0.205	5.811	0.184	5.211
508	Karakorum (Biafo Gyang)	16.05.2006	27.11.2007	1.534	2.9	-0.087	3.750	0.215	4.036	0.232	5.509	0.151	3.591
509	Karakorum (Biafo Gyang)	17.06.2006	08.11.2006	0.395	2.8	-0.144	3.878	0.037	4.178	0.148	5.700	0.376	14.449
510	Karakorum (Biafo Gyang)	17.06.2006	27.01.2007	0.614	2.9	0.042	4.129	-0.221	4.484	0.225	6.096	0.366	9.933
511	Karakorum (Biafo Gyang)	17.06.2006	11.06.2007	0.984	14.3	0.071	4.171	0.137	3.352	0.154	5.351	0.157	5.441
512	Karakorum (Biafo Gyang)	17.06.2006	27.06.2007	1.027	14.3	-0.078	4.304	0.211	3.523	0.225	5.562	0.219	5.414
513	Karakorum (Biafo Gyang)	17.06.2006	27.11.2007	1.447	0.0	-0.043	3.818	-0.067	4.157	0.080	5.644	0.055	3.902
514	Karakorum (Biafo Gyang)	24.06.2006	11.06.2007	0.964	0.0	0.131	2.970	0.106	2.714	0.168	4.024	0.175	4.172
515	Karakorum (Biafo Gyang)	24.06.2006	27.06.2007	1.008	0.0	-0.058	2.987	0.102	2.847	0.117	4.127	0.116	4.093
516	Karakorum (Biafo Gyang)	26.07.2006	27.06.2007	0.921	0.0	0.040	2.748	0.104	2.717	0.111	3.864	0.121	4.197
517	Karakorum (Biafo Gyang)	12.09.2006	27.11.2007	1.208	8.6	-0.246	4.843	-0.028	4.410	0.248	6.550	0.205	5.421
518	Karakorum (Biafo Gyang)	28.09.2006	27.11.2007	1.164	11.4	-0.320	4.704	0.065	3.954	0.326	6.146	0.280	5.278
519	Karakorum (Biafo Gyang)	30.10.2006	27.11.2007	1.077	8.6	0.012	4.635	0.042	3.983	0.044	6.111	0.041	5.675
520	Karakorum (Biafo Gyang)	08.11.2006	27.01.2007	0.219	0.1	0.479	3.557	-0.150	3.665	0.502	5.107	2.291	23.302
521	Karakorum (Biafo Gyang)	08.11.2006	27.11.2007	1.052	2.8	-0.095	3.046	0.269	3.008	0.285	4.281	0.271	4.069
522	Karakorum (Biafo Gyang)	11.01.2007	27.11.2007	0.877	2.9	0.270	3.987	-0.034	3.808	0.272	5.513	0.310	6.289
523	Karakorum (Biafo Gyang)	27.01.2007	27.11.2007	0.833	2.9	0.065	3.651	0.352	3.670	0.358	5.177	0.430	6.216
524	Karakorumk (Hispar)	30.09.2001	29.10.2003	2.079	8.6	0.052	4.378	0.057	3.613	0.077	5.676	0.037	2.730
525	Karakorumk (Hispar)	29.10.2003	13.09.2004	0.877	0.0	-0.234	3.510	0.112	3.489	0.260	4.949	0.296	5.645
526	Karakorumk (Hispar)	29.10.2003	29.09.2004	0.921	0.0	-0.342	4.166	-0.094	3.938	0.354	5.732	0.385	6.227
527	Karakorumk (Hispar)	29.10.2003	11.03.2006	2.367	0.0	0.100	3.538	-0.184	3.509	0.209	4.983	0.088	2.105
528	Karakorumk (Hispar)	11.03.2006	12.09.2006	0.507	8.6	0.044	4.669	0.274	4.145	0.278	6.244	0.548	12.319
529	Karakorumk (Hispar)	11.03.2006	01.05.2007	1.140	0.0	-0.058	4.075	-0.026	4.346	0.063	5.958	0.056	5.227
530	Karakorumk (Hispar)	30.09.2001	29.10.2003	2.079	8.6	0.327	4.809	0.133	3.808	0.354	6.134	0.170	2.950
531	Karakorumk (Hispar)	30.09.2001	13.09.2004	2.956	8.6	0.040	4.258	-0.050	3.332	0.064	5.407	0.022	1.829
532	Karakorumk (Hispar)	30.09.2001	12.09.2006	4.953	0.0	0.038	3.206	-0.192	3.265	0.195	4.576	0.039	0.924
533	Karakorumk (Hispar)	30.09.2001	28.09.2006	4.997	2.8	0.122	2.964	-0.025	2.953	0.124	4.184	0.025	0.837
534	Karakorumk (Hispar)	30.09.2001	30.10.2006	5.085	0.0	-0.044	3.419	0.306	3.563	0.310	4.938	0.061	0.971
535	Karakorumk (Hispar)	29.10.2003	13.09.2004	0.877	0.0	0.116	3.261	-0.148	2.998	0.188	4.430	0.215	5.053
536	Karakorumk (Hispar)	13.09.2004	12.09.2006	1.997	8.6	0.262	4.257	0.004	3.101	0.262	5.267	0.131	2.637
537	Karakorumk (Hispar)	05.11.2005	05.04.2006	0.414	11.4	-0.305	5.090	-0.270	4.038	0.408	6.498	0.986	15.706
538	Karakorumk (Hispar)	05.11.2005	21.04.2006	0.458	8.6	-0.921	4.952	-0.233	4.185	0.950	6.483	2.077	14.170
539	Karakorumk (Hispar)	05.11.2005	17.06.2006	0.614	0.0	0.741	4.240	-0.509	4.232	0.898	5.990	1.464	9.761
540	Karakorumk (Hispar)	05.11.2005	12.09.2006	0.852	8.6	-0.458	5.092	-0.240	4.042	0.517	6.501	0.606	7.630
541	Karakorumk (Hispar)	05.11.2005	28.09.2006	0.896	11.4	-0.348	5.041	-0.165	3.734	0.385	6.273	0.430	7.002
542	Karakorumk (Hispar)	05.11.2005	30.10.2006	0.984	8.6	-0.631	4.930	0.010	3.471	0.631	6.029	0.642	6.130
543	Karakorumk (Hispar)	05.11.2005	27.11.2007	2.060	0.0	-0.371	4.102	0.033	3.509	0.372	5.398	0.181	2.620
544	Karakorumk (Hispar)	05.04.2006	21.04.2006	0.044	2.9	-0.078	2.299	0.139	2.300	0.159	3.252	3.637	74.184
545	Karakorumk (Hispar)	05.04.2006	17.06.2006	0.200	11.4	0.079	4.748	-0.178	3.997	0.195	6.206	0.975	31.031
546	Karakorumk (Hispar)	05.04.2006	12.09.2006	0.438	2.9	-0.125	3.497	0.304	3.656	0.329	5.059	0.750	11.542
547	Karakorumk (Hispar)	05.04.2006	28.09.2006	0.482	0.0	-0.149	3.357	0.121	3.728	0.192	5.016	0.398	10.403
548	Karakorumk (Hispar)	05.04.2006	30.10.2006	0.570	2.9	-0.111	3.500	0.032	3.810	0.116	5.174	0.203	9.079
549	Karakorumk (Hispar)	21.04.2006	12.09.2006	0.395	0.0	-0.149	3.693	0.157	3.877	0.216	5.355	0.549	13.573
550	Karakorumk (Hispar)	21.04.2006	28.09.2006	0.438	2.9	-0.110	3.348	0.179	3.621	0.210	4.931	0.479	11.250
551	Karakorumk (Hispar)	21.04.2006	30.10.2006	0.526	0.0	-0.169	3.628	0.010	3.885	0.169	5.316	0.321	10.105
552	Karakorumk (Hispar)	17.06.2006	27.11.2007	1.447	0.0	-0.205	4.416	-0.062	4.123	0.215	6.041	0.148	4.176
553	Karakorumk (Hispar)	12.09.2006	28.09.2006	0.044	2.9	0.062	2.740	0.097	3.080	0.115	4.122	2.618	94.039
554	Karakorumk (Hispar)	12.09.2006	30.10.2006	0.132	0.0	-0.274	3.656	0.104	3.849	0.293	5.308	2.231	40.364

Appendix A: Satellite images and correlation details

No.	Geographic region	Date [yyyy-mm-dd] Scene 1	Scene 2	Time span [years]	Inci-dence angle diff. [°]	Residual offset [m] East-West Mean	SD	North-South Mean	SD	Total displacement uncertainty [m] Mean	SD	Velocity uncertainty [m/yr] Mean	SD
555	Karakorumk (Hispar)	12.09.2006	27.11.2007	1.208	8.6	-1.842	5.252	-0.440	4.326	1.894	6.804	1.567	5.632
556	Karakorumk (Hispar)	28.09.2006	30.10.2006	0.088	2.9	-0.157	2.989	0.237	3.223	0.284	4.396	3.241	50.141
557	Karakorumk (Hispar)	28.09.2006	27.11.2007	1.164	11.4	0.028	5.029	-0.023	3.972	0.036	6.408	0.031	5.504
558	Karakorumk (Hispar)	30.10.2006	27.11.2007	1.077	8.6	0.001	5.104	-0.086	3.949	0.086	6.453	0.080	5.993
559	Chitral (North)	31.08.2000	04.07.2002	1.841	0.0	0.313	3.084	-0.518	3.208	0.605	4.450	0.329	2.417
560	Chitral (North)	31.08.2000	22.09.2002	2.060	0.0	-0.029	2.253	0.096	2.065	0.100	3.056	0.049	1.484
561	Chitral (North)	14.10.2001	04.07.2002	0.721	9.0	0.036	3.771	0.027	3.748	0.045	5.317	0.062	7.378
562	Chitral (North)	14.10.2001	22.09.2002	0.940	9.0	-0.094	3.196	0.003	2.404	0.094	4.000	0.100	4.256
563	Chitral (North)	04.07.2002	16.08.2006	4.121	0.0	-0.209	3.216	0.274	3.112	0.344	4.475	0.084	1.086
564	Chitral (North)	04.07.2002	01.09.2006	4.164	0.0	-0.268	3.543	0.332	3.513	0.427	4.990	0.103	1.198
565	Chitral (North)	22.09.2002	16.08.2006	3.901	0.0	0.201	2.614	-0.030	2.613	0.203	3.696	0.052	0.947
566	Chitral (North)	22.09.2002	01.09.2006	3.945	0.0	0.093	2.970	0.051	2.889	0.106	4.144	0.027	1.050
567	Chitral (North)	16.08.2006	19.08.2007	1.008	0.0	-0.007	2.361	0.031	2.200	0.032	3.227	0.031	3.201
568	Chitral (North)	01.09.2006	27.07.2007	0.901	8.6	0.030	3.586	-0.041	3.107	0.051	4.744	0.056	5.264
569	Chitral (North)	01.09.2006	19.08.2007	0.964	0.0	-0.025	2.875	0.008	2.725	0.026	3.962	0.027	4.108
570	Chitral (South)	31.08.2000	22.09.2002	2.060	0.0	0.002	2.285	0.020	2.076	0.021	3.087	0.010	1.498
571	Chitral (South)	24.06.2001	28.09.2001	0.263	2.0	-0.058	3.042	0.147	3.232	0.158	4.438	0.601	16.875
572	Chitral (South)	24.06.2001	14.10.2001	0.307	2.4	-0.148	3.201	0.099	3.452	0.178	4.708	0.581	15.342
573	Chitral (South)	24.06.2001	22.09.2002	1.247	11.4	-0.074	3.446	0.151	3.055	0.168	4.606	0.135	3.695
574	Chitral (South)	24.06.2001	14.06.2003	1.973	2.8	0.208	3.042	-0.208	2.877	0.294	4.187	0.149	2.122
575	Chitral (South)	24.06.2001	20.10.2003	2.323	2.8	0.016	3.065	0.011	3.420	0.020	4.593	0.009	1.977
576	Chitral (South)	24.06.2001	16.06.2004	2.981	2.9	0.188	2.600	-0.141	2.614	0.235	3.687	0.079	1.237
577	Chitral (South)	24.06.2001	20.09.2004	3.244	0.0	-0.181	3.110	0.247	3.313	0.306	4.544	0.094	1.401
578	Chitral (South)	28.09.2001	14.06.2003	1.710	0.9	0.196	3.150	-0.220	3.620	0.295	4.799	0.172	2.807
579	Chitral (South)	28.09.2001	20.10.2003	2.060	0.8	-0.002	2.669	0.134	2.558	0.134	3.697	0.065	1.795
580	Chitral (South)	28.09.2001	16.06.2004	2.718	0.9	0.078	3.139	-0.061	3.612	0.099	4.786	0.036	1.761
581	Chitral (South)	28.09.2001	20.09.2004	2.981	2.0	-0.069	2.878	-0.079	2.925	0.105	4.104	0.035	1.377
582	Chitral (South)	14.10.2001	14.06.2003	1.666	0.5	0.156	3.457	-0.497	4.104	0.520	5.366	0.312	3.221
583	Chitral (South)	14.10.2001	20.10.2003	2.016	0.4	0.093	2.710	0.089	2.582	0.129	3.743	0.064	1.856
584	Chitral (South)	14.10.2001	16.06.2004	2.674	0.5	0.202	3.385	-0.311	3.900	0.371	5.164	0.139	1.931
585	Chitral (South)	14.10.2001	20.09.2004	2.937	2.4	0.049	2.693	-0.042	2.674	0.064	3.795	0.022	1.292
586	Chitral (South)	22.09.2002	20.09.2004	1.997	11.5	0.050	3.356	0.000	2.507	0.050	4.189	0.025	2.097
587	Chitral (South)	22.09.2002	19.08.2007	4.910	0.0	0.086	2.821	-0.084	2.647	0.121	3.868	0.025	0.788
588	Chitral (South)	08.10.2002	19.08.2007	4.866	2.8	0.116	3.221	-0.057	3.070	0.129	4.450	0.027	0.914
589	Chitral (South)	14.06.2003	15.05.2004	0.921	0.0	0.061	2.412	0.000	2.408	0.061	3.408	0.066	3.703
590	Chitral (South)	14.06.2003	16.06.2004	1.008	0.0	-0.044	2.565	0.018	2.434	0.047	3.536	0.047	3.507
591	Chitral (South)	14.06.2003	27.07.2007	4.121	0.0	-0.214	2.880	0.279	2.936	0.352	4.113	0.085	0.998
592	Chitral (South)	20.10.2003	15.05.2004	0.570	0.0	0.092	3.162	-0.133	3.581	0.162	4.778	0.284	8.384
593	Chitral (South)	20.10.2003	16.06.2004	0.658	0.0	0.041	3.323	-0.104	3.838	0.112	5.077	0.170	7.721
594	Chitral (South)	20.10.2003	20.09.2004	0.921	2.9	-0.027	3.257	0.043	3.233	0.051	4.589	0.056	4.985
595	Chitral (South)	16.06.2004	20.09.2004	0.263	2.9	-0.257	3.447	-0.130	4.076	0.288	5.338	1.095	20.296
596	Chitral (South)	16.06.2004	27.07.2007	3.112	0.0	-0.135	2.723	0.146	2.736	0.199	3.861	0.064	1.240
597	Chitral (South)	20.09.2004	16.08.2006	1.904	11.5	-0.022	3.570	0.041	2.877	0.047	4.585	0.025	2.408
598	Chitral (South)	20.09.2004	27.07.2007	2.849	2.9	0.120	2.950	-0.087	3.220	0.149	4.367	0.052	1.533
599	Chitral (South)	16.08.2006	15.05.2007	0.745	0.0	0.361	3.025	-0.187	2.904	0.407	4.193	0.546	5.627
600	Chitral (South)	16.08.2006	19.08.2007	1.008	0.0	0.032	2.774	-0.020	2.562	0.038	3.776	0.038	3.746
601	West Kunlun Shan	10.03.2001	10.10.2003	2.586	0.0	0.108	3.382	0.059	3.217	0.123	4.668	0.047	1.805
602	West Kunlun Shan	26.03.2001	16.02.2002	0.896	8.6	-0.120	3.832	0.093	3.447	0.152	5.154	0.170	5.753
603	West Kunlun Shan	26.03.2001	13.03.2002	0.964	0.0	-0.014	3.689	-0.051	3.752	0.053	5.262	0.055	5.457
604	West Kunlun Shan	26.03.2001	18.03.2004	2.981	0.0	0.015	3.274	-0.013	3.264	0.020	4.623	0.007	1.551
605	West Kunlun Shan	16.02.2002	14.10.2002	0.658	2.9	0.133	3.481	0.339	3.488	0.364	4.928	0.554	7.495
606	West Kunlun Shan	16.02.2002	08.04.2003	1.140	0.0	0.238	3.169	0.015	3.211	0.239	4.511	0.210	3.958
607	West Kunlun Shan	16.02.2002	06.12.2004	2.805	0.0	-0.012	3.308	0.261	3.355	0.261	4.711	0.093	1.679
608	West Kunlun Shan	13.03.2002	18.03.2004	2.016	0.0	0.005	3.796	0.139	4.003	0.139	5.517	0.069	2.736
609	West Kunlun Shan	13.03.2002	16.01.2005	2.849	0.0	-0.068	3.348	0.127	3.656	0.144	4.958	0.051	1.740
610	West Kunlun Shan	13.03.2002	01.02.2005	2.893	0.0	0.046	3.202	0.006	3.382	0.046	4.657	0.016	1.610
611	West Kunlun Shan	14.10.2002	06.12.2004	2.148	2.9	0.066	3.613	0.298	3.565	0.305	5.076	0.142	2.363
612	West Kunlun Shan	14.10.2002	12.03.2005	2.411	2.9	-0.120	3.344	-0.160	3.455	0.200	4.808	0.083	1.994
613	West Kunlun Shan	14.10.2002	06.10.2005	2.981	2.9	0.025	3.393	0.126	3.508	0.129	4.881	0.043	1.637

Appendix A: Satellite images and correlation details

No.	Geographic region	Date [yyyy-mm-dd] Scene 1	Scene 2	Time span [years]	Incidence angle diff. [°]	Residual offset [m] East-West Mean	SD	North-South Mean	SD	Total displacement uncertainty [m] Mean	SD	Velocity uncertainty [m/yr] Mean	SD
614	West Kunlun Shan	08.04.2003	06.12.2004	1.666	0.0	-0.111	3.674	0.468	3.730	0.481	5.235	0.289	3.143
615	West Kunlun Shan	08.04.2003	12.03.2005	1.929	0.0	0.019	3.326	0.232	3.281	0.233	4.672	0.121	2.422
616	West Kunlun Shan	08.04.2003	06.10.2005	2.499	0.0	0.003	3.537	0.166	3.641	0.166	5.076	0.066	2.032
617	West Kunlun Shan	08.04.2003	11.02.2006	2.849	0.0	-0.062	3.338	0.226	3.423	0.234	4.782	0.082	1.678
618	West Kunlun Shan	10.10.2003	06.10.2005	1.992	14.3	0.115	3.274	0.087	2.969	0.145	4.419	0.073	2.219
619	West Kunlun Shan	18.03.2004	16.01.2005	0.833	0.0	-0.012	3.382	0.088	3.527	0.089	4.886	0.106	5.867
620	West Kunlun Shan	18.03.2004	01.02.2005	0.877	0.0	0.041	3.223	0.035	3.401	0.054	4.686	0.061	5.345
621	West Kunlun Shan	18.03.2004	04.02.2006	1.885	0.1	0.055	3.266	0.007	3.343	0.055	4.673	0.029	2.479
622	West Kunlun Shan	18.03.2004	12.04.2007	3.068	0.0	-0.067	2.951	0.113	2.941	0.132	4.166	0.043	1.358
623	West Kunlun Shan	06.12.2004	01.02.2005	0.156	8.6	0.005	3.371	-0.259	3.095	0.259	4.576	1.661	29.305
624	West Kunlun Shan	06.12.2004	12.03.2005	0.263	0.0	0.128	3.147	-0.299	3.290	0.325	4.552	1.236	17.309
625	West Kunlun Shan	06.12.2004	06.10.2005	0.833	0.0	0.047	3.206	-0.202	3.231	0.208	4.551	0.250	5.465
626	West Kunlun Shan	06.12.2004	04.02.2006	1.164	8.6	0.020	3.735	-0.431	3.371	0.431	5.032	0.370	4.321
627	West Kunlun Shan	06.12.2004	11.02.2006	1.184	0.0	0.019	3.209	-0.312	3.144	0.312	4.492	0.264	3.796
628	West Kunlun Shan	06.12.2004	12.04.2007	2.348	8.6	0.208	3.710	-0.317	3.446	0.379	5.063	0.161	2.157
629	West Kunlun Shan	06.12.2004	29.11.2007	2.981	0.0	0.092	3.279	-0.127	3.290	0.157	4.645	0.053	1.558
630	West Kunlun Shan	16.01.2005	12.03.2005	0.151	8.6	0.248	3.487	0.166	3.312	0.299	4.809	1.982	31.917
631	West Kunlun Shan	16.01.2005	04.02.2006	1.052	0.0	0.191	2.962	0.031	3.166	0.193	4.335	0.184	4.121
632	West Kunlun Shan	16.01.2005	11.02.2006	1.071	8.6	-0.011	3.417	0.400	3.226	0.400	4.699	0.374	4.386
633	West Kunlun Shan	16.01.2005	12.04.2007	2.236	0.0	-0.071	3.464	0.188	3.592	0.201	4.990	0.090	2.232
634	West Kunlun Shan	01.02.2005	12.03.2005	0.107	8.6	0.047	3.234	-0.086	3.108	0.098	4.485	0.920	41.974
635	West Kunlun Shan	01.02.2005	06.10.2005	0.677	8.6	0.021	3.996	0.019	3.697	0.028	5.444	0.042	8.045
636	West Kunlun Shan	01.02.2005	04.02.2006	1.008	0.0	0.180	2.708	0.050	2.826	0.186	3.915	0.185	3.883
637	West Kunlun Shan	01.02.2005	11.02.2006	1.027	8.6	-0.069	3.282	-0.157	2.961	0.171	4.421	0.166	4.303
638	West Kunlun Shan	01.02.2005	12.04.2007	2.192	0.0	0.021	3.415	0.065	3.537	0.069	4.916	0.031	2.243
639	West Kunlun Shan	01.02.2005	08.12.2007	2.849	0.0	0.039	3.603	-0.071	3.686	0.081	5.154	0.028	1.809
640	West Kunlun Shan	01.02.2005	25.01.2008	2.981	0.0	0.154	2.900	0.009	3.109	0.154	4.251	0.052	1.426
641	West Kunlun Shan	12.03.2005	06.10.2005	0.570	0.0	-0.065	3.369	-0.062	3.335	0.090	4.741	0.158	8.319
642	West Kunlun Shan	12.03.2005	04.02.2006	0.901	8.6	0.012	3.631	-0.085	3.415	0.086	4.984	0.095	5.530
643	West Kunlun Shan	12.03.2005	11.02.2006	0.921	0.0	0.054	3.163	0.178	3.178	0.186	4.484	0.202	4.871
644	West Kunlun Shan	12.03.2005	12.04.2007	2.085	8.6	0.001	3.552	0.026	3.182	0.026	4.769	0.012	2.287
645	West Kunlun Shan	12.03.2005	29.11.2007	2.718	0.0	0.043	3.333	0.151	3.438	0.157	4.788	0.058	1.762
646	West Kunlun Shan	06.10.2005	11.02.2006	0.351	0.0	0.186	3.413	-0.201	3.322	0.274	4.763	0.780	13.581
647	West Kunlun Shan	06.10.2005	12.04.2007	1.515	8.6	0.140	3.738	0.173	3.346	0.222	5.016	0.147	3.311
648	West Kunlun Shan	06.10.2005	29.11.2007	2.148	0.0	0.047	3.644	0.133	3.649	0.141	5.157	0.066	2.401
649	West Kunlun Shan	06.10.2005	08.12.2007	2.173	8.6	0.087	4.028	0.032	3.811	0.093	5.545	0.043	2.552
650	West Kunlun Shan	04.02.2006	12.04.2007	1.184	0.0	-0.041	3.397	0.185	3.412	0.189	4.815	0.160	4.068
651	West Kunlun Shan	04.02.2006	08.12.2007	1.841	0.0	-0.280	3.944	0.137	3.809	0.312	5.483	0.169	2.978
652	West Kunlun Shan	04.02.2006	25.01.2008	1.973	0.0	0.253	3.097	0.002	3.292	0.253	4.520	0.128	2.291
653	West Kunlun Shan	11.02.2006	12.04.2007	1.164	8.6	0.085	3.551	-0.196	3.295	0.213	4.844	0.183	4.160
654	West Kunlun Shan	11.02.2006	29.11.2007	1.797	0.0	0.001	3.408	0.180	3.421	0.180	4.829	0.100	2.687
655	West Kunlun Shan	11.02.2006	08.12.2007	1.822	8.6	-0.043	3.990	0.018	3.759	0.046	5.482	0.026	3.009
656	West Kunlun Shan	11.02.2006	25.01.2008	1.953	8.5	0.083	3.783	-0.224	3.723	0.239	5.308	0.122	2.717
657	West Kunlun Shan	12.04.2007	29.11.2007	0.633	8.6	-0.068	3.693	0.003	3.486	0.068	5.079	0.108	8.025

Appendix B: Supplementary material for chapter 4

B1   Additional information on glacier-surface velocity measurements

The orthorectification in COSI-Corr was done using a digital elevation model (DEM), based on Shuttle Radar Topography Mission (SRTM) data. As the original SRTM-DEM contains significant holes without data in high-relief terrain [e.g., *Kääb*, 2005], we used a SRTM-based dataset, in which larger voids have been patched with digitized contours from topographic maps [publicly available from Jonathan de Ferranti; http://www.viewfinderpanoramas.org/]. All remaining holes are filled by bilinear interpolation.

   We attempted to co-register and correlate every available image that appeared suitable for velocity measurements, but used only those images that were accurately co-registered. As a rule of thumb, we considered images well co-registered when no obvious shifts were seen in the orthorectified images and when their correlation produced the characteristic across-track stripes in the east-west displacement maps which are on the order of ~5-10 m and associated with uncorrected attitude variations of the Terra spacecraft [*Avouac et al.*, 2006; *Leprince et al.*, 2007; *Scherler et al.*, 2008]. These artifacts were removed by subtracting the average across-track displacement using the post-processing tools provided in COSI-Corr [*Leprince et al.*, 2007]. On average, we used ~20 orthorectified images per study region and ~20-30 image correlations with velocity measurements per glacier (Table A4). Most of the image pairs we used in this study are separated by one or several years. However, in cases of fast flowing glaciers, it proved useful to correlate imagery separated by a couple of months only, as rapid surface changes cause the correlation to fail when the images are separated by a year or more. In a few cases, the obtained satellite images were found to be saturated, i.e., they were shot at high gain, leading to undifferentiated snow-covered areas, especially over strongly reflecting high and flat accumulation basins. In such cases, the cross-correlation procedure failed over saturated areas but still worked over debris-covered areas or in the presence of crevasses.

B2   Additional information on the uncertainties in the remotely-sensed velocity measurements

The residual uncertainties in the displacement measurements, i.e., after correcting for distortions related to attitude variations and after filtering out miscorrelations, are additive and Gaussian distributed, with zero mean and standard deviation that depends on the resolution of the image [*Leprince et al.*, 2007]. For ASTER images the standard deviation is usually ~2-4 m [*Scherler et al.*, 2008]. This noise accounts for measurement uncertainties induced by slight physical changes of the surface in between the correlated scenes, shadowing, lack of topographic resolution, uncorrected satellite induced artifacts, aliasing, quantization, noise of the sensors, and the intrinsic correlation accuracy [*Leprince et al.*, 2007]. The absolute values of these uncertainties can vary between the correlated images, the two displacement components (east-west, north-south), and even across one displacement map. We are unaware of any systematic study that addresses variations of these uncertainties over different surface types, i.e., stable

ground versus glacier surface. Hence, we assume that the above mentioned uncertainties are unrelated to surface type.

To obtain an estimate of the residual uncertainty in the displacement measurements, we take the mean and standard deviation in the east-west and north-south displacement maps over all pixels with <10 m absolute displacement [*Scherler et al.*, 2008]. Ideally, we first exclude all glacierized, non-stable areas and then compute these metrics over all the displacement values. However, this step is very labor intensive as it requires a manually generated mask hiding all glaciers, moving shadows, or other apparently moving features for each displacement map. Therefore, the 10-m absolute displacement threshold serves as a first-order mask for miscorrelated pixels and glacierized areas. This, however, leads to unintentional inclusion of some slow-moving ice, or shifting shadows in the statistics, ultimately resulting in a non-zero mean and a higher standard deviation. Therefore, we regard our estimates as upper limits for the expected uncertainties. Reported uncertainties (Table A4) in the annual velocities are derived from dividing the absolute displacement uncertainties by the temporal separation of the correlated images in years and adding the mean and standard deviation of the total displacement.

B3 Principles of ice flow

Ice movement is driven by gravitational stresses induced by the ice column and can be due to internal deformation, basal sliding, and shearing within a basal till layer, if present [*Patterson*, 1994]. Assuming that lateral and longitudinal stresses are small compared to driving stresses, ice flow due to internal deformation, u_{def}, can be described by

$$u_{def} = \frac{2A}{(n+1)} (\rho g \sin \alpha)^n h^{n+1} \qquad \text{(eq. A1)},$$

in which A is Glen's flow law coefficient, which depends mostly on temperature, ρ is ice density, g is gravitational acceleration, h and α are the glacier's thickness and its slope respectively, and n represents a parameter usually taken as 3 [*Paterson*, 1994: p.251; *Oerlemans*, 2001]. The details of basal sliding are the subject of ongoing research, but it is commonly assumed to depend on the effective pressure, which equals the ice overburden pressure, p_i, which is proportional to ice thickness, minus the basal water pressure, P_w, according to

$$u_{sliding} = k \frac{(\rho g h \sin \alpha)^m}{(p_i - P_w)^q} \qquad \text{(eq. A2)},$$

in which $u_{sliding}$ is basal sliding velocity, k is a parameter that depends on the mechanical and thermal propoerties of the ice and the bed roughness, and m and q are flow law parameters usually taken to be 2 or 3, and 1 respectively [e.g., *Budd et al.*, 1979; *Paterson*, 1994: p.157].

B4 Cold versus temperate ice

Principally, high-altitude and relatively dry, polar-like glaciers are colder than glaciers located at lower elevations and in a more maritime climate [*Paterson*, 1994]. Many of the studied glaciers cover large altitudinal ranges, and are probably polythermal, i.e., they possess zones where the ice is cold, and zones where the ice is temperate [*Fowler and Larson*, 1978]. However, the scarcity of ground-truth data on basal glacier conditions [e.g., *Liu et al.*, 2009] hampers assessing the regional distribution of cold versus temperate ice in the study region.

In order to obtain an idea about the thermal conditions of the studied glaciers, we analyzed surface air temperatures derived from the CRU 2.0 10-arc minute gridded data set [*New et al.*, 2002]. Regional differences in air temperature are most evident during winter and on the order of ~5 K, although significant intraregional variability exists (Figure A1). During summer, the variability and regional differences are slightly smaller (~4 K) and the data within each geographic region roughly follows a lapse rate of 0.65 K/100 m, which is in the mid-range of lapse rates that have been measured in different regions of High Asia and during different seasons [e.g., *de Scally*, 1997]. The limited regional temperature differences, suggest to first order similar thermal regimes of glaciers at similar elevations, except for the West Kunlun Shan.
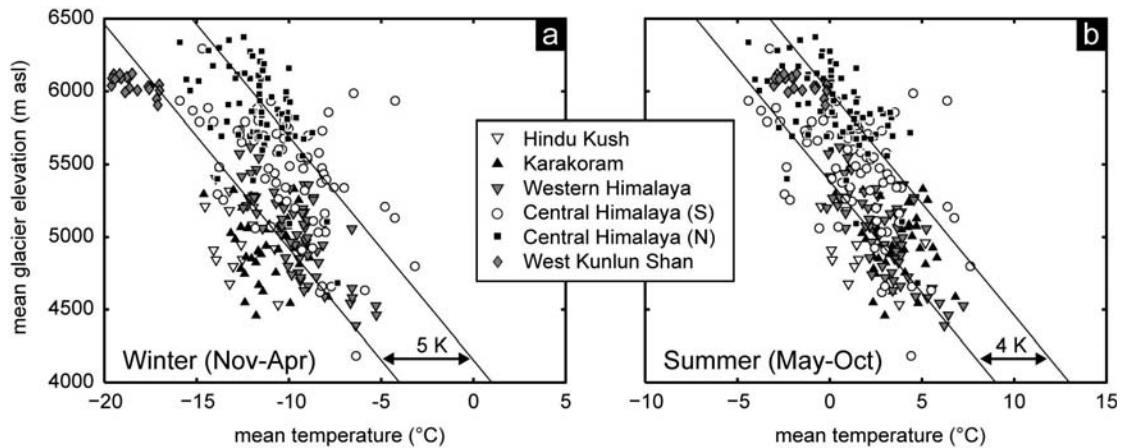
Figure A1: Surface air temperatures at the ELA of the studied glaciers during (a) winter and (b) summer. We interpolated mean seasonal temperatures at the center of a rectangle bounding the analyzed glaciers and plotted them against their mean elevation. Diagonal lines indicate atmospheric temperature profiles following a lapse rate of 0.65 K/100 m.

Most of the studied glaciers have their highest velocities at or slightly blow their mean elevation (Figure A2), where mean summer temperatures are for most regions above freezing, indicating significant melting taking place. This inference is supported by the limited avaiable mass balance studies from these regions [e.g., *Kulkarni et al.*, 1992; *Ageta et al.*, 1980; *Fujita et al.*, 1998, 2001; *Shi and Zhang*, 1984; *Wagnon et al.*, 2008; *Dobhal et al.*, 2008; *Mihalcea et al.*, 2006]. In principle, the refreezing of melt water in the upper snow and firn layers releases heat that quickly removes the cold wave of the previous winter, and if the water flows via fractures or moulins to the base it may increase basal water pressures and facilitate sliding (eq. A2) [*Paterson*, 1994]. In the West Kunlun Shan and part of the northern central Himalaya, however, mean summer temperatures barely reach above freezing (Figure A1). In these regions, most of the ice is located at high elevations (>5.0-5.5 km asl), precipitation is low [e.g., *Miehe et al.*, 2001; *Ohata et al.*, 1989], and due to low temperatures but high incoming solar radiation, sublimation is regarded to be more important than melting [*Odell*, 1925; *Ageta et al.*, 1989; *Liu et al.*, 1996; *Fujita et al.*, 2000; *Aizen et al.*, 2001; *Rupper et al.*, 2008]. Observed ice temperatures in the West Kunlun Shan [*Ageta et al.*, 1989] and the northern central Himalaya [*Liu et al.*, 2009] are low, potentially leading to significant amounts of cold-based ice. We note, however, our observations of significant glacier-surface velocity fluctuations in the lower parts of these glaciers (Figure 4.9) that may be related to variations in the annual amount of sliding, which requires temperate ice at the base [e.g., *Willis*, 1995]. Similar interannual velocity variations are evident over extended portions of glaciers in the Karakoram (cf., Figure 4.7) [*Quincey et al.*, 2009].
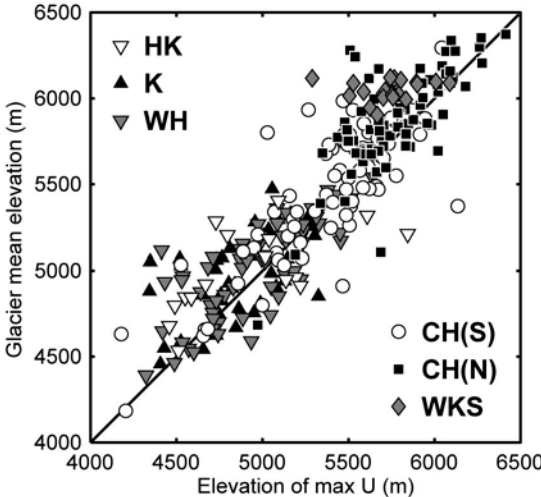
Figure A2: Elevation of maximum velocity along the profile vs. mean elevation of the studied glaciers.

Appendix C: Supplementary material for chapter 6

Table C1: Published and recalculated exposure ages from different regions in High Asia.

Region	Sample ID	Glacial stage	Latitude (°N)	Longitude (°E)	Elevation (m asl)	Sample thickness (cm)	Sample density (g/cm)	Shielding correction	Erosion rate (cm/yr)	^{10}Be concentration (atoms/g) (±1σ)	Age after *Lifton* [2005] (ka) (±1σ)	Comment
1a	MUST-1	Olimde	38.467	75.061	3689	5.0	2.67	1.00	0.0003	501000±13000	9.017±0.923	a
1a	MUST-2	Olimde	38.467	75.062	3681	5.0	2.67	1.00	0.0003	496000±13000	8.973±0.919	a
1a	MUST-3	Olimde	38.465	75.065	3700	5.0	2.67	1.00	0.0003	516000±16000	9.216±0.958	a
1a	MUST-4	Olimde	38.464	75.065	3709	5.0	2.67	1.00	0.0003	499000±13000	8.878±0.909	a
1a	MUST-5	Olimde	38.466	75.062	3688	5.0	2.67	1.00	0.0003	490000±13000	8.833±0.906	a
1a	MUST-6	Olimde	38.467	75.061	3685	5.0	2.67	1.00	0.0003	488000±12000	8.814±0.899	a
1a	MUST-7	Olimde	38.511	75.034	3535	5.0	2.67	1.00	0.0003	467000±17000	9.224±0.976	a
1a	MUST-8	Olimde	38.516	75.032	3534	5.0	2.67	1.00	0.0003	457000±12000	9.039±0.926	a
1a	MUST-9	Olimde	38.520	75.031	3521	5.0	2.67	1.00	0.0003	439000±11000	8.765±0.895	a
1a	MUST-10	Olimde	38.521	75.032	3517	5.0	2.67	1.00	0.0003	408000±11000	8.204±0.84	a
1a	MUST-11	Olimde	38.520	75.034	3494	5.0	2.67	1.00	0.0003	405000±11000	8.257±0.847	a
1a	MUST-12	Olimde	38.521	75.034	3490	5.0	2.67	1.00	0.0003	424000±11000	8.637±0.884	a
1a	MUST-13	Olimde	38.514	75.035	3511	5.0	2.67	1.00	0.0003	421000±14000	8.475±0.885	a
1a	MUST-14	Olimde	38.513	75.035	3521	5.0	2.67	1.00	0.0003	428000±11000	8.557±0.875	a
1a	MUST-15	Olimde	38.391	75.128	3986	5.0	2.67	1.00	0.0003	8168000±213000	132.429±19.427	
1a	MUST-16	Subaxh	38.394	75.131	3987	5.0	2.67	1.00	0.0003	7018000±162000	108.756±14.739	
1a	MUST-17	Subaxh	38.394	75.132	3988	5.0	2.67	1.00	0.0003	4577000±106000	65.108±7.759	
1a	MUST-18	Subaxh	38.394	75.132	3989	5.0	2.67	1.00	0.0003	2942000±69000	39.623±4.393	
1a	MUST-19	Subaxh	38.394	75.132	3991	5.0	2.67	1.00	0.0003	8826000±201000	148.587±22.724	
1a	MUST-20	Subaxh	38.393	75.133	4006	5.0	2.67	1.00	0.0003	5928000±188000	87.839±11.451	
1a	MUST-21	Olimde	38.393	75.171	3862	5.0	2.67	1.00	0.0003	433000±11000	7.126±0.725	b
1a	MUST-22	Olimde	38.393	75.172	3864	5.0	2.67	1.00	0.0003	405000±11000	6.611±0.675	
1a	MUST-23	Olimde	38.393	75.172	3862	5.0	2.67	1.00	0.0003	394000±14000	6.41±0.671	
1a	MUST-24	Olimde	38.393	75.171	3862	5.0	2.67	1.00	0.0003	403000±15000	6.581±0.693	b
1a	MUST-25	Olimde	38.393	75.171	3862	5.0	2.67	1.00	0.0003	419000±11000	6.89±0.702	
1a	MUST-26	Olimde	38.393	75.172	3861	5.0	2.67	1.00	0.0003	422000±11000	6.946±0.707	
1a	MUST-27	Olimde	38.364	75.171	4023	5.0	2.67	0.99	0.0003	431000±13000	6.447±0.663	
1a	MUST-28	Olimde	38.364	75.171	4024	5.0	2.67	0.99	0.0003	458000±12000	6.917±0.705	b
1a	MUST-29	Olimde	38.364	75.171	4025	5.0	2.67	0.99	0.0003	443000±12000	6.649±0.679	
1a	MUST-30	Olimde	38.364	75.171	4026	5.0	2.67	0.98	0.0003	467000±12000	7.12±0.725	
1a	MUST-31	Olimde	38.363	75.171	4028	5.0	2.67	0.98	0.0003	431000±11000	6.501±0.66	
1a	MUST-32	Olimde	38.361	75.171	4082	5.0	2.67	0.99	0.0003	119000±6000	1.748±0.191	
1a	MUST-33	Olimde	38.361	75.171	4081	5.0	2.67	0.99	0.0003	124000±6000	1.829±0.198	
1a	MUST-34	Olimde	38.360	75.172	4094	5.0	2.67	0.99	0.0003	129000±6000	1.893±0.204	
1a	MUST-35	Olimde	38.359	75.172	4120	5.0	2.67	0.98	0.0003	150000±6000	2.218±0.233	
1a	MUST-36	Olimde	38.356	75.173	4167	5.0	2.67	0.99	0.0003	127000±6000	1.778±0.192	
1a	MUST-37	Olimde	38.356	75.173	4176	5.0	2.67	0.99	0.0003	125000±5000	1.738±0.182	
1a	MUST-38	Olimde	38.355	75.173	4180	5.0	2.67	0.99	0.0003	124000±9000	1.719±0.208	
1a	MUST-39	Olimde	38.353	75.171	4228	5.0	2.67	1.00	0.0003	29000±5000	0.426±0.084	
1a	MUST-40	Olimde	38.353	75.171	4227	5.0	2.67	1.00	0.0003	61000±5000	0.839±0.106	
1a	MUST-41	Olimde	38.353	75.170	4238	5.0	2.67	1.00	0.0003	39000±4000	0.56±0.079	
1a	MUST-42	Olimde	38.411	75.165	3719	5.0	2.67	1.00	0.0003	1009000±37000	17.026±1.842	
1a	MUST-43	Olimde	38.411	75.165	3715	5.0	2.67	1.00	0.0003	978000±24000	16.585±1.728	
1a	MUST-44	Olimde	38.410	75.165	3718	5.0	2.67	1.00	0.0003	1144000±27000	19.148±2.005	
1a	MUST-45	Olimde	38.397	75.168	3857	5.0	2.67	1.00	0.0003	859000±21000	13.607±1.406	
1a	MUST-46	Olimde	38.397	75.167	3861	5.0	2.67	1.00	0.0003	871000±27000	13.754±1.447	
1a	MUST-47	Olimde	38.397	75.167	3860	5.0	2.67	1.00	0.0003	870000±21000	13.747±1.42	
1a	MUST-48	Karasu	38.076	75.028	3594	5.0	2.67	1.00	0.0003	18231000±611000	NaN±NaN	
1a	MUST-49	Karasu	38.079	75.037	3623	5.0	2.67	1.00	0.0003	10909000±121000	366.904±114.295	
1a	MUST-50	Karasu	38.076	75.035	3624	5.0	2.67	1.00	0.0003	13499000±192000	NaN±NaN	

Appendix C: Supplementary material for chapter 6

Region	Sample ID	Glacial stage	Latitude (°N)	Longitude (°E)	Elevation (m asl)	Sample thickness (cm)	Sample density (g/cm)	Shielding correction	Erosion rate (cm/yr)	^{10}Be concentration (atoms/g) (±1σ)	Age after *Lifton* [2005] (ka) (±1σ)	Com-ment
1a	MUST-88	Karasu	38.066	75.041	3557	5.0	2.67	1.00	0.0003	7739000±115000	188.786±32.267	
1a	MUST-89	Karasu	38.066	75.035	3537	5.0	2.67	1.00	0.0003	7899000±215000	198.848±36.047	
1a	MUST-52	Olimde	38.285	75.023	4580	5.0	2.67	1.00	0.0003	13000±4000	0.158±0.051	
1a	MUST-53	Olimde	38.285	75.026	4568	5.0	2.67	1.00	0.0003	32000±4000	0.391±0.062	
1a	MUST-54	Olimde	38.287	75.024	4524	5.0	2.67	1.00	0.0003	25000±5000	0.313±0.07	
1a	MUST-55	Olimde	38.287	75.025	4504	5.0	2.67	1.00	0.0003	48000±5000	0.591±0.084	
1a	MUST-56	Olimde	38.287	75.025	4511	5.0	2.67	1.00	0.0003	41000±5000	0.514±0.08	
1a	MUST-57	Olimde	38.288	75.013	4357	5.0	2.67	1.00	0.0003	1137000±27000	13.499±1.392	
1a	MUST-58	Olimde	38.289	75.011	4313	5.0	2.67	1.00	0.0003	1083000±26000	13.207±1.362	
1a	MUST-59	Olimde	38.289	75.011	4308	5.0	2.67	1.00	0.0003	1074000±34000	13.14±1.383	
1a	MUST-60	Olimde	38.289	75.011	4300	5.0	2.67	1.00	0.0003	993000±24000	12.26±1.261	
1a	MUST-61	Olimde	38.289	75.008	4284	5.0	2.67	1.00	0.0003	1144000±27000	14.116±1.458	
1a	MUST-62	Olimde	38.301	74.984	4005	5.0	2.67	1.00	0.0003	1175000±46000	16.778±1.829	
1a	MUST-63	Subaxh	38.301	74.983	4001	5.0	2.67	1.00	0.0003	1676000±45000	23.39±2.499	
1a	MUST-64	Subaxh	38.302	74.969	3987	5.0	2.67	1.00	0.0003	1547000±37000	21.897±2.312	
1a	MUST-65	Subaxh	38.303	74.979	3979	5.0	2.67	1.00	0.0003	4953000±93000	72.036±8.677	
1a	MUST-66	Subaxh	38.302	74.980	3995	5.0	2.67	1.00	0.0003	3266000±56000	43.724±4.84	
1a	MUST-86	Subaxh	38.283	74.980	3988	5.0	2.67	1.00	0.0003	1585000±38000	22.392±2.368	
1a	MUST-67	Olimde	38.288	75.008	4246	5.0	2.67	1.00	0.0003	1049000±34000	13.291±1.403	
1a	MUST-68	Olimde	38.288	75.008	4244	5.0	2.67	1.00	0.0003	1027000±25000	13.045±1.345	
1a	MUST-69	Olimde	38.287	75.007	4234	5.0	2.67	1.00	0.0003	1078000±26000	13.723±1.417	
1a	MUST-70	Olimde	38.288	75.007	4244	5.0	2.67	1.00	0.0003	1021000±26000	12.974±1.342	
1a	MUST-71	Olimde	38.288	75.008	4248	5.0	2.67	1.00	0.0003	1037000±26000	13.135±1.357	
1a	MUST-72	Olimde	38.287	75.011	4295	5.0	2.67	1.00	0.0003	892000±22000	11.107±1.14	c
1a	MUST-73	Olimde	38.286	75.011	4298	5.0	2.67	1.00	0.0003	770000±19000	9.685±0.99	
1a	MUST-74	Olimde	38.286	75.011	4292	5.0	2.67	1.00	0.0003	807000±20000	10.141±1.039	
1a	MUST-75	Olimde	38.286	75.011	4293	5.0	2.67	1.00	0.0003	820000±32000	10.286±1.101	
1a	MUST-76	Olimde	38.292	75.025	4477	5.0	2.67	0.99	0.0003	399000±9000	4.719±0.474	
1a	MUST-77	Olimde	38.292	75.025	4473	5.0	2.67	0.99	0.0003	337000±10000	3.978±0.406	
1a	MUST-78	Olimde	38.293	75.024	4461	5.0	2.67	0.99	0.0003	353000±10000	4.21±0.428	
1a	MUST-79	Olimde	38.293	75.025	4473	5.0	2.67	0.99	0.0003	336000±10000	3.966±0.405	
1a	MUST-80	Subaxh	38.340	75.022	4181	5.0	2.67	1.00	0.0003	2963000±79000	36.055±3.989	
1a	MUST-81	Subaxh	38.342	75.021	4181	5.0	2.67	1.00	0.0003	1954000±46000	24.386±2.591	
1a	MUST-82	Subaxh	38.340	75.021	4168	5.0	2.67	1.00	0.0003	5717000±69000	74.548±8.948	
1a	MUST-83	Subaxh	38.342	75.015	4123	5.0	2.67	1.00	0.0003	1572000±47000	20.577±2.2	
1a	MUST-84	Subaxh	38.342	75.014	4113	5.0	2.67	1.00	0.0003	4290000±75000	55.325±6.334	
1a	MUST-90	Subaxh	38.340	75.017	4126	5.0	2.67	1.00	0.0003	7927000±117000	114.198±15.479	
1a	MUST-91	Subaxh	38.343	75.013	4117	5.0	2.67	1.00	0.0003	1784000±44000	23.213±2.465	
1a	MUST-92	Subaxh	38.342	75.014	4117	5.0	2.67	1.00	0.0003	4629000±158000	60.604±7.353	
1a	MUST-P1	Subaxh	38.276	74.917	4091	0.0	2.67	0.92	0.0003	595000±15000	8.847±0.904	k
1a	MUST-P2	Subaxh	38.276	74.917	4091	0.0	2.67	0.92	0.0003	405000±15000	5.98±0.628	k
1b	KONG_1	Subaxh	38.640	74.990	3480	5.0	2.67	1.00	0.0003	758000±19000	14.945±1.552	
1b	KONG_2	Subaxh	38.641	74.994	3502	5.0	2.67	1.00	0.0003	1328000±31000	24.86±2.643	
1b	KONG_3	Subaxh	38.642	74.994	3527	5.0	2.67	1.00	0.0003	916000±23000	17.293±1.808	
1b	KONG_4	Subaxh	38.642	74.994	3527	5.0	2.67	1.00	0.0003	1528000±37000	27.965±3.006	
1b	KONG_5	Olimde	38.642	74.995	3539	5.0	2.67	1.00	0.0003	588000±16000	11.361±1.175	
1b	KONG_6	Olimde	38.642	74.995	3539	5.0	2.67	1.00	0.0003	594000±16000	11.47±1.186	
1b	KONG_7	Olimde	38.642	74.995	3542	5.0	2.67	1.00	0.0003	604000±16000	11.634±1.202	
1b	KONG_8	Olimde	38.640	75.003	3639	5.0	2.67	0.98	0.0003	371000±11000	7.073±0.728	
1b	KONG_9	Olimde	38.640	75.004	3637	5.0	2.67	0.98	0.0003	366000±11000	6.985±0.719	
1b	KONG_10	Olimde	38.640	75.004	3638	5.0	2.67	0.98	0.0003	374000±11000	7.136±0.734	
1b	KONG_11	Olimde	38.641	75.004	3639	5.0	2.67	0.98	0.0003	372000±12000	7.092±0.736	
1b	KONG_12	Olimde	38.641	75.004	3641	5.0	2.67	0.98	0.0003	382000±11000	7.278±0.748	
1b	KONG_13	Olimde	38.641	75.004	3652	5.0	2.67	0.98	0.0003	373000±18000	7.054±0.776	
1b	KONG_14	Olimde	38.644	75.041	4168	5.0	2.67	1.00	0.0003	106000±11000	1.432±0.204	
1b	KONG_15	Olimde	38.644	75.040	4178	5.0	2.67	1.00	0.0003	57000±10000	0.799±0.16	
1b	KONG_16	Olimde	38.644	75.040	4179	5.0	2.67	1.00	0.0003	104000±10000	1.398±0.191	
1b	KONG_17	Olimde	38.643	75.039	4178	5.0	2.67	1.00	0.0003	88000±11000	1.195±0.189	
1b	KONG_18	Olimde	38.649	75.032	4057	5.0	2.67	1.00	0.0003	247000±8000	3.598±0.37	
1b	KONG_19	Olimde	38.649	75.032	4057	5.0	2.67	1.00	0.0003	240000±9000	3.496±0.365	

Region	Sample ID	Glacial stage	Latitude (°N)	Longitude (°E)	Elevation (m asl)	Sample thickness (cm)	Sample density (g/cm)	Shielding correction	Erosion rate (cm/yr)	^{10}Be concentration (atoms/g) (±1σ)	Age after *Lifton* [2005] (ka) (±1σ)	Comment
1b	KONG_20	Olimde	38.649	75.032	4060	5.0	2.67	1.00	0.0003	235000±9000	3.425±0.359	
1b	KONG_21	Olimde	38.645	75.031	4039	5.0	2.67	1.00	0.0003	60000±6000	0.902±0.126	
1b	KONG_22	Olimde	38.645	75.031	4042	5.0	2.67	1.00	0.0003	314000±10000	4.644±0.478	
1b	KONG_23	Olimde	38.644	75.028	4008	5.0	2.67	1.00	0.0003	195000±8000	2.979±0.315	
1b	KONG_24	Olimde	38.643	75.028	4005	5.0	2.67	1.00	0.0003	101000±7000	1.498±0.179	
1b	KONG_25	Olimde	38.645	75.026	3999	5.0	2.67	1.00	0.0003	224000±7000	3.388±0.347	
1b	KONG_26	Olimde	38.645	75.026	3997	5.0	2.67	1.00	0.0003	224000±8000	3.392±0.352	
1b	KONG_27	Olimde	38.646	75.026	4000	5.0	2.67	1.00	0.0003	157000±8000	2.428±0.267	
1b	KONG_28	Olimde	38.646	75.026	4000	5.0	2.67	1.00	0.0003	77000±6000	1.162±0.145	
1b	KONG_29	Subaxh	38.593	75.010	3573	5.0	2.67	1.00	0.0003	1566000±42000	27.881±3.016	
1b	KONG_30	Subaxh	38.595	75.003	3554	5.0	2.67	1.00	0.0003	3023000±71000	54.584±6.315	
1b	KONG_P1	Subaxh	38.594	74.995	3541	0.0	2.67	0.99	0.0003	2154000±54000	37.25±4.118	
1b	KONG_35	Olimde	38.709	75.280	3326	5.0	2.67	0.93	0.0003	34000±6000	0.849±0.171	
1b	KONG_36	Olimde	38.709	75.280	3328	5.0	2.67	0.93	0.0003	59000±7000	1.423±0.218	
1b	KONG_37	Olimde	38.711	75.280	3309	5.0	2.67	0.93	0.0003	63000±6000	1.537±0.209	
1b	KONG_38	Olimde	38.714	75.280	3299	5.0	2.67	0.93	0.0003	39000±7000	0.98±0.2	
1b	KONG_41	Olimde	38.738	75.273	3118	5.0	2.67	0.93	0.0003	14000±5000	0.424±0.157	
2	K2-1	Skardu	35.315	75.626	2598	3.0	2.67	1.00	0.0003	3497000±110000	156.445±25.098	
2	K2-2	Skardu	35.314	75.625	2601	3.0	2.67	1.00	0.0003	4657000±70000	260.46±56.331	
2	K2-3	Skardu	35.314	75.625	2611	3.0	2.67	1.00	0.0003	3867000±90000	182.197±31.003	
2	K2-4	Skardu	35.315	75.623	2598	3.0	2.67	1.00	0.0003	4717000±90000	268.486±60.089	
2	K2-5	Skardu	35.314	75.626	2602	3.0	2.67	1.00	0.0003	2947000±50000	120.941±16.792	
2	K2-6	Skardu	35.314	75.627	2613	3.0	2.67	1.00	0.0003	4027000±110000	192.771±34.279	
2	K2-7	Skardu	35.317	75.621	2545	3.0	2.67	1.00	0.0003	2537000±60000	105.765±14.225	
2	K2-8	Skardu	35.318	75.618	2557	3.0	2.67	1.00	0.0003	3107000±70000	135.722±19.938	
2	K2-9	Skardu	35.318	75.617	2557	3.0	2.67	1.00	0.0003	1917000±50000	74.647±9.213	
2	K2-12	?	35.677	75.469	2950	3.0	2.67	1.00	0.0003	587000±10000	17.255±1.773	
2	K2-13	?	35.677	75.469	2952	3.0	2.67	1.00	0.0003	607000±20000	17.77±1.903	
2	K2-14	?	35.677	75.475	2945	3.0	2.67	1.00	0.0003	587000±20000	17.308±1.857	
2	K2-15	?	35.679	75.469	2950	3.0	2.67	1.00	0.0003	587000±20000	17.254±1.851	
2	K2-16	?	35.678	75.469	2951	3.0	2.67	1.00	0.0003	587000±20000	17.244±1.85	
2	K2-17	?	35.676	75.469	2950	3.0	2.67	1.00	0.0003	587000±20000	17.256±1.851	
2	K2-18	?	35.675	75.466	2868	3.0	2.67	1.00	0.0003	567000±10000	17.572±1.809	
2	K2-19	?	35.675	75.466	2865	3.0	2.67	1.00	0.0003	507000±20000	15.907±1.732	
2	K2-23	Mungo	35.718	75.520	2646	3.0	2.67	0.96	0.0003	377000±10000	13.941±1.399	
2	K2-24	Mungo	35.718	75.520	2631	3.0	2.67	0.96	0.0003	357000±10000	13.393±1.35	
2	K2-25	Mungo	35.718	75.520	2631	3.0	2.67	0.96	0.0003	347000±10000	13.054±1.318	
2	K2-26	Mungo	35.719	75.520	2650	3.0	2.67	0.96	0.0003	367000±10000	13.572±1.365	
2	K2-31	Mungo	35.721	75.676	3164	3.0	2.67	0.94	0.0003	407000±10000	11.448±1.176	
2	K2-32	Mungo	35.722	75.674	3166	3.0	2.67	0.94	0.0003	67000±10000	2.007±0.359	
2	K2-33	Mungo	35.724	75.672	3052	3.0	2.67	0.96	0.0003	397000±10000	11.422±1.142	
2	K2-48	Mungo	35.671	75.799	3633	3.0	2.67	1.00	0.0003	607000±20000	11.971±1.261	
2	K2-49	Mungo	35.671	75.799	3631	3.0	2.67	1.00	0.0003	617000±20000	12.169±1.281	
2	K2-50	Mungo	35.671	75.799	3640	3.0	2.67	1.00	0.0003	657000±20000	12.838±1.345	
2	K2-51	Mungo	35.671	75.799	3644	3.0	2.67	1.00	0.0003	607000±20000	11.894±1.253	
2	K2-52	Mungo	35.667	75.798	3636	3.0	2.67	1.00	0.0003	607000±20000	11.951±1.259	
2	K2-53	Mungo	35.667	75.797	3643	3.0	2.67	1.00	0.0003	657000±20000	12.818±1.343	
2	K2-54	Mungo	35.666	75.797	3824	3.0	2.67	1.00	0.0003	487000±10000	8.781±0.887	
2	K2-55	Mungo	35.666	75.796	3825	3.0	2.67	1.00	0.0003	717000±20000	12.55±1.305	
2	K2-56	Mungo	35.668	75.797	3881	3.0	2.67	1.00	0.0003	737000±20000	12.48±1.294	
2	K2-58	Mungo	35.694	75.719	3879	3.0	2.67	1.00	0.0003	727000±30000	12.323±1.338	
2	K2-59	Mungo	35.694	75.719	3811	3.0	2.67	1.00	0.0003	727000±20000	12.798±1.33	
2	K2-60	Mungo	35.694	75.719	3031	3.0	2.67	0.94	0.0003	417000±10000	12.349±1.231	
2	K2-61	Mungo	35.694	75.718	3032	3.0	2.67	0.93	0.0003	407000±10000	12.189±1.217	
2	K2-62	Mungo	35.672	75.814	3017	3.0	2.67	0.94	0.0003	387000±20000	11.637±1.277	
2	K2-63	Mungo	35.672	75.814	2944	3.0	2.67	0.69	0.0003	297000±10000	12.604±1.292	
2	K2-65	Askole	35.672	75.814	3113	3.0	2.67	0.80	0.0003	407000±10000	13.733±1.42	
2	K2-66	Askole	35.672	75.814	3128	3.0	2.67	0.80	0.0003	167000±10000	5.8±0.669	
2	K2-67	Askole	35.672	75.814	3122	3.0	2.67	0.80	0.0003	177000±10000	6.169±0.701	
2	K2-68	Askole	35.672	75.814	3113	3.0	2.67	0.80	0.0003	187000±10000	6.598±0.741	

Region	Sample ID	Glacial stage	Latitude (°N)	Longitude (°E)	Elevation (m asl)	Sample thickness (cm)	Sample density (g/cm)	Shielding correction	Erosion rate (cm/yr)	[10]Be concentration (atoms/g) (±1σ)	Age after *Lifton* [2005] (ka) (±1σ)	Comment
2	K2-69	Askole	35.703	75.954	3109	3.0	2.67	0.80	0.0003	217000±10000	7.68±0.839	
2	K2-70	Askole	35.703	75.952	3106	3.0	2.67	0.79	0.0003	187000±10000	6.718±0.755	
2	K2-72	?	35.703	75.953	4209	3.0	2.67	1.00	0.0003	917000±20000	12.789±1.31	
2	K2-73	?	35.704	75.952	4213	3.0	2.67	1.00	0.0003	937000±20000	13.02±1.333	
2	K2-74	?	35.703	75.952	4212	3.0	2.67	1.00	0.0003	947000±20000	13.155±1.347	
2	K2-75	?	35.703	75.948	4215	3.0	2.67	1.00	0.0003	927000±30000	12.877±1.358	
2	K2-76	?	35.703	75.947	4211	3.0	2.67	1.00	0.0003	1197000±30000	16.257±1.695	
2	K2-77	?	35.703	75.943	4211	3.0	2.67	1.00	0.0003	967000±20000	13.417±1.374	
2	K2-78	?	35.695	75.957	4225	3.0	2.67	1.00	0.0003	947000±20000	13.069±1.338	
2	K2-79	?	35.694	75.958	4221	3.0	2.67	1.00	0.0003	897000±20000	12.453±1.276	
2	K2-80	Mungo	35.694	75.958	3823	3.0	2.67	0.81	0.0003	717000±20000	15.196±1.591	
2	K2-81	Mungo	35.693	75.960	3821	3.0	2.67	0.81	0.0003	737000±20000	15.591±1.631	
2	K2-82	Mungo	35.692	75.960	3818	3.0	2.67	0.81	0.0003	707000±20000	15.049±1.577	
2	K2-83	Mungo	35.692	75.961	3779	3.0	2.67	1.00	0.0003	2567000±60000	41.138±4.579	
2	K2-84	Mungo	35.689	75.941	3768	3.0	2.67	1.00	0.0003	687000±20000	12.446±1.298	
2	K2-85	Mungo	35.689	75.941	3766	3.0	2.67	0.99	0.0003	697000±30000	12.747±1.395	
2	K2-86	?	35.689	75.941	3445	3.0	2.67	0.98	0.0003	517000±10000	11.691±1.188	
2	K2-87	?	35.689	75.941	3442	3.0	2.67	0.98	0.0003	547000±20000	12.353±1.319	
2	K2-88	?	35.688	75.927	3447	3.0	2.67	0.98	0.0003	587000±20000	13.157±1.396	
2	K2-89	?	35.688	75.927	3441	3.0	2.67	0.98	0.0003	517000±10000	11.719±1.191	
2	K2-90	Askole	35.688	75.927	3095	3.0	2.67	0.97	0.0003	27000±2700	0.841±0.117	
2	K2-91	Askole	35.695	75.927	3096	3.0	2.67	0.96	0.0003	47000±10000	1.421±0.333	
2	K2-92	Askole	35.687	75.926	3094	3.0	2.67	0.96	0.0003	37000±3700	1.136±0.158	
2	K2-93	Askole	35.686	75.926	3090	3.0	2.67	0.96	0.0003	87000±10000	2.719±0.411	
2	K2-94	Askole	35.688	75.925	3096	3.0	2.67	0.96	0.0003	47000±10000	1.421±0.333	
2	K2-95	Askole	35.292	75.662	3087	3.0	2.67	0.96	0.0003	27000±2700	0.864±0.12	
2	K2-96	Askole	35.292	75.662	3116	3.0	2.67	0.97	0.0003	57000±10000	1.721±0.346	
2	K2-116	?	35.292	75.662	2276	3.0	2.67	1.00	0.0003	127000±20000	6.366±1.196	d
2	K2-117	?	35.292	75.662	2276	3.0	2.67	1.00	0.0003	97000±9700	4.978±0.701	d
2	K2-118	?	35.315	75.626	2276	3.0	2.67	1.00	0.0003	117000±11700	5.843±0.825	d
2	K2-119	?	35.314	75.625	2276	3.0	2.67	1.00	0.0003	97000±9700	4.973±0.7	d
3	RAM-5	Holocene maximum	35.211	74.810	2634	3.0	2.57	0.92	0.0003	279000±33000	11.464±1.804	
3	ZIAP-1	mid Holocene	35.231	74.746	2900	5.0	2.65	0.93	0.0003	241000±23000	8.548±1.187	
3	SLOAN-18	mid Holocene	35.176	74.883	3573	4.0	2.61	0.91	0.0003	269000±36000	6.38±1.071	
3	SLOAN-17	mid Holocene	35.194	74.604	3577	3.0	2.65	0.90	0.0003	235000±47000	5.577±1.257	
3	SLOAN-12	Holocene maximum	35.400	74.675	3355	2.0	2.65	1.00	0.0003	451000±32000	10.609±1.308	
3	SLOAN-1	mid Holocene	35.390	74.577	3400	4.0	2.65	0.93	0.0003	281000±23000	7.256±0.936	
3	SLOAN-4	mid Holocene	35.388	74.578	3255	4.0	2.65	0.91	0.0003	260000±24000	7.507±1.023	
3	INDUS-7	Holocene maximum	35.402	74.415	1730	9.0	2.55	0.96	0.0003	146000±35000	11.36±3.025	
3	INDUS-6	Holocene maximum	35.401	74.415	1730	5.0	2.52	0.97	0.0003	150000±29000	11.207±2.493	
3	INDUS-5	Holocene maximum	35.401	74.405	1575	5.0	2.60	0.93	0.0003	310000±60000	25.635±5.941	e
3	SLOAN-7	pre-Holocene	35.421	74.566	3846	4.0	2.65	0.96	0.0003	3883000±246000	66.388±9.226	
3	INDUS-1	pre-Holocene	35.465	74.502	1892	3.0	2.63	0.94	0.0003	709000±45000	43.366±5.642	
3	INDUS-2	pre-Holocene	35.463	74.503	1845	5.0	2.53	0.98	0.0003	1126000±59000	74.595±10.007	
3	GOR-1	pre-Holocene	35.514	74.517	2103	12.0	2.61	0.96	0.0003	3543000±487000	406.808±245.682	
4	L7	Batal	32.400	77.600	4340	3.0	2.67	1.00	0.0003	922000±62000	13.066±1.593	
4	L8	Batal	32.500	77.600	4350	3.0	2.67	1.00	0.0003	1110000±39000	15.319±1.641	
4	L9	Batal	32.500	77.600	4350	3.0	2.67	1.00	0.0003	1035000±47000	14.4±1.598	
4	L10	Kulti	32.300	77.200	2390	3.0	2.67	0.99	0.0003	298000±23000	14.071±1.807	
4	L12	Kulti	32.300	77.200	2415	3.0	2.67	0.99	0.0003	275000±9000	12.853±1.357	
4	L15	Batal	32.300	77.200	2430	3.0	2.67	0.99	0.0003	419000±13000	18.687±1.994	
4	L20	Kulti (Batal)	32.600	76.900	2865	3.0	2.67	0.90	0.0003	280000±15000	10.716±1.218	
4	L21	Kulti (Batal)	32.600	76.900	2700	3.0	2.67	1.00	0.0003	304000±21000	11.609±1.422	
4	L24	Kulti	32.500	77.000	2985	3.0	2.67	0.86	0.0003	82000±4000	3.298±0.36	f
4	L25	Kulti	32.500	77.000	2985	3.0	2.67	0.93	0.0003	93000±6000	3.448±0.404	f
4	L26	Batal	32.500	77.000	3050	3.0	2.67	0.89	0.0003	444000±19000	14.89±1.637	
4	L27	Batal	32.500	77.000	2975	3.0	2.67	0.84	0.0003	416000±19000	15.425±1.718	
4	L28	Kulti	32.500	77.000	3000	3.0	2.67	0.90	0.0003	382000±12000	13.231±1.392	

Appendix C: Supplementary material for chapter 6

Region	Sample ID	Glacial stage	Latitude (°N)	Longitude (°E)	Elevation (m asl)	Sample thickness (cm)	Sample density (g/cm)	Shielding correction	Erosion rate (cm/yr)	^{10}Be concentration (atoms/g) (±1σ)	Age after *Lifton* [2005] (ka) (±1σ)	Comment
4	L29	Kulti	32.500	77.000	2985	3.0	2.67	0.97	0.0003	401000±11000	13.043±1.356	
4	L31	Batal (Kulti)	32.500	77.100	3020	3.0	2.67	0.98	0.0003	357000±9000	11.347±1.167	f
4	L32	Batal (Kulti)	32.500	77.100	3020	3.0	2.67	0.96	0.0003	552000±34000	17.217±2.066	
4	L33	Batal (Kulti)	32.500	77.100	3036	3.0	2.67	0.98	0.0003	624000±17000	18.722±1.976	
4	L37	Batal	32.400	77.600	4555	3.0	2.67	1.00	0.0003	1273000±34000	15.697±1.641	
4	L40	Batal (Chandra)	32.400	77.600	4780	3.0	2.67	1.00	0.0003	1272000±35000	13.671±1.376	
4	L41	Batal (Chandra)	32.400	77.600	4770	3.0	2.67	1.00	0.0003	1348000±33000	14.932±1.549	
4	L42	Batal (Chandra)	32.400	77.600	4890	3.0	2.67	1.00	0.0003	1391000±56000	14.525±1.58	
4	L44	Kulti (Batal)	32.400	77.600	4070	3.0	2.67	0.99	0.0003	766000±22000	12.778±1.332	g
4	L48	Sorapani II	32.400	77.600	4045	3.0	2.67	0.99	0.0003	10000±1000	0.207±0.029	
4	L49	Batal (Kulti)	32.400	77.600	4190	3.0	2.67	0.99	0.0003	872000±22000	13.524±1.4	
4	L50	Batal (Kulti)	32.400	77.600	4070	3.0	2.67	0.99	0.0003	912000±23000	14.969±1.555	
5	BH1d	no moraine	31.000	78.930	3028	3.0	2.67	0.93	0.0003	710000±100000	23.148±4.213	h
5	BH2	no moraine	31.000	78.930	3015	3.0	2.67	0.93	0.0003	109000±4000	4.195±0.438	h
5	BH3	no moraine	31.000	78.930	3021	3.0	2.67	0.93	0.0003	143000±5000	5.323±0.554	h
5	BH6	no moraine	30.960	78.950	3810	3.0	2.67	0.91	0.0003	173000±11000	4.24±0.496	h
5	BH7	no moraine	30.960	78.940	3878	3.0	2.67	0.91	0.0003	96000±7000	2.303±0.28	h
5	BH9	no moraine	30.960	78.940	3896	3.0	2.67	0.93	0.0003	103000±14000	2.401±0.403	h
5	BH14	no moraine	30.940	78.950	4396	3.0	2.67	0.97	0.0003	460000±11000	7.236±0.734	h
5	BH16	no moraine	30.940	78.950	4314	3.0	2.67	0.97	0.0003	445000±11000	7.313±0.743	h
5	BH19	Kedar	30.940	78.950	4323	3.0	2.67	0.97	0.0003	493000±12000	7.986±0.812	
5	BH20	Kedar	30.940	78.950	4242	3.0	2.67	0.97	0.0003	438000±10000	7.478±0.757	
5	BH21	no moraine	31.000	78.920	3015	3.0	2.67	0.95	0.0003	172000±6000	6.161±0.643	h
5	BH24	no moraine	31.000	78.920	3040	3.0	2.67	0.95	0.0003	159000±7000	5.654±0.609	h
5	BH25	no moraine	30.930	79.080	3960	3.0	2.67	0.99	0.0003	39000±5000	0.841±0.135	h
5	BH26	Bhujbas	30.940	79.060	3917	3.0	2.67	0.97	0.0003	58000±3000	1.265±0.139	
5	BH27	Bhujbas	30.940	79.060	3918	3.0	2.67	0.97	0.0003	102000±4000	2.245±0.235	
5	BH29	Gangotri	30.940	79.060	3973	3.0	2.67	0.97	0.0003	33000±9000	0.731±0.212	
5	BH30	Gangotri	30.940	79.060	3956	3.0	2.67	0.97	0.0003	16000±7000	0.377±0.169	
5	BH31	Gangotri	30.940	79.060	3973	3.0	2.67	0.97	0.0003	12000±7000	0.28±0.166	
5	BH32	Gangotri	30.940	79.060	3956	3.0	2.67	0.97	0.0003	46000±7000	1±0.181	
5	BH33	no moraine	30.950	79.060	4140	3.0	2.67	0.97	0.0003	214000±9000	4.096±0.436	h
5	BH34	no moraine	30.950	79.060	4145	3.0	2.67	0.97	0.0003	115000±8000	2.229±0.267	h
5	BH35B	Bhagirathi	30.950	79.060	4093	3.0	2.67	0.97	0.0003	940000±28000	16.127±1.702	
5	BH36	Bhagirathi	30.950	79.060	4112	3.0	2.67	0.97	0.0003	695000±19000	12.168±1.262	
5	BH37	Bhagirathi	30.950	79.060	4098	3.0	2.67	0.97	0.0003	513000±15000	9.29±0.961	b
5	BH38	no moraine	30.950	79.060	3857	3.0	2.67	0.97	0.0003	40000±8000	0.925±0.206	h
5	BH39	no moraine	30.950	79.060	3863	3.0	2.67	0.97	0.0003	51000±8000	1.154±0.213	h
5	BH41	no moraine	30.990	78.940	3063	3.0	2.67	0.99	0.0003	14000±10000	0.536±0.387	h
5	BH43	Bhagirathi	31.010	78.710	2510	3.0	2.67	0.95	0.0003	6000±13000	0.341±0.739	i
5	BH44	Bhagirathi	31.010	78.710	2499	3.0	2.67	0.95	0.0003	35000±11000	1.834±0.606	i
5	BH45	Bhagirathi	31.010	78.710	2490	3.0	2.67	0.95	0.0003	12000±11000	0.666±0.615	i
5	BH46	Bhagirathi	31.010	78.710	2495	3.0	2.67	0.95	0.0003	27000±11000	1.412±0.594	i
6	LT12	not given	28.200	85.500	2978	2.0	2.67	0.91	0.0003	20000±6000	0.895±0.283	h
6	LT13	not given	28.200	85.500	2978	4.0	2.67	0.90	0.0003	30000±11000	1.331±0.506	h
6	LT14	not given	28.200	85.500	2980	2.0	2.67	0.90	0.0003	15000±6000	0.695±0.287	h
6	LT15	not given	28.200	85.500	2980	1.0	2.67	0.90	0.0003	13000±4000	0.607±0.196	h
6	LT16	not given	28.200	85.500	3016	1.5	2.67	0.83	0.0003	44000±7000	2.014±0.377	h
6	LT17	not given	28.200	85.500	3016	4.0	2.67	0.83	0.0003	38000±11000	1.772±0.543	h
6	LT18	not given	28.200	85.500	3020	2.0	2.67	0.82	0.0003	14000±4000	0.694±0.21	h
6	LT22	not given	28.200	85.600	4150	3.0	2.67	0.99	0.0003	903000±45000	15.801±1.792	
6	LT23	not given	28.200	85.600	4156	1.0	2.67	0.99	0.0003	844000±32000	14.626±1.578	
6	LT24	not given	28.200	85.600	4156	2.0	2.67	0.99	0.0003	893000±47000	15.489±1.776	
6	LT26	not given	28.200	85.600	4154	2.0	2.67	0.99	0.0003	735000±36000	13.001±1.458	
6	LT32	not given	28.200	85.600	3853	2.5	2.67	0.97	0.0003	431000±17000	9.472±1.013	
6	LT33	not given	28.200	85.600	3851	2.5	2.67	0.96	0.0003	403000±16000	8.974±0.96	
6	LT35	not given	28.200	85.600	3846	1.0	2.67	0.98	0.0003	458000±21000	9.842±1.08	
6	LT36	not given	28.200	85.600	3846	2.0	2.67	0.93	0.0003	192000±8000	4.744±0.505	b
6	LT61	not given	28.200	85.500	3523	1.5	2.67	0.96	0.0003	129000±8000	3.748±0.434	
6	LT63	not given	28.200	85.500	3525	1.0	2.67	0.95	0.0003	134000±7000	3.907±0.433	

Region	Sample ID	Glacial stage	Latitude (°N)	Longitude (°E)	Elevation (m asl)	Sample thickness (cm)	Sample density (g/cm)	Shielding correction	Erosion rate (cm/yr)	[10]Be concentration (atoms/g) (±1σ)	Age after *Lifton* [2005] (ka) (±1σ)	Com- ment
7	E5	Periche II	27.890	86.820	4328	3.0	2.67	0.99	0.0003	1143000±33000	17.853±1.889	
7	E6	Periche II	27.890	86.820	4433	3.0	2.67	0.99	0.0003	966000±23000	14.643±1.515	
7	E7	Periche II	27.890	86.820	4310	3.0	2.67	0.99	0.0003	973000±24000	15.625±1.624	
7	E9	Periche I	27.880	86.820	4401	3.0	2.67	0.99	0.0003	1466000±35000	21.594±2.278	
7	E10	Periche I	27.880	86.820	4401	3.0	2.67	0.99	0.0003	1473000±33000	21.686±2.28	
7	E11	Periche I	27.880	86.820	4401	3.0	2.67	0.99	0.0003	1473000±33000	21.686±2.28	
7	E29	Chhukung	27.900	86.870	4755	3.0	2.67	0.99	0.0003	1319000±16000	16.589±1.688	j
7	E30	Chhukung	27.900	86.870	4837	3.0	2.67	0.99	0.0003	710000±21000	9.056±0.937	
7	E31	Chhukung	27.900	86.870	4812	3.0	2.67	0.99	0.0003	697000±16000	9.006±0.915	
7	E32	Lobuche & Historical	27.900	86.870	4773	3.0	2.67	0.99	0.0003	53000±7000	0.826±0.135	
7	E36	Lobuche & Historical	27.910	86.870	4525	3.0	2.67	0.99	0.0003	5000±3000	0.095±0.058	
7	E37	Lobuche & Historical	27.900	86.870	4691	3.0	2.67	0.99	0.0003	75000±21000	1.171±0.348	
7	E38	Lobuche & Historical	27.900	86.870	4718	3.0	2.67	0.99	0.0003	8000±3000	0.139±0.054	
7	E39	Periche I	27.910	86.880	5074	3.0	2.67	0.99	0.0003	1714000±45000	18.122±1.905	
7	E40	Periche I	27.910	86.880	5074	3.0	2.67	0.99	0.0003	2181000±54000	22.501±2.385	
7	E41	Periche I	27.910	86.880	5060	3.0	2.67	0.99	0.0003	5096000±138000	47.483±5.433	j
7	E45	Periche I	27.910	86.870	5050	3.0	2.67	0.99	0.0003	2698000±47000	27.455±2.904	
7	E46	Periche I	27.910	86.870	5047	3.0	2.67	0.99	0.0003	1606000±48000	17.311±1.834	
7	E57	Periche I	27.920	86.890	5280	3.0	2.67	0.98	0.0003	2071000±66000	19.799±2.125	
7	E58	Periche I	27.920	86.890	5064	3.0	2.67	0.98	0.0003	2179000±106000	22.778±2.621	
7	E59	Periche I	27.920	86.890	5324	3.0	2.67	0.99	0.0003	694000±17000	7.098±0.72	j
7	E61	Thuklha	27.910	86.890	5005	3.0	2.67	0.99	0.0003	297000±22000	3.834±0.471	
7	E62	Thuklha	27.910	86.880	4955	3.0	2.67	0.99	0.0003	274000±11000	3.634±0.383	
7	E63	Thuklha	27.910	86.880	5032	3.0	2.67	0.98	0.0003	257000±15000	3.339±0.38	
7	E71	Periche II	27.910	86.810	4579	3.0	2.67	0.98	0.0003	2134000±122000	27.927±3.384	j
7	E73	Periche II	27.910	86.810	4557	3.0	2.67	0.98	0.0003	1047000±32000	14.97±1.579	
7	E75	Thyangboche II	27.920	86.810	4647	3.0	2.67	0.98	0.0003	2542000±38000	31.554±3.362	
7	E76	Thyangboche II	27.920	86.810	4651	3.0	2.67	0.98	0.0003	2980000±467000	36.179±7.362	
7	E77	Thyangboche II	27.920	86.810	4674	3.0	2.67	0.98	0.0003	2362000±77000	29.175±3.221	
7	E79	Chhukung	27.920	86.810	4624	3.0	2.67	0.98	0.0003	660000±16000	9.471±0.967	
7	E80	Chhukung	27.920	86.810	4624	3.0	2.67	0.98	0.0003	671000±31000	9.615±1.056	
7	E81	Chhukung	27.920	86.810	4628	3.0	2.67	0.98	0.0003	676000±26000	9.661±1.03	
7	E82	Lobuche & Historical	27.920	86.810	4270	3.0	2.67	0.99	0.0003	85000±10000	1.614±0.247	
7	E84	Thyangboche I	27.920	86.800	4739	3.0	2.67	0.99	0.0003	7233000±131000	90.28±11.458	
7	E85	Thyangboche I	27.920	86.800	4725	3.0	2.67	0.99	0.0003	6830000±123000	84.712±10.574	
7	E86	Thyangboche I	27.920	86.800	4739	3.0	2.67	0.99	0.0003	6254000±113000	75.077±9.112	
7	E87	Thyangboche I	27.930	86.800	4930	3.0	2.67	0.99	0.0003	3646000±94000	37.452±4.151	
7	E88	Thyangboche I	27.930	86.800	5017	3.0	2.67	0.99	0.0003	2514000±39000	26.182±2.751	
7	E89	Thyangboche I	27.930	86.800	5021	3.0	2.67	0.99	0.0003	2585000±88000	26.791±2.952	

Regions: (1a) Mustagh Ata [*Seong et al.*, 2009]; (1b) Kongur Shan [*Seong et al.*,2009]; (2) Karakoram [*Seong et al.*, 2007]; (3) Nanga Parbat [*Phillips et al.*, 2000]; (4) Lahul [*Owen et al.*, 2001]; (5) Garhwal [*Barnard et al.*, 2004]; (6) Langtang [*Abramowski*, 2003]; (7) Khumbu [*Finkel et al.*, 2003].

Comments: (a) We argue that the interpretation of the sampled boulders as glaciogenic in origin is ambiguous: (1) the authors do not provide convincing evidence that the sampled landform is a moraine. The only evidence is seen in the presence of large boulders. The authors point out that the associated glacial advance and ELA-depression (no values given) is exceptionally large compared to any other advance in their study area, but only suggest that hypsometry may explain this without providing further details; (2) no other moraines have been identified by the authors in between the sampled deposits and the glaciers; whereas in neighboring valleys, several younger distinct moraines have been described, mapped and sampled; (3) in between the sampled deposits and the present-day glacier, a large debris fan can be seen in high-resolution satelite imagery in Google Earth which could potentially be the source for the boulders; (4) the main river of the valley as well as smaller tributaries have incised between the sampled deposits and the present-day glaciers, indicating fluvial modification of the land surfaces. Thus, although the sampled deposit may indeed represent a moraine, we find the presently available evidence too scarce to firmly support an interpretation of this landform as a moraine. (b) The authors assume that erosion or toppling of the boulder affected the sampled surface and lead to a too young age. (c) Age considered by authors too old and probably related to an older landform (preexposure). (d) The sampled deposits have been interpreted differently by *Hewitt* [1999]. Also, the authors do not explain which glacier could have produced these deposits. At present, no glacier exists nearby, which may be invoked to have descended thus far down, i.e., to an elevation of ~2200 m asl. This elevation stands in contrast to all of the other sampled and dated deposits, which are found at significantly higher elvations (>3000 m asl) and which were produced by some very large glaciers, e.g., Biafo glacier. (e) The age difference to samples of the same assumed glacial episode is >15 kyr. Thus, cosmogenic nuclide inheritance is likely. (f) Authors note the boulder surface is weathered and

exfoliated. (g) The age aparently violates the morphostratigraphic order. (h) No moraine. (i) Questionable if landform is a moraine. If so, then the age violates the morphostratigraphic order. See *Barnard et al.* [2004] for discussion. (j) Rejected by authors without explanation. (k) Depth profile.

Appendix D: Supplementary material for chapter 7

Glacier-surface velocities. Obtaining glacier-surface velocities from optical satellite imagery is a well established method [*Bindschadler and Scambos*, 1991; *Scambos et al.*, 1992; *Kääb*, 2005; *Stearns and Hamilton*, 2005; *Howat et al.*, 2007; *Scherler et al.*, 2008]. We used the program COSI-Corr [*Leprince et al.*, 2007] for precise orthorectification, co-registration, and correlation of Advanced Spaceborne Thermal Emission and reflection Radiometer (ASTER) satellite imagery and followed the procedures outlined in ref. [*Scherler et al.*, 2008] to obtain accurate velocity profiles following the central flow line of the glaciers. Along these profiles, we recorded the elevation and slope of the glacier surface, determined from an SRTM digital elevation model (DEM). The temporal separation of the satellite images is generally close to a year or multiple years and thus not biased by seasonal velocity variations [*Scherler et al.*, 2008]. Each profile is constructed from several measurements and final velocities reflect mean annual velocities averaged over the years 2000-2008. Uncertainties in the velocity measurements are usually on the order of ~5% (Table A4) and were calculated from the correlation uncertainties [*Leprince et al.*, 2007; *Scherler et al.*, 2008].

Ice-flux estimates. We identified the approximate position of the transient equilibrium line altitude (ELA) during the study period using satellite images taken at the end of the hydrological year, i.e., late summer to fall [*Rabatel et al.*, 2005]. Note that these estimates (1) depend on the availability of suitable satellite images, which differs from region to region, and (2) do not represent the steady-state ELA, corresponding to a zero net-mass balance. We estimated the ice-flux as close to the ELA as possible, but in cases where the ELA was found located in complex glacial terrain, e.g., in broad accumulation basins, we have chosen the next suitable location downstream where a parabolic channel form appears likely (Figure D1, Figure D2). In cases of complex branching glaciers, we have chosen the largest contributing glacier branch if the ELA is located much higher than major confluences. The ice-flux q, is given by

$$q = h_{\max} \overline{w} \overline{u} \qquad \text{(eq. D1)},$$

where h_{max} is the maximum cross-glacier thickness, $\overline{w}$ is the depth-averaged glacier width, and $\overline{u}$ is the average cross-sectional velocity [*Budd and Allison*, 1975]. Using analytical and numerical solutions for ice flow through channels of various shape, Nye [1965] derived shape factors, s_1 and s_2, to relate $\overline{w}$ to the surface width w_{max}, and $\overline{u}$ to the maximum centre-line surface velocity, u_{max}, respectively, so that q can be expressed as [*Budd and Allison*, 1975]

$$q = h_{\max} w_{\max} s_1 u_{\max} s_2 \qquad \text{(eq. D2)}$$

We obtained a first-order estimate of the ice thickness, h, assuming perfect plasticity and constant driving-stresses [*Paterson*, 1994],

$$\tau = \rho_i g h \sin(\alpha) \qquad \text{(eq. D3)},$$

in which ρ_i is ice density (~900 kg/m^3), g is gravity (9.81 m/s²), α is the local slope along the direction of flow, and τ is the driving stress, in this study taken to be 1.25x10^5 Pa, an average value for valley glaciers [*Paterson*, 1994]. We calculated uncertainties for our ice-flux estimates

using the velocity uncertainties, and a range of estimated uncertainties for the parameters s1, s2, and τ, which are least constrained, and also α. For uncertainties of 0%, 10%, and 20% in the parameters s_1, s_2, and τ, as well as 0%, 5%, and 10% in the slope values (Table D1), mean (median) uncertainties are 9(6)%, 21(19)%, and 38(37)% of the ice flux, respectively.

Topographic analyses. We measured local relief for each pixel in the 90-m resolution DEM by taking the elevation range, i.e., the difference between the maximum and minimum elevation, in circular areas of 5 km radius. Topographic statistics in the swath profiles were obtained across their 100-km widths and at 90-m spacing. Catchment hypsometry was calculated for contributing areas above the glacier termini. Glacier areas were calculated from digitzed glacier outlines.

Present-day snowlines. We used two sources of snowlines: a map of regional climatic snowline contours [*von Wissmann*, 1959], and glacier-snowline elevations provided in the World Glacier Inventory (WGI) [*National Snow and Ice Data Center*, 2009]. For the purpose of our study, we found the regional snowline elevations [*von Wissmann*, 1959] more useful than the irregularly distributed and in places extremely variable snowline dataset from the WGI that largely misses data from India. Comparison between the two datasets revealed that the map of regional climatic snowlines [*von Wissmann*, 1959] misses small-scale variations, probably related to topography, overestimates WGI snowlines in central Tibet, and the Karakoram, and underestimates WGI snowlines in the central Himalaya (Figure D4-Figure D6). Note that these discrepancies do not affect our results, but tend to accentuate the east-west differences that we show.

Quaternary euilibrium line altitude (ELA) lowering. To reconstruct the Quaternary land surface above the snowline, which is approximately equal to the ELA [*von Wissmann*, 1959; *Ohmura et al.*, 1992; *Paterson*, 1994], we used the map of regional climatic snowlines [*von Wissmann*, 1959] and the map of ELA-lowering during the last glacial maximum (LGM) by *Shi* [2002]. It should be noted that the LGM in High Asia occurred earlier during the last glacial cycle than the global LGM [*Shi*, 2002; *Owen et al.*, 2009; *Scherler et al.*, 2010]. However, reliable data on local-LGM extents of glaciers and associated ELA-lowering across High Asia is extremely rare, and we therefore use the more numerous and accurate global LGM data. In a recent review, *Owen and Benn* [2005] concluded that the map by *Shi* [2002] may not be very accurate in detail, but that the general pattern appears to be realistic (Figure D7). As this map does not cover the western Pamir and Hindu Kush, we assume LGM-ELAs ~1000 m lower than today, which is equal, or close to reported values from these regions [*von Wissmann*, 1959; *Owen et al.*, 2005; *Abramowski et al.*, 2006].

Climate data sets. For climatic analyses, we used 5-km resolution maps of mean annual and seasonal rainfall derived from Tropical Rainfall Measuring Mission (TRMM) data from 1998 to 2006, calibrated to meteorological station data [*Bookhagen and Burbank*, 2006]. Reliable estimates of snow-water equivalent in mountainous terrain are difficult to obtain and unavailable for the study region. Thus, we content ourselves with 0.05°-resolution data on fractional snow cover from the MODerate resolution Imaging Spectroradiometer (MODIS) collected between March 2000 and March 2008 [*Hall et al.*, 2007], as a proxy from snowfall. This is legitimate for the scope of our study and in the study region, as snow melting is predominantly driven by summer temperatures and longer snow cover is to first order related to the amount of snowfall [*Bookhagen and Burbank*, in press].
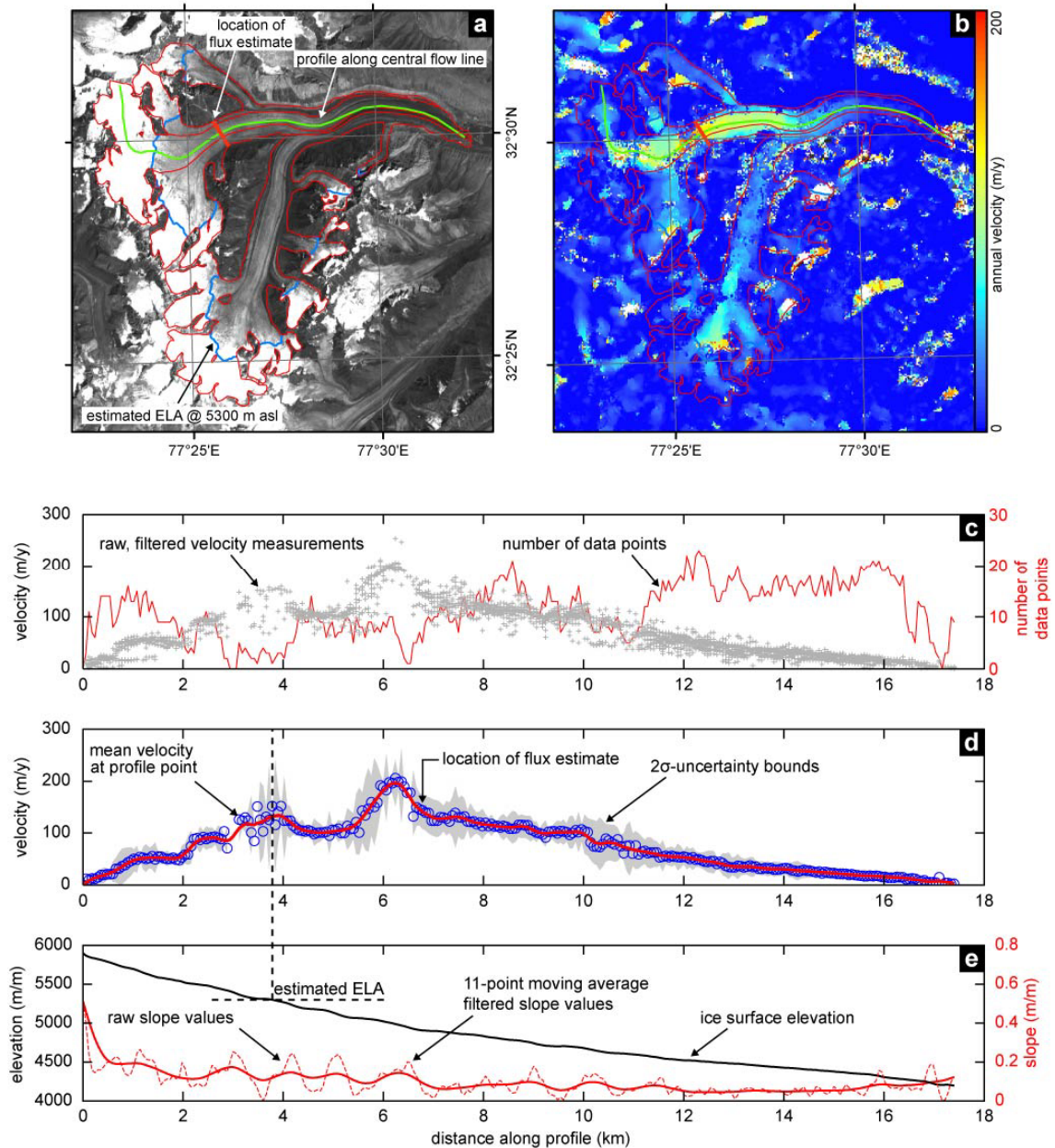
Figure D1: Sample glacier and derived velocity profile. (a) Orthorecified ASTER image of Samundar Tapu Glacier in the upper Chenab basin, Himachal Pradesh, India. (b) Mean annual surface-velocity field (Sep 2004-Sep 2006). (c) All available annual surface-velocity measurements along the central flow line, obtained from 23 image correlations within the measurement period 2000-2008. (d) Average velocity profile (red line) obtained from interpolation and smoothing of average velocities at each profile point (blue circles). (e) Surface elevation and surface slope along central-flow line from 90-m resolution SRTM DEM. For the thickness estimate, we smoothed the elevation profile over a length of five or eleven (this example) profile points, depending on glacier size, which we found was most efficient in suppressing distorting noise in the slope values while still preserving its overall shape.
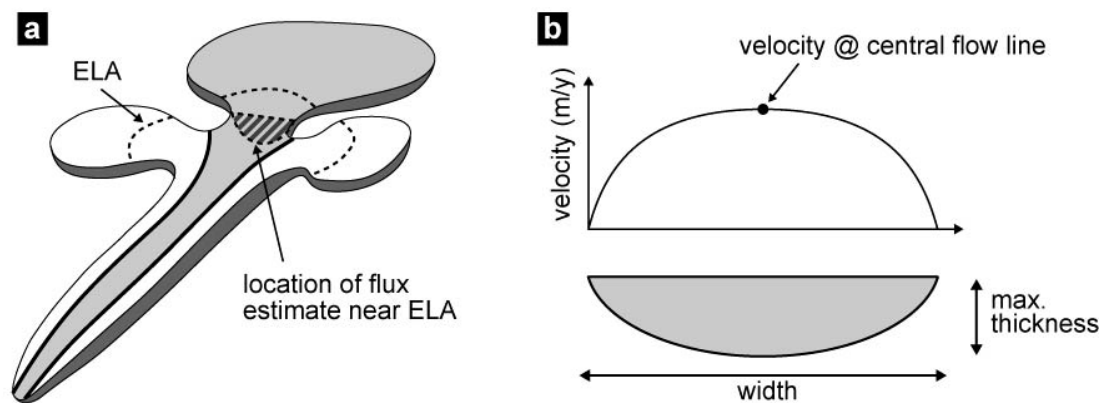
Figure D2: Determination of ice flux estimates near ELA. (a) Sketch showing the methodological principles for estimating the ice flux near the ELA. When the ELA is located in complex terrain, e.g., as in broad accumulation basins, estimating the ice flux from surface velocities and geometric glacier properties at the ELA is difficult. In such cases, we selected the next suitable location downstream, where the cross-sectional glacier shape is more easily approximated by a parabola. The glacier area related to the estimated ice flux is kept in grey and does not include the tributary accumulation basins and their corresponding ice lobes. The mean (median) altitudinal offsets of the positions where we estimated the ice flux from the ELAs are ~195 (92) m (Table D1). Several of the investigated glaciers are heavily fed by snow and ice avalanches, and have accumulation areas that are partly disconnected from the main glacier body, leading to estimated ELAs that are above or very close to the maximum elevation of the glacier. In such cases, flux estimates were only possible at considerable lower elevations. Note, however that in such cases the along-profile position of the flux estimate is still located in the upper half of the glacier-velocity profile. The mean ($\pm 1\sigma$) normalized along-profile point of all flux estimate is 0.39 ± 0.13 (Table D1). (b) The glacier surface velocity is highest at the central flow line, in the center of a transverse profile across the glacier surface.
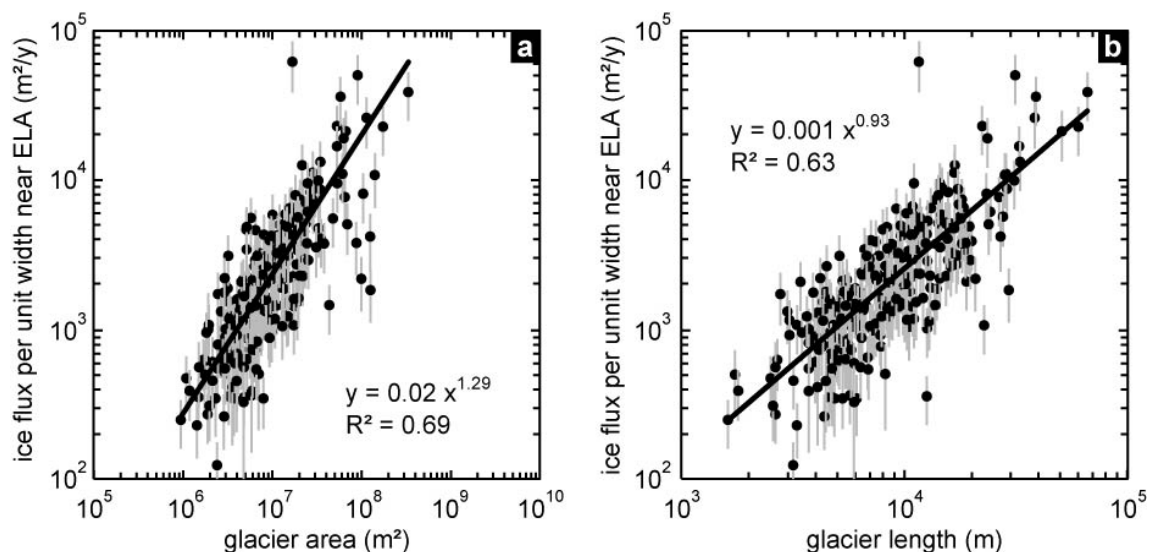
Figure D3: Uncertainties in the ice flux estimates. To estimate the uncertainties in the ice flux estimates, we propagated the uncertainties in the velocity measurements and made assumptions about the uncertainties in the other quantities. The glacier-surface velocity uncertainties are relatively small and contribute ~5 % to the ice flux uncertainties. The largest uncertainties are associated with our assumptions about constant driving stresses, the simplified parabolic glacier cross-sectional areas, and the scheme of relating the average cross-sectional area to the maximum surface velocity. We computed ice-flux uncertainties for 0 %, 10 %, and 20 % uncertainties in these factors, as no other information is available (Table D1). Inaccuracies in gravitational acceleration and the density of ice are minor and negligible. The plots above include error bars for the case of 20-% uncertainties in these factors, and include additional 10-% uncertainties in the slope values. We note that further ambiguity in our estimates is given by the choice of the location where we estimated the flux-estimate, in particular with respect to major confluences along the glacier. However, by differentiating between glacier areas from different glacier branches, we try to take such variations partly into account when comparing ice flux to glacier area (a), whereas such variations may be more important when comparing ice flux with glacier length (b). Lastly, it should be noted that in the Himalaya, glacier flow velocities are most likely not in full equilibrium with glacier sizes, i.e., glacier area and length. Thus, for given glacier areas, or lengths, we

expect steady state glacial-ice fluxes to be somewhat higher than they are at present. This would result in the data following a steeper slope in the trend, but the overall direction and main point of our argument is robust.

Table D1: Details of the ice-flux estimates.

ID	Length (km)	Area (km²)	Min. elev. (m asl)	Max. elev. (m asl)	Esti-mated ELA (m asl)[a]	Elev. of flux estimate (m asl)	Elev. diff. (m)[b]	Down-stream distance of flux estimate (norm.)	No. of data points	Glacier-surface velocity (m/yr)[c] Mean	SD	Average velocity (m/yr)[d]	Slope (°)	Width S1 (m)	S2	Depth (m)	Ice flux (m³/yr)	Ice flux uncertainties (%)[e] Low	Med.	High
101	8.70	7.64	4126	6151	5000	4889	111	0.255	2	56.5	12.6	54.6 ±1.3	9.7	567	0.7	0.60 84	1095635	2.47	18.18	36.11
102	12.59	3.26	4161	6167	5400	5421	-21	0.162	2	18.8	0.8	14.4 ±0.3	13	574	0.7	0.56 63	204751	2.10	18.13	36.07
103	9.35	7.13	3781	5864	5000	4491	509	0.250	0	NaN	NaN	66.9 ±0.0	14	499	0.7	0.57 59	790143	0.06	18.00	36.00
104	11.52	15.61	4139	6777	4850	4740	110	0.313	5	66.3	8.9	65.4 ±0.9	4.7	823	0.7	0.64 172	4146227	1.34	18.07	36.07
105	18.45	15.41	3641	6920	5200	4681	519	0.324	3	94.1	36.7	115.2 ±1.3	8.4	606	0.7	0.61 97	2878551	1.14	18.05	36.05
106	3.96	3.72	4244	4788	4600	4497	103	0.288	7	14.8	2.0	14.1 ±1.3	5.6	824	0.7	0.62 145	734733	9.13	20.21	37.19
107	3.17	2.41	4406	5653	4850	4758	92	0.358	0	NaN	NaN	8.4 ±1.9	21	516	0.7	0.53 40	63573	22.66	28.92	42.48
108	4.59	1.49	4396	5920	5100	5102	-2	0.300	2	13.2	1.1	20.2 ±0.3	18	491	0.7	0.54 46	171793	1.57	18.05	36.00
202	8.02	5.11	4348	5811	5150	5145	5	0.298	1	80.7	0.0	106.0 ±2.6	7.9	631	0.7	0.61 103	2952397	2.45	18.18	36.12
203	10.85	6.42	3676	6298	5200	4590	610	0.342	1	122.6	0.0	107.6 ±3.1	16	374	0.7	0.58 51	839856	2.90	18.22	36.10
204	7.19	3.79	4340	5962	5200	5178	22	0.334	4	58.3	36.1	63.2 ±6.8	18	552	0.7	0.53 45	585565	10.69	20.92	37.52
206	10.37	6.47	3567	5155	**5200**	4435	765	0.173	5	37.9	5.5	36.6 ±1.5	3	1038	0.7	0.66 273	4793897	4.00	18.46	36.27
208	18.61	20.03	3401	6383	5200	4624	576	0.190	5	59.1	8.5	59.8 ±1.2	4.7	974	0.7	0.62 174	4402750	2.05	18.14	36.11
209	16.82	21.51	3727	5919	5100	4966	134	0.413	11	96.5	13.1	98.1 ±7.6	2.9	1016	0.7	0.60 277	12765952	7.76	19.63	36.88
210	18.99	9.82	4023	7011	5550	5502	48	0.161	2	100.1	5.8	94.4 ±0.5	14	710	0.7	0.53 60	1485098	0.54	18.01	36.01
211	26.57	64.99	3960	6848	5180	5148	32	0.273	1	65.3	0.0	63.4 ±3.7	3	1076	0.7	0.65 267	8280988	5.81	18.94	36.52
301	6.63	5.15	3990	5768	4700	4563	137	0.368	14	72.0	13.8	69.3 ±10.0	7	724	0.7	0.61 116	2485201	14.39	23.06	38.81
302	16.77	28.48	3525	6835	4750	4091	659	0.449	10	209.3	39.6	210.0 ±29.6	6.1	1105	0.7	0.57 134	12413797	14.07	22.87	38.70
303	22.29	53.11	2971	6899	4850	4374	476	0.416	1	851.1	0.0	823.6 ±11.5	11	1221	0.7	0.53 75	28131987	1.40	18.07	36.05
304	31.38	90.73	3245	7070	4800	4732	68	0.423	4	291.3	55.8	279.1 ±15.3	2	1718	0.7	0.65 397	86627560	5.48	18.84	36.47
305	38.42	113.34	3339	6388	4700	4397	303	0.366	15	331.5	20.8	328.8 ±34.9	4.1	1698	0.7	0.57 199	44326822	10.60	20.91	37.58
306	38.84	58.13	3649	6203	4900	4951	-51	0.276	2	234.1	1.3	234.2 ±1.7	2.4	1314	0.7	0.65 339	47496151	0.72	18.04	36.06
307	50.69	66.60	3100	5558	4500	4568	-68	0.189	14	94.4	12.0	95.4 ±8.0	1.7	2066	0.7	0.65 490	43916189	8.35	19.87	37.01
308	5.27	4.85	4480	6005	4700	4790	-90	0.579	7	42.9	9.5	39.5 ±4.5	8.7	453	0.7	0.63 93	735625	11.33	21.28	37.77
309	28.81	27.92	2940	6767	4800	4599	201	0.311	1	328.7	0.0	274.2 ±11.8	9.5	1182	0.7	0.53 86	10322480	4.29	18.52	36.28
401	66.06	334.75	3074	5724	4850	4642	208	0.332	0	NaN	NaN	248.9 ±3.5	2.2	2491	0.7	0.60 372	96794020	1.41	18.08	36.08
402	7.08	6.51	4037	5488	4700	4711	-11	0.271	38	56.6	6.7	56.4 ±4.6	7.4	821	0.7	0.59 111	2115636	8.20	19.80	36.96
403	11.58	19.76	3770	5475	4900	4643	257	0.440	19	77.5	10.4	78.0 ±3.8	7.1	908	0.7	0.58 115	3318003	4.88	18.67	36.37
404	11.64	12.09	3643	4831	4400	4391	9	0.232	2	69.4	4.0	70.9 ±0.5	5	917	0.7	0.62 164	4621948	0.76	18.04	36.06
405	14.22	23.66	3696	4878	4000	4375	-375	0.325	2	42.9	4.3	42.4 ±0.6	3	1425	0.7	0.63 274	7288857	1.41	18.08	36.08
407	32.70	52.90	3953	5883	4800	4794	6	0.327	48	150.4	17.0	151.7 ±6.5	3.1	1638	0.7	0.61 259	27530790	4.29	18.53	36.31
408	28.56	60.89	4473	6100	5050	4937	113	0.456	5	101.1	20.9	90.0 ±2.8	2.8	1870	0.7	0.60 292	20628239	3.10	18.29	36.19
409	33.06	34.60	3507	5848	4600	4596	4	0.300	14	94.7	15.5	93.0 ±3.1	2.6	1427	0.7	0.64 318	18893283	3.34	18.33	36.21
410	5.28	4.04	4255	5571	4700	4713	-13	0.443	13	56.6	7.2	55.2 ±2.9	11	761	0.7	0.55 75	1213981	5.23	18.75	36.40
501	6.94	7.23	4039	5539	5050	4770	280	0.353	6	99.4	10.3	94.0 ±4.9	13	727	0.7	0.54 64	1656007	5.18	18.74	36.38
502	7.54	6.30	4505	5610	5150	5204	-54	0.277	12	32.2	12.1	33.0 ±4.5	5.4	837	0.7	0.62 150	1795824	13.64	22.60	38.54
503	7.65	6.97	4168	5473	5000	4602	398	0.529	7	49.4	3.5	49.0 ±5.0	7.6	541	0.7	0.63 107	1254890	10.25	20.73	37.47
504	8.35	3.29	3912	5831	5000	4446	554	0.412	2	93.9	18.2	79.3 ±0.5	16	759	0.7	0.53 52	1167859	0.68	18.01	35.99
505	9.12	17.02	3921	5335	4900	4538	362	0.402	9	35.2	6.7	35.1 ±1.9	5.5	839	0.7	0.62 149	1901021	5.39	18.81	36.45
506	11.78	21.72	4124	5806	4900	4714	186	0.553	5	32.7	8.8	27.9 ±0.8	4.1	1241	0.7	0.61 198	2920954	3.01	18.27	36.18
507	11.63	16.89	3473	4664	**4850**	4160	690	0.407	15	51.2	12.4	51.2 ±5.2	0.3	891	0.7	0.66 2618	55167632	10.13	20.68	37.45
508	14.42	53.34	3479	5473	4800	4183	617	0.418	13	94.7	13.6	92.9 ±5.9	3.4	1295	0.7	0.62 236	12326192	6.39	19.13	36.61
509	14.74	30.41	3768	6248	4900	4531	369	0.472	9	112.0	24.0	119.2 ±6.0	4.8	833	0.7	0.63 169	7382863	5.01	18.71	36.40
510	15.74	27.01	3831	5951	5100	4867	233	0.349	20	81.7	14.4	83.9 ±8.1	3.7	976	0.7	0.64 221	8094219	9.59	20.42	37.31
511	15.68	7.99	3905	5887	5200	4821	379	0.282	6	98.7	4.4	94.9 ±4.9	11	637	0.7	0.57 77	1849814	5.16	18.74	36.39
512	19.34	19.11	3496	5896	5000	4515	485	0.331	5	45.4	4.1	46.9 ±4.5	4.5	885	0.7	0.63 180	3301630	9.57	20.41	37.30
513	2.51	1.09	3899	4726	5000	4427	573	0.308	4	24.2	9.2	20.5 ±3.6	15	285	0.7	0.62 53	134335	17.54	25.13	40.04
514	2.70	1.69	4941	5765	5250	5168	82	0.511	7	26.7	6.2	29.5 ±3.5	16	379	0.7	0.58 52	236602	11.99	21.62	37.93
515	4.72	1.91	4363	5742	5200	5239	-39	0.405	4	32.8	1.1	31.8 ±21.0	11	489	0.7	0.60 75	487869	65.99	68.41	75.19
516	3.98	2.14	4230	5622	5000	5057	-57	0.313	13	24.1	10.4	24.7 ±7.4	13	503	0.7	0.57 61	303575	29.86	34.87	46.77
517	5.44	2.88	4104	5460	4900	4723	177	0.361	7	15.3	5.1	16.6 ±1.3	9.1	531	0.7	0.61 89	336814	7.67	19.58	36.84
518	5.13	4.23	4409	6283	5100	5065	35	0.474	7	19.3	1.6	18.6 ±0.9	6.6	1040	0.7	0.57 124	960107	4.96	18.69	36.38
519	4.07	4.44	4857	5700	5200	5150	50	0.544	8	49.1	6.5	47.2 ±3.8	12	666	0.7	0.56 70	861836	8.13	19.76	36.92
520	4.31	3.21	4431	5758	4950	4864	86	0.458	10	33.5	5.4	37.5 ±5.3	8.7	541	0.7	0.62 94	827314	14.14	22.90	38.71
521	4.89	2.60	4414	5928	5100	5094	6	0.424	5	37.7	1.3	34.0 ±4.5	14	689	0.7	0.54 60	527954	13.21	22.33	38.35
522	6.04	3.18	4066	5806	4950	4702	248	0.523	4	55.3	7.9	54.3 ±3.8	10	396	0.7	0.63 79	745449	6.94	19.30	36.69
523	60.14	173.56	3421	6300	5050	4869	181	0.244	11	142.8	5.9	143.4 ±4.6	2.2	2293	0.7	0.61 371	52107216	3.19	18.31	36.19
601	8.19	7.29	4526	5797	5200	5232	-32	0.329	5	40.1	9.4	39.6 ±1.3	5	1149	0.7	0.59 162	3052352	3.27	18.32	36.20
602	7.13	8.17	4601	5509	5000	4994	6	0.443	9	36.8	9.8	35.9 ±2.0	4.2	1305	0.7	0.60 196	3853106	5.68	18.90	36.49
603	7.71	5.83	4017	5193	4850	4742	108	0.252	6	14.5	2.3	14.5 ±1.9	3.3	837	0.7	0.66 246	1376563	13.36	22.44	38.45
604	12.65	5.58	4091	5497	5000	4908	92	0.197	8	11.5	2.0	11.9 ±1.9	5.4	767	0.7	0.63 150	780616	6.44	19.14	36.62
605	9.61	9.77	4127	5544	4900	4834	66	0.358	0	NaN	NaN	90.0 ±2.1	14	755	0.7	0.53 60	1506684	2.32	18.15	36.08
606	10.87	22.45	3892	5121	4850	4432	418	0.542	7	62.7	6.2	59.3 ±1.1	3.3	852	0.7	0.66 244	5682472	1.91	18.13	36.10
607	9.21	20.01	4216	5471	5050	5020	30	0.355	8	50.7	2.0	50.8 ±2.0	2.8	1462	0.7	0.63 287	9394002	3.99	18.46	36.27
608	10.57	5.50	3702	5278	4650	4409	241	0.190	8	26.0	1.8	25.7 ±4.0	5.2	753	0.7	0.64 156	1354662	15.48	23.76	39.23
609	10.71	11.96	4492	5656	5150	5104	46	0.389	1	30.1	5.0	30.7 ±1.9	2.7	1125	0.7	0.66 303	4833784	6.12	19.04	36.57
610	10.90	13.97	3731	5653	4900	4394	506	0.526	7	90.4	4.1	90.3 ±1.9	5.4	870	0.7	0.62 151	5144179	2.12	18.15	36.11
611	11.31	19.22	3954	5139	4700	4554	146	0.383	9	28.5	4.1	28.2 ±1.3	3.1	1127	0.7	0.65 263	3809022	4.74	18.64	36.36
612	11.75	5.77	4168	5707	5000	4994	6	0.236	4	65.5	3.8	62.8 ±1.4	4.2	649	0.7	0.66 192	3623231	2.27	18.17	36.12
613	13.81	20.46	4247	5547	4900	4881	19	0.320	3	79.6	4.6	77.1 ±2.0	3.7	1137	0.7	0.63 217	8399929	2.59	18.21	36.14
614	14.69	10.07	4247	5521	5000	4988	12	0.330	2	44.3	0.6	45.2 ±0.2	2.9	885	0.7	0.66 280	5188486	0.41	18.03	36.06

ID	Length (km)	Area (km²)	Min. elev. (m asl)	Max. elev. (m asl)	Esti-mated ELA (m asl)[a]	Elev. of flux estimate (m asl)	Elev. diff. (m)[b]	Down-stream distance of flux estimate (norm.)	No. of data points	Glacier-surface velocity (m/yr)[c] Mean	SD	Average velocity (m/yr)[d]	Slope (°)	Width (m)	S1	S2	Depth (m)	Ice flux (m³/yr)	Ice flux uncertainties (%)[e] Low	Med.	High
615	15.98	13.90	3862	5238	4650	4595	55	0.310	8	43.8	7.3	42.9 ±1.4	3.1	986	0.7	0.66	259	5074507	3.19	18.31	36.19
616	18.43	16.37	3945	5773	4900	5124	-224	0.261	5	106.6	5.5	105.7 ±0.3	5.4	1041	0.7	0.59	151	6840641	0.30	18.03	36.05
617	18.08	28.14	4034	5524	4800	4669	131	0.359	10	35.7	3.6	33.8 ±2.4	1.7	1333	0.7	0.67	469	9901566	6.98	19.33	36.72
618	23.55	63.05	4119	6047	5050	4768	282	0.492	14	83.1	11.7	82.6 ±4.2	1.6	1799	0.7	0.66	500	34335236	5.05	18.72	36.41
619	2.79	2.46	4942	5586	5150	5191	-41	0.596	14	20.4	2.9	19.7 ±2.6	4.3	657	0.7	0.66	190	1134609	13.10	22.28	38.36
620	2.99	2.67	4918	5537	5200	5209	-9	0.545	10	24.6	3.0	24.6 ±3.7	6.3	929	0.7	0.59	129	1219006	15.17	23.56	39.11
621	4.48	6.35	4786	5497	5000	5003	-3	0.668	8	22.2	9.9	21.2 ±2.2	3	873	0.7	0.66	270	2311575	10.32	20.77	37.50
622	6.47	5.19	4290	5108	4850	4710	140	0.369	7	12.2	2.5	11.6 ±2.0	4.2	1051	0.7	0.62	195	1032553	17.59	25.19	40.11
623	5.31	4.45	4868	5965	5200	5227	-27	0.543	5	12.7	4.1	11.0 ±1.4	3	611	0.7	0.67	274	862759	12.75	22.08	38.24
624	5.11	3.20	4141	4961	4650	4628	22	0.202	4	30.5	15.5	35.4 ±3.0	4.1	878	0.7	0.64	196	2733258	8.33	19.86	37.00
625	5.52	4.71	3904	4523	**4600**	4331	269	0.187	2	31.8	5.8	27.7 ±2.2	4.7	772	0.7	0.64	173	1662727	8.07	19.75	36.94
626	7.45	10.49	4824	5613	5180	5174	6	0.694	7	20.9	3.0	20.9 ±2.7	2.1	1150	0.7	0.67	395	4454528	12.72	22.06	38.23
627	5.81	4.42	4084	5346	4850	4865	-15	0.319	3	53.6	12.5	48.3 ±1.6	15	1065	0.7	0.56	55	1109125	3.35	18.31	36.15
701	6.36	6.64	3876	5476	5000	4745	255	0.528	7	26.7	4.8	28.1 ±2.3	5.7	707	0.7	0.63	143	1251257	8.23	19.81	36.97
702	7.20	5.99	4486	5318	5250	4972	278	0.367	12	27.8	3.0	25.3 ±3.5	7.6	953	0.7	0.56	108	1014600	13.66	22.61	38.54
703	7.02	6.44	4280	5428	5200	5016	184	0.479	5	28.9	6.7	30.5 ±0.5	3.8	974	0.7	0.64	213	2825917	1.73	18.11	36.09
704	8.82	7.24	4750	6162	5350	5286	64	0.395	2	25.4	13.9	36.6 ±1.3	4	988	0.7	0.63	201	3199748	3.50	18.36	36.22
705	9.60	13.70	4537	5799	5400	5023	377	0.431	8	38.0	3.6	35.9 ±2.5	2.7	957	0.7	0.66	299	4743156	6.97	19.33	36.72
706	9.84	13.90	4524	5767	5300	4959	341	0.451	16	19.9	10.1	19.7 ±3.2	4.5	1104	0.7	0.61	179	1664734	16.02	24.11	39.45
707	8.70	14.90	4830	5781	5350	5195	155	0.407	13	33.9	10.1	33.7 ±4.0	3.2	1333	0.7	0.63	251	4974796	11.73	21.50	37.91
708	10.08	5.37	4062	5785	5200	4929	271	0.327	0	NaN	NaN	73.8 ±1.0	11	756	0.7	0.54	71	1502433	1.33	18.06	36.04
709	10.44	11.83	4529	5642	5300	5052	248	0.374	7	73.4	10.6	69.8 ±0.3	7.2	701	0.7	0.61	113	2351649	0.37	18.02	36.04
710	13.62	11.23	3974	5544	5200	4759	441	0.247	3	28.0	11.1	32.3 ±0.4	7.5	763	0.7	0.59	109	1103580	1.25	18.06	36.06
711	13.14	15.84	3860	5631	5200	4966	234	0.338	5	86.2	7.8	85.5 ±0.8	4.4	1279	0.7	0.59	184	8292882	1.00	18.05	36.06
712	17.40	34.04	4195	5899	5300	4905	395	0.390	5	144.6	15.8	141.2 ±0.8	5.3	1163	0.7	0.58	152	10142567	0.56	18.03	36.05
713	3.72	2.42	5055	5555	5500	5348	152	0.387	8	8.5	3.8	10.3 ±1.5	7	401	0.7	0.66	116	219784	14.65	23.23	38.91
714	3.78	3.44	4272	5011	5400	4558	842	0.429	6	14.0	1.8	15.7 ±1.7	6.1	798	0.7	0.61	133	715384	10.72	20.97	37.60
715	4.44	5.49	4511	5376	5250	4989	261	0.568	0	NaN	NaN	79.5 ±0.9	14	590	0.7	0.55	58	1048756	1.12	18.03	36.02
716	4.56	3.53	4441	5023	5000	4806	194	0.329	7	13.8	4.2	14.6 ±2.5	5.6	729	0.7	0.63	146	682929	17.36	25.02	40.01
717	4.26	3.91	4893	5526	5450	5336	114	0.310	13	17.9	5.6	16.6 ±0.8	6.7	1021	0.7	0.57	122	823540	4.76	18.64	36.36
718	5.28	6.20	4507	5527	5400	4774	626	0.364	4	18.9	3.5	18.1 ±0.5	3.2	932	0.7	0.66	253	1967770	2.85	18.25	36.16
719	5.22	4.67	5032	5545	5400	5443	7	0.287	1	12.2	0.0	14.7 ±0.3	4.5	1365	0.7	0.58	179	1454561	2.22	18.16	36.12
720	5.64	4.77	4091	5202	4800	4314	486	0.415	3	30.0	4.9	25.2 ±0.2	7.7	590	0.7	0.62	105	679481	0.86	18.04	36.05
801	4.92	4.67	5115	5981	5550	5553	-3	0.268	5	19.9	4.5	20.9 ±2.0	7.8	658	0.7	0.61	105	617320	9.52	20.38	37.28
802	5.52	5.31	4066	4651	**5000**	4480	520	0.250	20	21.0	5.4	20.2 ±5.2	4	695	0.7	0.66	201	1307110	25.52	31.24	44.17
803	7.26	9.09	4248	5526	5000	4827	173	0.595	2	36.3	15.7	44.5 ±1.7	14	714	0.7	0.53	60	702900	3.75	18.39	36.20
804	7.44	6.13	4524	5535	5150	5142	8	0.282	14	19.6	3.6	20.1 ±3.6	6.4	780	0.7	0.61	128	855555	18.02	25.49	40.06
805	7.80	4.54	4876	5906	5450	5457	-7	0.308	8	28.5	5.7	30.0 ±3.1	10	866	0.7	0.54	81	793558	10.25	20.73	37.46
806	8.88	8.41	4644	5556	5100	5170	-70	0.378	10	17.4	3.7	19.0 ±2.9	4.3	732	0.7	0.65	191	1210351	15.41	23.71	39.21
807	8.46	6.02	4247	5317	5000	4928	72	0.291	7	33.5	3.7	33.1 ±0.7	5.4	885	0.7	0.61	151	1884065	2.18	18.16	36.11
808	10.50	5.49	4124	5371	5000	4882	118	0.240	14	19.8	3.8	18.9 ±3.5	6.7	519	0.7	0.65	121	538043	18.34	25.71	40.44
809	11.28	10.78	4229	5417	4950	4917	33	0.282	2	46.9	7.5	40.9 ±0.0	6.4	540	0.7	0.65	126	1271163	0.04	18.02	36.04
810	10.20	16.72	3905	5611	5000	4541	459	0.529	8	90.8	28.1	84.7 ±1.4	5.2	673	0.7	0.65	155	4031533	1.65	18.10	36.09
811	15.42	19.91	3943	5315	4900	4713	187	0.319	21	34.0	10.9	31.5 ±5.1	2.4	960	0.7	0.67	345	4890088	16.06	24.14	39.47
812	27.60	23.85	3977	5651	5150	5140	10	0.278	13	42.9	8.6	44.3 ±3.6	2.9	987	0.7	0.66	278	5603854	8.06	19.75	36.94
813	4.14	3.79	4198	5511	5100	4639	461	0.638	23	21.3	7.3	23.0 ±4.9	9.2	550	0.7	0.61	88	477199	21.38	27.96	41.90
814	4.74	2.96	5109	5930	5500	5524	-24	0.304	1	12.5	0.0	10.7 ±1.3	7.7	481	0.7	0.64	106	243442	12.39	21.87	38.15
815	5.04	3.93	5016	6124	5450	5413	37	0.369	12	10.3	1.1	10.5 ±1.9	5.4	727	0.7	0.64	150	513638	18.14	25.57	40.35
816	6.48	7.56	4390	5246	4900	4707	193	0.435	23	14.9	2.3	14.5 ±5.1	3.9	952	0.7	0.64	207	1281369	35.30	39.64	50.46
817	5.70	5.84	3695	4998	**5850**	4101	1749	0.379	0	NaN	NaN	17.3 ±0.3	15	564	0.7	0.55	54	204324	1.87	18.09	36.04
901	6.30	6.21	5440	5985	5750	5768	-18	0.486	10	10.7	2.1	10.8 ±1.8	4.1	867	0.7	0.65	200	843648	16.62	24.52	39.70
902	8.52	14.65	5215	6154	5500	5521	-21	0.592	17	16.7	2.5	16.2 ±2.1	4.9	699	0.7	0.65	167	859194	12.89	22.16	38.28
903	8.52	15.01	5057	6429	5450	5425	25	0.542	10	15.2	1.6	16.0 ±0.8	4.7	907	0.7	0.63	173	1108352	5.25	18.77	36.43
904	3.30	1.43	5388	6228	5800	5762	38	0.509	8	9.5	2.9	9.7 ±1.7	14	450	0.7	0.58	58	102368	17.38	25.02	39.98
905	4.38	2.88	5595	6151	5750	5917	-167	0.370	1	4.7	0.0	3.9 ±0.7	5.5	661	0.7	0.64	148	172476	17.99	25.46	40.29
906	5.58	3.65	5283	6028	5650	5620	30	0.505	10	10.9	1.9	11.4 ±2.0	6.2	553	0.7	0.65	130	363755	17.95	25.44	40.27
907	6.12	3.72	5197	6048	5500	5526	-26	0.637	14	7.9	1.9	7.3 ±1.9	7.6	522	0.7	0.63	107	179448	25.31	31.07	44.04
1001	7.86	6.22	4560	5630	5200	5075	125	0.366	3	14.2	6.4	15.2 ±1.6	6.9	733	0.7	0.61	119	563897	10.30	20.76	37.49
1002	10.68	8.07	4025	5842	5150	5058	92	0.275	2	192.4	3.0	182.2 ±1.4	13	623	0.7	0.55	61	2684479	0.78	18.02	36.01
1003	13.98	13.58	4115	5683	4900	4898	2	0.279	4	21.9	2.9	22.0 ±3.0	4.3	774	0.7	0.65	187	1449367	13.83	22.72	38.61
1004	17.10	18.78	4330	5930	4950	4963	-13	0.442	1	13.7	0.0	13.8 ±0.7	3.3	951	0.7	0.65	245	2595494	3.00	18.27	36.18
1005	3.72	4.03	4753	5478	5200	5065	135	0.307	4	44.7	11.2	38.6 ±3.0	15	938	0.7	0.54	56	763424	7.78	19.61	36.83
1006	8.10	17.49	3788	5335	4750	4216	534	0.385	6	28.8	3.5	26.8 ±1.3	6.1	1159	0.7	0.57	133	1652920	4.83	18.66	36.37
1007	5.58	4.91	4360	5255	5000	4731	269	0.398	5	21.6	3.8	22.6 ±1.3	4.6	775	0.7	0.64	176	1377547	5.53	18.85	36.47
1101	6.00	5.89	5015	6076	5500	5530	-30	0.260	6	16.2	2.5	14.7 ±2.2	3.8	833	0.7	0.65	213	1192162	15.14	23.54	39.10
1102	10.86	7.31	4775	5932	5400	5434	-34	0.326	0	NaN	NaN	21.7 ±1.4	5.4	823	0.7	0.62	151	1166267	6.56	19.18	36.64
1103	10.32	15.44	5062	6285	5650	5578	72	0.326	8	21.0	5.2	20.1 ±2.3	3.4	853	0.7	0.66	239	1897215	11.26	21.25	37.77
1104	12.60	14.67	3829	4966	**5350**	4501	849	0.271	5	32.5	2.1	32.1 ±1.6	2.8	1024	0.7	0.66	293	4451588	5.02	18.71	36.40
1105	12.90	7.70	4608	6596	5700	5739	-39	0.298	2	51.5	17.1	61.8 ±0.6	17	797	0.7	0.54	48	899699	0.89	18.01	35.99
1106	18.78	10.23	4350	6424	5500	5517	-17	0.166	2	59.4	7.2	68.0 ±0.4	6.6	959	0.7	0.58	124	3283101	0.55	18.00	36.01
1107	19.98	20.93	3749	6011	5450	4721	729	0.348	7	36.1	5.4	36.8 ±3.3	3.5	817	0.7	0.66	229	3183130	7.84	19.66	36.89
1108	31.08	32.89	4003	6329	5150	5134	16	0.214	1	79.3	0.0	84.2 ±3.0	3	1410	0.7	0.63	268	14043799	3.54	18.37	36.23
1109	4.74	2.47	5433	6147	5700	5700	0	0.468	6	13.4	2.6	13.8 ±1.2	6.6	381	0.7	0.67	123	302350	8.50	19.92	37.03
1110	4.98	6.16	5036	5501	5450	5296	154	0.494	4	13.4	2.3	12.1 ±2.3	3.5	964	0.7	0.65	232	1237541	19.23	26.35	40.86
1111	4.86	2.32	5169	5864	5700	5680	20	0.173	5	6.8	2.3	6.1 ±1.6	6.5	554	0.7	0.64	126	190111	25.87	31.53	44.37
1112	4.92	2.96	4075	5659	5400	4679	721	0.366	5	30.3	3.2	28.9 ±1.2	12	399	0.7	0.62	71	353770	3.97	18.44	36.24
1113	5.00	6.41	5201	5980	5700	5712	-12	0.424	9	19.8	3.7	20.5 ±3.2	8.7	1061	0.7	0.54	94	772597	15.54	23.79	39.24
1114	6.36	5.85	5316	6484	5750	5741	9	0.293	4	19.5	4.9	18.1 ±1.4	5.4	819	0.7	0.62	152	975714	7.47	19.51	36.81
1115	6.24	6.74	4985	6322	5500	5459	41	0.279	11	20.1	3.1	17.6 ±3.0	5.8	856	0.7	0.61	141	904448	16.89	24.70	39.81
1201	6.72	7.55	5308	5890	5650	5674	-24[b]	0.277	5	15.4	2.4	16.2 ±0.3	3.9	1239	0.7	0.61	210	1799587	1.71	18.11	36.09

Appendix D: Supplementary material for chapter 7

ID	Length (km)	Area (km²)	Min. elev. (m asl)	Max. elev. (m asl)	Esti-mated ELA (m asl)[a]	Elev. of flux estimate (m asl)	Elev. diff. (m)[b]	Down-stream distance of flux estimate (norm.)	No. of data points	Glacier-surface velocity (m/yr)[c] Mean	SD	Average velocity (m/yr)[d]	Slope (°)	Width S1 (m)	S2	Depth (m)	Ice flux (m³/yr)	Ice flux uncertainties (%)[e] Low	Med.	High
1202	6.18	9.62	5286	5987	5700	5690	10	0.437	3	22.7	1.4	22.1 ±0.4	5.3	928	0.7	0.61	152	1334343	1.68	18.10	36.09
1203	9.18	10.43	5139	5835	5650	5660	-10	0.209	1	40.8	0.0	40.1 ±1.8	5.3	1225	0.7	0.58	154	3070684	4.56	18.59	36.33
1204	11.04	24.80	5191	5911	5650	5595	55	0.380	2	68.5	5.0	65.3 ±1.1	2.5	1635	0.7	0.63	330	15538993	1.73	18.11	36.10
1205	11.10	22.80	5086	5993	5650	5565	85	0.497	1	52.0	0.0	50.7 ±1.6	3.9	1144	0.7	0.62	207	5202406	3.14	18.30	36.16
1206	5.16	7.13	5376	5889	5650	5610	40	0.430	11	11.9	1.1	12.0 ±1.5	3	791	0.7	0.67	268	1191693	12.08	21.70	38.02
1207	7.68	8.64	5405	6147	5800	5751	49	0.453	3	21.8	3.7	23.7 ±1.6	2.9	1031	0.7	0.66	282	3192861	6.71	19.23	36.67
1301	6.00	4.56	5182	6089	5850	5815	35	0.330	2	28.9	0.3	29.3 ±0.3	7.3	466	0.7	0.65	111	690194	1.03	18.05	36.06
1302	6.54	4.35	5046	5832	5600	5454	146	0.431	1	29.4	0.0	28.4 ±1.4	7.7	505	0.7	0.64	106	681426	4.75	18.64	36.35
1303	6.42	13.15	5131	6333	5600	5595	5	0.495	3	44.8	3.0	44.6 ±0.4	6.4	838	0.7	0.60	128	2011927	0.82	18.04	36.05
1304	7.50	9.61	5472	6304	5950	5956	-6	0.352	0	NaN	NaN	21.0 ±1.6	3.6	951	0.7	0.65	224	2034782	7.69	19.60	36.86
1305	7.92	9.54	4148	5522	**5700**	4817	883	0.189	6	37.8	2.7	39.4 ±4.4	10	946	0.7	0.54	82	1152509	11.20	21.21	37.73
1306	9.30	7.66	4980	6854	5750	5704	46	0.290	3	57.6	5.0	57.2 ±1.9	7.4	907	0.7	0.57	110	2273783	3.28	18.32	36.19
1307	8.46	11.71	5441	6668	5950	5876	74	0.497	5	29.1	3.2	29.4 ±1.0	4.6	788	0.7	0.64	177	1835979	3.50	18.36	36.22
1308	9.60	9.35	3982	5069	**5700**	4545	1155	0.213	1	34.1	0.0	38.1 ±1.7	4.4	727	0.7	0.65	186	2343894	4.57	18.60	36.34
1309	10.68	23.33	5327	6422	6000	5778	222	0.517	8	32.6	2.9	31.4 ±1.0	3.8	1199	0.7	0.62	217	3538348	3.15	18.30	36.19
1310	10.80	11.57	4112	6524	5950	5899	51	0.267	3	97.4	7.5	95.7 ±2.5	7.2	1088	0.7	0.56	114	4637267	2.63	18.21	36.14
1311	13.86	12.04	4467	6226	5850	5080	770	0.329	2	60.4	15.3	54.8 ±1.1	5.2	860	0.7	0.62	157	3216628	1.92	18.13	36.10
1312	12.72	20.08	3441	4529	**5700**	4106	1594	0.208	7	64.0	10.1	61.5 ±5.2	4.1	1150	0.7	0.62	200	6128415	8.40	19.89	37.02
1313	15.30	16.48	4469	6411	5800	5028	772	0.451	5	94.6	6.8	94.9 ±2.8	6.7	589	0.7	0.64	122	3055383	2.98	18.27	36.17
1314	17.52	28.98	3674	6243	5800	5686	114	0.329	1	170.1	0.0	166.2 ±1.3	7.3	1613	0.7	0.53	111	11058124	0.77	18.04	36.05
1315	4.26	3.03	5274	6251	5800	5789	11	0.451	2	30.5	3.3	30.9 ±0.4	13	499	0.7	0.57	62	380309	1.24	18.05	36.03
1316	3.30	1.95	5478	6178	5700	5678	22	0.509	5	23.0	3.9	18.5 ±0.8	6.6	385	0.7	0.67	123	411014	4.53	18.58	36.33
1317	3.72	3.00	5267	6101	5650	5466	184	0.532	6	22.5	1.0	22.0 ±1.0	7.7	565	0.7	0.62	106	568525	4.35	18.54	36.30
1318	4.38	4.84	5118	6031	5650	5461	189	0.562	2	31.0	2.6	35.1 ±0.2	8.9	573	0.7	0.61	91	784726	0.67	18.03	36.04
1319	4.14	3.18	5465	6384	5900	5883	17	0.406	3	25.5	3.3	21.4 ±2.4	9.7	650	0.7	0.58	84	474947	11.09	21.15	37.70
1320	4.74	9.88	5450	6253	5800	5690	110	0.658	10	15.7	3.1	15.9 ±1.7	5.6	958	0.7	0.60	144	920773	10.74	20.98	37.61
1321	4.98	6.56	5053	6372	5900	5816	84	0.410	0	NaN	NaN	48.0 ±0.4	10	865	0.7	0.54	78	1223594	0.86	18.03	36.03
1322	5.10	1.78	4066	4829	**5700**	4655	1045	0.141	2	12.2	1.7	12.4 ±0.2	7.3	506	0.7	0.64	112	314124	1.92	18.12	36.10
1323	5.34	7.87	5525	6339	6000	5849	151	0.506	3	20.0	4.4	19.0 ±2.3	4.8	1152	0.7	0.60	171	1568097	11.87	21.58	37.95
1324	5.46	5.32	5258	6042	5800	5552	248	0.648	6	31.8	3.6	31.4 ±1.1	12	442	0.7	0.60	66	383776	3.54	18.35	36.19
1325	6.42	8.83	5516	6428	5900	5760	140	0.617	1	20.3	0.0	18.2 ±1.5	4.3	1184	0.7	0.61	190	1746852	8.49	19.92	37.04
1326	5.70	5.08	5328	6088	5800	5703	97	0.421	4	31.2	0.8	31.5 ±0.7	8.3	652	0.7	0.60	98	846507	2.05	18.13	36.09
1401	5.28	5.61	5641	7154	6150	6154	-4	0.511	4	15.6	2.6	13.3 ±0.7	6.2	860	0.7	0.60	131	632105	5.43	18.82	36.45
1402	10.02	9.82	4996	6106	5600	5511	89	0.192	49	22.0	2.0	21.3 ±5.4	5	976	0.7	0.61	163	1439763	25.62	31.33	44.23
1403	8.40	9.77	5051	5802	5750	5374	376	0.450	6	20.8	5.3	20.6 ±1.3	5.2	956	0.7	0.61	157	1318476	6.39	19.12	36.61
1404	7.02	12.99	5167	6293	6000	5807	193	0.419	28	20.7	1.0	20.6 ±3.6	6.8	710	0.7	0.61	119	744262	17.58	25.18	40.10
1405	7.38	13.14	5152	6056	5800	5540	260	0.325	10	40.4	4.3	40.7 ±0.8	6.4	590	0.7	0.64	126	1327247	1.91	18.12	36.09
1406	6.96	9.08	4812	5324	**6300**	5156	1144	0.198	32	35.8	3.6	36.2 ±3.6	4.3	1062	0.7	0.62	188	3136323	10.05	20.64	37.43
1407	8.58	6.61	4942	5806	5800	5370	430	0.196	24	22.5	2.2	23.0 ±3.6	4.1	797	0.7	0.65	197	1646446	15.62	23.85	39.29
1408	8.82	13.65	5619	6729	5950	5862	88	0.667	24	41.0	9.3	37.9 ±2.8	3.8	873	0.7	0.65	215	3244377	7.33	19.46	36.79
1409	8.76	10.29	5031	7554	6300	5243	1057	0.493	32	23.0	2.1	22.9 ±3.7	5.1	1439	0.7	0.56	159	2061026	16.14	24.20	39.50
1410	8.82	8.39	5575	7017	6200	6169	31	0.354	1	23.1	0.0	23.3 ±0.3	6.2	755	0.7	0.62	131	996988	1.29	18.07	36.07
1411	10.26	9.57	5406	6360	6150	5981	169	0.345	17	19.8	3.9	19.4 ±2.2	5.9	786	0.7	0.62	137	910464	11.54	21.40	37.85
1412	12.66	13.88	5341	6520	6050	6065	-15	0.185	16	47.7	3.2	47.5 ±2.6	6	676	0.7	0.63	137	1934726	5.41	18.82	36.45
1413	10.86	8.72	5394	6411	6150	6054	96	0.238	5	33.8	4.8	34.3 ±0.3	4.3	744	0.7	0.65	189	2186900	0.85	18.05	36.06
1414	11.04	10.74	4794	5682	**5700**	5230	470	0.152	6	19.9	0.9	18.0 ±1.2	5.5	758	0.7	0.63	148	892641	6.46	19.15	36.62
1415	11.28	19.02	5611	6648	6300	6012	288	0.590	59	20.1	2.2	19.7 ±5.2	4.5	1083	0.7	0.61	180	1646714	26.16	31.77	44.54
1416	15.36	22.11	4950	6111	6000	5675	325	0.211	16	39.9	2.7	40.1 ±2.9	5.9	997	0.7	0.59	137	2264076	7.26	19.43	36.77
1417	13.08	12.73	4564	6466	6050	5854	196	0.358	23	27.4	2.8	26.7 ±3.6	4.9	1046	0.7	0.61	167	1993407	13.55	22.55	38.51
1418	16.14	11.22	5097	6623	6150	6015	135	0.227	14	32.6	5.6	32.2 ±2.5	4.5	868	0.7	0.64	182	2281506	7.78	19.63	36.88
1419	14.40	13.28	5420	6463	6200	5890	310	0.275	46	41.7	4.3	40.8 ±4.9	6.4	840	0.7	0.60	128	1838598	11.96	21.63	37.98
1420	16.38	13.79	5180	6456	5800	5803	-3	0.227	7	56.4	8.7	56.5 ±2.0	5.7	1242	0.7	0.57	144	4027725	3.45	18.35	36.21
1421	1.62	0.95	5470	5964	5700	5751	-51	0.296	5	17.3	2.8	15.0 ±0.5	19	404	0.7	0.55	43	100150	3.24	18.27	36.10
1422	15.96	19.53	4566	5614	5500	5359	141	0.241	20	43.6	4.3	43.3 ±3.8	3.2	1547	0.7	0.61	257	7353213	8.73	20.03	37.09
1423	17.34	15.06	4921	7841	5800	5908	-108	0.374	0	NaN	NaN	179.9 ±0.0	18	779	0.7	0.54	46	2429199	0.01	17.98	35.97
1424	1.74	1.75	5542	5824	5650	5629	21	0.690	24	7.9	1.4	7.3 ±2.1	5.2	807	0.7	0.62	156	432868	28.31	33.56	45.83
1425	19.62	21.71	4705	7056	6000	5322	678	0.229	2	118.6	24.2	121.0 ±6.0	7.8	1015	0.7	0.55	105	4961906	0.49	18.03	36.04
1426	2.64	1.88	5871	6718	6200	6065	135	0.591	3	7.8	1.0	7.5 ±0.5	9.6	575	0.7	0.60	85	154778	6.31	19.09	36.58
1427	5.64	3.89	5187	5735	5600	5533	67	0.213	32	12.9	1.9	13.2 ±2.4	6.1	652	0.7	0.63	133	507281	17.97	25.45	40.27
1428	4.08	3.57	4821	5334	**6300**	5041	1259	0.265	16	6.1	1.1	5.8 ±2.7	5.1	842	0.7	0.63	161	345333	47.00	50.33	59.23
1429	3.48	1.83	5040	5777	5750	5511	239	0.362	6	23.7	1.3	23.1 ±0.6	8.2	704	0.7	0.59	100	668545	2.65	18.21	36.13
1430	4.62	3.29	4970	5783	**6300**	5151	1149	0.338	22	9.2	0.9	8.6 ±3.0	4.9	737	0.7	0.64	165	470620	34.61	39.03	49.98
1431	3.72	5.88	5968	6539	6250	6228	22	0.516	13	5.5	1.2	5.8 ±2.9	5.1	1066	0.7	0.60	159	410549	49.61	52.78	61.32
1432	6.84	4.48	4986	5662	**5700**	5323	377	0.193	8	10.1	2.3	10.2 ±1.6	5.6	807	0.7	0.62	146	521628	15.43	23.73	39.21
1433	8.22	7.04	4787	6059	5550	5005	545	0.402	11	4.9	1.4	4.8 ±2.2	3.5	900	0.7	0.65	231	452093	45.55	48.99	58.09
1434	5.34	6.98	5107	5700	**5800**	5374	426	0.393	49	24.4	2.2	24.5 ±5.0	4.7	1111	0.7	0.60	173	1980673	20.41	27.23	41.43
1435	5.34	6.76	5028	5644	**5700**	5400	300	0.270	7	16.2	2.6	15.9 ±1.6	6.8	696	0.7	0.62	120	577137	9.75	20.49	37.34
1436	4.74	4.83	5744	6350	6100	6071	29	0.405	2	4.6	0.5	5.0 ±0.1	4.9	995	0.7	0.61	164	349879	2.57	18.21	36.14
1437	5.28	7.99	5900	6548	6300	6244	56	0.432	3	5.1	0.8	6.0 ±0.6	6	939	0.7	0.60	136	323690	10.47	20.84	37.54
1438	5.46	5.21	5679	6460	6200	6183	17	0.286	1	15.3	1.3	15.2 ±1.7	7.7	708	0.7	0.60	106	628067	7.87	19.66	36.89
1501	10.14	8.46	4691	7289	5500	5208	292	0.426	4	48.9	5.0	47.8 ±2.1	8.5	483	0.7	0.63	95	971043	4.48	18.57	36.31
1502	5.64	4.67	5283	6338	5600	5591	9	0.489	2	12.2	6.3	14.5 ±0.8	3.2	697	0.7	0.67	257	1219668	5.44	18.83	36.46
1503	6.42	9.30	5166	6000	5500	5577	-77	0.579	4	26.4	2.3	25.9 ±1.5	10	1801	0.7	0.60	81	1582202	5.67	18.88	36.47
1504	9.42	6.06	5019	5840	5650	5630	20	0.191	4	28.0	6.6	25.7 ±1.7	6.4	727	0.7	0.62	127	1028133	6.53	19.17	36.63
1505	7.08	9.28	5152	7240	5550	5560	-10	0.449	20	54.3	2.2	54.4 ±3.9	4.8	1067	0.7	0.61	170	4212027	7.23	19.42	36.73
1506	9.18	17.56	5496	7141	5950	5887	63	0.366	17	35.5	2.5	35.4 ±4.1	7.1	1038	0.7	0.56	115	1659785	11.53	21.39	37.84
1507	9.66	9.76	4193	5499	5400	4911	489	0.236	4	81.9	3.1	80.0 ±0.8	6.1	1199	0.7	0.56	134	5053150	0.98	18.05	36.06
1508	22.74	17.40	4303	8021	5450	5429	21	0.219	0	NaN	NaN	52.6 ±2.1	15	905	0.7	0.54	54	965016	3.99	18.43	36.21
1509	19.74	25.30	4584	8098	5500	5385	115	0.283	16	86.1	6.6	83.3 ±2.6	9.2	822	0.7	0.56	89	2384720	3.09	18.28	36.16
1510	24.30	24.95	4216	6383	5400	5182	218	0.242	13	54.9	5.9	54.3 ±3.4	3.3	1081	0.7	0.65	249	6644612	6.28	19.09	36.59

ID	Length (km)	Area (km²)	Min. elev. (m asl)	Max. elev. (m asl)	Estimated ELA (m asl)[a]	Elev. of flux estimate (m asl)	Elev. diff. (m)[b]	Downstream distance of flux estimate (norm.)	No. of data points	Glacier-surface velocity (m/yr)[c] Mean	SD	Average velocity (m/yr)[d]	Slope (°)	Width (m)	S1	S2	Depth (m)	Ice flux (m³/yr)	Ice flux uncertainties (%)[e] Low	Med.	High
1511	1.80	1.19	5327	6009	5700	5696	4	0.367	16	31.9	5.6	27.7 ±2.9	23	627	0.7	0.55	36	243381	10.30	20.70	37.36
1512	2.64	1.51	5701	6467	5850	5852	-2	0.500	10	10.6	1.9	10.7 ±3.2	7.1	476	0.7	0.65	115	265825	30.31	35.26	47.09
1513	4.80	2.79	4754	5764	5400	5390	10	0.325	8	34.8	2.5	32.5 ±1.9	16	484	0.7	0.55	51	306240	5.74	18.88	36.44
1514	2.58	1.98	5528	6350	5800	5670	130	0.791	9	13.3	2.4	12.6 ±2.8	14	353	0.7	0.61	58	109003	22.35	28.70	42.37
1515	3.06	3.38	5401	6294	5650	5548	102	0.784	7	39.6	3.0	39.0 ±1.2	11	550	0.7	0.58	73	634043	3.08	18.27	36.15
1516	3.66	3.41	5473	6127	5750	5766	-16	0.574	7	28.5	5.6	28.0 ±2.4	8.1	555	0.7	0.62	100	678574	8.70	20.01	37.07
1517	3.42	4.51	5206	5906	5600	5614	-14	0.351	2	47.6	25.7	48.1 ±0.4	7.5	899	0.7	0.57	108	1866857	0.77	18.04	36.05
1518	4.62	8.53	5567	6586	6000	5681	319	0.714	11	33.9	1.0	33.1 ±3.3	7.6	563	0.7	0.63	108	884367	10.06	20.64	37.42
NaN	NaN	NaN	5246	6489	5750	NaN	NaN	0.000	NaN	NaN	NaN	NaN ±NaN	NaN	NaN	NaN	NaN	NaN	NaN	NaN	NaN	NaN
1520	3.90	2.87	5167	6126	5700	5712	-12	0.539	5	59.8	4.0	58.2 ±1.4	11	733	0.7	0.56	77	1294740	2.34	18.16	36.10
1521	4.32	4.68	5484	6449	5800	5669	131	0.694	21	29.0	5.7	29.0 ±5.1	8.4	746	0.7	0.58	98	855124	17.57	25.16	40.09
1522	4.68	4.17	5504	6703	5900	5855	45	0.526	21	19.2	2.9	19.6 ±4.2	10	608	0.7	0.58	79	381647	21.26	27.86	41.83
1523	4.68	6.29	5547	6560	5950	5921	29	0.436	13	31.7	8.2	29.8 ±4.2	6.9	776	0.7	0.60	118	1148887	13.92	22.77	38.64
1524	4.80	3.63	5282	6159	5650	5639	11	0.575	8	14.6	2.4	13.9 ±0.7	4.8	708	0.7	0.65	170	759630	5.36	18.80	36.45
1525	5.22	3.30	5205	6539	5600	5580	20	0.506	7	37.8	5.3	36.4 ±1.6	11	473	0.7	0.61	76	559572	4.33	18.53	36.28
1526	5.58	4.86	5264	6060	5800	5770	30	0.505	8	41.5	5.7	39.0 ±2.0	8	682	0.7	0.60	101	1133380	5.03	18.71	36.39
1527	5.46	6.50	5286	6166	5700	5703	-3	0.407	3	43.1	5.7	35.6 ±0.6	8.4	636	0.7	0.60	96	916256	1.67	18.10	36.07
1601	6.96	8.63	4523	5897	4950	4991	-41	0.612	9	123.7	12.9	117.7 ±1.4	14	502	0.7	0.56	57	1323083	1.15	18.04	36.02
1602	6.48	7.75	5504	6658	6050	6039	11	0.482	1	39.1	0.0	44.5 ±0.9	6.1	1245	0.7	0.56	133	2887204	1.99	18.13	36.10
1603	6.78	6.82	5359	6628	5950	5759	191	0.593	35	56.0	3.1	55.4 ±4.9	6.4	660	0.7	0.63	127	2048350	8.92	20.11	37.13
1604	9.78	12.05	4128	5570	5300	4597	703	0.313	10	24.3	4.2	22.9 ±2.3	2.8	987	0.7	0.66	286	2993123	10.05	20.64	37.43
1605	8.34	5.19	4483	5986	5400	5244	156	0.417	3	65.8	16.6	75.2 ±0.6	5.7	678	0.7	0.64	144	3287035	0.81	18.04	36.06
1606	8.40	13.30	5185	6513	5650	5603	47	0.514	0	NaN	NaN	61.0 ±1.6	5.5	1452	0.7	0.55	148	5047768	2.59	18.21	36.14
1607	9.36	11.25	5002	6691	5750	5738	12	0.583	13	29.4	9.5	25.2 ±3.4	2.8	1312	0.7	0.64	287	4259609	13.29	22.40	38.43
1608	10.92	15.91	5345	6906	6150	5615	535	0.462	13	42.7	8.2	45.3 ±4.1	3.9	807	0.7	0.65	210	3486167	8.97	20.13	37.15
1609	12.12	19.69	4808	6408	5700	5102	598	0.431	1	64.8	0.0	66.6 ±0.6	12	966	0.7	0.53	66	1564771	0.89	18.03	36.02
1610	11.94	14.63	5084	6638	5650	5657	-7	0.427	1	48.6	0.0	65.0 ±1.1	4.6	1105	0.7	0.61	176	5392028	1.64	18.10	36.09
1611	14.22	18.24	5163	6483	5750	5689	61	0.422	29	91.8	6.4	91.3 ±4.8	4.1	1129	0.7	0.62	200	8952906	5.24	18.77	36.43
1612	17.64	19.36	4300	5867	5300	4877	423	0.248	34	59.2	13.0	60.2 ±6.1	3.9	1006	0.7	0.64	209	5678899	10.17	20.70	37.46
1613	16.74	33.30	4061	6180	5100	4471	629	0.333	7	53.7	3.6	52.9 ±0.7	3.9	1161	0.7	0.62	207	5521264	1.40	18.08	36.08
1614	15.60	35.30	5318	6825	5850	5838	12	0.365	7	71.7	9.0	73.1 ±0.7	5.5	2021	0.7	0.53	149	8170970	0.96	18.05	36.06
1615	3.06	4.03	5349	5868	5650	5645	5	0.490	20	23.9	3.4	23.3 ±4.2	7.8	1119	0.7	0.54	104	1024654	18.18	25.59	40.36
1616	4.20	2.92	4904	5865	5200	5182	18	0.571	12	52.5	4.5	56.2 ±2.0	9.2	440	0.7	0.63	89	971144	3.47	18.35	36.20
1617	3.18	2.14	4709	5832	5300	5066	234	0.604	0	NaN	NaN	30.1 ±0.8	20	505	0.7	0.53	41	228563	2.68	18.17	36.04
1618	4.68	4.01	5517	6558	5950	5869	81	0.551	45	13.4	1.6	13.4 ±6.3	7	572	0.7	0.63	116	391918	47.19	50.52	59.38

[a] ELAs were approximated by snowlines, which we estimated from satellite images near the end of the hydrological year. Where the estimated ELA is higher than maximum glacier elevation (bold numbers), a large amount of accumulation occurs by snow and ice avalanches. [b] Elevation differences between the estimated ELA and the point on the profile where the ice flux was estimated. Profiles of large differences are usually associated with glaciers that are fed to a high degree by snow and ice avalanches and where a large portion of the ice is situated below the estimated ELA. Note, however that the point of ice flux estimation along the profile is usually located in the upper half of the glacier (see column 'Downstream distance of flux estimate'). [c] In case of no direct velocity measurements at the profile point of the flux estimate, the surface velocity and its uncertainty are obtained by interpolation of neighboring velocity measurements. [d] Average velocity at profile point of flux estimate is obtained from smoothing the interpolated, mean velocity measurements along the profile with a running average filter of 11 data points (660 m), or 5 data points (300 m) for profiles <2 km length. [e] Assuming uncertainties for s_1, s_2, τ = 0% (low)/ 10% (medium)/ 20% (high), and for α = 0 (low)/ 5% (medium)/ 10% (high).
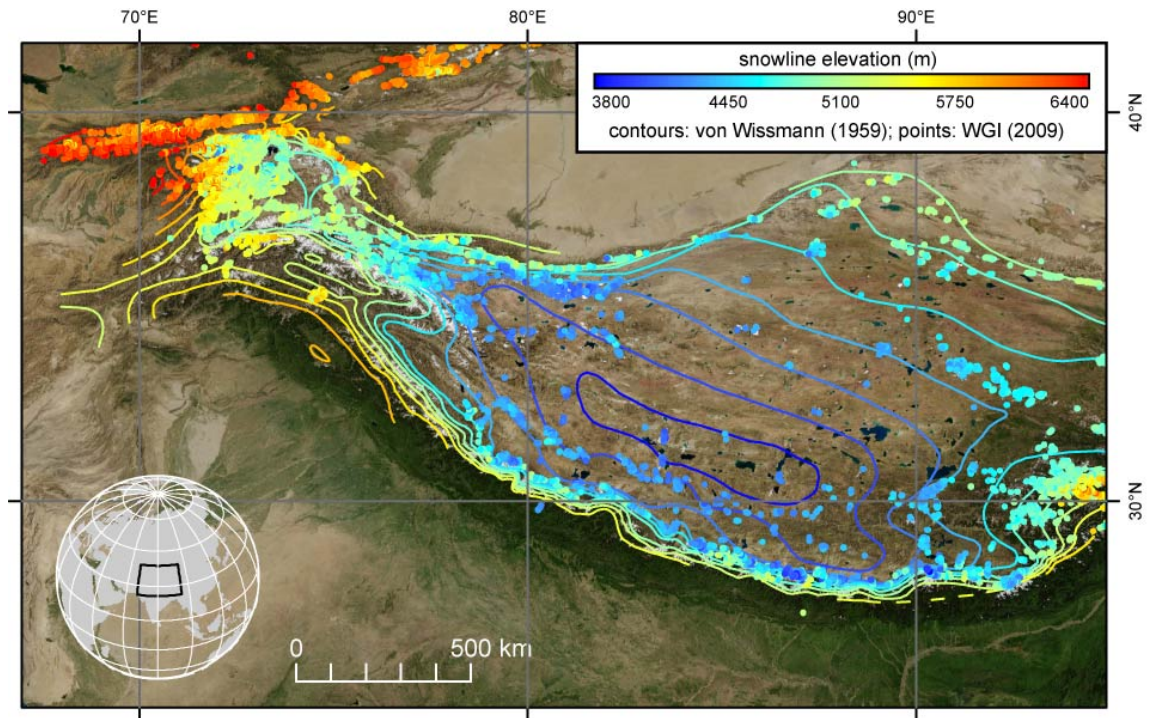
Figure D4: Snowline data sets from High Asia. The 200-m spaced contours are based on point-observations mostly from the first part of the 20th century, which have been compiled by *von Wissmann* [1959]. Note that most of the observations were made 60-100 years ago. The points refer to snowline observations taken from the World Glacier Inventory (WGI) [*National Snow and Ice Data Center*, 2009]. The data set from Central Asia includes over 16197 observations from the Pamirs/Tian Shan, the Tarim Basin, the Tibetan Plateau, and the Huang He, Salween/Irrawaddy, Sikiang Hong/Mekong, Yangtse, Ganges, and Indus River Basins. Most of the snowline data from China are lacking a date, but they are probably relatively recent and the result of the newly completed Chinese Glacier Inventory (available from the World Data Center for Glaciology and Geocryology, Lanzhou; see http://wdcdgg.westgis.ac.cn/). Snowline data from the Pamirs and Tian Shan have been obtained between 1943 and 1980. Unfortunately, snowline data from Afghanistan, Pakistan, India, and Bhutan are rare and mostly missing dates.
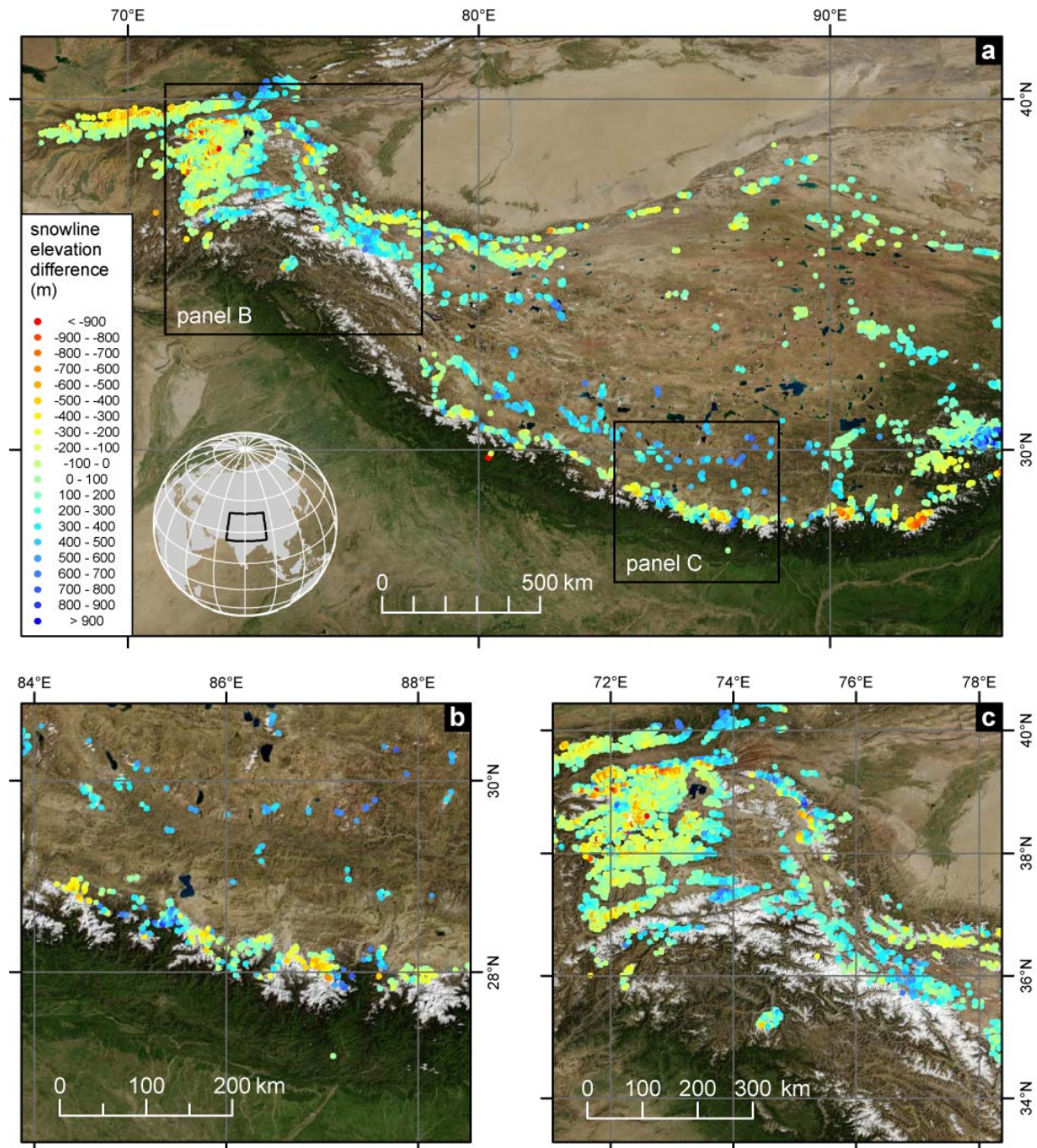
Figure D5: Differences in snowline datasets across High Asia. (a) Point-wise snowline data from WGI [*National Snow and Ice Data Center*, 2009] are subtracted from interpolated snowline elevations taken from the map by *von Wissmann* [1959]. We first interpolated the contour-map by *von Wissmann* [1959] to produce a grid with 6280-m cellsize, and then interpolated a single snowline elevation for each point where snowline elevations are given in the WGI dataset. The results indicate the following: (i) most snowline data from the map by *von Wissmann* [1959] and the WGI are within a few 100 meters (green and cyan colors); (ii) extreme differences occur locally and sometimes adjacent with extreme differences of opposite sign; (iii) in some regions, a systematic positive (von Wissmann snowlines > WGI snowlines; e.g., Karakoram, south-central Tibet) or negative difference (von Wissmann snowlines < WGI snowlines; e.g., northwestern Pamir) exists. (b) Close-up view of the central Himalaya, and (c) the Pamir and Karakoram. Extreme small-scale variability in snowline differences between adjacent regions in the central Himalaya indicates the possibility of biases in the WGI-snowline data set and/or small-scale variability, related to, e.g., topography, which is not resolved in the map of regional climatic snowlines by von Wissmann. Note also that small-scale topography-related variability of satellite-imagery derived ELAs is not reflected in the snowline map by *von Wissmann* [1959] as documented by differences in the range of ELA and snowline elevations within a region (Figure 7.2). Different mean values of satellite-imagery derived ELAs and snowlines after *von Wissmann* [1959] are possibly associated with shifts in snowlines during the last ~50-100 years, i.e., since the snowline data were collected. Note that the snowline elevations after von Wissmann that we used for the reconstruction (Figure 7.3) are somewhat lower than our glacier ELAs in the central Himalaya, but higher in the Karakoram (Figure 7.4), indicating even more pronounced east-west differences in the recosntruction.
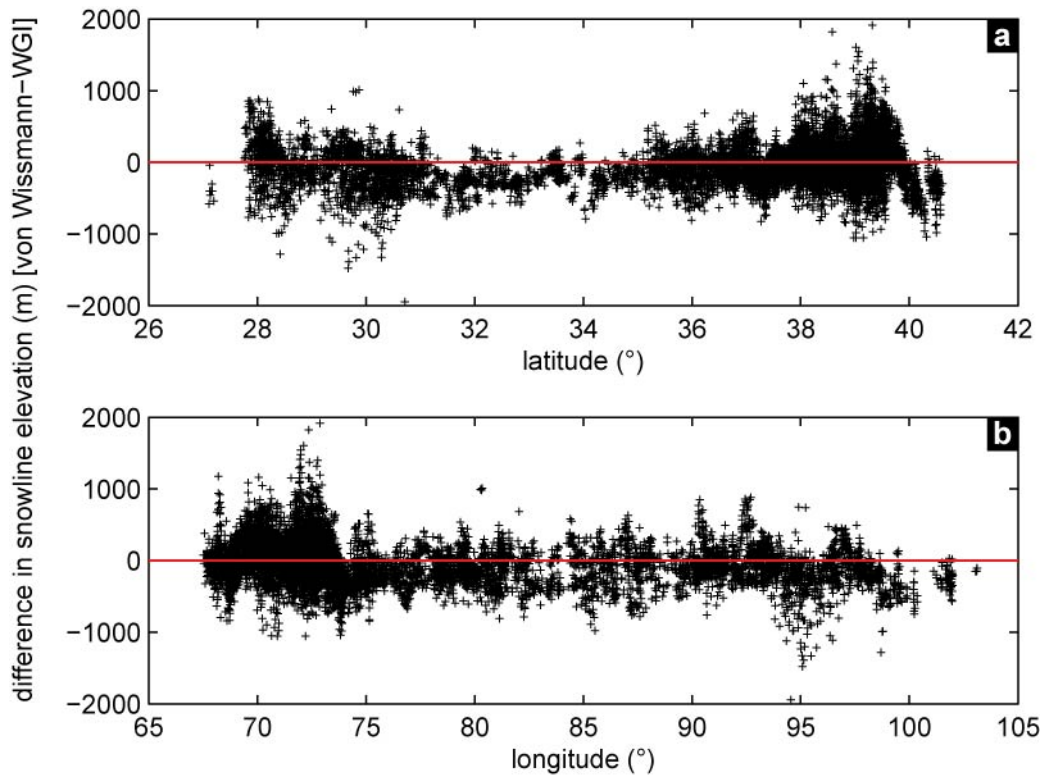
Figure D6: Latitudinal and longitudinal differences in snowline data sets. Scatter plots of the difference in snowline elevation (m) between the data by *von Wissmann* [1959] and the WGI [*National Snow and Ice Data Center*, 2009] show no trends. Larger scatter in the differences are seen at higher latitudes and lower longitudes, corresponding to the Pamir and Tien Shan Mountains.
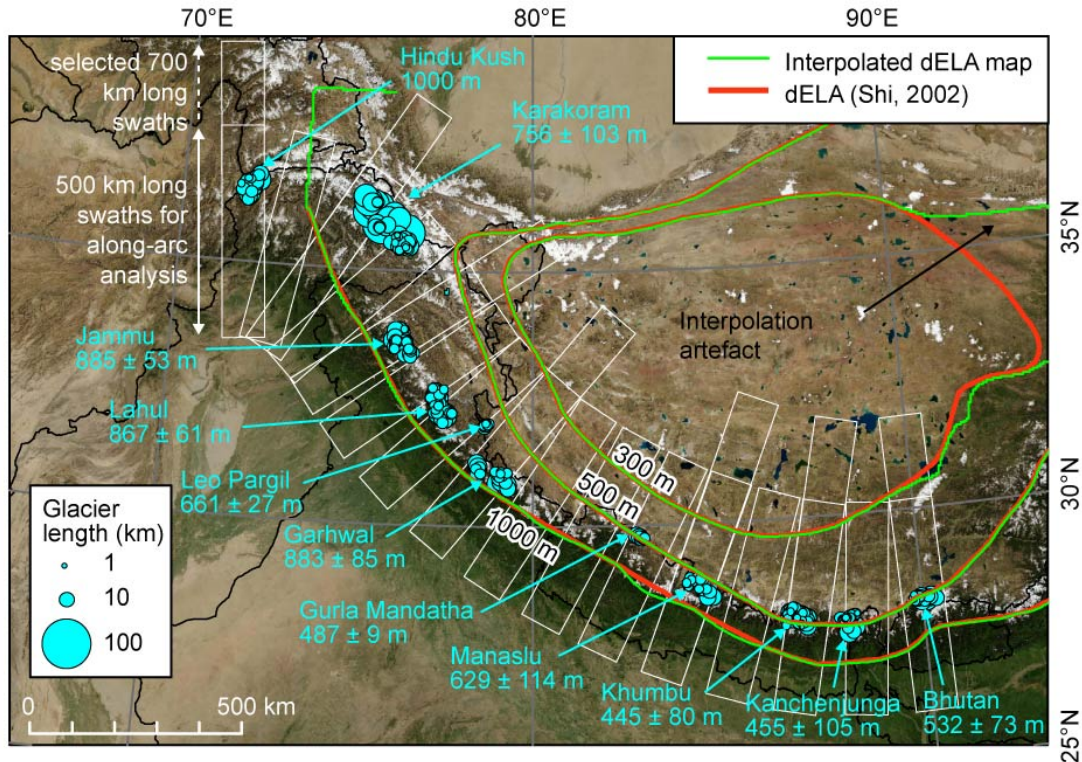

Figure D7: ELA-depression (ΔELA) during the Last Glacial Maximum (LGM). ΔELA-contours show original data by *Shi* [2002] in red, and contours derived from the interpolated continuous ΔELA-surface used for this study in green. The map of LGM ELA-depressions [*Shi*, 2002] that we used for the reconstruction of the land surface above the LGM ELA does not extend across the entire part of the study area, but ends in the central Pamir at ~73.5°E. Observations from the Pamir indicate ELA-depressions of as much as ~1000 m along the humid orogenic front in the western Pamir to values between ~300 and ~400 m in the arid central and eastern part of the Pamir Plateau [*von Wissmann*, 1959;

Abramowski et al., 2006]. In order to have an LGM-ΔELA map extending across the entire study area, we assume uniform LGM-ELA depressions of 1000 m along the western edge of the Pamirs.

We note that the LGM-ΔELA map [*Shi*, 2002] misses small-scale variations in ELA-depressions related to, e.g., topography, hence under- or overestimating ΔELAs locally. For the purpose of our study, the general pattern is more important than local variability, and according to *Owen and Benn* [2005], who compiled LGM ΔELAs from the literature, the map appears to be realistic. However, we note that the data reported in *Owen and Benn* [2005], shows considerable scatter and some inconsistencies with respect to newer assessments. For instance, ΔELAs of 450 m and 950 m [*Owen and Benn*, 2005], north and south of Mount Everest stand in contrast with more recent estimates of 150 m and 280 m [*Owen et al.*, 2009]. In order to assess potential biases, we compared ΔELA-values at the location of the glaciers that we derived from the map by *Shi* [2002] (see cyan-colored text in Figure D8) with newer or records not cited in *Owen and Benn* [2005].

For glaciers located in the Bhutanese Himalaya, *Meyer et al.* [2009] used the toe to summit altitude method (TSAM) and the maximum elevation of lateral moraines method (MELM), and estimated Marine Isotope Stage (MIS) 3 ΔELAs of ~580 m, compared to LGM-ΔELAs of ~532 +/- 73 m obtained from Shi [2002]. Around the Kanchenjunga massif, *Asahi* [2010] used the MELM method, and estimated ΔELAs of assumed LGM age that rise from ~1000 m at the southernmost front of the Himalaya to ~500 m at the edge of the Tibetan Plateau, where most of our studied glaciers are located and LGM-ΔELAs of ~455 +/- 105 m are obtained from *Shi* [2002]. A problem in this work is the different methods applied for obtaining present-day and palaeo ELAs, thus making the values difficult to interpret. We further stress that the MELM method commonly overestimates ΔELAs, and that the values are therefore probably too high [*Müller*, 1980; *Benn and Lehmkuhl*, 2000]. *Asahi* [2010] applied the same methods in the Khumbu region and obtained ΔELAs that rise from ~1000 at the wet mountain front to ~250 m at Mount Everest, but these are based on very few data points with considerable scatter. *Duncan et al.* [1998] used the toe to headwall are ratio (THAR) method on glaciers reconstructed from valley shapes, and obtained ΔELA values of 100-900 m, with a mean (+/- 1σ) of ~500 +/-180 m. *Müller* [1980] used the TSAM, MELM, and other methods to obtain present-day ELAs and the elevation of empty cirques to estimate Pleistocene ELAs in the same region. The obtained ΔELAs rise from ~600 m in the south to ~200 m in the north of this area. These values are similar to ΔELA values of 280 m and 150 m that have been obtained by *Owen et al.* [2009] from glacier reconstructions based on dated LGM-moraines and using the accumulation area ration (AAR) method on the Khumbu and Rongbuk glaciers, located south and north of Mount Everest, respectively. The values derived from the map by *Shi* [2002] in this area give LGM-ΔELAs of ~445 +/- 80 m for glaciers located north and south of Mount Everest. Thus, the ΔELA-estimates we used are probably a little too high north of Mount Everest, but appear reasonable in the southern part of the Khumbu region.

A steep north-south gradient in ΔELAs has been documented by *Schäfer et al.* [2008] from dated LGM to Lateglacial moraines in the Nyalam region (~86°E), in between the Khumbu and Manaslu regions. Using the THAR method, *Schäfer et al.* [2008] found ΔELAs that rise from ~450 +/- 100 m in the south to ~250 +/- 50 m farther north, on the edge of the Tibetan Plateau. *Gayer et al.* [2006] used the AAR and THAR methods in the Ganesh Himal, farther to the west (~85°E), and obtained an LGM ΔELA of ~750 m at the wet, monsoon-soaked front of the Himalaya. Palaeo ELAs from the Manaslu, Gurla Mandatha, and Leo Pargil regions are so far missing. *Sharma and Owen* [1996] provide ΔELA-data from the Gangotri Valley in Garhwal which is difficult to evaluate due to interpretation and dating issues of older glacial deposits [*Barnard et al.*, 2004]. *Scherler et al.* [2010] obtained Lateglacial, post-LGM ELAs from dated moraines in Western Garhwal, and found ΔELAs that rise from ~400 m within the High Himalaya to <300 m in deeper parts of the orogen. *Owen and Benn* [2005] summarized the data available from Lahul, which indicates LGM ΔELAs of ~780-840 m, similar to the values derived from *Shi* [2002], with ~867 +/- 61 m. Data from Jammu is presently lacking, but estimates by *Damm* [2006], using the TSAM method, and data given by *Owen and Benn* [2005], suggest LGM-ELAs farther to the north in the Zanskar Range, and in westernmost Tibet of ~500-600 m, which is close to the values provided by *Shi* [2002]. New geochronological data from the central Karakoram [*Seong et al.*, 2007] suggest extensive valley glaciers that advanced >60 km during the Lateglacial down to elevations of ~2300 m asl., but corresponding shifts in the ELA are missing. In contrast, *Owen and Benn* [2005] reconstructed an LGM ΔELA for Batura glacier of <100 m, which stands in contrast to earlier estimates of ~1100 m. We think that the values of 756 +/- 103 m provided by *Shi* [2002] are possibly a little too high but closer to the true values for the entire range as compared to the very low value obtained for Batura Glacier alone. Clearly, more data are needed from this part of High Asia. Finally, data from the Hindukush are limited and the LGM-ΔELA values of ~1000 m that have been reported in *Owen et al.* [2002], lack clear indication of which method was used, but are similar to the ΔELA values reported by *Porter* [1970] from the Swat Valley, Pakistan, farther to the south.

In summary, the currently available data suggests that the ΔELA-map by *Shi* [2002] probably overestimates ΔELAs in more interior regions of Tibet, but is in reasonable agreement with data from the external parts of the orogen. The possibly too high ΔELA-values assumed for more interior regions of Tibet, however, have little effect on our study, as the present-day snowlines are quite high above the land surface and a greater LGM-ELA lowering would induce only minor changes and does not affect our results. Furthermore, the steep northward decline in ΔELAs is observed in all places along the central Himalaya where data exist. Importantly, the southward bulge of ΔELA-contours seen in the central Himalaya in the map by *Shi* [2002] is supported by the available data from these regions [*Müller*, 1980; *Duncan*

et al., 1998; *Schäfer et al.*, 2008; *Owen et al.*, 2009; *Meyer et al.*, 2009; *Asahi*, 2010;]. Thus, we suggest that the ΔELA map by *Shi* [2002] depicts the LGM-ELA depressions fairly well and serves as a reasonable data source for our reconstruction of LGM-glacial environments across High Asia. The results that we base our conclusions on are not affected by changes on the order of the discrepancies observed between different data sources.
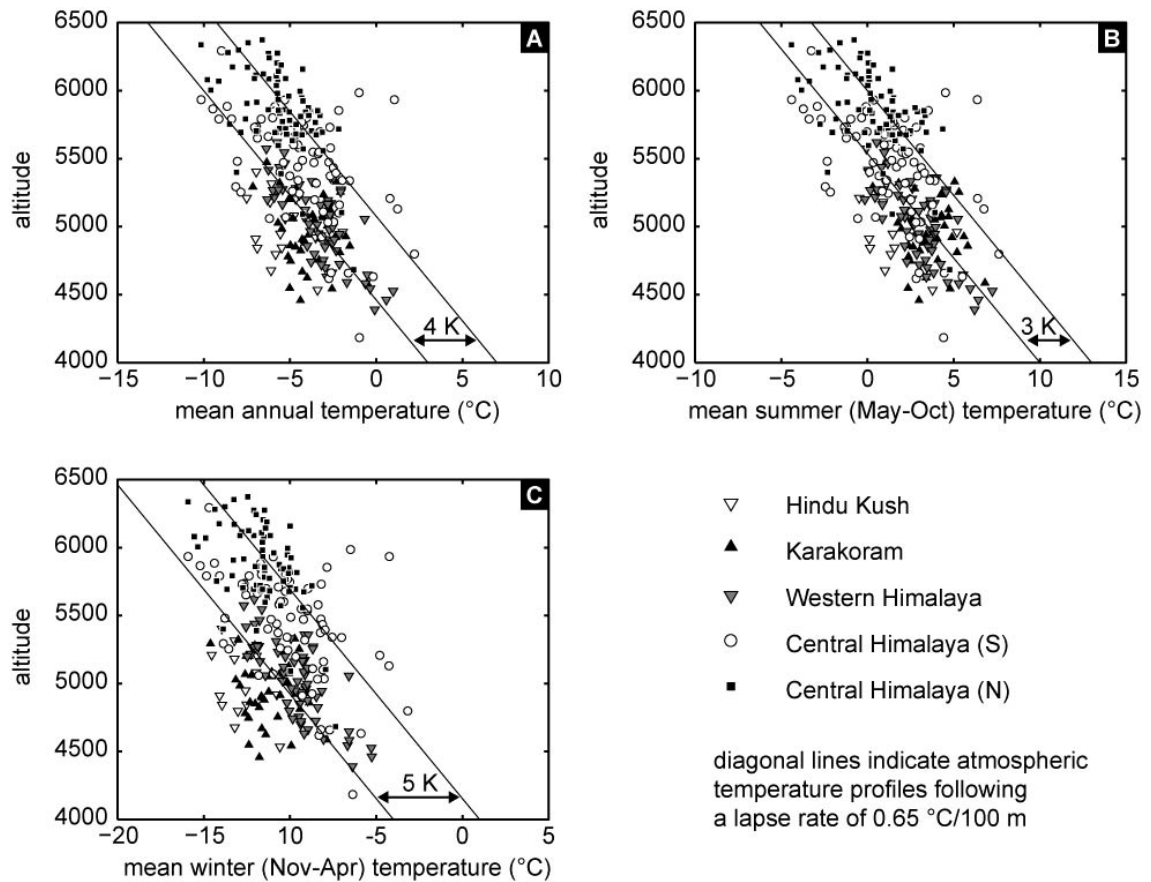

Figure D8: Seasonal and annual temperatures at the analyzed glaciers. (A) Mean annual temperatures, (B) mean summer temperatures, and (C) mean winter temperatures. The temperature data is derived from the 10-arc minutes resolution CRU 2.0 data set (Climate Research Unit; available at http://www.cru.uea.ac.uk/), which is based on mean monthly meteorological station data from 1961 to 1990 [*New et al.*, 2002], measured at screen height, i.e., 1.25-2 m above ground. We interpolated the temperatures at the location of the glaciers and plotted them against mean glacier elevation. Differences in air temperatures between the five geographical regions are most evident during winter but show high interregional variability. During summer, the differences are generally smaller and the data from each region roughly follows a lapse rate of 0.65 K/100 m. Such a lapse rate is in the mid-range of lapse rates that have been obtained for different regions in High Asia during different seasons [*de Scally*, 1997; *Thayyen et al.*, 2005; *Jain et al.*, 2008]. On average, however, the temperature differences between the geographical regions are not large, suggesting similar thermal regimes of the glaciers.